공학박사 학위논문

Shear Strength and Degradation Model for Performance Based Seismic Design/Evaluation of RC Walls

RC 벽체의 성능기반 내진설계 및 평가를 위한
전단 강도와 강도저하 예측모델

2021년 8월

서울대학교 대학원

건축학과

김 성 현

Shear Strength and Degradation Model for Performance Based Seismic Design/Evaluation of RC Walls

지도 교수 박 홍 근

이 논문을 공학박사 학위논문으로 제출함

2021년 7월

서울대학교 대학원

건축학과

김 성 현

김성현의 공학박사 학위논문을 인준함

2021 년 8 월

위 원 장 _____

부위원장 _____

위 원 _____

위 원 _____

위 원 _____

위 원 _____

Abstract

Shear Strength and Degradation Model for Performance Based Seismic Design/Evaluation of RC Walls

Kim, Sung Hyun
Department of Architecture and Architectural Engineering
College of Engineering
Seoul National University

In the performance based seismic design/evaluation, the behavior of structure by earthquakes is evaluated by the nonlinear analysis. In the slender walls of high-rise residential buildings, because the large shear force is applied by a dynamic mode effect, the high-strength reinforcement is required for economic design. Therefore, in this dissertation, experimental studies were conducted to provide the evidence of validity of RC walls with 700 MPa high-strength reinforcement. In the case of walls in the existing buildings, because the deformation capacity is limited by not applying the seismic design, it is necessary to evaluate the shear strength and inelastic deformation of the walls accurately. Therefore, the present dissertation investigated the major design parameters affecting the shear strength of wall, and developed the shear strength and strength degradation model based on the shear failure mechanism.

The large demand force is applied by the gravity loads and earthquake loads at the walls in the high-rise residential buildings. Thus, the validity of 700 MPa reinforcement should be verified for the walls with high shear reinforcement ratio and high axial force. Even the demand force is small, the current design code requires

the minimum reinforcement ratio for serviceability and safety. Thus, it is required to investigate the effects of the low reinforcement ratio on the strength and deformation capacity of the walls. For these purpose, the cyclic loading tests were conducted for the 700 MPa RC walls with various test parameters. The test results showed that the shear strength of walls with 700 MPa reinforcement was greater than the design strength, regardless of the test parameters. 700 MPa shear reinforcement was yielded at the peak shear strength. However, because of the greater yield strain and less reinforcement ratio, the walls with 700 MPa rebars showed the less strength margin, the greater crack width, the less energy dissipation and the less drift ductility ratio.

Based on the test results, the effects of design parameters on the shear strength were investigated. The major design parameters were the yield strength of shear reinforcement, the vertical web reinforcement ratio, the axial load ratio, and the shape of the cross section. Since such parameters are closely related to the compression zone depth, the shear strength and shear strength degradation of walls are explained based on the effective compressive stress of concrete and effective area of concrete in compression. Based on the consideration, the present study developed the shear strength and strength degradation model. The major failure mechanisms of diagonal tension cracking and web crushing were addressed.

The diagonal tension strength was defined by the compression zone depth and the normal stress of concrete in the compression zone. As the inelastic deformation increased, concrete crushing occurred in the compression zone. Thus, the effective compression zone gradually decreased, and diagonal tension strength degraded.

The web crushing strength was defined by effective compressive stress of diagonal strut. By the compression softening effect, the effective concrete stress decreased as the crack width increased. Therefore, the web crushing strength degraded as the lateral deformation increased.

Based on these shear failure mechanisms, simplified shear strength and strength degradation models were developed. Compared to existing design method, the proposed model agreed with the existing test results.

To implement the proposed model into the practical design, design tables and guideline were suggested. The proposed model was applied in the Perform 3D, and the analysis results were compared with the test results. The Perform 3D analysis results showed that the strength degradation occurred after flexural yielding, and the deformation capacity was limited by the strength degradation.

Keywords: Performance based seismic design/evaluation, 700 MPa reinforcement, cyclic loading, wall shear strength, wall deformation capacity, diagonal tension cracking, and web crushing.

Student ID: 2017-35111

Contents

List of Tables

List of Figures

List of Symbols

a : modeling parameter, rotation corresponding to the initiation of strength degradation

a : $M_u/(V_u l_w)$ = shear span ratio

A_c : area of concrete

A_{cv} : net shear area in the cross section

A_g : gross area of cross section

A_{sl} : the area of the tensile reinforcement

A_{st} : the area of transverse reinforcement within spacing s

b : modeling parameter, rotation corresponding to the termination of strength degradation

b_w : width of cross-section

c : compression zone depth

c : modeling parameter, residual strength ratio

c_v : shear contribution ratio

d : depth of cross section

d_b : nominal diameter of vertical rebars

E_c : elastic modulus of concrete

e_l : elongation in the plastic hinge region

f_c' = concrete compressive strength

f_{ce} : effective compressive strength of diagonal strut

f_t : concrete tensile strength

f_{vbe} : yield strength of vertical boundary reinforcement

f_{vh} : yield strength of horizontal reinforcement (= yield strength of shear reinforcement)

List of Symbols

f_{vv} : yield strength of vertical web reinforcement

f_{vwd} : design yield strength of shear reinforcement

f_y : yield strength of rebar

G_c : shear modulus of concrete

H : height of the wall

h_{be} : width of boundary element or flange

h_w : thickness of web

h_w/l_w : aspect ratio

I_g : moment of inertia

k_c : coefficient related to the compression zone depth

k_s : size effect factor

l_p : plastic hinge length

M_u : required flexural moment

n : elastic modulus ratio of steel and concrete

N_u : axial force

$N_u/A_g f_c'$: Axial force ratio

R : plastic hinge rotation

R_{sle} : reduction factor of equivalent stress block of flange

s : the spacing of transverse reinforcement

t_{be} : thickness of boundary element or flange

t_w : wall thickness

v_{cc} : shear capacity of concrete controlled by compression failure

v_{ct} : shear capacity of concrete controlled by tensile failure

V_f : shear force corresponding to the nominal flexural strength

V_n : nominal shear strength

V_u : required shear force

V_{wc} : web crushing strength

V_{wcm} : maximum web crushing shear strength

z : distance from the zero normal strain

Δ : overall lateral displacement

δ : overall lateral drift ratio

δ_{cr} : drift ratio at cracking

Δ_{ef} : lateral displacement in the elastic region

δ_f : flexural lateral drift ratio

Δ_f : lateral flexural displacement

δ_m : drift ratio at the peat strength

Δ_p : lateral displacement in the plastic hinge region

Δ_{pf} : lateral flexural displacement in the plastic hinge region

Δ_{ps} : lateral shear displacement in the plastic hinge region

Δ_s : lateral shear displacement

δ_s : shear lateral drift ratio

δ_u : ultimate drift ratio

Δ_θ : lateral displacement by the rigid body rotation of the elastic region

ε_c : principal compressive strain of web concrete

$\varepsilon_c(z)$: concrete normal strain at the distance z

ε_{co} : concrete crushing strain

ε_t : principal tensile strain

ε_y : yield strain of reinforcement

ε_{yh} : yield strain of shear reinforcement

η : contribution ratio of the concrete to shear strength

θ : angle of shear crack

ρ : flexural reinforcement ratio

ρ_h : horizontal reinforcement ratio (= shear reinforcement ratio)

ρ_t : transverse reinforcement ratio

List of Symbols

ρ : transverse reinforcement ratio in the boundaty element

$\rho_{t,min}$: minimum transverse reinforcement ratio

ρ_v : vertical web reinforcement ratio

ρ_w : longitudinal reinforcement ratio

$\sigma_c(z)$: normal stress of concrete at the distance z

σ_{ct} : average compressive stress of the compression zone

ϕ : curvature

ϕ_p : plastic curvature

ϕ_y : yielding curvature

ω_1, and ω_2 : strength margin ratios

Chapter 1. Introduction

1.1 General

In 2017, an earthquake in Pohang caused damges to buildings. Unlike the damages caused by the Gyeongju earthquake (2016), as shown in Fig. 1-1, major damages on the structural members occurred by Pohang earthquake. In particular, severe damage occurred at the walls and piloties of the existing buildings that were not applied by the seismic design. Further, the wall damages also occurred at the new residential buildings.

According to the record of the Korea Meteorological Administration, since the start of earthquake recording, the frequency and magnitude of earthquakes have increased gradually (see Fig. 1-2). To address the increasing seismic hazard, the seismic design code has been strengthened, since it was first introduced in 1988. Currently, seismic design is mandatory for all buildings with multiple stories (see Fig. 1-3). Thus, the economic seismic design is one of the important issues in the design of building.

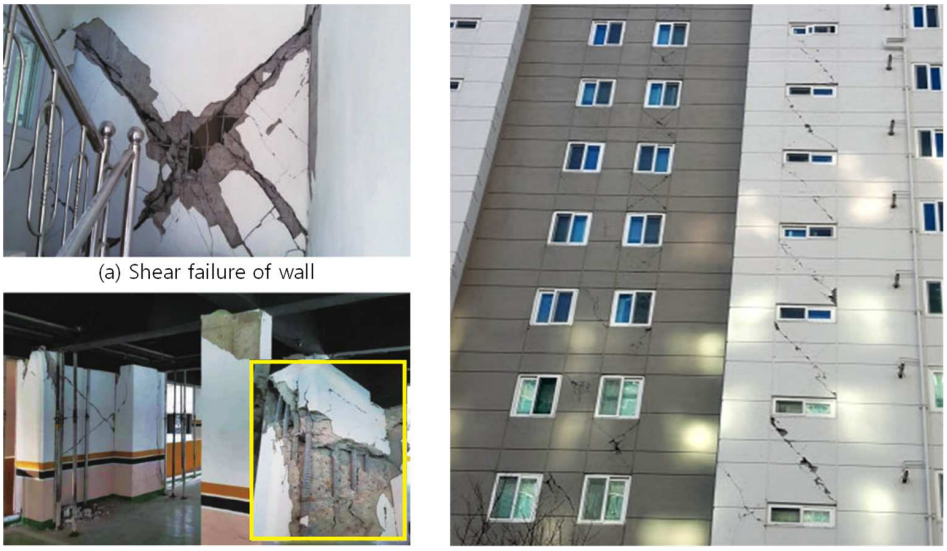

Fig. 1-1 Structural damages by Pohang earthquake

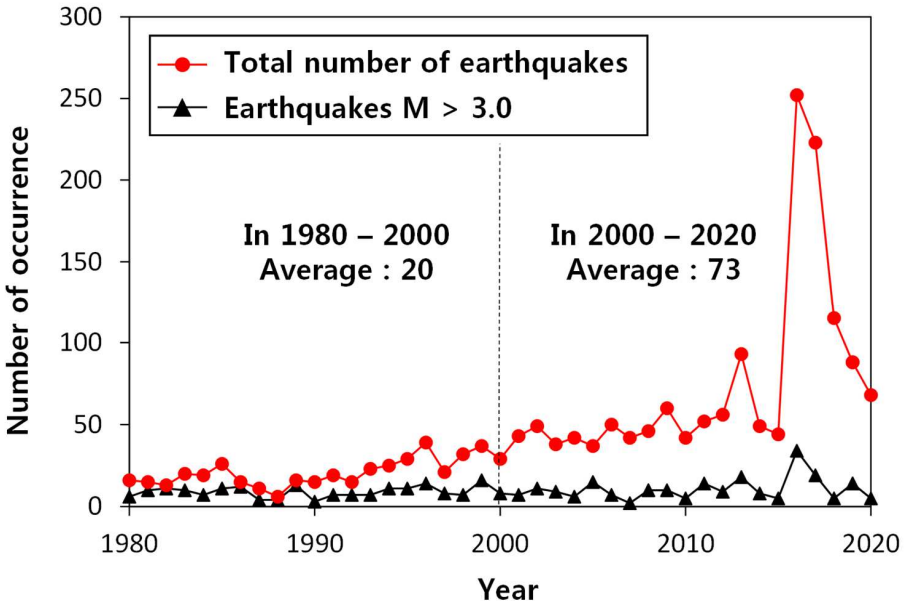

Fig. 1-2 Frequency and magnitude of earthquakes in Korea

(Korea Meteorological Administration).

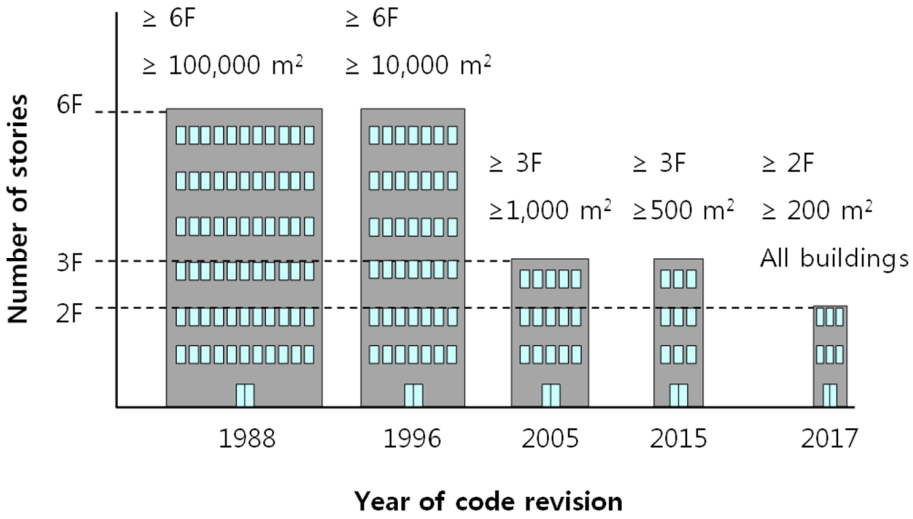

Fig. 1-3 Buildings subject to seismic design obligations

Recently, performance based seismic design/evaluation method (PBD) is frequently used for seismic design of new residential buildings and seismic performance evaluation of existing buildings. Fig. 1-4 shows the concept of the performance based seismic design/evaluation. In the performance based seismic design/evaluation method, the structural members are designed and evaluated so that the building satisfies the target performance level for the design earthquakes. As long as the performance level is satisfied, the plastic deformation and energy dissipation of the building are allowed. Therefore, the performance based design is economic design method that can use the performance of materials and structural members more efficiently than the existing ultimate strength design method.

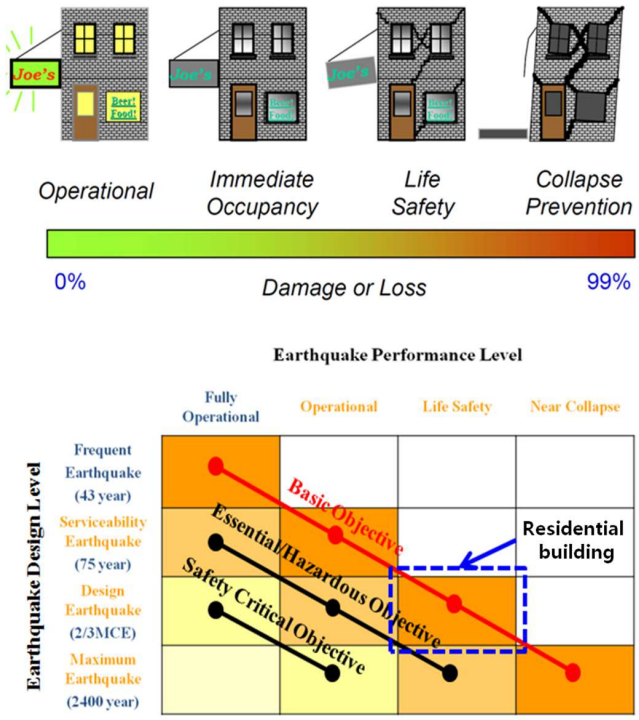

Fig. 1-4 Concept of the performance based seismic design/evaluation

Table 1-1 compares the structural characteristics of the new residential buildings and existing residential buildings, which are subjects of performance based design.

The new residential buildings have following characteristics:

1) High-rise: Due to overpopulation in the metropolitan area and limited land, the new residential buildings are becoming taller to accommodate more residents. High-rise residential buildings commonly have over than 25 stories.

2) Decrease in wall area: Because the lifespan of the building increased, and in order to protect the environment, remodeling is preferred rather than redevelopment. In order to facilitate the remodeling, total wall area is decreased, which can increase the demand force per unit length of the wall.

3) Increase in slab thickness: The inter-story noise and vibration are one of the important issues in the modern apartment building. To block them, the slab thickness should be greater than 210 mm. Due to the greater slab thickness, the structural mass of the building increases, which can increase the earthquake loads.

4) Vertical and horizontal discontinuity: Due to architectural requirements, various type of plan, such as L-shape, C-shape, and Y-shape, are used. Further, in the lower stories, piloties are frequently used. In the case of building with horizontal and vertical discontinuity, the design code require the building to be designed by using special earthquake loads.

5) Seismic design category D: The new residential buildings usually have a seismic design category D due to unfavorable ground conditions. In that case, if the total height of the building is greater than 60 m, the building should be designed as special structural wall system. Special boundary element is required to secure the ductility capacity.

On the other hand, the existing residential buildings have following contrasting characteristics:

1) Low to mid-rise: The total number of stories was usually less than 15 in the existing residential buildings. This is because the regulations were stricter for the residential buildings greater than 16 stories before 2005.

2) Greater wall area: The existing residential buildings had a flat-type plan, where the wall arrangement was relatively inefficient and had a large amount of walls. Further, because the concrete strength was lower in the past, the wall area was greater.

3) Smaller slab thickness: Before 2005, there was no regulation on the inter-story noise. The slab thickness was less than 150 mm, usually 120 mm.

4) Typical plan: In the past, the plate-shape plan was preferred. The flat-type residential building was easy to construct and it can place all households in the same direction.

5) Seismic design category less than C: The existing residential buildings was constructed on the relatively favorable ground conditions. Further, because the total height was low, the ordinary structural wall system was used. The boundary confinement was not provided, and ductility of the walls were low.

Table 1-1 Comparisons of the new and exiting residential buildings.

Items	New residential buildings	Existing residential buildings
Height and total number of stories	▪ High-rise ▪ Greater than 20F	▪ Low to mid-rise ▪ Less than 15F
Wall area	▪ Less, ▪ Efficient plan, ▪ Consideration of remodeling	▪ Greater, ▪ Greater wall area due to low concrete strength
Slab thickness	210 mm	< 150 mm, usually 120 mm
Type of plan	▪ Various type: L-shape, C-shape, Y-shape, etc.… ▪ Piloties in lower stories.	▪ Typical plan, flat-type
Seismic design category (SDC)	SDC D	SDC B, C
Material strength	▪ High-strength concrete ▪ High-strength reinforcement f_y = 500 – 600 MPa	▪ Low-strength concrete ▪ Normal-strength reinforcement f_y = 400 MPa

Considering these characteristics, in the new residential buildings, the demand forces by earthquake loads can be significantly increased compared to the existing buildings. Further, because the increase of stories, the shear force demand can be significantly increased by the higher mode effects (i.e. shear force amplification effect). Kim et al. (2019) reported actual demand shear force was increased 1.5 to 2.5 times shear force resulting from elastic analysis. Such shear demand amplification is addressed in current design codes such as Eurocode 8 and ACI 318-19 (see Fig. 1-5). The existing walls, which were not designed considering shear amplification, can be subjected to severe shear damage under earthquake loading.

To address the increase of demand forces, the use of high-strength reinforcement can be one of the efficient options. The several experimental studies have investigated the walls with high-strength reinforcement to reduce the reinforcement ratio. Based on the test results, the permissible yield strength of reinforcement has increased in the design codes. KCI 2017, Eurocode 8, and Model code 2010 allow yield strength of 600 MPa for vertical and horizontal reinforcement of walls. Further, in ACI 318-19, which is recently revised, the permissible yield strength of vertical reinforcement of walls increased to 690 MPa (100 ksi), and the permissible yield strength of horizontal reinforcement of special walls increased to 690 MPa (100 ksi). Based on these structural design codes, the high-rise residential buildings in Korea usually use 500 MPa for reinforcement less than D13 (diameter of 13 mm), and 600 MPa for reinforcement greater than D16 (diameter of 16 mm). However, for 700 MPa reinforcement, the experimental verification is required.

For the performance based seismic design/evaluation of both new and existing residential buildings, the shear strength and deformation capacity of walls are major factors to evaluate the performance of structure. For walls in the new residential building, high axial load is applied due to increase of the number of stories. Further,

high strength reinforcement and high reinforcement ratio are used to resist increased demand forces. Such design parameters are limitedly addressed in the existing model for shear strength and deformation capacity. Thus, for economic and safe design, accurate model to predict the shear strength and deformation capacity of walls should be provided.

Further, the walls in the existing residential building are vulnerable to shear failure, when applied by the earthquake loads. In the RC members subjected to high shear demand, the inelastic deformation can be limited by shear strength degradation after flexural yielding. When shear strength is less than the shear demand required for flexural yielding, brittle shear failure occurs before flexural yielding ($V_n < V_f$), Even the shear strength is greater than the yield strength demand ($V_n \geq V_f$), shear strength degradation can occur as the inelastic deformation increases after flexural yielding. For seismic performance evaluation of buildings, inelastic deformation capacity is important. Thus, shear strength degradation and the corresponding deformation capacity should be accurately predicted for performance based seismic evaluation of the existing buildings.

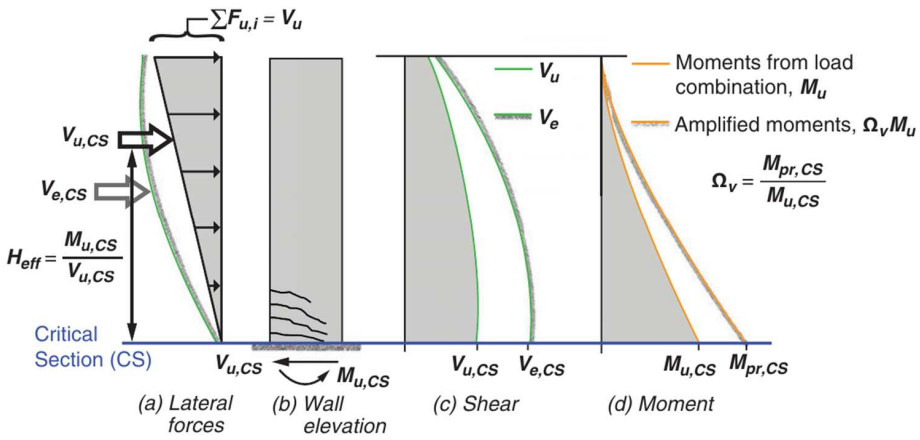

Fig. 1-5 Shear force amplification model of ACI 318-19

1.2 Scope and objectives

Based on the background of study, the major objectives of this dissertation are as follows: 1) to verify the validity of 700 MPa reinforcement for RC shear wall; 2) to improve the shear strength model considering the various design parameters; 3) to develop the shear strength degradation-deformation capacity model after flexural yielding.

For the first objectives, experimental tests on shear walls with 700 MPa reinforcement were conducted. 15 wall specimens were tested under cyclic lateral loading. To address the general design of shear walls in the high-rise residential buildings, high shear reinforcement ratio (ρ_h = 0.42 – 0.66 %) or significantly low reinforcement ratio (ρ_v = 0.14 – 0.27 %, and ρ_h = 0.14 – 0.25 %), and high axial force ($N_u/A_g f_c'$ = 0.30) were addressed as test parameters. Because these test parameters have been limitedly addressed by the existing studies, the test results of the present study complement the experimental basis for the development of shear strength model.

For the second objective, the effects of design parameters on the shear strength was discussed based on the test results of the present study and existing studies. A simplified shear strength model was developed addressing the effects of major design parameters: flexural reinforcement, axial force ratio, and boundary element. The proposed model was derived by considering the general shear failure mechanisms of walls: diagonal tension cracking and web crushing. For applicability in practical design, the proposed shear strength equation was simplified in the practical range of design parameters. The proposed shear strength model was verified by the existing test specimens failed by shear failure before flexural yielding.

For the last objective, simplified load-deformation model was developed. Unlike existing models, the proposed model was developed based on the shear failure mechanisms of diagonal tension cracking and web crushing. The initial load-deformation model was derived as function of the curvature. Thus, to transform the curvature to the deformation, plastic hinge deformation model of wall was developed. The proposed load-deformation model was verified by the existing test specimens failed by shear failure after flexural yielding. In order to apply the proposed model in the practical design, inelastic deformation capacity was defined according to major design parameters. Design tables and guideline were suggested.

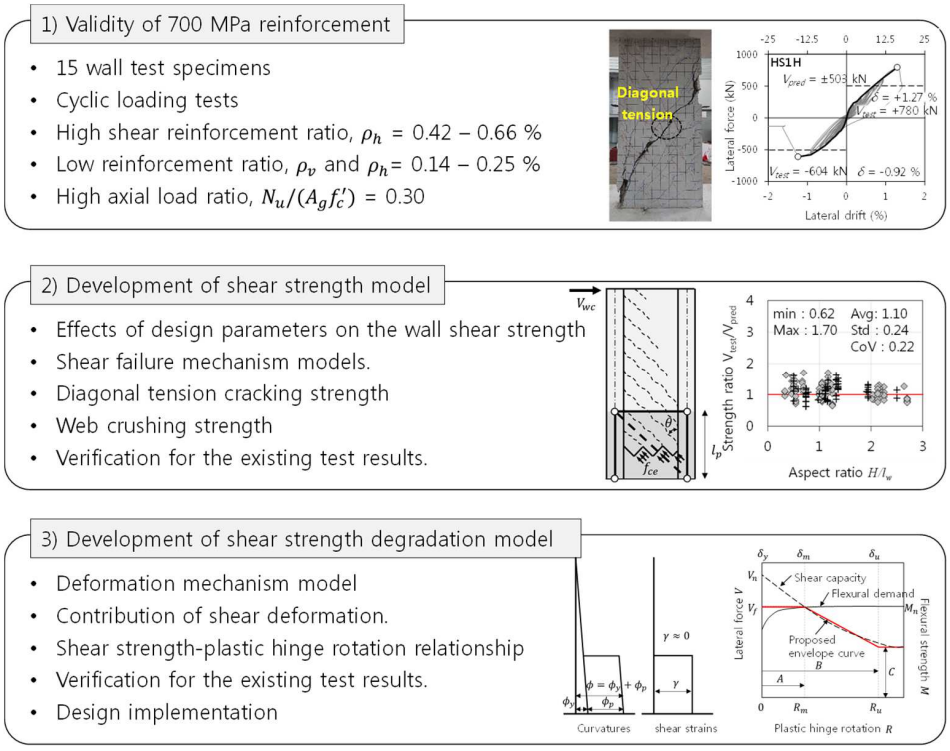

Fig. 1-6 Research scope and objectives

1.3 Outline of dissertation

In Chapter 2, the current design codes and the existing studies were reviewed. Design shear strength and strength-deformation model specified in the current design codes were compared. Existing studies to improve and develop the shear strength and deformation capacity model were investigated. Lastly, the existing theoretical models to predict shear failure mechanism of RC wall were introduced. They were used for the derivation of proposed shear strength and deformation model of this dissertation.

In Chapter 3, experimental tests on RC shear walls with 700 MPa reinforcement were performed. The detail of specimens, test parameters, test setups and instrumentation were reported in detail. For test parameters, yield strength of reinforcement (f_y = 470 – 809 MPa), vertical and horizontal web reinforcement ratio (ρ_v = 0.14 – 1.99 %, and ρ_h = 0.14 – 0.66 %), failure mode (Flexural yielding mode, and shear failure mode), aspect ratio (h_w/l_w = 1.0, and 2.0), and axial load ratio ($N_u/A_g f_c'$ = 0 – 0.30) were considered. The test strengths, failure modes, strain of vertical and horizontal reinforcement, contribution of the deformations, energy dissipations, and drift ductility ratio of the test specimens were evaluated. Based on the test results, the validity of 700 MPa shear reinforcement was evaluated by the current design codes and existing studies.

In Chapter 4, the effect of various design parameters on the shear strength of wall was discussed based on the test results of the present study and existing studies. The major design parameters affecting the shear strength of the walls are the yield strength of reinforcement, the wall aspect ratio, the vertical reinforcement ratio, the axial load ratio, and the shape of the section.

In Chapter 5, the simplified design method was developed to predict the shear strength of RC walls. Based on two shear failure mechanisms of diagonal tension cracking and web crushing, simplified shear strength equations were derived, considering the effects of major design parameters: vertical reinforcement ratio, axial load ratio, and the shape of cross-section (rectangular wall, barbell shaped wall, and flanged wall). The proposed shear strength model was verified by the existing test results.

In Chapter 6, the simplified load-deformation model were proposed to predict the shear strength – deformation relationship of the walls. Based on two shear failure mechanisms, diagonal tension cracking and web crushing, the simplified shear strength – deformation models were derived. For the load-displacement relationship of existing test specimens, the proposed models were compared with the current ASCE 31-17 model.

In Chapter 7, the proposed shear strength degradation model was applied in the Perform 3D. The proposed model was transformed as shear spring model to applicate in the Perform 3D. Design tables including the modeling parameters of shear stress-shear strain relationship of the shear spring model were suggested. A guideline for the modeling of shear wall was suggested. The analysis results of Perform 3D was compared with actual test results.

Finally, summary and conclusions presented in Chapter 8.

Fig. 1-7 shows the hierarchy between chapters.

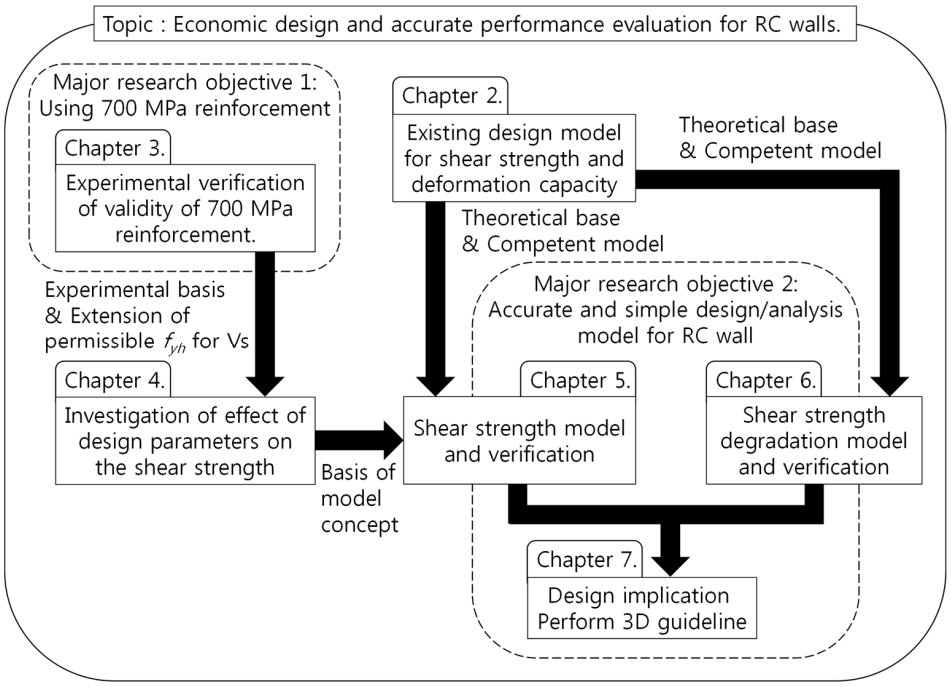

Fig. 1-7 Hierarchy between chapters

Chapter 2. Literature Review

This section provides reviews of current design codes and the literature on experimental studies for RC walls. This section consists of three sections: 1) Section 2.1 summarizes the current design codes; 2) Section 2.2 summarizes the existing model to predict shear strength and deformation capacity of RC walls; and 3) Section 2.4 introduces the existing theoretical models to predict shear failure mechanism of RC wall.

2.1 Current design codes

In this section, the current design codes, which are generally used in the practical design, are summarized. The current design codes provide the design equations for the shear strength and deformation capacity of RC walls.

2.1.1 ACI 318-19 (ACI Committee 318, 2019)

In ACI 318-19, the general provisions for wall shear strength (Section 11.5.4) were revised to be the same as the seismic provisions (Section 18.10.4). The only difference is the permissible yield strength of shear reinforcement: f_y = 420 MPa for ordinary wall, and f_y = 690 MPa for special wall.

$$V_n = \left(\alpha_c\sqrt{f_c'} + \rho_h f_y\right) A_{cv} \leq V_{nmax} = 2/3\sqrt{f_c'}A_{cv} \quad (2\text{-}1)$$

Where, A_{cv} = net shear area in the cross section (mm^2), f_c' = concrete compressive strength (MPa), f_y = yield strength of horizontal reinforcement (MPa), ρ_h = horizontal reinforcement ratio, with α_c = 1/6 for aspect ratio greater than 2.0 (h_w/l_w > 2.0), and

1/4 for aspect ratio less than 1.5 ($h_w/l_w < 1.5$). The maximum shear strength is $V_{nmax} = 2/3\sqrt{f_c'}A_{cv}$.

On the other hand, section 22.5 of ACI 318-19 specifies the one-way shear strength of RC members. The nominal shear strength is defined as the sum of the contributions of concrete and shear reinforcement ($V_n = V_c + V_s$). The concrete shear strength is defined as a function of the longitudinal rebar ratio, concrete strength, and axial load.

When $\rho_t \geq \rho_{t,min}$

$$V_c = \left(0.17\sqrt{f_c'} + \frac{N_u}{6A_g}\right) b_w d \text{ or } \left(0.66\rho_w^{1/3}\sqrt{f_c'} + \frac{N_u}{6A_g}\right) b_w d \quad \text{(2-2a)}$$

When $\rho_t < \rho_{t,min}$

$$V_c = \left(0.66\rho_w^{1/3}\lambda_s\sqrt{f_c'} + \frac{N_u}{6A_g}\right) b_w d \quad \text{(2-2b)}$$

Where, N_u = axial force, A_g = gross area of cross section, b_w = width of cross-section (= t_w), d = depth of cross section (=0.8l_w), ρ_t and $\rho_{t,min}$ = transverse reinforcement ratio and minimum transverse reinforcement ratio, respectively, and ρ_w = longitudinal reinforcement ratio ($\rho_w = A_s/(b_w d)$).

The contribution of shear reinforcement is defined as follows:

$$V_s = A_{st} f_y d/s \quad \text{(2-3)}$$

Where, s = the spacing of transverse reinforcement, and A_{st} = the area of transverse reinforcement within spacing s.

2.1.2 Eurocode 2 and 8 (British Standards Institution, 2004)

In Eurocode 2, a variable angle truss model approach is used for shear design. For a member not requiring the shear reinforcement, contribution of concrete to shear strength is as follows:

$$V_{Rd,c} = \left[C_{Rd,c}k(100\rho_l f_c')^{1/3} + k_1\sigma_{cp}\right]t_w d \quad (2\text{-}4)$$

Where $k = 1+\sqrt{(200/d)} \leq 2.0$, $\rho_l = A_{sl}/(t_w d) \leq 0.02$, A_{sl} = the area of the tensile reinforcement, $\sigma_{cp} = N_u/A_{cv} < 0.2f_{cd}$ (MPa), A_{cv} = the area of concrete cross section (mm^2). The values of $C_{Rd,c}$ and k_1 for use in a Country may be found in its National Annex.

On the other hand, for a member requiring the shear reinforcement, contribution of concrete to shear strength is neglected and only the shear resistance of shear reinforcement is considered.

$$V_{Rd,s} = \frac{A_{vh}}{s_h} z f_{ywd} \cot\theta \quad (2\text{-}5)$$

Where, z = inner lever arm corresponding to the flexural moment (mm) (approximately $z = 0.9d$), f_{vwd} = design yield strength of shear reinforcement (MPa), θ = angle of shear crack (rad).

In Eurocode 8, which is seismic design code, when the shear span ratio is greater than 2.0 ($a = M_u/(V_u l_w) \geq 2.0$), the provisions of Eurocode 2 shall be used with the limitation of $z = 0.8 l_w$, $\theta = 45°$. On the other hand, if $a < 2.0$, following equation is used:

$$V_{Rd} = V_{Rd,c} + 0.75 \alpha_s \rho_h f_{ywd} t_w l_w \tag{2-6}$$

The permissible yield strength of the shear reinforcement is 600 MPa.

The maximum shear strength is calculated as follows:

$$V_{Rd,max} = \alpha_{cw} v_1 f_c' h_w z / (\tan\theta + \cot\theta) \tag{2-7}$$

Where, h_w = the thickness of the wall, z = the inner lever arm corresponding to the bending moment, θ = the crack angle between the concrete compression strut and the member axis perpendicular to the shear force, α_{cw} = a coefficient addressing the state of the stress in the compression chord, and v_1 = a strength reduction factor for concrete cracked in shear. The values of α_{cw} and v_1 for use in a specific country may be found in its National Annex. The recommended values of α_{cw} and v_1 are as follows:

$$\alpha_{cw} = \begin{bmatrix} 1 \\ 1 + \sigma_{cp} / f_{cd} \\ 1.25 \\ 2.5\left(1 - \sigma_{cp} / f_{cd}\right) \end{bmatrix} \begin{pmatrix} \text{for non-prestressed structures} \\ \text{for } 0 < \sigma_{cp} \leq 0.25 f_{cd} \\ \text{for } 0.25 f_{cd} < \sigma_{cp} \leq 0.5 f_{cd} \\ \text{for } 0.5 f_{cd} < \sigma_{cp} < 1.0 f_{cd} \end{pmatrix} \tag{2-8a}$$

$$v_1 = \begin{bmatrix} 0.6 \\ 0.9 - f_{ck} / 200 \end{bmatrix} \begin{pmatrix} \text{for } f_{ck} \leq 60 \text{ MPa} \\ \text{for } f_{ck} \geq 60 \text{ MPa} \end{pmatrix} \tag{2-8b}$$

2.1.3 KDS 14 20 22 (Korean Concrete Institute, 2020)

In KDS 14 20 22, the shear strength equations are similar to those of the previous version of ACI 318 (ACI 318-19 14, 2014).

Section 4.2 specifies the one-way shear strength of RC member. The concrete shear strength in a member subjected to shear force and flexural moment only shall be calculated as follows:

$$V_c = \frac{1}{6}\sqrt{f_c'}\,b_w d \tag{2-9}$$

Where, f_c' = concrete compressive strength (MPa), b_w = width of cross-section, and d = depth of cross section.

The concrete shear strength in a member subjected to axial force shall be permitted to be calculated as follows:

$$V_c = \frac{1}{6}\left(1 + \frac{N_u}{14A_g}\right)\sqrt{f_c'}\,b_w d \tag{2-10}$$

Where, N_u = axial force (positive value, N), and A_g = gross area of cross section (mm^2).

The concrete shear strength V_c shall be permitted to be calculated with more detailed methods provided in following equations:

$$V_c = \left(0.16\sqrt{f_c'} + 17.6\rho_w \frac{V_u d}{M_u}\right) b_w d \tag{2-11}$$

Where, ρ_w = flexural reinforcement ratio (=A_s/($b_w d$), where A_s = area of flexural

reinforcement (mm^2)), V_u = factored shear force, and M_u = factored flexural moment simultaneously occurring with V_u.

However, V_c defined by Eq. (2-11) shall not exceed $0.29\sqrt{f_c'}b_w d$, and $V_u d/M_u$ in Eq. (2-11) shall not exceed 1.0.

For a member subjected to axial compression, M_u in Eq. (2-11) is permitted to be replaced with M_m in order to calculate V_c, where $V_u d/M_u$ is not limited to 1.0.

$$M_m = M_u - N_u \frac{(4h - d)}{8} \tag{2-12}$$

Where, h = entire depth of the member (= l_w, length of the wall).

However, V_c defined by Eq. (2-12) shall not be exceed following:

$$V_c = 0.29\sqrt{f_c'}b_w d\sqrt{1 + \frac{N_u}{3.5A_g}} \tag{2-13}$$

The contribution of shear reinforcement is defined as follows:

$$V_s = A_{st} f_y d/s \tag{2-14}$$

Where, s = the spacing of transverse reinforcement, and A_{st} = the area of transverse reinforcement within spacing s.

On the other hand, in section 4.9.2, the shear strength of wall is provided. The concrete shear strength V_c is calculated as the lesser of the values computed from following equations:

$$V_c = 0.28\sqrt{f_c'}t_w d + \frac{N_u d}{4l_w} \quad \text{(2-15a)}$$

$$V_c = \left[0.05\sqrt{f_c'} + \frac{l_w\left(0.1\sqrt{f_c'} + 0.2\frac{N_u}{4l_w t_w}\right)}{\frac{M_u}{V_u} - \frac{l_w}{2}}\right] t_w d \quad \text{(2-15b)}$$

When ($M_u/V_u - l_w/2$) is negative, Eq. (2-15b) shall not be used.

The maximum shear strength is $V_{nmax} = 5/6\sqrt{f_c'}t_w d$.

2.1.4 ASCE/SEI 41-17 (American Society of Civil Engineers, 2017)

ASCE 41-17, a design guideline for the performance based design (PBD), a multi-linear envelope curve model is used to define the lateral load-displacement relationship of RC wall. Fig. 2-1 shows the load-displacement model of ASCE 41-17. The wall is classified by the governing failure mode, flexural yielding or post-yielding shear failure.

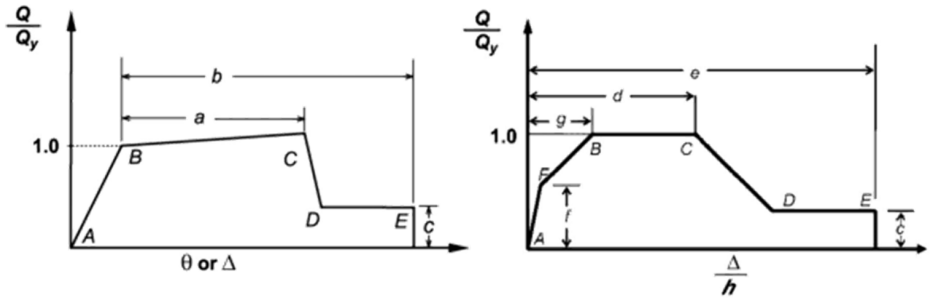

(a) Load-displacement relationship of flexural controlled wall

(b) Load-displacement relationship of shear controlled wall

Fig. 2-1 Generalized load-deformation relationship of wall (ASCE 41-17)

Table 2-1 shows the values of modeling parameters of wall controlled by flexure. In the case of wall with flexural yielding, the envelope curve model is defined by three modeling parameters: 1) a plastic hinge rotation at the peak strength ("*a*" in ASCE 41-17), 2) a plastic hinge rotation at the ultimate state ("*b*" in ASCE 41-17), and 3) a residual strength ratio ("*c*" in ASCE 41-17). These modeling parameters are affected by axial load, shear force demand, and boundary confinement. The peak strength is defined by nominal flexural strength.

Table 2-2 shows the values of modeling parameters of wall controlled by shear. In the case of wall with shear failure after yielding, the envelope curve model is defined by five modeling parameters: 1) a lateral drift ratio (story drift) at the peak

strength "*d*", 2) a lateral drift ratio at the ultimate state "*e*", 3) a lateral drift ratio at the cracking "*g*", 4) a residual strength ratio "*c*", and 5) an elastic strength to peak strength ratio "*f*". These modeling parameters are only affected by axial load. Further, when the axial load ratio is greater than 0.15, the wall should be treated as a force-controlled component. The peak shear strength of a wall is defined according to ACI 318 code.

FEMA 273, and FEMA 356, which are design guidelines for PBD, share the same provisions of ASCE 41-17.

Table 2-1 Modeling parameters of reinforced concrete wall controlled by flexure (ASCE 41-17)

Conditions			Plastic rotation		Residual strength
$\frac{(A_s - A_s')f_y + P}{t_w l_w f_c'}$	$\frac{V}{t_w l_w \sqrt{f_c'}}$	Confined boundary	*a*	*b*	*c*
≤ 0.1	≤ 4	Yes	0.015	0.020	0.75
≤ 0.1	≥ 6	Yes	0.010	0.015	0.40
≥ 0.25	≤ 4	Yes	0.009	0.012	0.60
≥ 0.25	≥ 6	Yes	0.005	0.010	0.30
≤ 0.1	≤ 4	No	0.008	0.015	0.60
≤ 0.1	≥ 6	No	0.006	0.010	0.30
≥ 0.25	≤ 4	No	0.003	0.005	0.25
≥ 0.25	≥ 6	No	0.002	0.004	0.20

Table 2-2 Modeling parameters of reinforced concrete wall controlled by shear (ASCE 41-17)

Conditions	Total drift ratio (%)			Residual strength	
$\frac{(A_s - A_s')f_y + P}{t_w l_w f_c'}$	*d*	*e*	*g*	*c*	*f*
≤ 0.05	1.0	2.0	0.4	0.2	0.6
> 0.05	0.75	1.0	0.4	0.0	0.6

2.1.5 Design guideline for performance based design of RC structure (Architectural Institute of Korea, 2020)

In Korea, the bearing wall structure is majority of the residential building. For economic design, the performance based seismic design is frequently used for design of the buildings. Therefore, Architectural Institute of Korea has developed "Design guideline for performance based design of RC structures" in order to help practical engineers understand and apply the PBD.

In recent revision of this design guideline (2020), the modeling methods for RC beam, column, and beam column joint are revised. In particular, the one-way shear strength of RC beam is provided based on the study of Choi et al. as follows:

$$V_c = k_s f_t b_w c_s \cot\theta \tag{2-16}$$

where,

$$k_s = \left(\frac{0.3}{d}\right)^{0.25} \leq 1.1 \tag{2-17a}$$

$$f_t = 0.2\sqrt{f_c'} \tag{2-17b}$$

$$c = \left(-\rho n + \sqrt{(\rho n)^2 + 2\rho n}\right) d \tag{2-17c}$$

$$\cot\theta = \sqrt{1 + \overline{\sigma_{ct}}/f_t} \tag{2-17d}$$

$$\overline{\sigma_{ct}} = \frac{M_u}{b_w c_s j d} \tag{2-17e}$$

where, k_s = size effect factor, f_t = concrete tensile strength developed in the diagonal tension crack, θ = crack angle of diagonal tension crack, b_w = breadth of the member, c = compression zone depth, ρ = flexural reinforcement ratio, n = elastic modulus ratio of steel and concrete, d = depth of the member, σ_{ct} = average compressive stress of the compression zone, M_u = required flexural moment, and jd

= inner lever arm corresponding to the flexural moment.

In the present study, the theoretical base used in derivation of Eq. (2-16) is applied. Using the compression zone failure mechanism, the diagonal tension strength of RC wall is defined. Detailed process of derivation is introduced in Chapter 5.

On the other hand, the guideline provides the numerical modeling method to predict the load-displacement relationship of RC wall. In the modeling of wall, fiber model method is basically used. The shear behavior of wall is classified to flexural control or shear control. In the case of flexural control wall, the wall is considered as force controlled member. Thus, the shear behavior is modeled as a linear elastic behavior. In the case of shear control wall, the nonlinear ductile shear model can be applied only with axial load ratio less than 0.15. The modeling parameters of envelope curve model are the same those provided in ASCE 41-17.

2.2 Existing model for shear strength and deformation capacity of RC shear walls

In this section, the existing models, which predict the shear strength and deformation capacity of RC wall, are summarized. The existing models are developed based on the wall test results.

2.2.1 Cardenas et al. (1973)

Cardenas et al. summarized the background material for special provisions for walls of ACI 318-71. Prior to the publication of ACI 318-71, the provisions for wall was relatively little.

In their study, the shear strength prediction was derived according to two types of inclined cracking: 1) web-shear cracking, and 2) flexural-shear cracking.

The web-shear cracking is expected in a shear wall when the principal tensile stress exceeds the tensile strength of concrete. In an un-cracked rectangular wall, assuming that the concrete tensile strength is $0.33\sqrt{f_c'}$ ($4\sqrt{f_c'}$ in USC unit), the shear stress of section subjected to combined axial load was derived by using Mohr's circle.

$$v_c = 0.28\sqrt{f_c'} + \frac{N_u}{4l_w t_w} \quad (2\text{-}18)$$

Where, l_w = length of the wall, t_w = thickness of the wall, and N_u = applied axial force.

The flexural-shear cracking occurs when a flexural crack turns and becomes inclined in the direction of increasing moment. The flexural-shear capacity was

derived, assuming that the flexural tensile stress of $0.5\sqrt{f_c'}$ at a section located a distance $l_w/2$ above the section was produced by shear force.

$$v_c = 0.05\sqrt{f_c'} + \frac{l_w\left(0.1\sqrt{f_c'} + 0.2\frac{N_u}{4l_w t_w}\right)}{\frac{M_u}{V_u} - \frac{l_w}{2}} \tag{2-19}$$

Where, M_u = applied flexural moment, and V_u = applied shear force.

The design provisions in Eqs. (2-18) and (2-19) were compared with experimental results. The model safely predicts the existing test results. Eqs. (2-18) and (2-19) were applied to ACI 318-71, and they have been used until revised in ACI 318-19.

2.2.2 Barda et al. (1977)

Results of eight test specimens with low aspect ratio were reported and analyzed. The following range of design parameters were addressed: aspect ratio of wall a = 0.25 – 1.0, vertical and horizontal web reinforcement ratio ρ_v and ρ_h = 0 – 0.5 %, vertical boundary reinforcement ratio ρ_{be} = 1.8 – 6.4 %, and yield strength of reinforcement f_y = 413 – 551 MPa.

The test results showed that as the aspect ratio decreased, the contribution of horizontal reinforcement to shear strength decreased, while the contribution of vertical reinforcement to shear strength increased. Nevertheless, the horizontal web reinforcement contributed to control the number of cracks and crack width. Based on this result, they suggested that the minimum reinforcement should be provided in the walls.

The peak shear strength was affected by the aspect ratio. In the specimens with aspect ratio of 1.0, the peak shear strength 20 % less than that of specimens with lower aspect ratio. Further, shear strength of flanged walls was greater than that of rectangular walls.

Based on the test results, Barda et al. proposed the shear strength equation for low-rise walls with boundary elements as follows:

$$V_c = \left(0.67\sqrt{f_c'} - 0.208a\sqrt{f_c'} + \frac{N_u}{4l_w t_w}\right) A_{cv} \qquad (2\text{-}20)$$

Where, a = aspect ratio, N_u = applied axial force, l_w = length of wall, t_w = thickness of web, and A_{cv} = shear resisting area. The concrete shear strength in Eq. (2-20) is included in the shear prediction by ASCE 43-05, which is a design standard for nuclear power plants.

2.2.3 Duffey et al. (1994)

Duffey et al. (1994) investigated the displacement capacity of shear wall with low aspect ratio. For the 50 existing studies, the drift data were screened. For the typical load-displacement curve, the drift limits at ultimate load and beyond (at 90, 80, 70, 60, and 50 percent of ultimate load) were determined and their statistical properties were examined.

They found that the lateral drift was lognormally distributed (see Fig. 2-2). For the squat walls with aspect ratio ≤ 1.0, the average of drift capacity at ultimate load was 0.80 %, and the average of drift capacity at the failure, where the load dropped 50 % of peak strength, was 1.81 %.

The drift ratios in this model consists of the flexural and shear deformation, $\delta = \delta_f + \delta_s$.

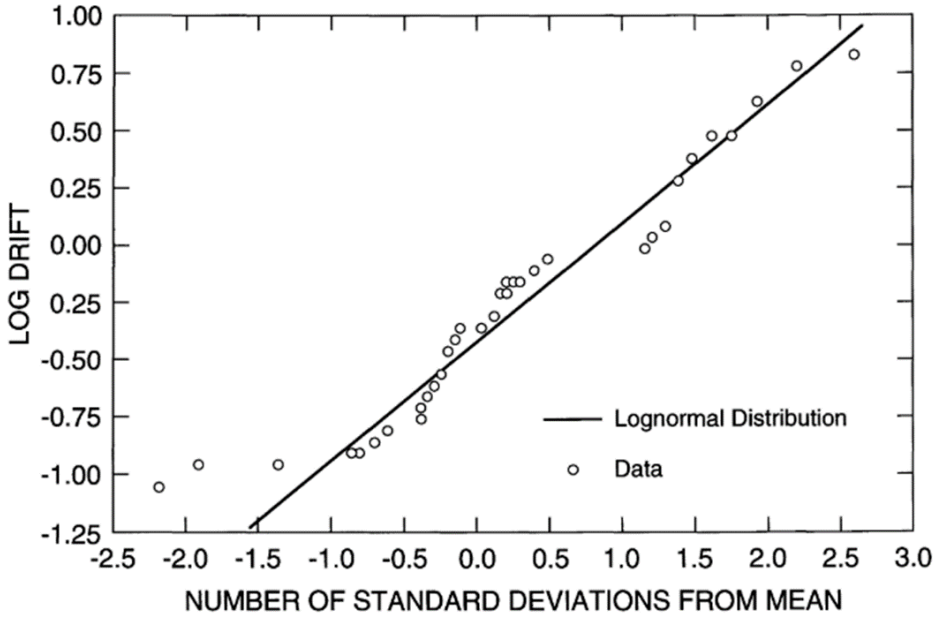

Fig. 2-2 Log frequency plot of existing test results (Duffey et al., 1994)

2.2.4 Hidalgo and Jordan (1996)

Hidalgo and Jordan developed a load-displacement envelope curve model based on the observations of the shear wall tests. The wall tests addressed the following range of the design parameters: aspect ratio a (= M/Vl_w) = 0.35 – 1.0, horizontal reinforcement ratio ρ_h = 0.125 – 0.381 %, and vertical reinforcement ratio ρ_v = 0.125 – 0.259 %.

Fig. 2-3 shows the envelope curve model of Hidalgo and Jordan. The envelope curve model was defined by three points: 1) drift at cracking, 2) drift at peak strength, and 3) ultimate drift at residual strength. The peak shear strength of the envelope curve was defined by using the shear strength equation specified in ACI 318. The cracking strength V_{cr} was defined as the concrete shear strength V_c, estimated by ACI 318. The ultimate drift ratio was defined as a drift when the load dropped 80 % of peak strength.

From the linear regression of the experimental results, the drift ratio at cracking δ_{cr}, the drift ratio at the peak strength δ_m, and the ultimate drift ratio δ_u were proposed as follows:

$$\delta_{cr} = 0.0019a \tag{2-21a}$$

$$\delta_m = 0.00185 + 0.0045a \tag{2-21b}$$

$$\delta_u = 0.016a \tag{2-21c}$$

Where, a = aspect ratio of the wall.

As shown in Eq. (2-21a), the drift ratios were only affected by the aspect ratio. The drift ratios in this model included the flexural and shear deformation, $\delta = \delta_f + \delta_s$.

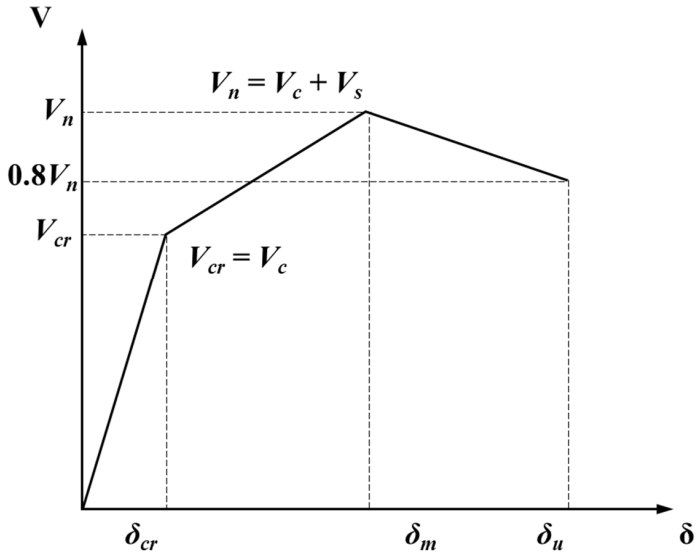

Fig. 2-3 Load-displacement envelope curve model (Hidalgo and Jordan, 1996)

2.2.5 Carrillo and Alcocer (2012)

In several Latin American countries, the walls of low-rise economic housing are typically thin, and they have web reinforcement ratios that are less than the minimum ratio specified in the design codes. Carrillo and Alcocer (2012) investigated the structural performance of such lightly reinforced low-rise walls.

They conducted several experimental studies. The total number of specimens was 39, addressing the following design parameters: type of concrete (normal weight, light weight, and self-consolidating); type of reinforcement (deformed bar, and welded-wire); yield strength of reinforcement (f_y = 447 and 605 MPa); vertical and horizontal web reinforcement ratio ($\rho_v = \rho_h$ = 0 – 0.28 %); wall aspect ratio (a = 0.45 – 1.99); and type of loading (monotonic loading, reversed-cyclic loading, and dynamic shaking table loading).

Because of low aspect ratio, the test specimens were controlled by shear deformations. The major shear failure modes observed in the tests were as follows: 1) a diagonal tension failure (DT), where most of the web shear reinforcement yielded but there was no crushing of the web concrete; 2) a diagonal compression failure (DC), where some of the reinforcement yielded and noticeable concrete spalling and crushing occurred in the web; and 3) a mixed failure mode (DT + DC).

Based on the test results, they developed the shear strength and deformation capacity model. The shear strength of wall was defined as follows:

$$V_n = V_c + V_s = \left[\alpha_1\sqrt{f_c'} + \eta_h\rho_h f_{yh}\right] A_{cv} \leq \alpha_2\sqrt{f_c'}A_{cv} \tag{2-22}$$

where,

$$\alpha_1 = 0.21 - 0.02a \tag{2-23a}$$

$$\alpha_2 = 0.40 \tag{2-23b}$$

where, α_1, and α_2 = coefficients defining the relative contribution of the concrete to diagonal tension and diagonal compression strength, respectively, ρ_h = shear reinforcement ratio, f_c' = concrete compressive strength, f_{yh} = yield strength of shear reinforcement, a = aspect ratio of the wall, A_{cv} = gross area resisting shear (=$l_w t_w$, where l_w = length of the wall, and t_w = thickness of the wall), and η_h = efficiency of shear reinforcement (η_h = 0.8 for deformed bar).

Fig. 2-4 shows the load-displacement envelope model of Carrillo and Alcocer (2012). The concept of model was the same the model of Hialgo and Jordan (1996). However, the definition of shear strength and deformation was different. In this model, the cracking shear strength was defined as follows:

$$V_{cr} = V_c = \alpha_1 \sqrt{f_c'} A_{cv} \tag{2-24}$$

The lateral drift ratio at the cracking load δ_{cr} was calculated, assuming the linear elastic relationship with effective lateral stiffness.

$$\delta_{cr} = \frac{V_{cr}}{K_{cr} H} \tag{2-25}$$

where,

$$K_{cr} = \frac{0.5}{\frac{H^3}{3E_c I_g} + \frac{H}{G_c A_c}} \tag{2-26}$$

Where, K_{cr} = effective lateral stiffness including flexural and shear stiffness, H = height of the wall, E_c = elastic modulus of concrete, G_c = shear modulus of concrete, I_g = moment of inertia, and A_c = area of concrete.

In Eq. (2-26), the effective stiffness was assumed as 50 % of the initial stiffness.

The lateral drift ratio at the peak strength δ_m and the ultimate lateral drift ratio δ_u were derived from observed trends and nonlinear regression analysis:

$$\delta_m = \frac{V_n}{t_w\sqrt{f_c'}}\frac{e^{1.3a}}{5.2\times10^4} \quad \text{(2-27a)}$$

$$\delta_u = \frac{V_n}{t_w\sqrt{f_c'}}\frac{e^{1.35a}}{3.65\times10^4} \quad \text{(2-27b)}$$

The residual strength at the ultimate deformation was defined as 80 percent of the peak shear strength, $0.8V_n$.

The drift ratios in this model defined as sum of the flexural and shear deformation, $\delta = \delta_f + \delta_s$.

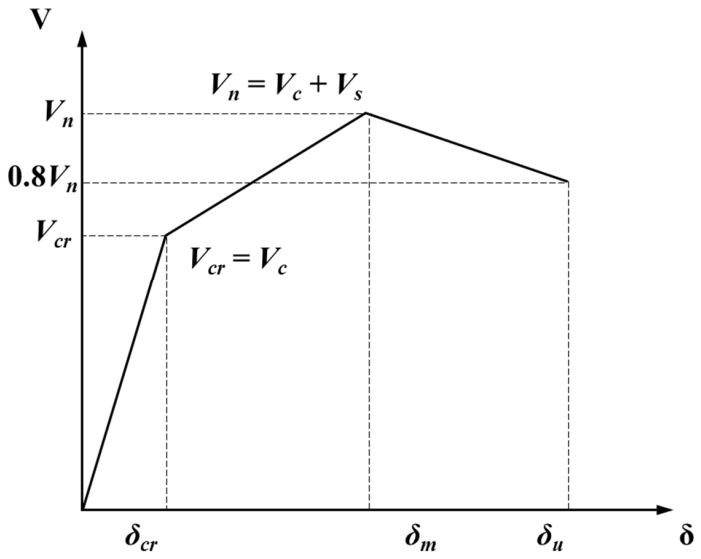

Fig. 2-4 Load-displacement envelope curve model (Carrillo and Alcocer, 2012)

2.2.6 Sanchez (2013)

Sanchez (2013) proposed a shear strength model and calibrated it with the experimental tests. The model assumed that shear strength is the sum of contributions of concrete and shear reinforcement. The model was developed by a simplified strut-and-tie model which was dependent upon the maximum inclined crack width.

The shear strength was defined as a function of the aspect ratio, vertical load, and the vertical and horizontal reinforcement ratio:

$$V_n = V_c + V_s = \left[(\gamma\eta_v + 0.04N_u/A_{cv})\sqrt{f_c'} + \eta_h\rho_h f_{yh}\right] A_{cv} \quad (2\text{-}28)$$

where,

$$\gamma = 0.42 - 0.08a \quad (2\text{-}29a)$$

$$\eta_v = 0.75 + 0.05\rho_v f_{yv} \quad (2\text{-}29b)$$

$$\eta_h = 1 - 0.16\rho_h f_{yh} \quad (2\text{-}29c)$$

Where, N_u = applied axial load, ρ_v and ρ_h = vertical and horizontal web reinforcement ratios, respectively, f_{yv} and f_{yh} = yield strengths of vertical and horizontal reinforcement, η_v and η_h = efficiency of vertical and horizontal reinforcement, respectively, and A_{cv} = gross area of concrete,

In code equations, a typical assumption is that web reinforcement yields at wall strength. In the model proposed herein, the extent of plasticity is accounted for through an efficiency factor. For the horizontal web reinforcement, efficiency diminishes with the percentage of horizontal web reinforcement and the drift demand on the wall. Efficiency factor η_h approximates 1.0 for horizontal reinforcement similar to the code minimum ($\rho_h f_{yh} \approx 1.0$ MPa), and linearly reduces to 0.20 for high reinforcement ratio ($\rho_h f_{yh} \approx 5.0$ MPa).

Further, Sanchez (2013) proposed the load-displacement envelope model. The model is similar to the models of Hidalgo and Jordan (1996), and Carrillo and Alcocer (2012), but differs that the flexural cracking in the elastic behavior was addressed. Fig. 2-5 shows the lateral load-displacement envelope model of Sanchez (2013).

Based on the test results, the lateral drift ratio at flexural cracking $\delta_{cr,f}$ and the lateral drift ratio at diagonal cracking δ_{cr} were defined as functions of aspect ratio:

$$\delta_{cr,f} = 0.0001 + 0.00005a \tag{2-30a}$$

$$\delta_{cr} = 0.00025 + 0.0013a \tag{2-30b}$$

The lateral loads corresponding to $\delta_{cr,f}$ and δ_{cr} were defined as follows:

$$V_{cr,f} = K_i \delta_{cr,f} H \tag{2-31a}$$

$$V_{cr} = (0.32 - 0.045a)\sqrt{f_c'} A_{cv} \tag{2-31b}$$

Where, H = height of the wall, K_i = initial lateral stiffness (= $H^3/(3E_cI_g)$, where, E_c = elastic modulus of concrete, and I_g = moment of inertia of gross section), and A_{cv} = gross area of concrete.

The lateral drift ratio at the peak strength δ_m was defined as the sum of flexural deformation and shear deformation:

$$\delta_m = \delta_f + \delta_s = \frac{V_n H^2}{3E_c I_g} + \frac{1}{3}\frac{V_n}{A_{cv}\sqrt{f_c'}}\frac{l_w}{H} e^{1.33a} \tag{2-32}$$

Where, V_n = shear strength calculated by (2-28), and l_w = length of the wall.

The ultimate lateral drift ratio δ_u was calculated from the lateral drift ratio at the peak strength δ_m.

$$\delta_u = \left(\delta_m + \frac{9}{\rho_h f_{yh} H}\right)(0.6a + 0.5) \geq 1.2\delta_m \tag{2-33}$$

Where, ρ_h = shear reinforcement ratio, and fyh = yield strength of shear reinforcement.

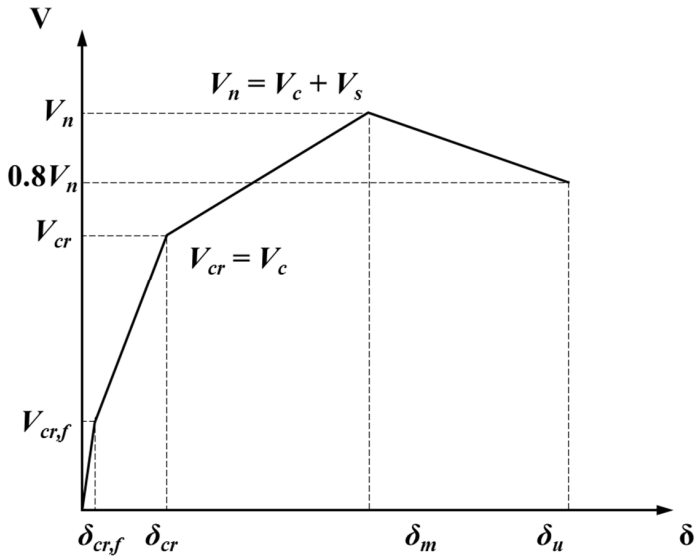

Fig. 2-5 Load-displacement envelope curve model (Sanchez, 2013)

2.2.7 Carlos (2016)

Carlos (2016) developed a shear strength and deformation prediction model based on the existing wall test. He constructed a wall test database, which included 207 wall test results. Only walls with symmetric cross sectional shapes were considered for this database. From them, 70 specimens had rectangular cross section, whereas 137 specimens had enlarged boundary elements. The group of walls with boundary elements consisted of 56 wall specimens with flanges (simulating intersecting walls) and 81 wall specimens with boundary columns (barbell shaped cross section).

Based on this database, a statistical approach was used to develop and calibrate the shear strength prediction model. From the multi-variable regression analysis, the shear strength of wall was defined as follows:

For rectangular wall

$$V_n = \begin{pmatrix} 0.35 + 0.068f_c' - 0.080f_c'a + 0.41\dfrac{N_u}{A_g} \ldots \\ +0.47\rho_{se}f_{yse} + 0.39\rho_{be}f_{ybe} \end{pmatrix} A_{cv} \qquad (2\text{-}34a)$$

For barbell-shaped or flanged wall

$$V_n = \begin{pmatrix} 0.54 + 0.19f_c' - 0.17a + 0.45\dfrac{N_u}{A_g} \ldots \\ +0.39\rho_{se}f_{yse} + 0.31\rho_{be}f_{ybe} \end{pmatrix} A_{cv} \qquad (2\text{-}34b)$$

where,

$$\rho_{se} = \xi\rho_v + (1-\xi)\rho_h \qquad (2\text{-}35a)$$

$$f_{yse} = \xi f_{yv} + (1-\xi)f_{yh} \qquad (2\text{-}35b)$$

$$\xi = 1.5 - a, 0 \le \xi \le 1.0 \qquad (2\text{-}35c)$$

where, a = wall aspect ratio, N_u = applied axial force, A_g = total cross sectional area, A_{cv} = shear resisting area (= $l_w t_w$), ρ_{se} = effective steel ratio, ρ_v = vertical

reinforcement ratio, ρ_{be} = vertical boundary reinforcement ratio, ρ_h = shear reinforcement ratio, f_{yse} = effective yield strength of reinforcement, f_{yv} = yield strength of vertical reinforcement, f_{ybe} = yield strength of vertical boundary reinforcement, f_{yh} = yield strength of shear reinforcement,

Further, Carlos proposed the load-displacement model, which is similar to the model of Carrillo and Alcocer. The lateral drift ratio at cracking δ_{cr}, lateral drift ratio at the peak strength δ_m, and ultimate lateral drift ratio δ_u were defined as follows:

For rectangular walls

$$\delta_{cr} = \left(0.06 + 12.4\rho_{be} + 9.3\rho_h + \frac{0.0024 l_w}{t_w}\right) \times 10^{-2} \quad \text{(2-36a)}$$

$$\delta_m = \left(0.94 - 0.0006 f_{yh} + 0.0063 f_c' - \frac{0.044 s_h}{t_w}\right) \times 10^{-2} \quad \text{(2-36b)}$$

$$\delta_u = \left(1.3 + 30.2\rho_v - \frac{0.46 s_h}{t_w} + \frac{0.42 s_v}{t_w} + \frac{0.1P}{A_g}\right) \times 10^{-2} \geq \delta_m \quad \text{(2-36c)}$$

For barbell-shaped or flanged walls

$$\delta_{cr} = \left(0.08 + 0.12\rho_{be} + 0.041\rho_h - \frac{0.031 s_v}{t_w}\right) \times 10^{-2} \quad \text{(2-36d)}$$

$$\delta_m = \left(0.67 + 0.24a - \frac{0.0077 l_w}{t_w} + 0.006 f_c' - 0.0005 f_{ybe}\right) \times 10^{-2} \quad \text{(2-36e)}$$

$$\delta_u = \mu_u \delta_m \quad \text{(2-36f)}$$

$$\mu_u = 2.39 - 0.001 f_{yh} - 0.164\rho_{be} - 31.3\rho_h - \frac{0.38 s_h}{t_w} + \frac{0.32 s_v}{t_w} \quad \text{(2-36g)}$$

Where, s_h = spacing of vertical reinforcement, and s_v = spacing of shear reinforcement. The lateral drift ratios in Eq. (2-36a) were included both flexural and shear deformations, $\delta = \delta_f + \delta_s$.

2.2.8 Epackachi et al. (2019)

Epackachi et al. (2019) studied to improve the load-deformation model of ASEC 41-17, based on the data from 240 tests of rectangular, barbell, and flanged shear-critical walls. The influence of wall aspect ratio, vertical web reinforcement ratio, and horizontal web reinforcement ratio, vertical reinforcement ratio in the boundary elements, normalized axial compressive load, and concrete uniaxial compressive strength on the deformation capacity of walls were investigated.

The force–displacement relationship reported in the literature for each of the 240 walls was digitized. Reported properties, including dimensions, details of reinforcement, and material properties were investigated. Using an equal-energy dissipation method, the load-displacement envelope curves of test results were idealized as an equivalent multi-linear envelope curve model per ASCE 41-17.

Table 2-3 shows the modeling parameters for the envelope curve model. The modeling parameters were proposed to address the effects of wall aspect ratio, axial load ratio, and shape of cross section. In this model, the peak shear strengths of rectangular walls were calculated by ACI 318-19 (Eq. (2-1)), while the peak shear strengths of barbell-shaped or flanged walls were calculated by strength model of Barda et al. (1977) (Eq. (2-20)).

Table 2-3 Modleing parmeters of reinforced concrete wall controlled by shear

Conditions			Total drift ratio (%)			Residual strength	
Shape	Aspect ratio	Axial load ratio	*d*	*e*	*g*	*c*	*f*
Rectangle	$a < 1$	$0 \le N_u/(A_g f_c') \le 0.2$	1.0	2.1	0.4	0.0	0.5
	$1 \le a \le 2$	$0 \le N_u/(A_g f_c') \le 0.2$	1.0	2.5	0.4	0.0	0.5
Barbell and flanged	$a < 1$	$0 \le N_u/(A_g f_c') < 0.05$	0.7	1.8	0.4	0.0	0.5
		$0.05 \le N_u/(A_g f_c') \le 0.2$	0.7	1.4	0.4	0.0	0.5
	$1 \le a \le 2$	$0 \le N_u/(A_g f_c') < 0.05$	0.9	2.6	0.4	0.0	0.5
		$0.05 \le N_u/(A_g f_c') \le 0.2$	0.9	1.6	0.4	0.0	0.5

2.2.9 Gulec and Whittaker (2011)

Gulec and Whittaker developed empirical equations to predict the shear strength of low-rise walls (aspect ratio ≤ 2.0). The strength equations were developed separately for rectangular cross section, and barbell-shaped or flanged cross section. The shear strength of walls with rectangular cross section was defined as follows:

$$V_n = \frac{0.125f_c'A_{cv} + 0.25F_{vw} + 0.20F_{vbe} + 0.40N_u}{\sqrt{h_w/l_w}} \leq 0.83A_{cv}\sqrt{f_c'} \qquad (2\text{-}37)$$

Where, A_{cv} = the wall area (mm^2), f_c' = the compressive strength of the concrete (MPa), ρ_v and ρ_{be} = the vertical reinforcement ratio in the web and boundary element, respectively, f_{yv} and f_{ybe} = yield strengths of vertical reinforcement in the web and boundary element, respectively (MPa), N_u = the axial force (N), h_w = the wall height, and l_w = the wall length.

For barbell-shaped and flanged wall, the shear strength was defined as follows:

$$V_n = \frac{0.04f_c'A_{eff} + 0.40F_{vw} + 0.15F_{vbe} + 0.35N_u}{\sqrt{h_w/l_w}} \leq 1.25A_t\sqrt{f_c'} \qquad (2\text{-}38)$$

Where, A_{eff} = the total wall area for barbell walls and the effective area for flanged walls (equal to the sum of the areas of the web plus the effective flanges area, where the area of an effective flange is the product of the flange thickness and one-half of the wall height minus the web thickness), A_t = the total gross area of concrete section. Equation (2-38) can be applied to barbell walls and flanged walls with $A_t/A_{cv} \geq 1.25$. For the design of flanged walls with $1.0 \leq A_t/A_{cv} \leq 1.25$, the peak shear strength should be taken as the smaller of the values calculated from Eqs. (2-37) and (2-38).

2.2.10 Zeynep and Cagri (2021)

Zeynep and Cagri developed empirical equations to predict the shear strength of conventional reinforced concrete walls. They focused on the exiting shear walls not including the adequate reinforcement and seismic detailing. They categorized the failure mode of the conventional walls by using the strength index V_n/V_f, where, V_n = nominal shear strength, and V_f = shear force corresponding to nominal flexural strength. Three failure modes were addressed; 1) shear-controlled walls ($V_n/V_f \leq 1$); 2) transition walls ($1 < V_n/V_f < 1.67$); and 3) flexure-controlled walls ($V_n/V_f \geq 1.67$).

The strength equations were developed based on the wall database of 246 test specimens. To develop the strength equation model, multilinear regression analysis was conducted on the training dataset. Different combinations of various key parameters were tried until the best correlation between the proposed equation and the test results were obtained while also being physically meaningful with consistent units. The generic equation for to estimate peak shear stress was suggested as follows:

$$V_n = \left((a)\frac{N_u}{A_{cv}} + (b)\frac{\left(1+\frac{1}{s/d_b}\right)(1+\rho_{be})f_c'\frac{t_w}{l_w}}{M/(Vl_w)} + (c)\rho_h f_{yh} \right) A_{cv} \qquad (2\text{-}39)$$

Where, A_{cv} = gross cross section area of wall, f_c' = concrete compressive strength, f_{yh} = yield strength of shear reinforcement, ρ_h = shear reinforcement ratio, ρ_{be} = vertical boundary reinforcement ratio, t_w = thickness of wall, l_w = length of wall, s/d_b = ratio of transverse boundary reinforcement spacing to longitudinal boundary bar diameter, $M/(Vl_w)$ = shear span ratio, and N_u = axial force.

In Eq.(2-39), the values of (a), (b), and (c) depends on the governing failure mode of walls: 1) 0.067, 0.38, 0.0040 for shear controlled walls; 2) 0.022, 0.33, 0.0042 for transition walls; and 3) 0.039, 0.36, 0.0038 for flexure controlled walls, respectively.

2.3 Shear wall failure mechanism models

The previous section reviewed the existing models for prediction of shear strength and deformation capacity of walls. Most of design models were proposed based on the statistical calibration of the existing test results. Such methodology is effective to develop an optimized model. However, since the model can be validate only for the limited test results, there is a limit to address the various range of design parameters.

The present section reviews the analytic and theoretic models to predict the behavior of shear wall. Fig. 2-6 shows the classification of theoretical models. The present study classified the models in three types: 1) a microscopic model, 2) an intermediate-scopic model, and 3) a macroscopic model. The microscopic model divides the wall in several microscopic segments to calculate the behavior of wall accurately (i.e. finite element model). Compared to the finite element model, the intermediate-scopic model decreases the number of segments, and calculate more efficiently (i.e. fiber model). The macroscopic model defines the overall behavior of wall, such as load-displacement envelope, by one function (i.e. concentrated hinge model). As the number of segments decreases, the accuracy decreases, but the simplicity of model increases.

The present study uses the macroscopic method to develop the simplified strength-deformation model. The strength-deformation capacity of wall is developed based on the shear failure mechanism in the plastic hinge region. Following sections review the existing theories for shear failure mechanism of wall, diagonal tension cracking, and web crushing.

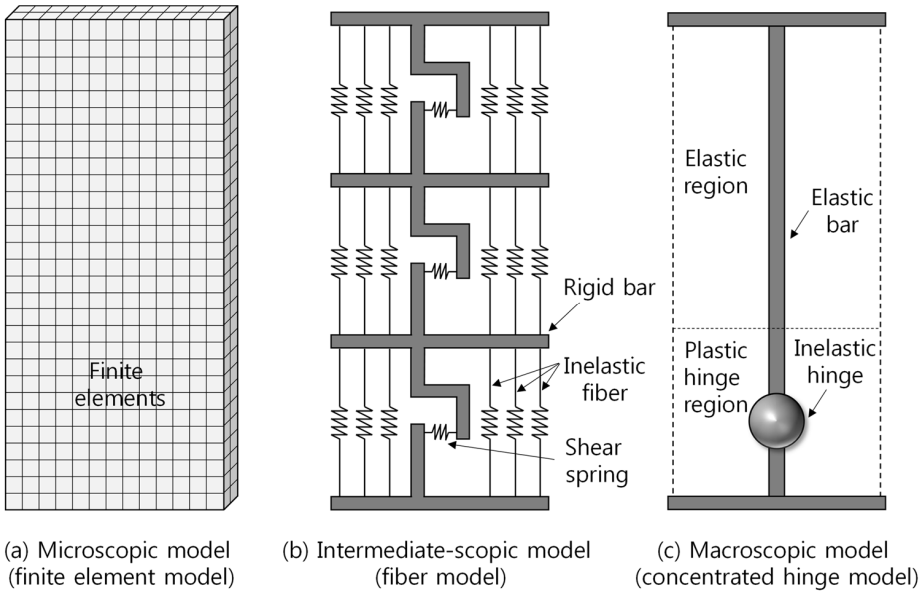

Fig. 2-6 Classification of wall behavior models

2.3.1 Compression zone failure mechanism model (Choi et al., 2007)

Choi et al. (2007) developed a compression zone failure mechanism model to predict the shear strength of RC members. Park and Choi (2017) reported that the compression zone depth can be used to describe the major trend of shear strength; as the flexural reinforcement ratio and axial compression increase, the compression zone depth increases. This trend is the same as that of shear strength. As the concrete strength increases, the compression zone depth does not significantly increase due to the force-equilibrium in the cross section, which is also similar to the trend of shear strength. For this reason, several recent studies have considered the compression zone depth as a major design parameter.

Fig. 2-7 shows the concept of the compression zone failure mechanism model. In this model, applying the Rankine's failure criteria, the shear capacity of a section is calculated at each deformation level. In stage AB which is in elastic state, the entire wall section can resists shear force. However, after flexural cracking (stage BC), only concrete in compression zone depth c is assumed to resist shear, and the concrete shear stress capacity v_c is controlled by tension failure v_{ct}. In stage CD, in the region of the compression zone experiencing compression softening, v_c is controlled by compression failure v_{cc}. Further, after the concrete strain exceeds the crushing strain ε_{co} = 0.002 (stage DE), shear resistance is gradually decreased. The effective compression area is decreased by crushing of the concrete. The shear demand curve is calculated from the flexural moment-curvature relationship of the section. At the intersection of the shear capacity and shear demand curves, the strength and deformation capacity are defined.

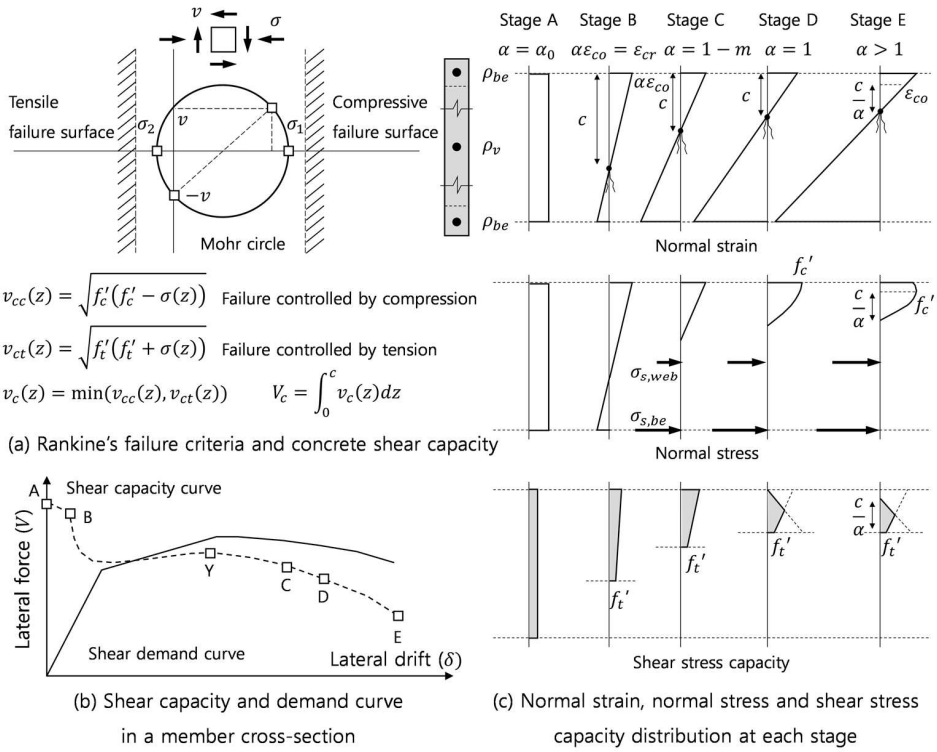

Fig. 2-7 Concept of compression zone failure mechanism model

In the compression zone failure mechanism model, the shear demand and shear capacity are calculated from the nonlinear sectional analysis (i.e. flexural moment−curvature analysis). Baek (2017), and Kim and Park (2021) proposed the simple calculating method for sectional analysis. In this studies, for simple calculations, distributed vertical bars in the boundary element and web were simplified as concentrated steel fibers (see Fig. 2-7 (c)). Using the plane assumption, the strain in a cross section was assumed to be linearly distributed.

Fig. 2-8 shows the stress-strain relationships of concrete and reinforcement. As shown in Fig. 2-8 (a), tor concrete, a parabolic strain−stress relationship was used as follows:

$$\sigma_c(\varepsilon) = f_c' \left[2\left(\frac{\varepsilon}{\varepsilon_{co}}\right) - \left(\frac{\varepsilon}{\varepsilon_{co}}\right)^2 \right] \geq 0 \quad (2\text{-}40)$$

Where $\sigma_c(\varepsilon)$ = concrete stress, ε = concrete strain, f_c' = compressive strength of the concrete, and ε_{co} = concrete strain at compressive strength f_c' (=0.002).

When concrete confinement effect was provided, concrete peak strength f_{cc}', concrete crushing strain ε_{cc}, and post peak behavior were defined according to the Kent and Park (1971) model.

$$\sigma_c(\varepsilon) = f_{cc}' \left[2\left(\frac{\varepsilon}{\varepsilon_{cc}}\right) - \left(\frac{\varepsilon}{\varepsilon_{cc}}\right)^2 \right] \quad (\varepsilon \leq \varepsilon_{1c}) \quad (2\text{-}41a)$$

$$\sigma_c(\varepsilon) = f_{cc}'(1 - Z(\varepsilon - \varepsilon_{cc}) \geq 0.2 f_{cc}' \quad (\varepsilon > \varepsilon_{cc}) \quad (2\text{-}41b)$$

where,

$$f_{cc}' = K f_c' \quad (2\text{-}42a)$$

$$\varepsilon_{cc} = K \varepsilon_{co} \quad (2\text{-}42b)$$

$$K = 1 + \frac{\rho_t f_{yh}}{f_c'} \quad (2\text{-}42c)$$

Where, ρ_t = transverse reinforcement ratio in the boundary element, f_{yh} = yield strength of transverse reinforcement, and Z = slope of the post-peak strain-stress relationship.

For rebars, the simple bilinear strain-stress relationship was used (Fig. 2-8 (b)). The shear demand curve is defined from the moment-curvature relationship calculated from sectional analysis.

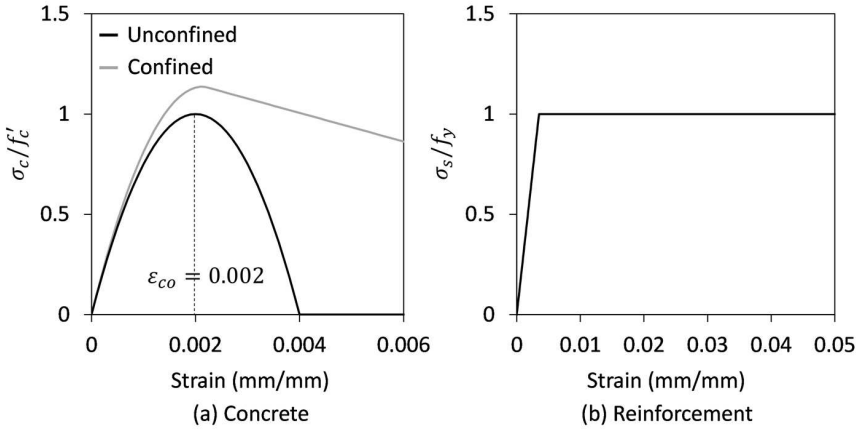

Fig. 2-8 Stress-strain relationships of concrete and rebar

At a location in a concrete cross-section, the shear stress capacity of the concrete subjected to normal stress is derived from the Rankine's failure criteria:

For failure controlled by tension

$$v_{ct}(z) = \sqrt{f_t'\left(f_t' + \sigma(z)\right)} \tag{2-43a}$$

For failure controlled by compression

$$v_{cc}(z) = \sqrt{f_c'\left(f_c' - \sigma(z)\right)} \tag{2-43b}$$

Where, f_t is concrete tensile strength ($f_t = 0.2\sqrt{f_c'}$, Metha and Monteiro, 2014).

The governing shear stress of concrete v_c is determined as the smaller of the two stress capacities in Eq. (2-43a). Before the normal stress of concrete reaches a reference stress $\sigma_{cr} = (f_c' - f_t)$, the shear stress capacity of concrete is controlled by tensile failure. Otherwise, it is controlled by compression failure. At the reference stress σ_{cr}, the strain coefficient is defined as $\alpha = 1 - m$, where $m = \sqrt{(f_t/f_c')}$. From the shear stress capacity v_c, the shear capacity of concrete V_c is calculated.

As shown in Fig. 2-7 (b) and (c), the governing shear stress of concrete v_c varies according to the deformation state. In stage AB (elastic state), concrete shear stress capacity v_c is controlled by tension failure v_{ct}, and the entire wall cross-section can resist shear force.

$$V_c = \int v_c \, dz t_w = \int_{-l_w/2}^{l_w/2} \sqrt{f_t'(f_t' + \sigma(z))} \, dz t_w \tag{2-44}$$

After flexural cracking, only the concrete in the compression zone is assumed to resist shear force (stage BE). Further, after concrete normal stress reaches σ_{cr} ($\alpha > 1 - m$), in the region of the compression zone with normal stress exceeding σ_{cr}, the shear stress capacity of concrete v_c is governed by v_{cc} (stage CE). In stage DE, the compressive strain of extreme fiber exceeds crushing strain ($\alpha\varepsilon_{co} > \varepsilon_{co}$, in that, $\alpha > 1.0$). In this case, the region subjected to concrete crushing cannot resist shear force. Thus, only the region where the normal strain is less than the crushing strain is considered in the calculation of shear capacity. Referring to Park et al. (2012), for indices α, m, and compression depth c, the concrete shear capacity V_c was derived for each deformation state:

$$V_c = \int v_c \, dz t_w = k f_c' t_w \, c/\alpha \tag{2-45}$$

Where, k is calculated at each deformation level as follows:

$$k_{\mathrm{BC}} = \frac{m}{2}\left[\begin{array}{c} m - (1-\alpha)\sqrt{m^2 - (1-\alpha)^2} + \cdots \\ (1+m^2)\left\{\tan^{-1}\left(\frac{1}{m}\right) + \sin^{-1}\left(\frac{\alpha^2 - 1}{\sqrt{1+m^2}}\right)\right\} \end{array}\right] \tag{2-46a}$$

$$k_{\mathrm{CD}} = m(1+m^2)\left(\frac{\pi}{4} - \tan^{-1}(m)\right) + \frac{1}{2}(m^2 - (1-\alpha)^2) \tag{2-46b}$$

$$k_{\mathrm{DE}} = m(1+m^2)\left(\frac{\pi}{4} - \tan^{-1}(m)\right) + \frac{m^2}{2} \tag{2-46c}$$

The contribution of shear reinforcement was defined as follows:

$$V_s = \rho_h f_{yh} A_{cv} \tag{2-47}$$

Where, ρ_h = horizontal bar ratio, f_{yh} = actual yield strength of shear reinforcement, and A_{cv} = net area of the shear section.

The total shear capacity is defined as the sum of the contributions of concrete and shear reinforcement:

$$V_n = V_c + V_s \tag{2-48}$$

From the curvature of the wall bottom, lateral drift of the wall δ was calculated as follows:

$$\delta = \phi(a/3)\mu \quad (\phi \le \phi_y) \tag{2-49a}$$

$$\delta = \phi(a/3)\mu + (\phi - \phi_y) l_p \quad (\phi \le \phi_y) \tag{2-49b}$$

Where, the curvature $\phi = \alpha\varepsilon_{co}/c$, curvature at yielding $\phi_y = \varepsilon_y/(d-c)$, ε_y = yield strain of vertical reinforcement in tension, a = shear span (=M/V), and l_p = plastic hinge length (= $0.5ad/l_w$, $0.75d \le l_p \le d$, Lee and Watanabe (2003)).

To address the effect of bond-slip and shear deformation, μ (= $EI_{flex}/EI_{y,eff}$), which is the ratio of the flexural yield stiffness to the effective yield stiffness was used according to Elwood and Eberhard (2009).

$$\mu = \frac{EI_{flex}}{EI_{y,eff}} = \left(\frac{EI_{flex}}{EI_g}\right) \Big/ \left(\frac{EI_{y,eff}}{EI_g}\right) = \alpha/\beta \tag{2-50a}$$

$$\alpha = \frac{EI_{flex}}{EI_g} \cong \alpha_{approx.} = 0.2 + 1.3\left(\frac{N_u}{A_g E_c \varepsilon_{co}}\right) + \rho n \leq 1.0 \tag{2-50b}$$

$$\beta = \frac{EI_{y,eff}}{EI_g} = \frac{0.45 + 2.5\left(\frac{N_u}{A_g f_c'}\right)}{1 + 110\left(\frac{d_b}{l_w}\right)\left(\frac{l_w}{a}\right)} \leq 1.0 \text{ and } \geq 0.2 \tag{2-50c}$$

where EI_g = gross flexural stiffness, N_u = axial compression force, A_g = the cross-sectional area of the wall, E_c = elastic modulus of concrete, ε_{co} = strain at concrete peat strength (0.002 in the present study), ρ = vertical rebar ratio, n = modulus ratio of rebar to concrete (= E_s/E_c), d_b = nominal diameter of vertical rebars, l_w = wall length, and a = shear span (=M/V).

2.3.2 Truss mechanism model (Eom and Park, 2010)

Eom and Park (2010) developed a truss mechanism model to predict the cyclic behavior of web. In low-rise walls subjected to cyclic lateral loading, longitudinal elongation occurs in the plastic hinge region, as the residual strain of vertical reinforcement is accumulated by the repeated cyclic loading (see Fig. 2-9). The elongation of plastic hinge region accelerates the web crushing failure. Because the elongation increases the principal tensile strain of web concrete, which leads the decrease of the effective compressive strength of diagonal strut.

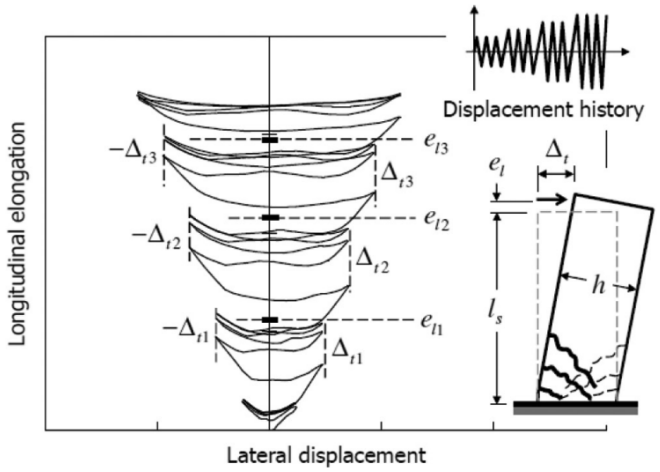

Fig. 2-9 Longitudinal elongation of reinforce concrete wall subjected to lateral cyclic loading (Eom and Park, 2010)

Fig. 2-10 shows the concept of the truss mechanism model. The truss model consists of a diagonal strut D_C and vertical reinforcement elements L_T and L_C. The elongation of the web is defined as the average elongations of the vertical truss elements, L_T and L_C. From this truss model, the elongation was calculated based on the displacement compatibility, force equilibrium, and constitutive rule.

The lateral displacement of wall Δ was defined as follows:

$$\Delta = \Delta_p + \Delta_\theta + \Delta_{ef} \tag{2-51}$$

Where, Δ_p = lateral displacement in the plastic hinge region, Δ_θ = lateral displacement by the rigid body rotation of the elastic region, and Δ_{ef} = lateral displacement in the elastic region.

The compressive strain in the diagonal concrete strut D_C was ignored because the compressive strain was significantly less than the tensile strain, according to test results. Therefore, in truss model, following relationship was defined:

$$-\Delta_p \sin\theta + \varepsilon_{lt} l_p \cos\theta \approx 0 \tag{2-52}$$

Where, ε_{lt} = the strain of vertical element L_T in tension, l_p = the length of the plastic hinge region (assumed as $l_p \approx d$, Lee and Watanabe, (2003)), d = the effective depth, and θ = the angle of diagonal concrete strut D_C

The elongation of the plastic hinge region was defined as the average of vertical elongations of vertical truss elements as follows:

$$e_l = \frac{(\varepsilon_{lt} + \varepsilon_{lc}) l_p}{2} \tag{2-53}$$

Where, ε_{lc} = the strain of vertical element L_C in compression.

From Eqs. (2-52) and (2-53), lateral displacement of plastic hinge region Δ_p was written as follows:

$$\Delta_p = \varepsilon_{lt} l_p \cot\theta = \left(2e_l - \varepsilon_{lc} l_p\right) \frac{l_p}{h_s} \tag{2-54}$$

Where, h_s = the distance between the vertical truss elements, L_T and L_C.

The lateral displacement due to rigid body rotation Δ_θ was defined as follows:

$$\Delta_\theta = \theta_p(H - l_p) = \frac{(\varepsilon_{lt} - \varepsilon_{lc})l_p(H - l_p)}{h_s} = \frac{2(e_l - \varepsilon_{lc}l_p)(H - l_p)}{h_s} \quad (2\text{-}55)$$

Where, H = height of the wall, and θ_p = the plastic hinge rotation.

Inserting Eqs. (2-54) and (2-55) into Eq. (2-51), the elongation e_l was defined as the function of the lateral displacement of wall Δ as follows:

$$e_l = \frac{(\Delta - \Delta_{ef})h_s}{2H} + \varepsilon_{lc}l_p\left(1 - \frac{l_p}{2H}\right) \quad (2\text{-}56)$$

The flexural displacement was calculated as $\Delta_{ef} = \phi_y(H - l_p)^2/3$.

Fig. 2-10 (a), shows the internal forces in the plastic hinge region. Force equilibriums in the plastic hinge region were as follows:

For lateral force equilibrium

$$F_D \sin\theta + V = 0 \quad (2\text{-}57a)$$

For axial force equilibrium

$$F_D \cos\theta + F_C + F_T - P = 0 \quad (2\text{-}58b)$$

For flexural moment equilibrium

$$VH + \frac{Ph_s}{2} = F_T h_s \quad (2\text{-}58c)$$

Where, F_T, F_C, and F_D = internal forces of the vertical truss elements, L_T, and L_C, and the diagonal concrete strut, D_C, respectively, and P = applied axial force.

In Eq. (2-57a), F_D can be eliminated and relationship between F_L and F_C was calculated as follows:

$$F_C = -F_T\left(1 - \frac{l_p}{H}\right) + P\left(1 - \frac{l_p}{2H}\right) \tag{2-58}$$

The forces in Eq. (2-58) were assumed that both the tensile and compressive forces were resisted entirely by longitudinal reinforcements with substantial elongation. Therefore, Eq. (2-58) was written as form of rebar stress as follows:

$$\begin{aligned}\sigma_{lc} &= -\sigma_{lt}\left(\frac{A_s}{A_s'}\right)\left(1 - \frac{l_p}{H}\right) + \frac{P}{A_s'}\left(1 - \frac{l_p}{2H}\right) \\ &\approx -f_y\left(\frac{A_s}{A_s'}\right)\left(1 - \frac{l_p}{H}\right) + \frac{P}{A_s'}\left(1 - \frac{l_p}{2H}\right)\end{aligned} \tag{2-59}$$

Where, σ_{lc}, and σ_{lt} = the stresses of the vertical truss elements, L_T, and L_C, respectively, A_s, and A_s' = the areas of vertical reinforcement in the vertical truss elements, L_T, and L_C, respectively, and f_y = yield strength of reinforcement. The compressive stress should not exceed the yield strength ($\sigma_{lc} \geq -f_y$).

Fig. 2-10 (c) shows the hysteretic stress-strain relationship of vertical truss element L_C. Considering the Baushinger effect, the stress-strain relationship was simplified as tri-linear curve in Fig. 2-10 (c). Thus, ε_{lc} corresponding to σ_{lc} was calculated as follows:

$$\varepsilon_{lc} = \varepsilon_1\left(1 + \eta\frac{\sigma_{lc}}{f_y}\right) - \varepsilon_y \tag{2-60}$$

Where, η = a factor for representing the Baushinger effect (= 0.6), and ε_1 = the maximum tensile strain of vertical truss element L_C in the previous load cycle.

Because the ε_1 should be updated as the loading cycle proceeds, the step-by-step

calculation was needed. However, for simple calculation, Eom and Park (2010) suggested the total elongation developed by repeated cyclic loading as follows:

$$e_l = \frac{(\Delta - \Delta_{ef})\frac{h_s}{H}\left(1+\eta\frac{\sigma_{lc}}{2f_y}\right) - \left(1-\frac{l_p}{2H}\right)\varepsilon_y l_p}{1-\left(1+\eta\frac{\sigma_{lc}}{f_y}\right)\left(1-\frac{l_p}{H}\right)} \quad (2\text{-}61)$$

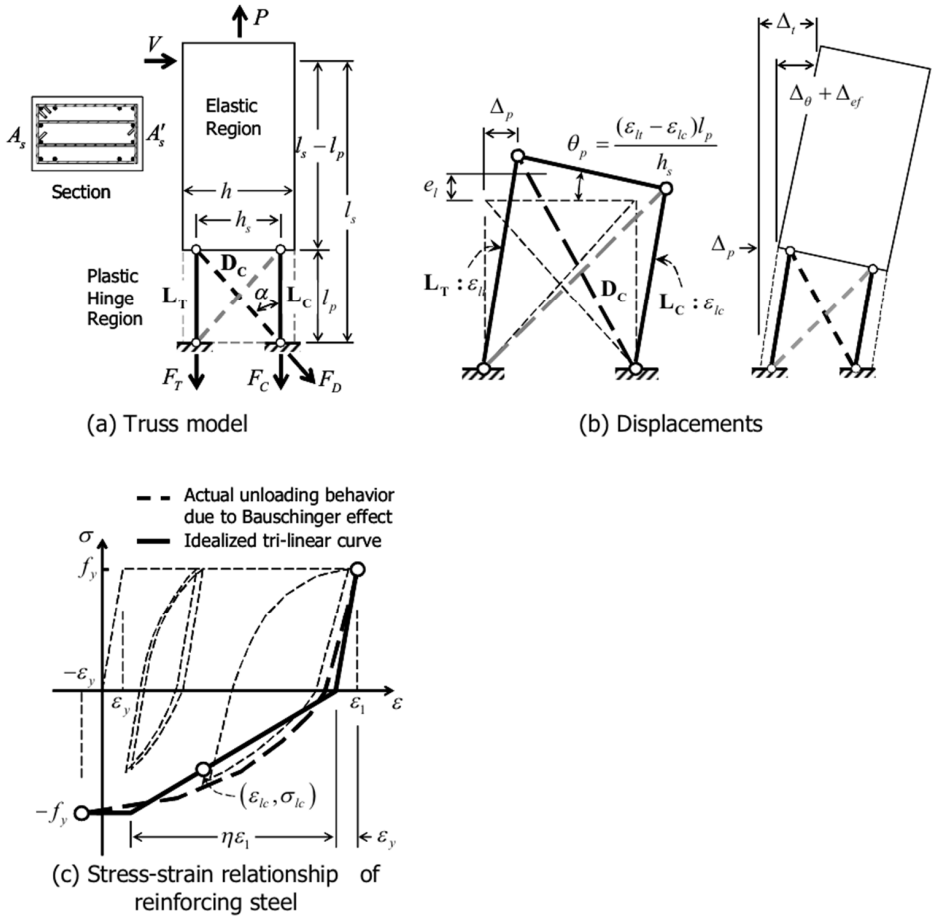

Fig. 2-10 Concept of truss mechanism model (Eom and Park, 2010)

Using the truss mechanism model, Eom et al. (2013) proposed the web crushing capacity of RC members with thin web. Fig. 2-11 shows the concept of the model. In this model, the crack angle in the web is assumed to be uniform in the plastic hinge region. The shear force in the plastic hinge zone is resisted by the diagonal concrete struts. Therefore, the shear capacity V_{wc} of the web wall due to web crushing is determined by the compressive strength of the web concrete as follows:

$$V_{wc} = f_{ce} l_{web} h_w \cos\theta \sin\theta \tag{2-62}$$

Where, f_{ce} = the effective compressive strength of the web concrete, h_w = the thickness of the web, l_{web} = the length of the web, and θ = the average crack angle in the web. The value of crack angle was assumed to be 45 degrees. Therefore, the shear capacity of the web V_{wc} was simplified as follows:

$$V_{wc} = \frac{1}{2} f_{ce} l_{web} h_w \tag{2-63}$$

As the elongation increases, the diagonal tensile strain of the web concrete increases, which degrades the strength of the compression strut (compression softening effect). According to Vecchio and Collins (1986), the effective compressive strength of concrete strut f_{ce} is defined as follows:

$$f_{ce} = \left(\frac{f_c'}{0.8 + 0.34(\varepsilon_t / \varepsilon_{co})} \right) \leq f_c' \tag{2-64}$$

Where, ε_t is the principal tensile strain. Eom et al. (2013) simplified the principal tensile strain based on Mohr's circle (see Fig. 2-11 (c)), as follows:

$$\varepsilon_t = \varepsilon_x + \varepsilon_y - \varepsilon_c \approx \varepsilon_{yh} + \frac{e_l}{d} + \varepsilon_{co} \tag{2-65}$$

Where, ε_x, and ε_y = the horizontal, and vertical strain of web concrete, respectively,

ε_c = the principal compressive strain of web concrete, ε_{yh} = the yield strain of shear reinforcement, e_l = the elongation in the plastic hinge region, d = the effective depth of the wall, and ε_{co} = the concrete crushing strain (= 0.002). Eom et al. (2013) assumed ε_{yh} = 0.002, because the permissible yield strength of wall shear reinforcement was limited to 420 MPa in the past design code.

Thus, Eq. (2-65) was simplified as follows:

$$\varepsilon_t = \frac{e_l}{d} + 0.004 \tag{2-66}$$

From Eqs. (2-63), Eq. (2-64), and (2-66), the web crushing strength V_{wc} was expressed as the function of longitudinal elongation e_l as follows:

$$V_{wc} = \frac{1}{2}\left(\frac{f_c'}{1.48 + 170(e_l/d)}\right) l_{web} h_w \leq \frac{1}{2} f_c' l_{web} h_w \tag{2-67}$$

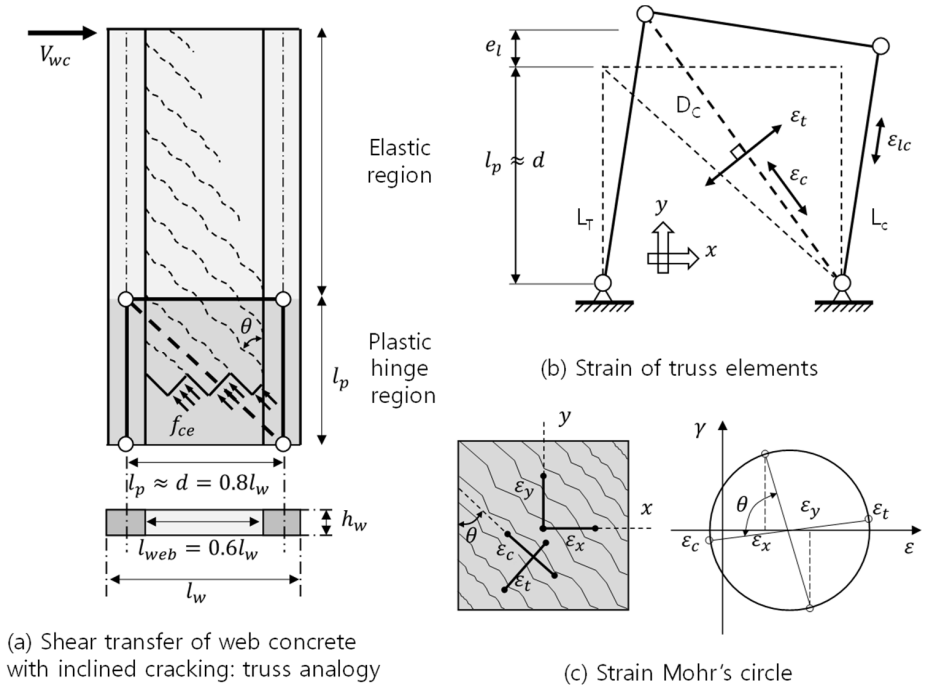

Fig. 2-11 Concept of web crushing model (Eom et al., 2013)

Chapter 3. Shear Strength of RC Walls with Various Design Parameters

3.1 Overview

In this chapter, to investigate the shear strength and deformation capacity of walls with various design parameters, fifteen wall specimens with aspect ratio 2.0 or 1.0 were tested under cyclic lateral loading. The major test parameters are the yield strength of reinforcement, reinforcement ratio, aspect ratio, and axial load ratio. Based on the test results, the structural performance of the walls, such as the failure mode, peak strength, deformation capacity, crack distribution, strains of rebar, ductility, and energy dissipation were discussed.

3.2 Backgrounds

Due to recent earthquakes, the earthquake load for design and evaluation of structures have been increased. In particular, shear demands for RC walls have increased: In the case of nuclear power plants (NPP), the safety requirements for earthquake has continued to increase for shear walls, which are the major structural component of NPP; and in the case of high rise buildings, the shear demand of walls was increased by considering the higher dynamic modes effects. For this reason, a large number of shear reinforcement is required, which degrades the constructability and economy.

To reduce the number of reinforcing bars in the wall, the use of high-strength reinforcement has been studied considering various design parameters. In the majority of existing studies for RC walls, the yield strength of horizontal rebars was less than 700 MPa (f_y = 520 to 667 MPa). The test results showed that when the effective shear reinforcement ratio ($\rho_h f_y$) was the same, the shear strength of walls with high-strength shear reinforcement was equivalent to that of walls with 420 MPa shear reinforcement.

On the other hand, studies for shear reinforcement with yield strength greater than 700 MPa (f_y > 700 MPa) are relatively limited. Kabeyasawa and Hiraishi (1998) reported the effect of ultra-high-strength bars (f_y = 753 to 1079 MPa) on barbell shaped shear walls. This study found that the yield strength of horizontal rebars was developed in relatively low horizontal bar ratios (ρ_h = 0.20 to 0.53 %), while in the walls with high shear reinforcement ratios (ρ_h = 0.99 to 1.44 %), horizontal rebars did not yield due to early web crushing failure. Cheng et al. (2016) reported that the shear capacity and deformation capacity of walls with high-strength bars (f_y = 786 to 806 MPa, ρ_h = 0.15 to 0.41 %) were comparable to those of walls with 420 MPa

grade bars (f_y = 440 to 475 MPa, ρ_h = 0.30 to 0.82 %). However, the crack width of the walls with high-strength bars was two times that of walls with 420 MPa bars because of the low horizontal bar ratio.

Based on the wall test results of Cheng et al. (2016) and Huq (2018), ACI 318-19 permitted the use of Grade 690 MPa (100 ksi) flexural reinforcement for both ordinary RC walls and special seismic RC walls. However, in the case of shear reinforcement, Grade 690 MPa (100 ksi) bar is permitted only for special seismic wall, while in the case of ordinary wall, the yield strength of shear reinforcement is still limited to 420 MPa (60 ksi). On the other hand, in KCI 2017 (KDS 14 20), Eurocode and Model code, Grade 600 MPa (87 ksi) bar is used for the shear reinforcement of RC walls.

As mentioned, existing studies of Kabeyasawa and Hiraishi (2016) and Cheng et al. (2018) verified the validity of 700 MPa reinforcement for shear design of RC walls. However, the test parameters were limited to low shear reinforcement ratio ($\rho_h/\rho_{h,max}$ = 0.29 – 0.85, where $\rho_{h,max}$ = shear reinforcement ratio corresponding to web crushing strength V_{nmax}) and low axial load ($N_u/(A_g f_c')$ = 0 – 0.16). On the other hand, in the case of high-rise building, the shear reinforcement ratio is relatively high, while in high-rise buildings, the axial load ratio is higher.

When using the 700 MPa reinforcement, the amount of reinforcement can be reduced by 40 percent compared to normal strength reinforcement (420/700 = 0.6). Therefore, the use of 700 MPa reinforcement enhance the constructability and economy. However, if the reinforcement ratio is significantly low, crack width increases and shear strength is degraded as the lateral deformation increases, which can results in brittle shear failure in the web wall after yielding of the wall. Further, the serviceability may not be satisfied, because the cracks due to drying shrinkage and concrete creep increase under service loads. Therefore, in structural design codes,

the minimum shear reinforcement ratio of the walls is suggested. In the actual design of walls, the shear reinforcement design is often governed by the minimum shear reinforcement ratio. In the case of 700 MPa reinforcement, the minimum shear reinforcement ratio is 0.25 %. It has an equivalent shear strength of shear reinforcement ratio of 0.42 % with normal strength reinforcement. Therefore, for better economy, it is necessary to investigate the effect of reduced minimum shear reinforcement ratio for 700 MPa reinforcement.

The existing studies investigated the effect of significantly low shear reinforcement ratio on the shear strength of walls. Hidalgo et al. (2002) tested wall specimens with reinforcement ratio equal to or less than the minimum reinforcement ratio (ρ_h = 0 – 0.38 %, and f_y = 366 – 471 MPa). Test results showed that the shear strengths of wall test specimens were greater than the nominal strength of design code (strength ratio V_{test}/V_n = 1.35 to 2.15), even in the wall with the shear reinforcement ratio less than the minimum shear reinforcement ratio. This result was confirmed by the study of Carrillo and Alcocer (2013). They tested ρ_h = 0.12 – 0.26 %, and f_y = 435 – 630 MPa. The test results showed that the minimum shear reinforcement ratio specified in ACI 318-19 (ρ_h = 0.25 %) appears to be excessive for controlling diagonal tension cracking. Thus, web shear reinforcement ratios less than the minimum ratio prescribed by ACI 318 are often used in several Latin American countries. Baek et al. (2018) investigated the effect of 0.2 % shear reinforcement ratio of 500 MPa reinforcement (actual yield strength f_y = 540 MPa) on the flexural and shear behavior of the wall. Test results showed that the failure modes were not significantly affected by the yield strength of shear reinforcement. Although the safety margin of the wall with 500 MPa reinforcement was slightly less than that of the wall with normal strength reinforcement, the effect of rebar yield strength on average crack width, lateral stiffness, and energy dissipation were neglected.

As mentioned, existing studies of Hidalgo et al. (2002), Carrillo and Alcocer (2013), and Baek et al. (2018), verified the effect of reduced minimum shear reinforcement ratio on shear strength of walls, in the range of rebar yield strength f_y = 336 – 630 MPa. Therefore, it is required to verify that the knowledges of existing studies can be applied to walls with 700 MPa reinforcement.

In the present study, the effect of 700 MPa high-strength rebars on the shear strength and deformation capacity of RC walls was investigated. There are two main purposes of experimental study: 1) to investigate the validity of 700 MPa rebar in the walls, and 2) to improve the wall test database with un-tested parameters for simplified shear strength and degradation model. For these purpose, the present study focused on the effects of significantly high or low reinforcement ratio, and high axial force. Further, the effect of high-strength shear reinforcement on the deformation capacity of walls after flexural yielding was investigated because inelastic deformation degrades shear capacity. For this purpose, 15 wall specimens were tested under cyclic lateral loading. For test parameters, failure modes, bar yield strength, aspect ratio, and axial load ratio were considered.

3.3 Test program

3.3.1 Test parameters and specimens details

The wall test specimens were classified in two groups by shear reinforcement ratio. First, considering the high demand forces of RC walls in high-rise buildings and NPPs, high vertical and horizontal reinforcement ratio (ρ_v = 1.27 %–1.99 %, ρ_h = 0.42 %–0.66 %, $\rho_h/\rho_{h,max}$ = 0.92 – 0.94) and high axial load ratio ($N_u/(A_g f_c^{'})$ =0 – 0.30) were tested by eight specimens. In these specimens, the effects of test parameters, such as yield strength of shear reinforcement, aspect ratio, and axial load ratio, were directly compared.

In the other group, considering lightly reinforced RC walls, which are designed only to resist gravity load, significantly low vertical and horizontal reinforcement ratio (ρ_v = 0.14 – 0.26 %, ρ_h = 0.14 – 0.25 %) were tested by seven specimens. The reinforcement ratio of 0.14 % is a reduced reinforcement ratio to have an effective rebar strength (ρf_y) equivalent to the minimum reinforcement ratio of 400 MPa rebar specified in ACI 318-19 (ρ = 0.25×400/700 = 0.14 %). In these specimens, the effect of reduced minimum shear reinforcement ratio on the shear strength and strength degradation after yielding was investigated. The effect of axial load was not considered.

15 specimens were tested under cyclic lateral loading. Fig. 3-1 to Fig. 3-4 show the details of the test specimens. Table 3-1 and Table 3-2 present the test parameters. The dimensions of walls with aspect ratio = 2.0 were 1,000 mm (length) × 2,000 mm (height) × 150 mm (thickness), and the walls with aspect ratio = 1.0 were 1,000 mm (length) × 1,000 mm (height) × 150 mm (thickness). To avoid unintended shear sliding failure at the interface between the foundation slab and the wall, the wall base was embedded to a depth of 50 mm below the top surface of the foundation slab.

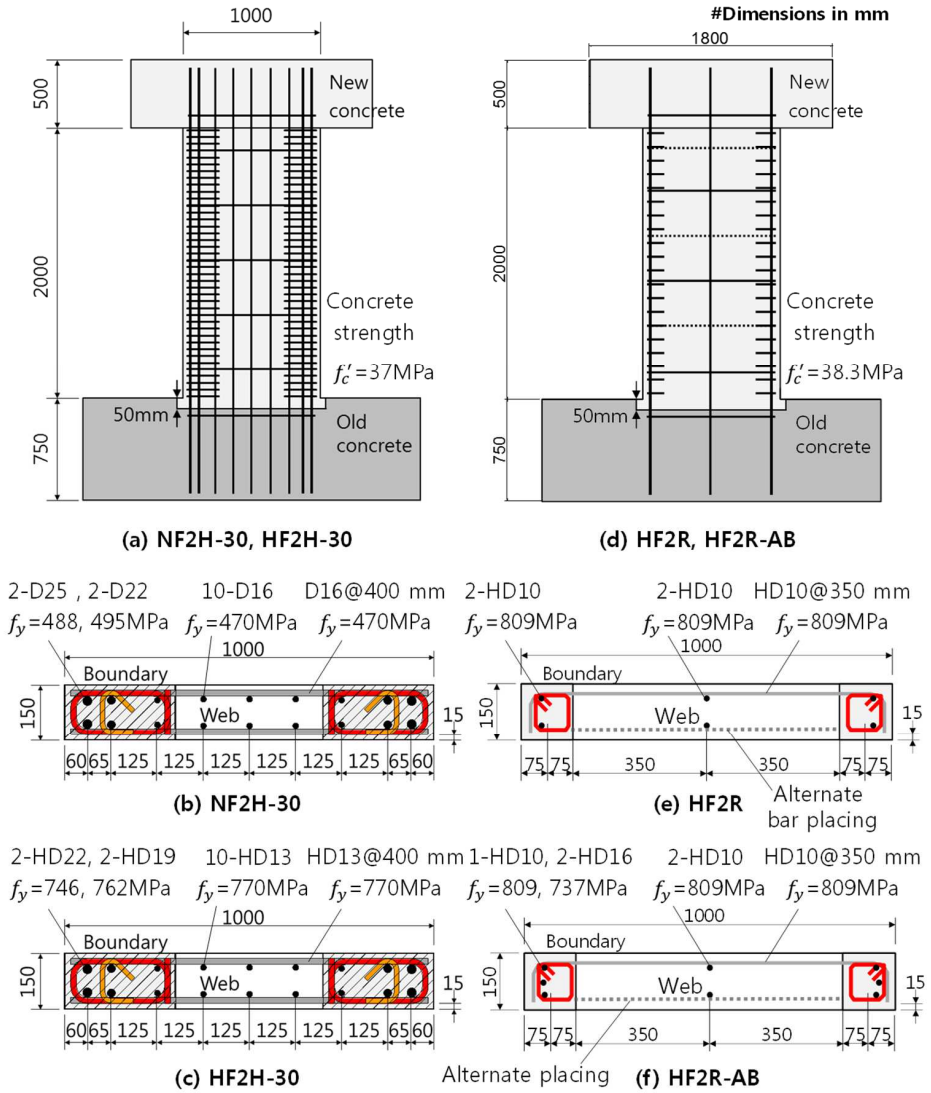

Fig. 3-1 Details of flexural yielding mode specimens

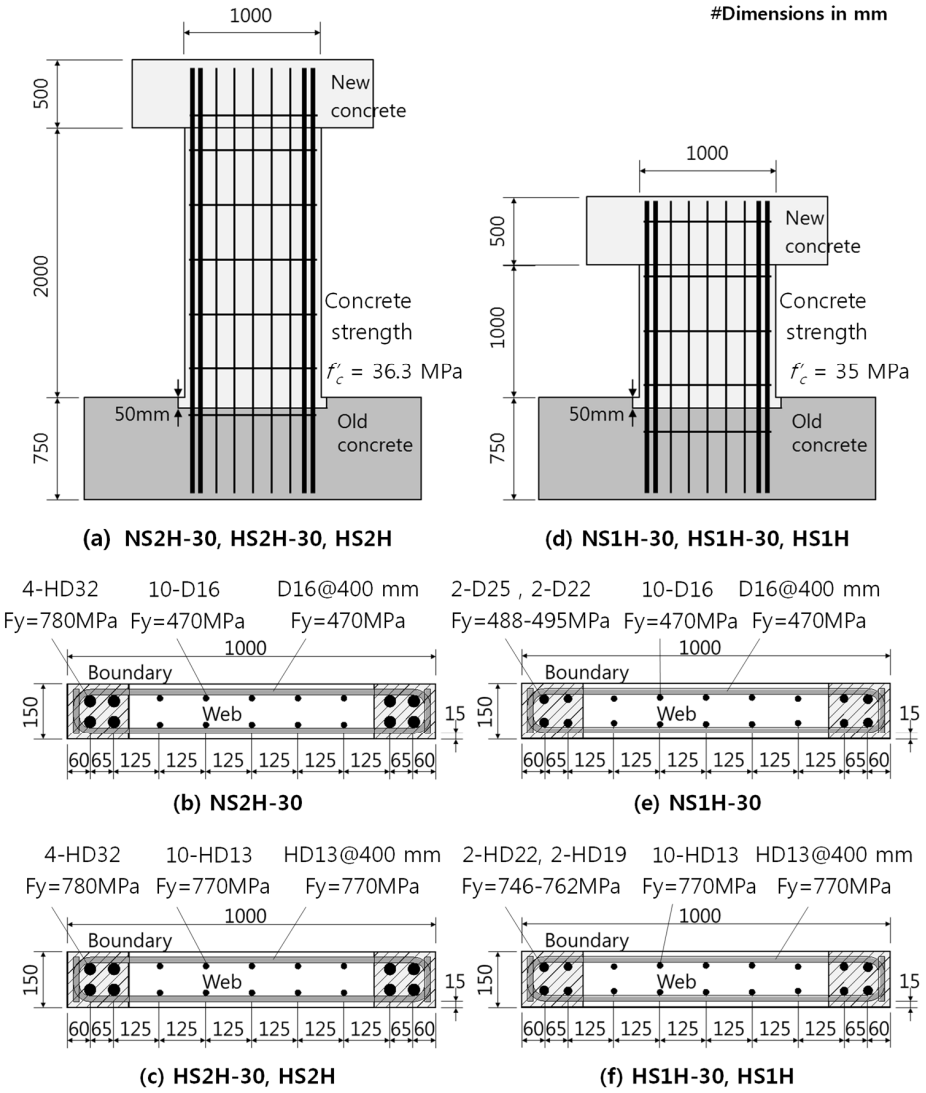

Fig. 3-2 Details of shear failure mode specimens with high shear reinf. ratio

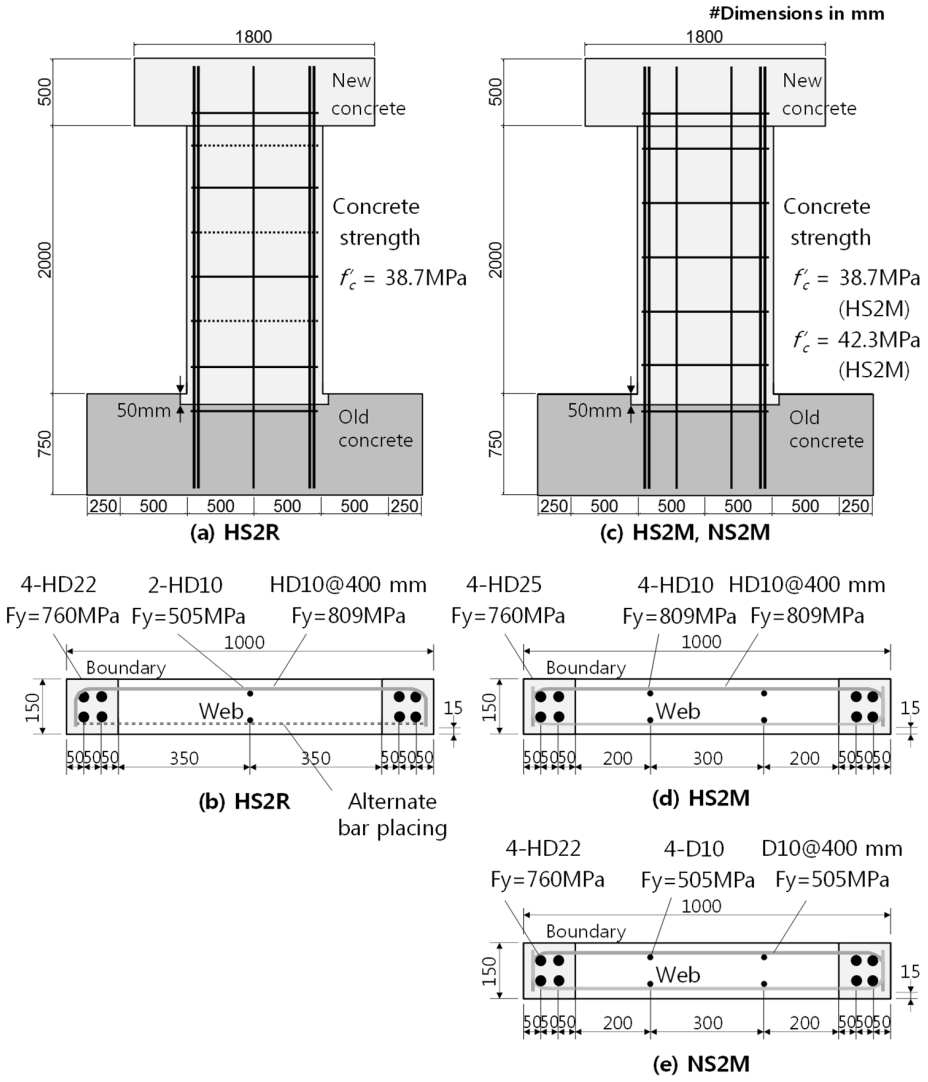

Fig. 3-3 Details of shear failure mode specimens with low shear reinf. ratio

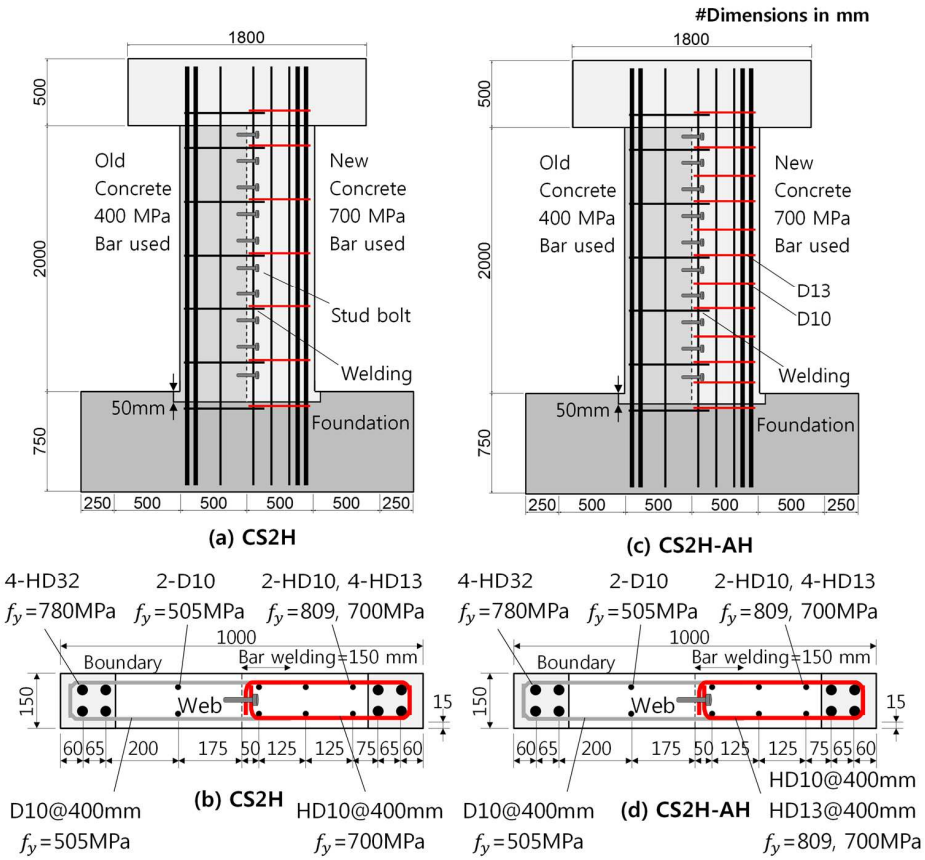

Fig. 3-4 Details of shear failure mode specimens with combined bar grade

Table 3-1 Design parameters of flexural yielding mode specimens

Specimens	Wall dimension (h_w × l_w) [mm x mm]	Concrete Strength f_c' [MPa]	Axial force Ratio $\frac{N_u}{A_g f_c'}$	Reinforcement							Strength prediction		
				Web					Boundary region		Shear strength V_n [kN]	Flexural strength V_f [kN]	$\frac{V_f}{V_n}$
				Horizontal			Vertical		Vertical				
				f_{yh} [MPa]	ρ_h [%]	$\rho_h f_{yh}$ [MPa]	f_{yv} [MPa]	ρ_v [%]	f_{yb} [MPa]	ρ_b [%]			
NF2H-30	1000 × 2000	37	0.3	470	0.66	3.10	470	1.99	470	5.96	584	622	1.07
HF2H-30		37	0.3	770	0.42	3.23	770	1.27	770	4.49	603	643	1.07
HF2R		38.3	0	809	0.14	1.13	809	0.14	809	0.63	325	79	0.25
HF2R-AB		38.3	0	809	0.14	1.13	809	0.27	707	2.08	325	173	0.53

Table 3-2 Design parameters of shear failure mode specimens

Specimens	Wall dimension (h_w × l_w) [mm x mm]	Concrete Strength f_c' [MPa]	Axial force Ratio $\frac{N_u}{A_g f_c'}$	Reinforcement							Strength prediction		
				Web					Boundary region		Shear strength V_n [kN]	Flexural strength V_f [kN]	$\frac{V_f}{V_n}$
				Horizontal			Vertical		Vertical				
				f_{yh} [MPa]	ρ_h [%]	$\rho_h f_{yh}$ [MPa]	f_{yv} [MPa]	ρ_v [%]	f_{yb} [MPa]	ρ_b [%]			
NS2H-30	1000 × 2000	36.3	0.3	470	0.66	3.10	470	1.99	770	10.59	580	1102	1.90
HS2H-30		36.3	0.3	770	0.42	3.23	770	1.27	770	10.59	599	1085	1.81
HS2H		36.3	0	770	0.42	3.23	770	1.27	770	10.59	506	1026	2.03
HS2R		38.7	0	809	0.14	1.13	809	0.14	760	6.88	325	505	1.55
HS2M		38.7	0	809	0.25	2.02	809	0.27	760	9.01	459	661	1.44
NS2M		42.3	0	505	0.25	1.26	505	0.27	760	6.88	352	509	1.45
CS2C		41.7	0	505/809	0.25/0.42	2.08	505/809	0.27/1.24	769	14.12	473	1191	2.52
CS2C-AH		41.7	0	505/809	0.25/0.66	3.04	505/809	0.27/1.24	769	14.12	617	1138	1.84
NS1H-30	1000 × 1000	35	0.3	470	0.66	3.10	470	1.99	470	5.96	572	1056	1.85
HS1H-30		35	0.3	770	0.42	3.23	770	1.27	770	4.49	592	1044	1.76
HS1H		35	0	770	0.42	3.23	770	1.27	770	4.49	503	920	1.83

For the test parameters, rebar grade, failure mode, aspect ratio, vertical reinforcement ratio, horizontal reinforcement ratio, and axial load ratio were considered. The name of each specimen indicates the test parameters. The first letter, **H**, **N**, or **C**, indicates the strength of rebars (Grade 700 MPa high-strength bar, Grade 400 MPa normal strength bar, or combined yield strength Grade 700 + 400 MPa). The second letters, **F** or **S** indicates the failure mode (flexural yielding mode or shear failure mode). The number **1** or **2** refers to the aspect ratio of the specimen. The third letter, **H**, **M**, **R**, or **C**, indicates the shear reinforcement ratio (high shear reinforcement ratio, minimum shear reinforcement ratio of 0.25%, reduced minimum shear reinforcement ratio, or combined shear reinforcement ratio). The last letters **30**, **AB** or **AH** following dash (-), if any, indicates additional details: **30** indicates high axial load ratio of 30 %, **AB** indicates use of additional vertical boundary reinforcement or **AH** indicates use of additional shear reinforcement. The axial load ratio is defined as $N_u/(A_g f_c')$, where N_u = axial load, A_g = cross-sectional area, and f_c' = concrete compressive strength.

The compressive strength of concrete was 35 – 42.3 MPa (Table 3-1 and 3-2). In the present study, focusing on the effect of high-strength reinforcement, concrete compressive strength was not considered as a test parameter. When high-strength concrete is combined with high-strength rebar, the shear strength, deformation capacity, and failure mode of walls can be affected by high concrete strength.

Table 3-3 presents the actual yield strength and tensile strength of rebars. Fig. 3-5 shows the strain-stress relationships of rebars. The actual yield strength of the vertical and horizontal reinforcement in the web was f_y = 505 MPa for Grade 400 D10 (bar diameter = 9.53 mm), f_y = 470 MPa for Grade 400 D16 (bar diameter = 15.9 mm), f_y = 809 MPa for Grade 700s HD10 (bar diameter = 9.53 mm, seismic grade), f_y = 770 MPa for Grade 700 HD13 (bar diameter = 12.7 mm), f_y = 700 MPa

for Grade 700s HD13 (bar diameter = 12.7 mm, and seismic grade). For vertical reinforcement in the boundary element, large diameter bars were used: Grade 400 D22 (f_y = 488 MPa, bar diameter = 22.2 mm), and D25 (f_y = 495 MPa, bar diameter = 25.4 mm) for **NF2H-30**, and **NS1H-30**; Grade 700s HD16 (f_y = 707 MPa, bar diameter = 15.9 mm) for **HF2R-AB**; Grade 700 HD22 (f_y = 762 MPa, bar diameter = 22.2 mm) for **HF2H-30**, **HS2R**, **NS2M**, **HS1H-30**, and **HS1H**; Grade 700 HD25 (f_y = 760 MPa, bar diameter = 25.4 mm) for **HS2M**; and Grade 700 HD32 (f_y = 780 MPa, bar diameter = 31.8 mm) for **NS2H-30**, **HS2H-30**, **HS2H**, **CS2C**, and **CS2C-AH**.

Table 3-3 Material properties of rebar

Grade	Grade 700s (700 MPa)				Grade 700 (700 MPa)				Grade 400 (400 MPa)			
Type	HD10	HD13	HD16	HD22	HD13	HD22	HD25	HD32	D10	D16	D22	D25
Bar diameter d_b, mm	9.53	12.7	19.1	22.2	12.7	22.2	25.4	31.8	9.53	15.9	22.2	25.4
Bar area A_s, mm^2	71.3	126.7	198.6	387.1	126.7	387.1	506.7	794.2	71.3	198.6	387.1	506.7
Yield strength f_y, MPa	809	700	707	760	770	762	760	780	505	470	488	495
Tensile strength f_t, MPa	1006	899	936	956	894	847	866	902	646	610	603	604

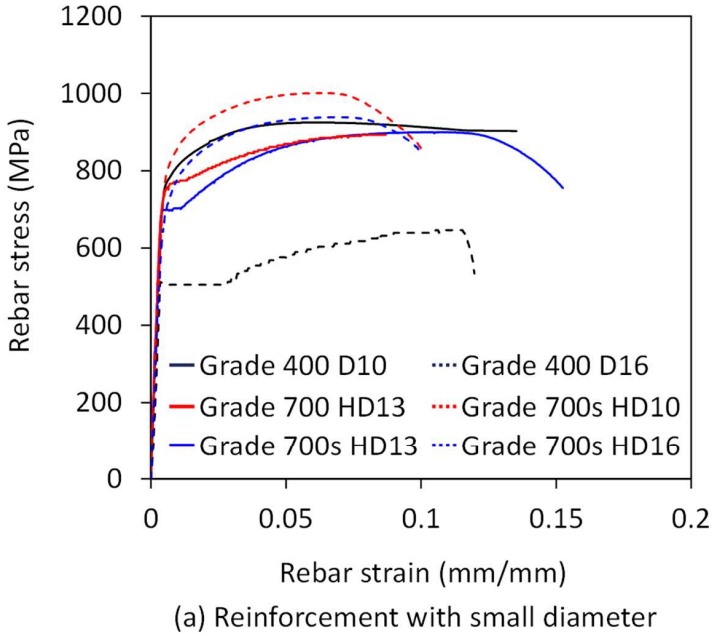

(a) Reinforcement with small diameter

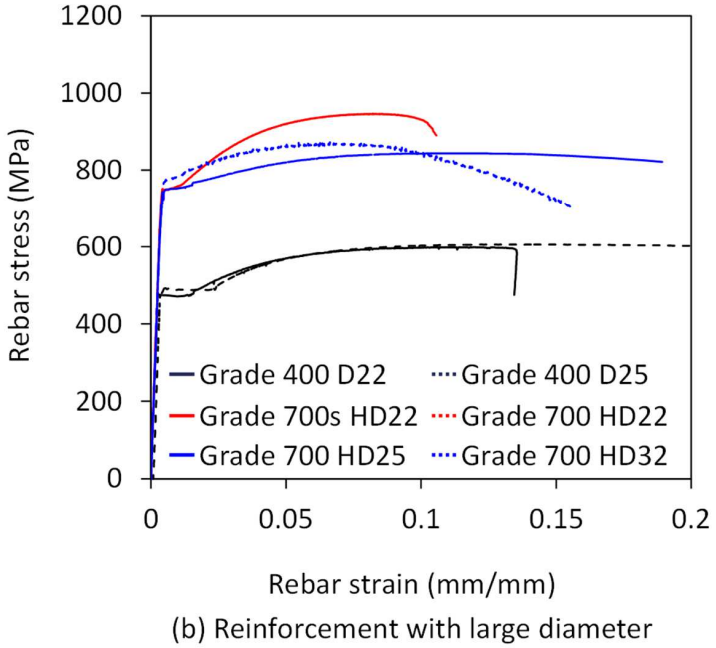

(b) Reinforcement with large diameter

Fig. 3-5 Stress-strain curves of reinforcement

Fig. 3-1 (a) – (c) show the details of **NF2H-30** and **HF2H-30** with flexural yielding mode and axial load ratio of 0.3. To investigate the effect of shear rebar grade on deformation ductility, the specimens were designed with special boundary confinement detail (ACI 318-19) to develop a large inelastic deformation. Considering the depth of compression zone c = 400 mm, which was estimated from the nominal flexural strength of the wall, the length of the boundary element was determined as 300 mm. Thus, the length of the web was 400 mm. In the web, the vertical bar ratio ρ_{vw} in **NF2H-30** was 1.99 %, while in **HF2H-30** with high-strength rebars, the ratio was reduced to 1.27 %. The web horizontal rebar ratios ρ_{hw} in **NF2H-30** were 0.66 %, and in **HF2H-30**, 0.42 %. In the boundary element, the vertical bar ratios ρ_{vb} in **NF2H-30** were 5.96 %, and in **HF2H-30**, 4.49 %. For boundary confinement, closed hoops and cross ties with a vertical spacing of 50 mm were used, conforming to the special seismic detail. In **NF2H-30** and **HF2H-30**, the nominal flexural strength V_f (i.e. horizontal force corresponding to the flexural capacity) was designed to be the same as the nominal shear strength V_n. Due to the conservation of nominal shear strength of ACI 318, in general, flexural yielding was expected to occur before shear failure.

Fig. 3-1 (d) – (f) show the details of **HF2R** and **HF2R-AB** with flexural yielding mode and horizontal bar ratio of 0.14 %. In these specimens, horizontal bar ratio having a shear strength equivalent to that of a wall with 400 MPa bars and the minimum reinforcement ratio (ρ_h = 0.25 %) was used. The nominal flexural strength V_f (i.e. horizontal force corresponding to the flexural capacity) of **HF2R** was designed to be the same as the half the concrete shear strength ($V_f = 0.5V_c$), while the nominal flexural strength of **HF2R-AB** was designed to be the same as the concrete shear strength ($V_f = 1.0V_c$). **HF2R** and **HF2R-AB** had common rebar details except for the vertical bars in the boundary element. To investigate the effect of reduced horizontal bar ratio on load carrying capacity under large lateral deformation, the

specimens were designed with special boundary confinement detail (ACI 318-19) to develop a large inelastic deformation. The depth of compression zone estimated from the nominal flexural strength of the wall was c = 80 mm in **HF2R**, and 100 mm in **HF2R-AB**. However, for conservative design, the length of the boundary element was determined as 150 mm. Thus, the length of the web was 700 mm. In the web, two 700 MPa HD10 bars were used for vertical reinforcement (vertical bar ratio ρ_v = 0.12 %), which was the minimum vertical reinforcement specified in ACI 318-19. For the web horizontal reinforcement, 700 MPa HD10 bar was alternately placed with spacing of 350 mm (horizontal bar ratio ρ_h = 0.14 %), which was smaller than the minimum horizontal reinforcement ratio $\rho_{h,min}$ = 0.25 %. For the vertical reinforcement in the boundary element, two 700 MPa HD10 bars were used in **HF2R** (ρ_{vb} = 0.63 %), while one 700 MPa HD10 + two 700 MPa HD16 bars were used in **HF2R-AB** (ρ_{vb} = 2.08 %). For boundary confinement, closed hoops with a vertical spacing of 50 mm were used.

Fig. 3-2 (a) – (c) show the details of **NS2H-30**, **HS2H-30**, and **HS2H** with shear failure mode. To induce shear failure mode, the nominal flexural strength V_f was increased to 2.0 times the nominal shear strength V_n. Thus, in the boundary element, the vertical bar ratios ρ_{vb} was increased to 10.59 %. In the web, the vertical and horizontal bar ratios were the same as those of the flexural yielding mode specimens **NF2H-30** and **HF2H-30**.

Fig. 3-2 (d) – (f) show the details of **NS1H-30**, **HS1H-30**, and **HS1H** with shear failure mode and aspect ratio of 1.0. To induce shear failure mode, the nominal flexural strength V_f was designed to be 1.8 times the nominal shear strength V_n. The sectional details of **NS1H-30** were the same as those of **NF2H-30**, except for the boundary confinement details. Similarly, the sectional details of **HS1H-30** and **HS1H** were the same as those of **HF2H-30**, except for the boundary confinement.

Fig. 3-3 (a) and (b) show the details of **HS2R** with shear failure mode and horizontal bar ratio of 0.14 %. To induce shear failure mode, the nominal flexural strength V_f was increased to 1.45 times the nominal shear strength V_n. Thus, for the vertical reinforcement in the boundary element, four 700 MPa HD22 bars were used (ρ_{vb} = 3.44 %). In the web, the vertical and horizontal bar ratios were the same as those of the flexural mode specimens. Boundary confinement was not considered in **HS2R**.

Fig. 3-3 (c) – (e) show the details of **HS2M**, and **NS2M** with shear failure mode and horizontal bar ratio of 0.25 %. To induce shear failure mode, the nominal flexural strength V_f was designed to be 1.37 – 1.45 times the nominal shear strength V_n. The diameter and number of rebars in the web wall were the same in **HS2M** and **NS2M**, except for the bar grade: four 400 MPa D10 or 700 MPa HD10 bars were used for vertical reinforcement (ρ_v = 0.24 %), and 400 MPa D10 or 700 MPa HD10 bars with vertical spacing of 400 mm were used for horizontal reinforcement (ρ_h = 0.25 %). For vertical reinforcement in the boundary element, four 700 MPa HD25 bars were used in **HS2M** (ρ_{vb} = 4.50 %), while four 700 MPa HD22 bars were used in **NS2M** (ρ_{vb} = 3.44 %).

Fig. 3-4 (a) – (d) show the details of **CS2C** and **CS2C-AH** with shear failure mode and combined bar grade. These specimens consisted of two segments of walls: one segment is a wall with low shear reinforcement ratio and normal strength bars (ρ_h = 0.25 %, f_{yh} = 400 MPa), which represented an old wall not conforming the seismic design; and the other segment is a wall with high shear reinforcement ratio and high-strength bars (ρ_h = 0.42 – 0.66 %, f_{yh} = 700 MPa), which represented a horizontally expanded wall to retrofit the old wall. To induce shear failure mode, the nominal flexural strength V_f was designed to be 1.68 – 2.19 times the nominal shear strength V_n. The nominal shear strength V_n of combined rebar grade specimens was

preliminarily estimated by sum of the nominal shear strength of two wall segments ($V_n = V_{n1} + V_{n2}$). In the old wall with normal grade rebars, two 400 MPa D10 bars were used as vertical bars in the web (ρ_v = 0.27 %), 400 MPa D10 bars with spacing of 400 mm were used as horizontal bars in the web (ρ_h = 0.25 %), and four 700 MPa HD32 bars were used as vertical bars in the boundary element (ρ_b = 14.12 %). After construction of old wall, to prevent unintended vertical sliding at the vertical interface between the wall segments, the interface was chipped to roughen and the headed bolts with a diameter of 16 mm were fixed into the old wall using the chemical anchor. In the expanded wall of **CS2C**, four 700 MPa HD13 + two 700 MPa HD10 (ρ_v = 1.24 %) were used for web vertical reinforcement. For web horizontal reinforcement, 700 MPa HD13 bars with spacing of 400 mm (ρ_h = 0.42 %) were used, and they were welded with the horizontal bars extended from the old wall. In **CS2C-AH**, the web horizontal rebar ratio of the expanded wall was increased to ρ_h = 0.66 %. Compared to **CS2C**, additional 700 MPa HD10 bars with a spacing of 400 mm were used.

3.3.2 Test setup and instrumentation

Fig. 3-6 shows the test setups and linear variable displacement transducers (LVDTs) for the measurement of displacement. In case of specimens with axial force, using 2,000 kN oil pressure machine, a compression force was applied to the top of the specimen. Then, by using a 1,500 kN actuator, cyclic lateral loading was applied to the specimen. The magnitude of the compressive force corresponding to the axial load ratio of 0.3 was calculated considering the actual compression strength of the concrete (see Table 3-1 and Table 3-2). In case of specimens without axial force, only cyclic lateral loading was applied to the specimens by using a 1,500 kN actuator.

The lateral loading protocol in Fig. 3-7 followed the "Guide for Testing Reinforced Concrete Structural Elements under Slowly Applied Simulated Seismic Loads (ACI 374.2R-13, 2013)". The increment of deformation control parameter is 1.25 to 1.5 times previous deformation level. The number of cycles at each deformation level is three. The lateral displacements of the specimen were measured at the center of the loading beam and foundation. The flexural deformation and shear deformation were measured using LVDTs (see Fig. 3-6).

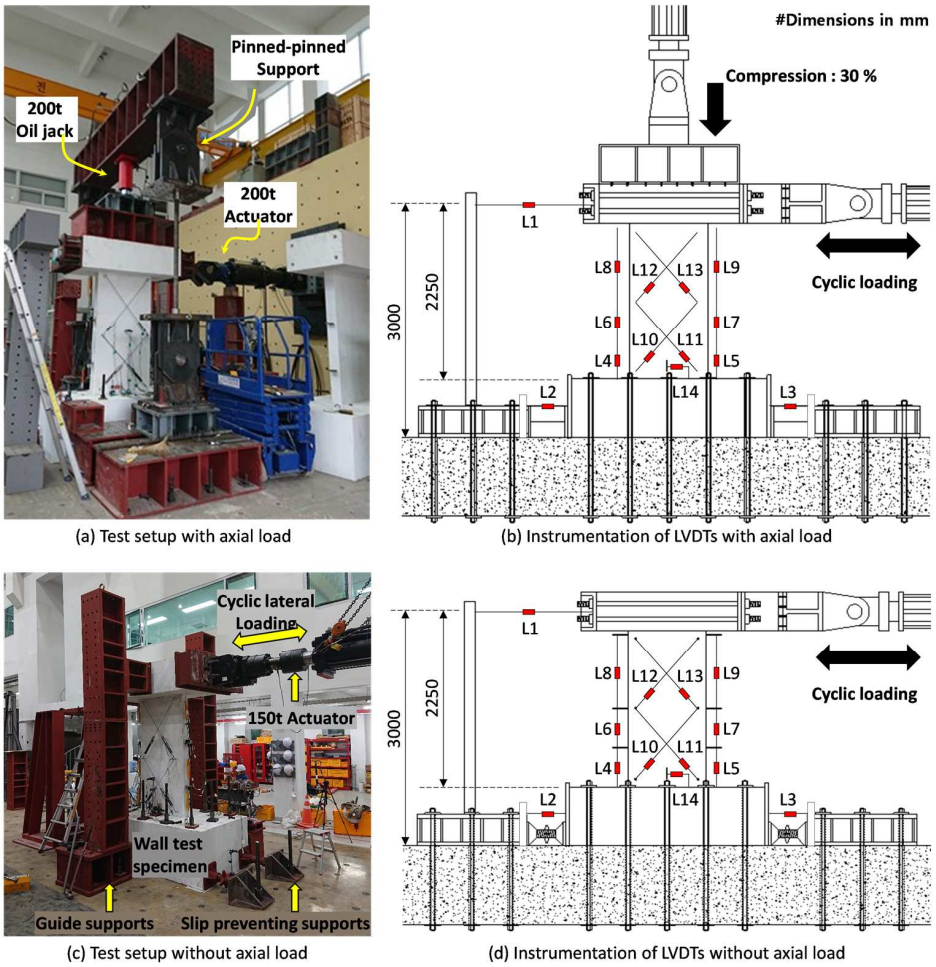

Fig. 3-6 Test setup

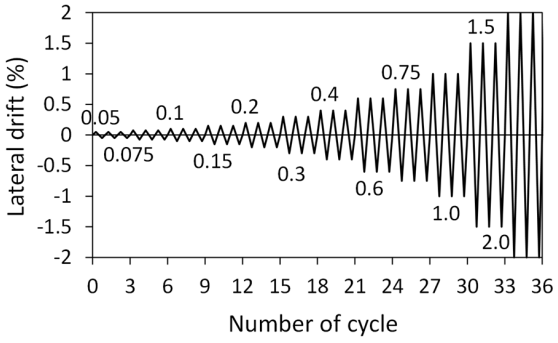

Fig. 3-7 Loading protocol

3.4 Test results

3.4.1 Failure modes

Fig. 3-8 to Fig. 3-12 show damage modes of the specimens at the end of the tests. Table 3-4 and Table 3-5 present failure modes of the specimens based on the damage corresponding to the peak strength.

In flexural mode specimen **NF2H-30** with Grade 400 MPa rebars (f_y = 470 MPa), as expected, flexural yielding occurred at the wall base (FY) (Fig. 3-8 (a) and Table 3-4). At both edges of the wall base, crushing and spalling of the cover concrete occurred. After the peak strength, as the lateral drift increased, vertical splitting cracks occurred at the interface between the boundary element and the web, but were not severe. However, in the web, severe spalling of cover concrete and buckling of vertical rebars occurred due to the high axial load ratio. In flexural specimen **HF2H-30** with Grade 700 MPa rebars (f_y = 770 MPa), flexural yielding occurred at the peak strength (FY) (Fig. 3-8 (b) and Table 3-4). At both edges of the wall base, crushing of the cover concrete occurred. After the peak strength, vertical splitting cracks occurred at the interface between the boundary element and the web, which resulted in gradual strength degradation (VS).

In flexural mode specimen **HF2R** (Grade 700 MPa, f_y = 809 MPa, ρ_h = 0.14 %, and $V_f = 0.5V_c$), as expected, flexural yielding occurred at the wall base (FY) (Fig. 3-8 (c) and Table 3-4). However, due to significantly low vertical reinforcement ratio in the boundary element (only two HD10 bars in each boundary element), most of the inelastic deformation occurred intensively at the base of the wall, while damages in upper part of the wall were limited. Further, this strain concentration caused premature tensile fracture of vertical bars in the boundary element, immediately after the peak strength (TF).

In flexural mode specimen **HF2R-AB** (Grade 700 MPa, f_y = 809 MPa, ρ_h = 0.14 %, and $V_f = 1.0V_c$), flexural yielding occurred at the peak strength (FY) (Fig. 3-8 (d) and Table 3-4). After the peak strength, as the lateral drift increased, diagonal tension cracking and web concrete crushing occurred in the plastic hinge zone, and the strength degradation gradually occurred (DT+WC).

In the shear failure specimens **NS2H-30**, **HS2H-30** and **HS2H**, to induce the shear failure mode, the area of vertical bars was increased in both edges of the wall. In **NS2H-30** with 400 MPa bars, initial diagonal cracks occurred at the lateral drift ratio δ = 0.3 %. At each loading step, the width of diagonal crack was greater than that of flexural horizontal tension cracks. At the peak strength, the major diagonal tensile crack penetrated through the wall section, resulting in a significant strength degradation (DT) (Fig. 3-9 (a) and Table 3-5). The crack angle was close to 45 degrees. At the compression zone of the wall base, concrete crushing occurred. Further, at the ends of the horizontal bar, loosening of the 90 degree hook and spalling of concrete cover occurred. The failure mechanism of **HS2H-30** with 700 MPa bars was similar to that of **NS2H-30** (Fig. 3-9 (b) and Table 3-5). However, at the maximum lateral drift ratio, because of the smaller horizontal bar ratio (ρ_{hw} = 0.42 % in **HS2H-30** vs ρ_{hw} = 0.66 % in **NS2H-30**), the width of the diagonal tensile crack was greater than that of **NS2H-30** (0.40 mm in **HS2H-30** vs 0.25 mm in **NS2H-30**).

In **HS2H** with no axial load, initial diagonal tensile cracking occurred earlier at the drift ratio δ = 0.2 %, when compared to **HS2H-30**. The width of the diagonal tensile crack was 0.5 mm, which was greater than that of **HS2H-30** (= 0.40 mm). After the peak strength, the width of diagonal tensile crack was significantly increased (> 1.0 mm) and crushing of the web concrete occurred, resulting in strength degradation (DT + WC) (Fig. 3-9 (c) and Table 3-5). In shear failure specimen

NS1H-30 with aspect ratio of 1.0, initial diagonal cracking occurred at the drift ratio of δ = 0.3 %. At the peak strength, the major diagonal crack penetrated into the entire wall and web crushing occurred (DT + WC) (Fig. 3-10 (a) and Table 3-5). In the compression zone at the wall base, concrete crushing occurred. The failure mechanism of **HS1H-30** was similar to that of **NS1H-30**. However, because of the lower horizontal bar ratio, the diagonal crack width was greater than that of **NS1H-30**. Further, failure occurred earlier at a lower drift ratio (δ_u = 0.6 % in **HS1H-30** vs δ_u = 0.75 % in **NS1H-30**) and the damage was severe. The failure mode of **HS1H-30** was a combined mode of diagonal tensile cracking and web concrete crushing (DT + WC) (Fig. 3-10 (b) and Table 3-5). In **HS1H** with no axial load, initial diagonal tensile cracking occurred earlier at the drift ratio of δ = 0.15 %. After the peak strength, diagonal tensile cracking and web concrete crushing occurred (DT + WC) (Fig. 3-10 (c) and Table 3-5). At the end of the horizontal bar, loosening of 90 degree hook was observed.

In shear failure mode specimen **HS2R** (Grade 700 MPa, f_y = 809 MPa, ρ_h = 0.14 %), initial diagonal cracks occurred at the lateral drift ratio δ = 0.2 %. At the peak strength, the major diagonal tensile crack penetrated through the wall section, causing strength degradation (DT) (Fig. 3-11Fig. 3-10 (a) and Table 3-5). Similar failure mechanism appeared in **HS2M** (Grade 700 MPa, f_y = 809 MPa, ρ_h = 0.25 %), and **NS2M** (Grade 400 MPa, f_y = 505 MPa, ρ_h = 0.25 %) (DT) (Fig. 3-11Fig. 3-10 (b) – (c) and Table 3-5). Further, in these specimens, after the peak strength, strength was suddenly dropped by tensile fracture of horizontal rebar.

In **CS2C** (Grade 400 and 700 MPa, f_y = 505 and 809 MPa, ρ_v = 0.27 and 1.24 %, ρ_h = 0.25 and 0.42 %), the horizontal bar ratio of the expanded wall was greater than that of the old wall. Therefore, the number of diagonal cracks in the expanded wall than that in the old wall. After peak strength, the major diagonal tension cracks

penetrated through the wall section, which causing sudden drop of load carrying capacity. The angle of diagonal tension crack was 45 degrees (DT), which was the same that of monolithic casted walls (i.e. **HS2R**, **HS2M**, and **NS2M**). A partial vertical cracks were developed at the vertical interface between the both wall segments. However, global vertical shear sliding did not occur, and damages on the vertical interface were limited (Fig. 3-12Fig. 3-10 (a) and Table 3-5).

In **CS2C-AH** (Grade 400 and 700 MPa, f_y = 505 and 809 MPa, ρ_v = 0.27 and 1.24 %, ρ_h = 0.25 and 0.66 %), the horizontal bar ratio of the expanded wall was increased than that of **CS2C**. Therefore, the diagonal cracks in the expanded wall were distributed along the vertical direction, and the average crack width was less in the expanded wall than in the old wall. After the peak strength, the major diagonal cracks were developed in the old wall, not penetrating through the expanded wall section (DT). The angle of diagonal crack was 60 degree, which was stiffer than that of **CS2C**. The damages on the vertical interface were limited (Fig. 3-12Fig. 3-10 (b) and Table 3-5).

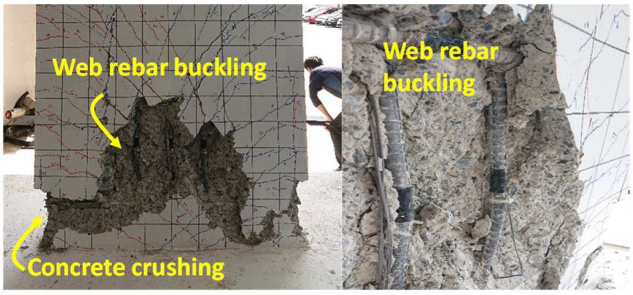

(a) NF2H-30

(b) HF2H-30

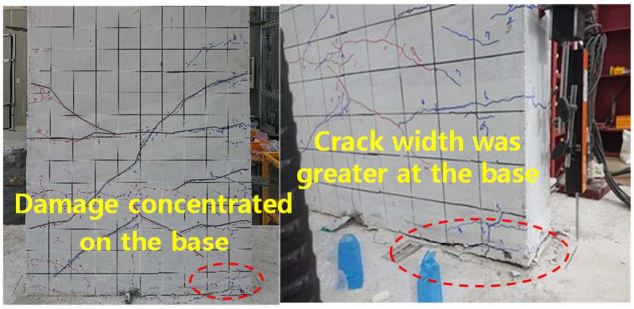

(c) HF2R

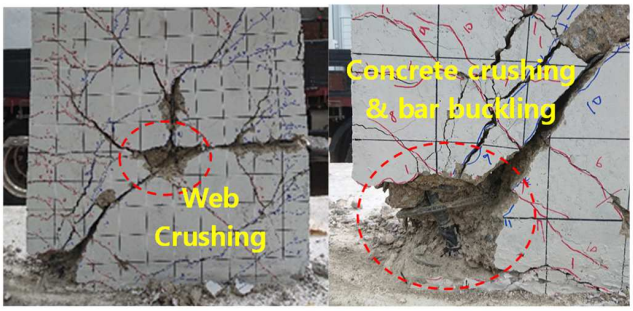

(d) HF2R-AB

Fig. 3-8 Damage mode of flexural yielding mode specimens

(NF2H-30, HF2H-30, HF2R, and HF2R-AB)

(a) NS2H-30

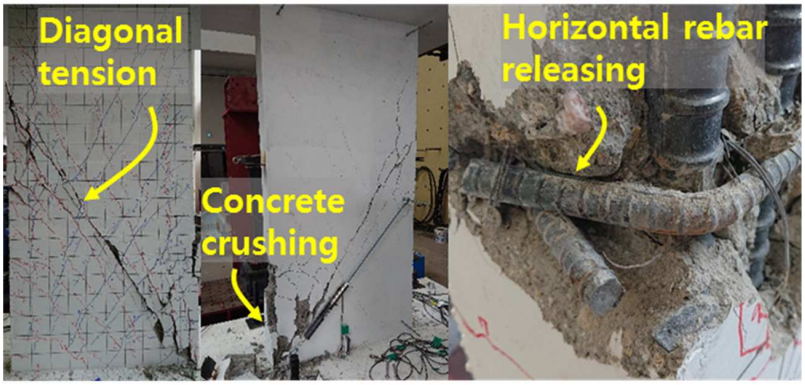

(b) HS2H-30

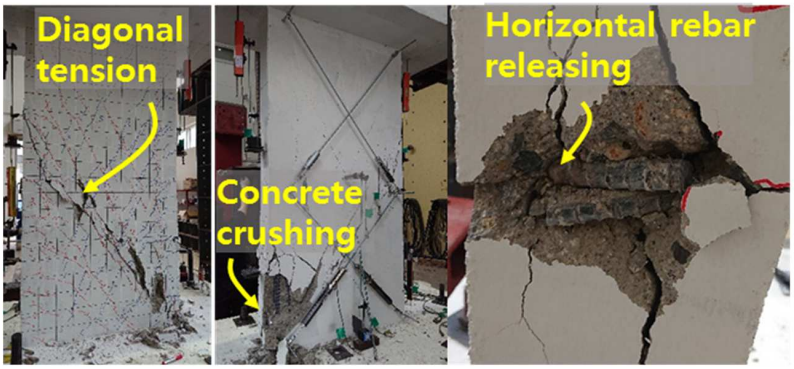

(c) HS2H

Fig. 3-9 Damage mode of shear failure mode specimens

(NS2H-30, HS2H-30, and HS2H)

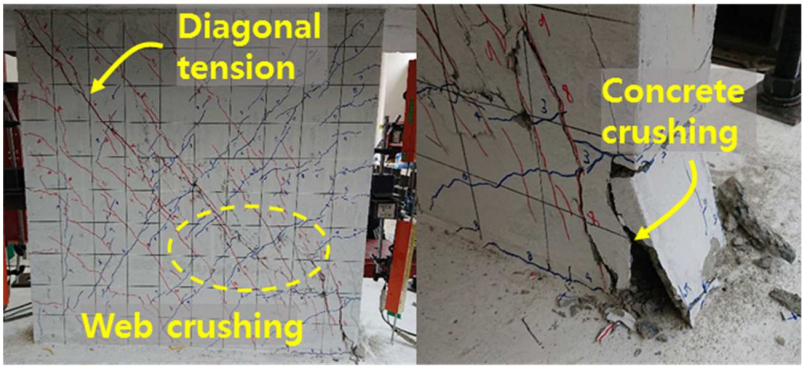

(a) NS1H-30

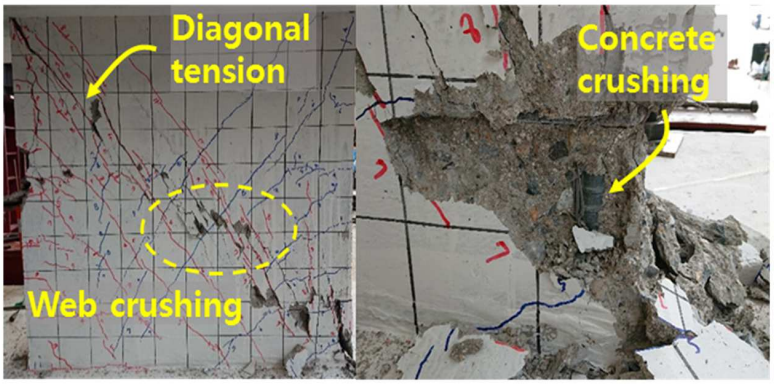

(b) HS1H-30

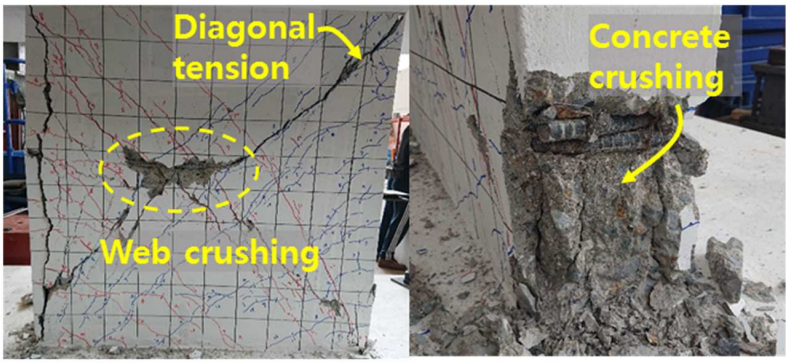

(c) HS1H

Fig. 3-10 Damage mode of shear failure mode specimens

(NS1H-30, HS1H-30, and HS1H)

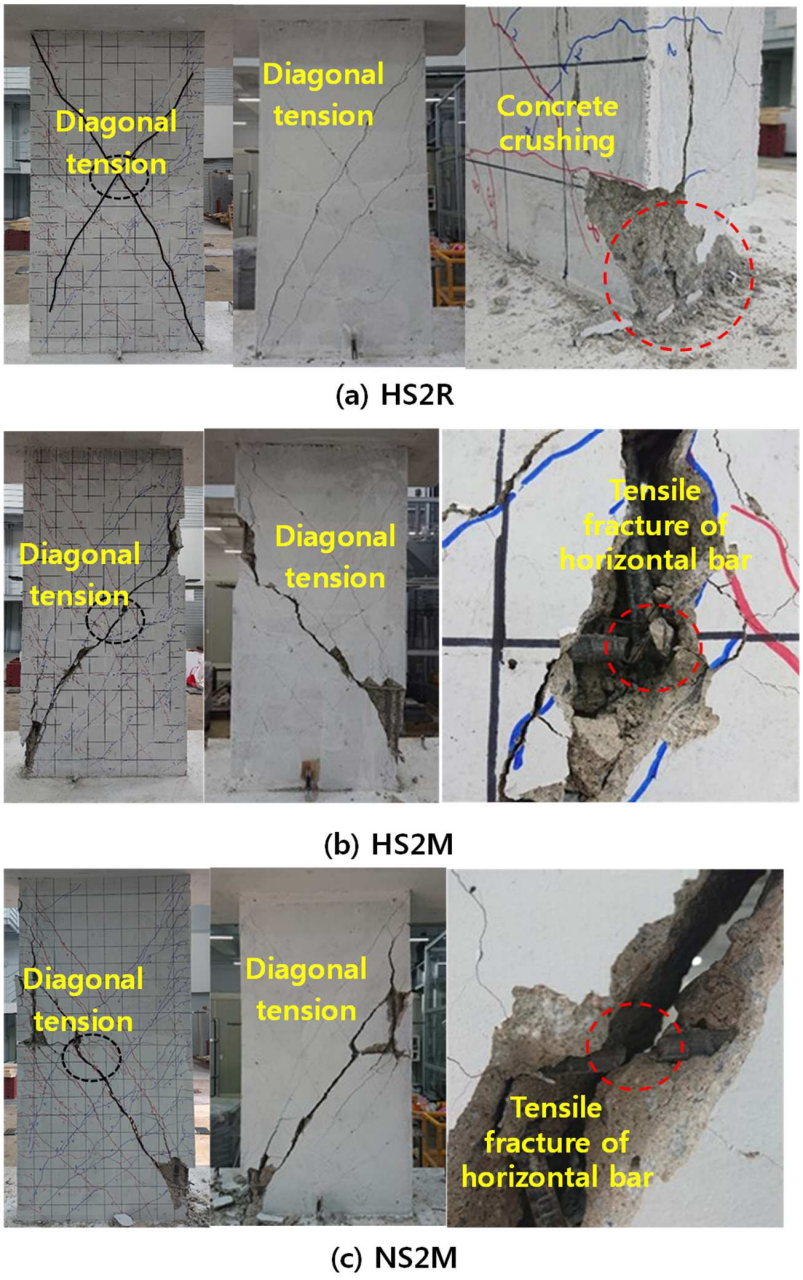

Fig. 3-11 Damage mode of shear failure mode specimens

(HS2R, HS2M, and NS2M)

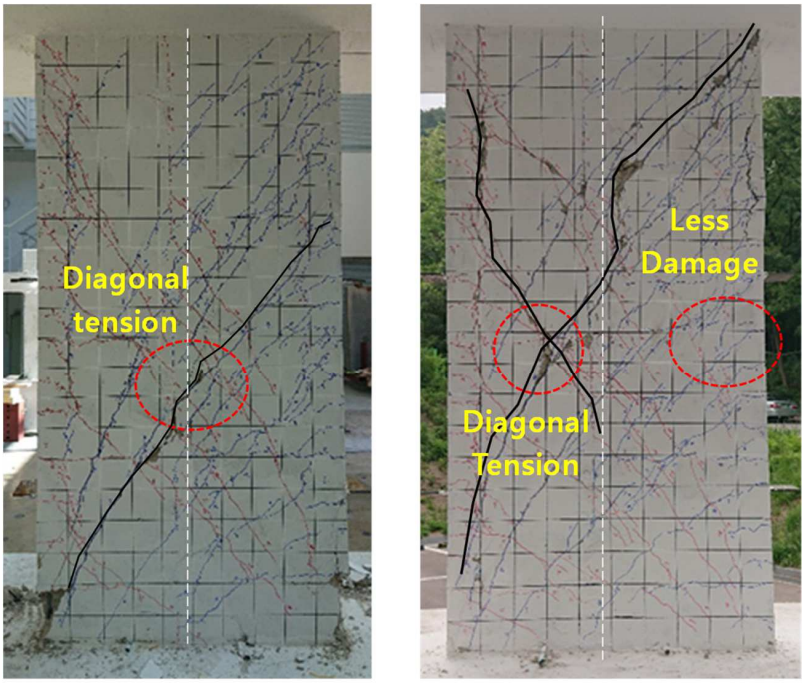

Fig. 3-12 Damage mode of combined rebar grade specimens

(CS2C, and CS2C-AH)

Table 3-4 Test results of flexural yielding mode specimens

Specimens	Wall dimension ($h_w \times l_w$) [mm × mm]	Tested strength V_{test} [kN]		Predicted strength V_{pred} [kN]	V_{test} / V_{pred}		Design failure Mode	Actual failure Mode
		Pos (+)	Neg (-)		Pos (+)	Neg (-)		
NF2H-30	1000 × 2000	650	634	622	1.05	1.02	FY	FY+CC+WC
HF2H-30		659	669	643	1.02	1.04	FY	FY+CC+VS
HF2R		81	95	79	1.03	1.20	FY	FY+TF
HF2R-AB		189	173	173	1.09	1.00	FY	FY+DT+WC

Notes: **FY** = flexural yielding mode, **CC** = concrete crushing mode, **VS** = vertical splitting mode, **TF** = tensile fracture of vertical bar mode, **WC** = web crushing failure mode, **DT** = Diagonal tension failure mode.

Table 3-5 Test results of shear failure mode specimens

Specimens	Wall dimension ($h_w \times l_w$) [mm × mm]	Tested strength V_{test} [kN]		Predicted strength V_{pred} [kN]	V_{test} / V_{pred}		Design failure Mode	Actual failure Mode
		Pos (+)	Neg (-)		Pos (+)	Neg (-)		
NS2H-30	1000 × 2000	829	694	580	1.43	1.20	WC	DT
HS2H-30		749	715	600	1.23	1.19	WC	DT
HS2H		708	706	506	1.40	1.40	WC	DT+WC
HS2R		347	347	325	1.07	1.07	DT	DT
HS2M		541	503	459	1.18	1.10	DT	DT
NS2M		450	475	352	1.28	1.35	DT	DT
CS2C		476	495	473	1.01	1.05	WC	DT
CS2C-AH		553	638	617	0.90	1.03	WC	DT
NS1H-30	1000 × 1000	991	862	572	1.73	1.51	WC	DT+WC
HS1H-30		889	761	592	1.50	1.29	WC	DT+WC
HS1H		780	604	503	1.55	1.20	WC	DT+WC

Notes: **WC** = web crushing failure mode, **DT** = Diagonal tension failure mode.

3.4.2 Lateral load- displacement relationships

Fig. 3-13 to Fig. 3-15 show the lateral load − displacement (lateral drift ratio) relationships of the test specimens. The lateral drift ratio δ indicates the net lateral displacement divided by the net wall height (H = 2250 mm for the specimens with aspect ratio = 2.0, H = 1250 mm for the specimens with aspect ratio = 1.0). The net lateral displacement (L1−L2) indicates the difference between the lateral displacements measured at the loading beam (L1) and the foundation slab (L2). The wall height H refers to the distance from the bottom of the wall to the lateral displacement measurement point.

Fig. 3-13 to Fig. 3-15 also show the nominal flexural strength V_f and shear strength V_n ($\leq V_{nmax}$, V_{nmax} = web crushing strength) predicted by ACI 318-19. In the calculation of nominal strength, the actual material strengths in Table 3-1 to Table 3-3 were used. In all specimens, the maximum tested strength V_{test} reached the predicted strength (V_{pred} = min(V_f, V_n)). This result indicates that the current design code is valid for the walls with Grade 700 MPa high-strength bar.

Fig. 3-13 shows the load-displacement relationships of flexural yielding mode specimens. In flexural mode specimen **NF2H-30** with Grade 400 D16 bars (f_y = 470 MPa, ρ_{hw} = 0.66 %, ρ_{vw} = 1.99 %), the peak strength occurred at the drift ratio of +1.49 and -1.41 %. The peak strength V_{test} was +650 and -634 kN in the positive and negative loading directions, respectively, which were 1.11 and 1.09 times the nominal flexural strength V_f = 584 kN predicted by sectional analysis (Fig. 3-13 (a)). After the peak strength, the load-carrying capacity decreased due to buckling of the vertical bars in the web. The ultimate drift ratio was δ_u = -2.0 %.

In flexural mode specimen **HF2H-30** with Grade 700 MPa rebars (f_y = 770 MPa, ρ_{hw} = 0.42 %, ρ_{vw} = 1.27 %), the peak strength occurred at the drift ratio of +1.52 and -1.45 %. The peak strength V_{test} was +659 and -669 kN, which were 1.13 and 1.15 times the nominal flexural strength V_f = 582 kN (Fig. 3-13 (b)). After the peak strength, the load-carrying capacity gradually decreased due to vertical splitting that occurred at the interface between the boundary element and the web. The ultimate drift ratio was δ_u = -2.0 %.

In flexural mode specimen **HF2R** (ρ_h = 0.14 %, ρ_v = 0.12 %, ρ_{vb} = 0.63 %, and V_f = 0.5V_c), because of the significantly low vertical bar ratio, the premature bar fracture occurred at the base of the wall. As a result, asymmetric structural behavior occurred, and the peak strength occurred at the drift ratio of +0.58 and -1.47 %. The peak strength V_{test} was +81.3 and -95.1 kN in the positive and negative loading directions, respectively, which were 1.03 and 1.20 times the nominal flexural strength V_f = 79.0 kN predicted by sectional analysis (Fig. 3-13 (c)). Immediately after the peak strength, the load-carrying capacity significantly decreased due to fracture of vertical bars in the boundary element. The ultimate drift ratio was δ_u = -1.47 %.

In flexural mode specimen **HF2R-AB** (ρ_h = 0.14 %, ρ_v = 0.12 %, ρ_{vb} = 2.08 %, and V_f = 1.0V_c), the peak strength occurred at the drift ratio of +2.84 and -2.00 %. The peak strength V_{test} was +189 and -173 kN, which were 1.15 and 1.05 times the nominal flexural strength V_f = 164 kN (Fig. 3-13 (d)). After the peak strength, in negative loading direction, the load-carrying capacity gradually decreased due to web crushing in the plastic hinge zone. The ultimate drift ratio was δ_u = 3.0 %.

Fig. 3-14 shows the load-displacement relationships of shear failure mode specimens with high shear reinforcement ratio. In **NS2H-30** with Grade 400 MPa rebars (f_y = 470 MPa, ρ_{hw} = 0.66 %, ρ_{vw} = 1.99 %), the peak strength V_{test} was +829 and -694 kN (at δ = +1.28 % and -1.02 %), which were 1.43 and 1.20 times the

nominal shear strength V_n = 580 kN (Fig. 3-14 (a)). Immediately after the peak strength, the load-carrying capacity significantly decreased and the diagonal crack width increased.

In shear failure mode specimen **HS2H-30** with Grade 700 MPa bars (f_y = 770 MPa, ρ_{hw} = 0.42 %, ρ_{vw} = 1.27 %), the peak strength occurred earlier at the drift ratio of +1.17 and -1.00 % than those of **NS2H-30**. The peak strength was V_{test} = +749 and -715 kN and the strength ratio was V_{test}/V_n = 1.23 and 1.19 (V_n = 600 kN) (Fig. 3-14 (b)). The load-carrying capacity significantly decreased immediately after the peak strength. Comparing the results of **NS2H-30** and **HS2H-30**, the peak strength of **HS2H-30** with 700 MPa bars was 10 percent lower than that of **NS2H-30** with 400 MPa bars. Because of the increased bar strength, the reinforcement ratio of **HS2H-30** was less than that of **NS2H-30**. Thus, concrete cracking initiated in a lower lateral deformation and the crack width increased, which resulted in the lower peak strength of **HS2H-30**.–

In shear failure specimen **HS2H** with Grade 700 MPa reinforcement (f_y = 770 MPa, ρ_{hw} = 0.42 %, ρ_{vw} = 1.27 %) and no axial load, the initial stiffness was less than that of **HS2H-30** with axial loading. The peak strength occurred at the drift ratio of +1.44 and -1.45 %. The peak strength was V_{test} = +708 and -706 kN and the strength ratio was V_{test}/V_n = 1.40 and 1.40 (V_n = 506 kN) (Fig. 3-14 (c)). After the peak strength, the load carrying capacity gradually degraded. The peak strength of **HS2H** were not significantly less than those of **HS2H-30** and **NS2H-30**. This result indicates that the effect of axial load on the shear strength was not significant.

In **NS1H-30** (Grade 400 MPa, h_w/l_w = 1.0), the peak strength V_{test} was +990 and -862 kN, (V_{test}/V_n = 1.73 and 1.50, V_n = 572 kN) at the drift ratio of +0.70 and -1.71 % (Fig. 3-14 (d)). Due to the low aspect ratio, the peak strength and initial stiffness of **NS1H-30** were greater than those of **NS2H-30**.

In **HS1H-30** (Grade 700 MPa, f_y = 770 MPa, ρ_{hw} = 0.42 %, ρ_{vw} = 1.27 %), the peak strength was V_{test} = +889 and -761 kN at the drift ratio of +0.98 and -0.73 %, and the strength ratio was V_{test}/V_n = 1.50 and 1.29 (V_n = 592 kN) (Fig. 3-14 (e)). After the peak strength, the load-carrying capacity decreased as the diagonal tensile crack width significantly increased.

In specimen **HS1H** (Grade 700 MPa), the peak strength was V_{test} = +780 and -604 kN at the drift ratio of +1.27 and -1.18 %, and the strength ratio was V_{test}/V_n = 1.55 and 1.20 (V_n = 503 kN) (Fig. 3-14 (f)). The peak strength of **HS1H** without axial load was less than those of **HS1H-30** and **NS1H-30**.

Fig. 3-15 shows the load-displacement relationships of shear failure mode specimens with low shear reinforcement ratio. In **HS2R** (f_y = 809 MPa, ρ_h = 0.14 %, and ρ_v = 0.12 %), the peak strength V_{test} was +347 and -347 kN (at δ = +1.16 % and -1.00 %), which were 1.07 and 1.07 times the nominal shear strength V_n = 323 kN (Fig. 3-15 (a)). Immediately after the peak strength, the load-carrying capacity decreased and the diagonal crack width increased.

In shear failure mode specimen **HS2M** (f_y = 809 MPa, ρ_h = 0.25 %, and ρ_v = 0.24 %), the peak strength occurred at the drift ratio of +1.50 and -1.37 %. The peak strength was V_{test} = +541 and -503 kN and the strength ratio was V_{test}/V_n = 1.18 and 1.10 (V_n = 459 kN) (Fig. 3-15 (b)). The peak strength of **HS2M** was greater than **HS2R** due to increase of shear reinforcement ratio. The load-carrying capacity significantly decreased due to fracture of horizontal rebar.

In shear failure specimen **NS2M** with 400 MPa bars (f_y = 505 MPa, ρ_h = 0.25 %, and ρ_v = 0.24 %), the peak strength occurred at the drift ratio of +1.50 and -1.49 %. The peak strength was V_{test} = +450 and -474 kN and the strength ratio was V_{test}/V_n = 1.28 and 1.35 (V_n = 352 kN) (Fig. 3-15 (c)). After the peak strength, the load-carrying

capacity significantly decreased due to fracture of horizontal rebar. Compared with **HS2R** and **NS2M**, which had the equivalent effective shear reinforcement ratio ($\rho_h f_y$ = 1.09 MPa in **HS2R** vs 1.26 MPa in **NS2M**), the peak strength of **NS2M** with 400 MPa bars was greater than that of **HS2R** with 700 MPa bars (V_{test} = 347 kN in **HS2R**, and 474 kN in **NS2M**). In **HS2R**, due to decrease of horizontal bar ratio, the crack width increased relatively low lateral drift, and the yielding of horizontal rebars occurred at relatively low lateral drift. Compared with **HS2M** and **NS2M**, which had the same horizontal rebar ratio, the peak strength of **HS2M** was 1.12 − 1.14 times that of **NS2M**, however, safety margin for the nominal strength decreased (V_{test}/V_n = 1.10 − 1.18 in **HS2M**, vs 1.28 − 1.35 in **NS2M**).

Fig. 3-15 also shows the load-displacement relationships of combined bar grade specimens. In **CS2C** (Grade 400 and 700 MPa, f_y = 505 and 809 MPa, ρ_v = 0.27 and 1.24 %, ρ_h = 0.25 and 0.42 %), the peak strength V_{test} was +476 and -495 kN, (V_{test}/V_n = 1.00 and 1.04, V_n = 474 kN) at the drift ratio of +0.95 and -0.94 % (Fig. 3-15 (d)). The peak strength was 1.04 – 1.06 times that of **NS2M**, which had the equivalent vertical and horizontal rebar ratio to those of old wall in **CS2C**.

In **CS2C-AH** (Grade 400 and 700 MPa, f_y = 505 and 809 MPa, ρ_v = 0.27 and 1.24 %, ρ_h = 0.25 and 0.66 %), the peak strength was V_{test} = +638 and -553 kN at the drift ratio of +1.50 and -1.35 %, and the strength ratio was V_{test}/V_n = 1.03 and 0.89 (V_n = 618 kN) (Fig. 3-15 (e)). Comparing **CS2C** and **CS2C-AH**, as the horizontal rebar ratio in the expanded wall increased, the peak strength increased.

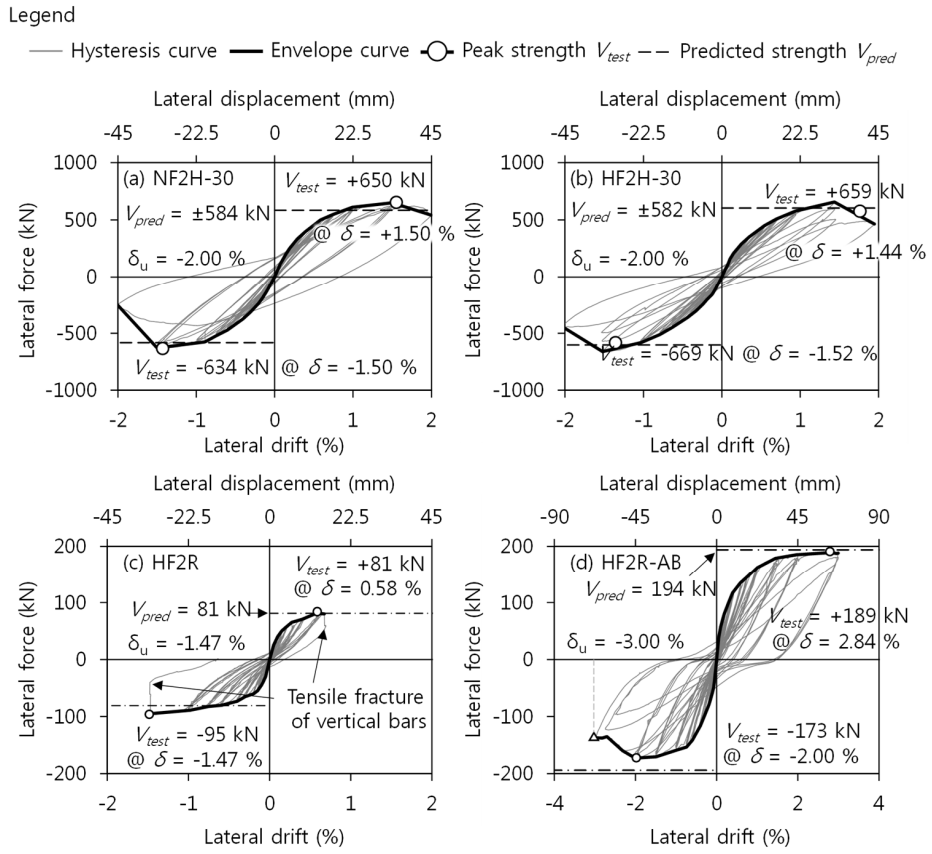

Fig. 3-13 Lateral load-displacement relationships of flexural yielding mode specimens (NF2H-30, HF2H-30, HF2R, and HF2R-AB)

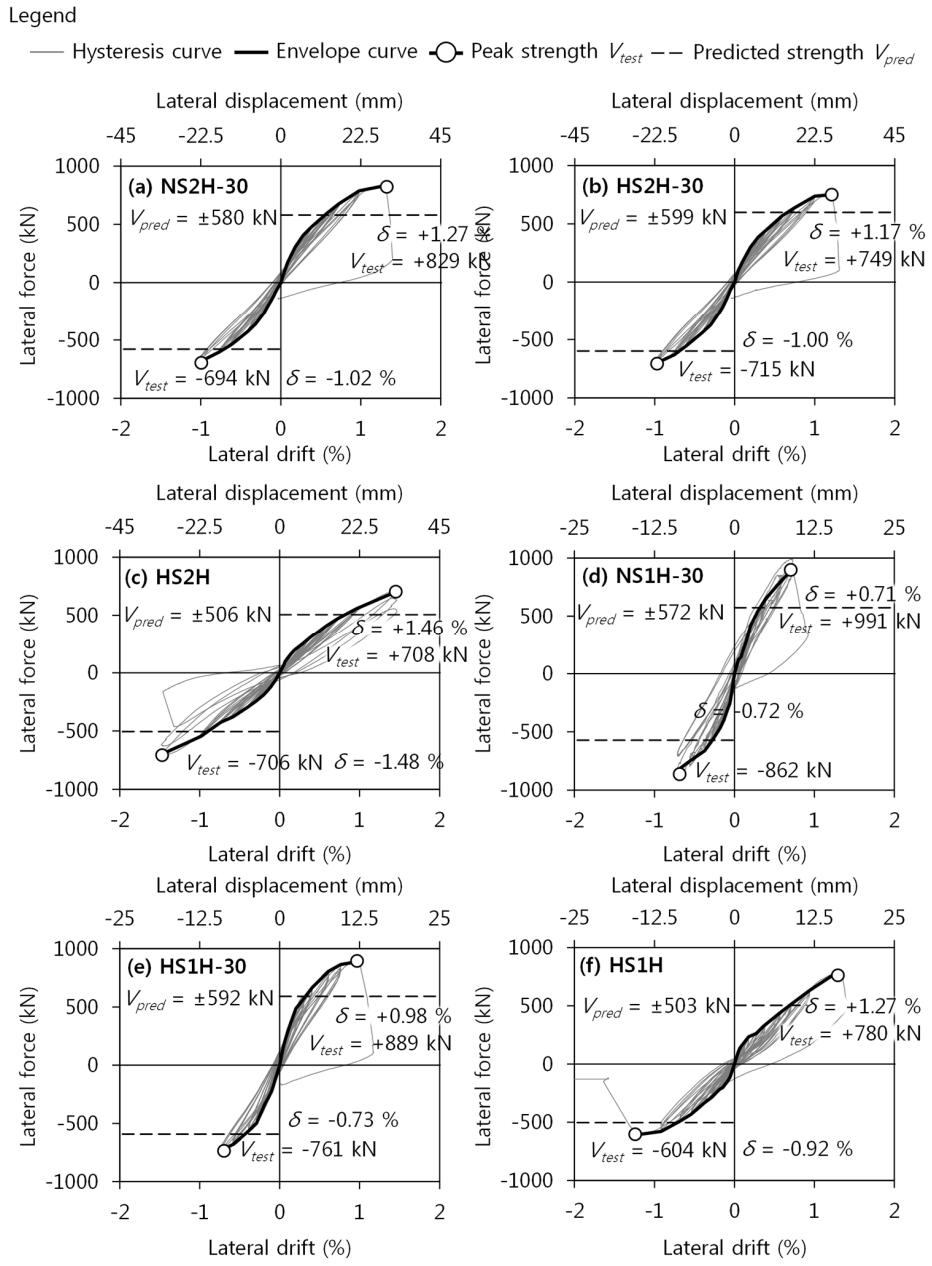

Fig. 3-14 Lateral load-displacement relationships of shear failure mode specimens (NS2H-30, HS2H-30, HS2H, NS1H-30, HS1H-30, and HS1H)

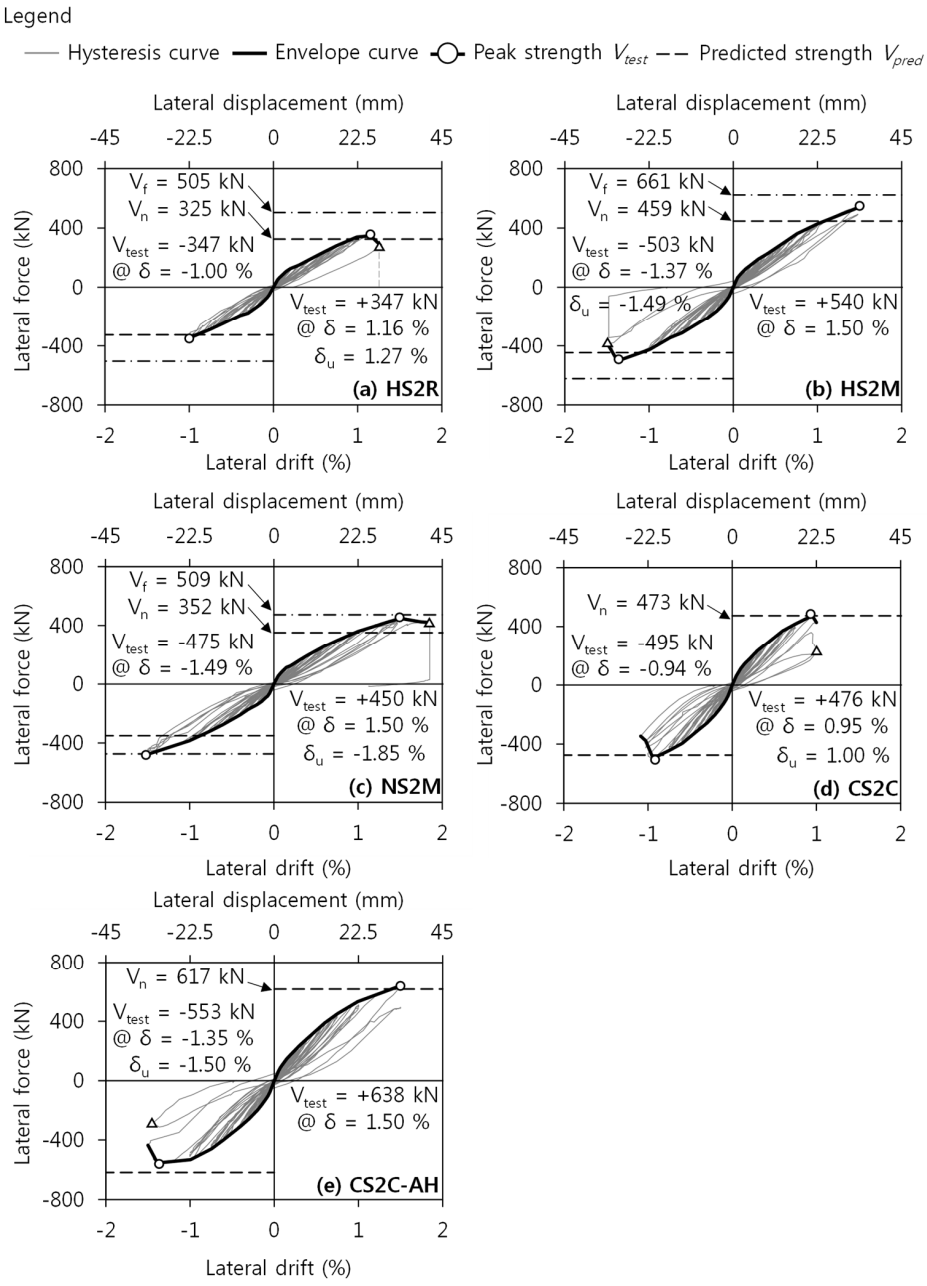

Fig. 3-15 Lateral load-displacement relationships of shear failure mode specimens (HS2R, HS2M, NS2M, CS2C, and CS2C-AH)

3.4.3 Strains of reinforcing bars

Fig. 3-16 to Fig. 3-21 show the strain distributions of the rebars in the wall specimens. In the figures, the strains were measured at lateral drift δ = 0.15, 0.3, 0.6, 1.0, and 1.5 %. The figures also show the locations of the rebars and strain gauges. The vertical bar strains were measured near the wall base, and the horizontal bar strains were measured in the middle of each horizontal rebar. In **CS2C**, and **CS2C-AH** with combined bar grade, strains of horizontal rebars were measured in the center of each wall segments.

In Fig. 3-16, Fig. 3-18, and Fig. 3-20, regardless of the failure modes of the specimens, the strains of vertical bars were linearly distributed under low lateral drift ratios δ = 0.15 – 0.3 % because of the flexural behavior. In the flexural mode specimens (**NF2H-30**, **HF2H-30**, **HF2R**, and **HF2R-AB**), vertical rebars in tension yielded at δ = 1.5 %. On the other hand, in the shear failure specimens (**NS2H-30**, **HS2H-30**, and **HS2H**), vertical rebars in tension did not yield as expected. As the shear crack width increased, the strain of vertical rebars in the web increased. In the shear failure specimen with aspect ratio = 1.0 (**NS1H-30**, **HS1H-30**, and **HS1H**), the vertical rebar strains were relatively small. At δ = 1.5 %, the tensile strain reached the yield strain. In the shear failure specimens with low shear reinforcement ratio (**HS2R**, **HS2M**, and **NS2M**), the tensile strain reached the yield strain. In the specimens with high axial load (**NF2H-30**, **HF2H-30**, **NS2H-30**, **HS2H-30**, and **NS1H-30**), the compressive strain was greater than concrete crushing strain (ε_{co} = 0.002).

As shown in Fig. 3-17, Fig. 3-19, and Fig. 3-21, the maximum horizontal rebar strain occurred in the middle of the wall height. In the flexural yielding mode specimens, both 400 and 700 MPa horizontal rebars did not yield at the peak strength. On the other hand, in the shear failure specimens, the strain of horizontal bars in the

middle of the wall height exceeded the yield strain regardless of the bar yield strength. In the specimens with axial load, the horizontal bar strain was smaller than that of the specimens without axial load. This result is because the crack width was decreased by applied axial load.

In the combined bar grade specimens (**CS2C**, and **CS2C-AH**), strains of horizontal bars in the old wall (Grade 400) were greater than those in the expanded wall (Grade 700). This indicates that the shear strength was limited by the yielding of Grade 400 horizontal bars in the old wall.

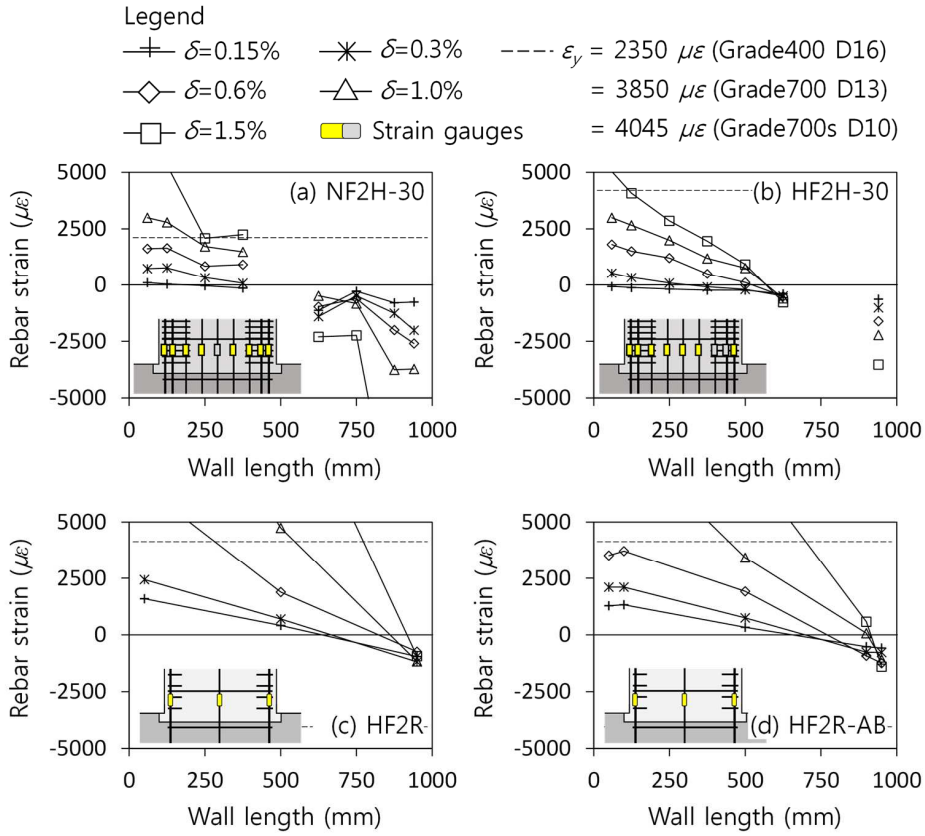

Fig. 3-16 Strain distribution of vertical reinforcement in flexural yielding mode specimens (NF2H-30, HF2H-30, HF2R, and HF2R-AB)

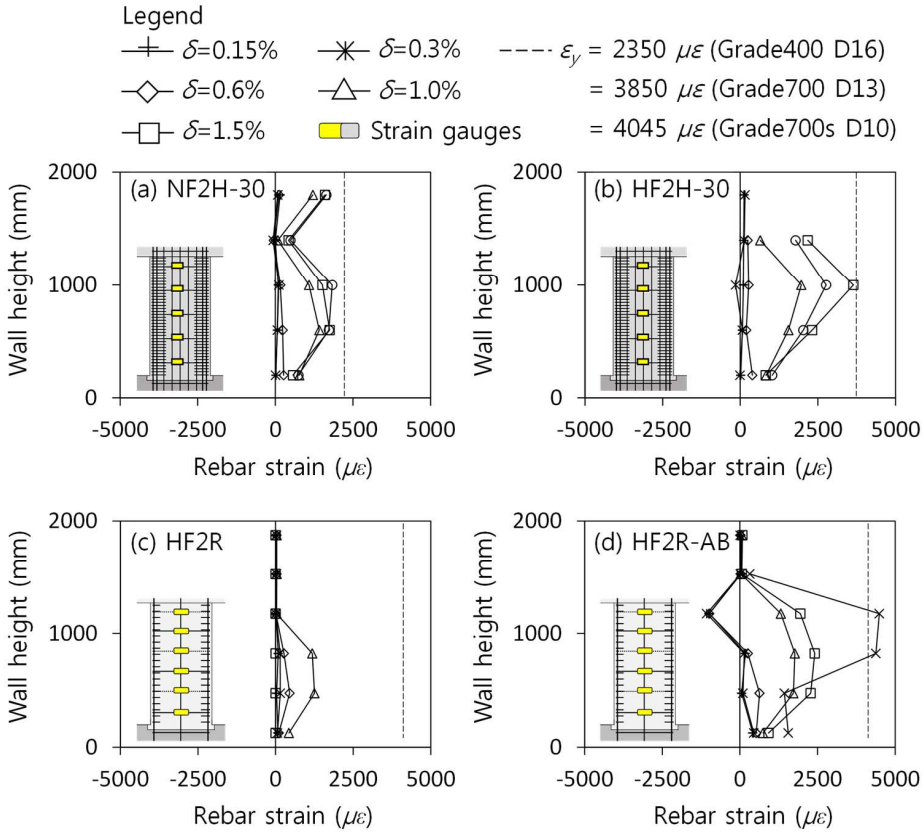

Fig. 3-17 Strain distribution of shear reinforcement in flexural yielding mode specimens (NF2H-30, HF2H-30, HF2R, and HF2R-AB)

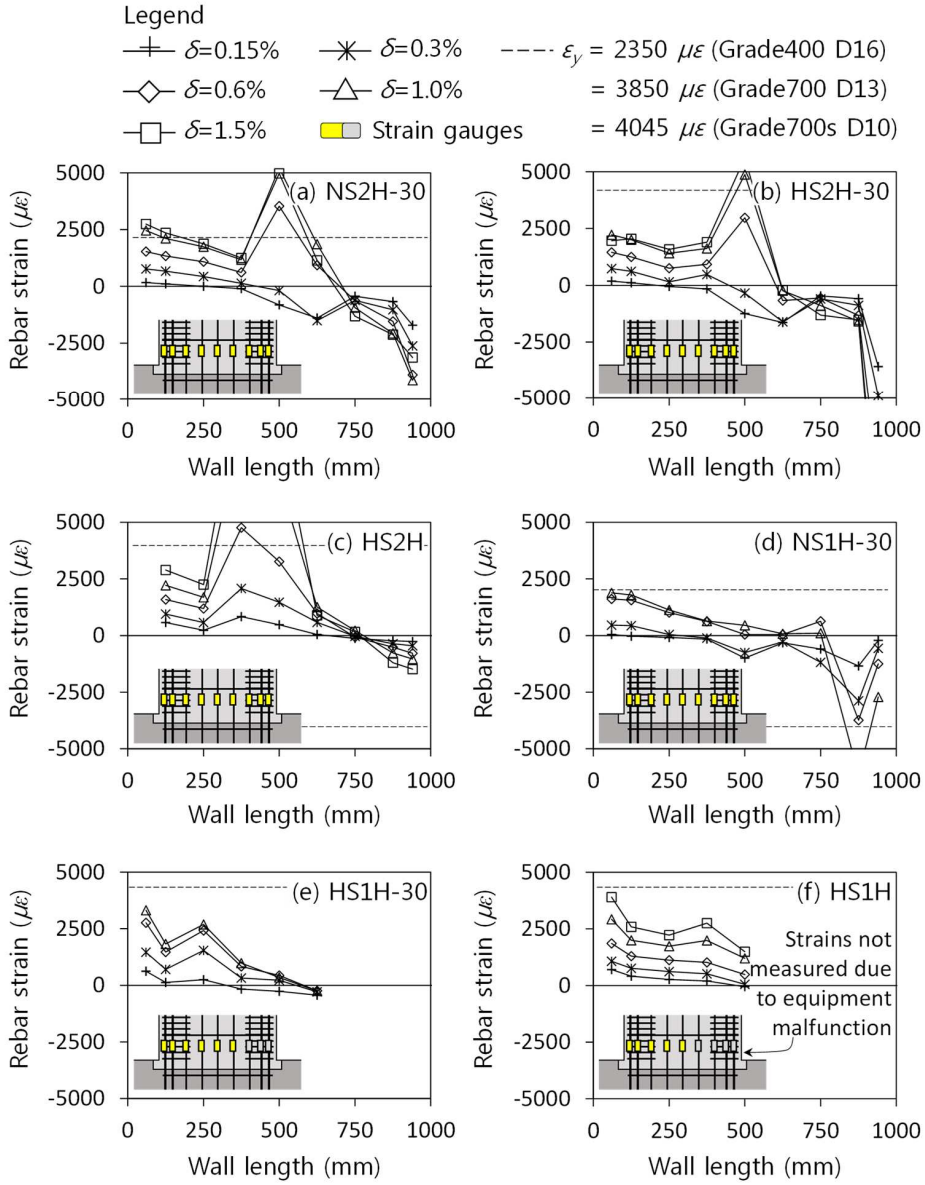

Fig. 3-18 Strain distribution of vertical reinforcement in shear failure mode specimens (NS2H-30, HS2H-30, HS2H, NS1H-30, HS1H-30, and HS1H)

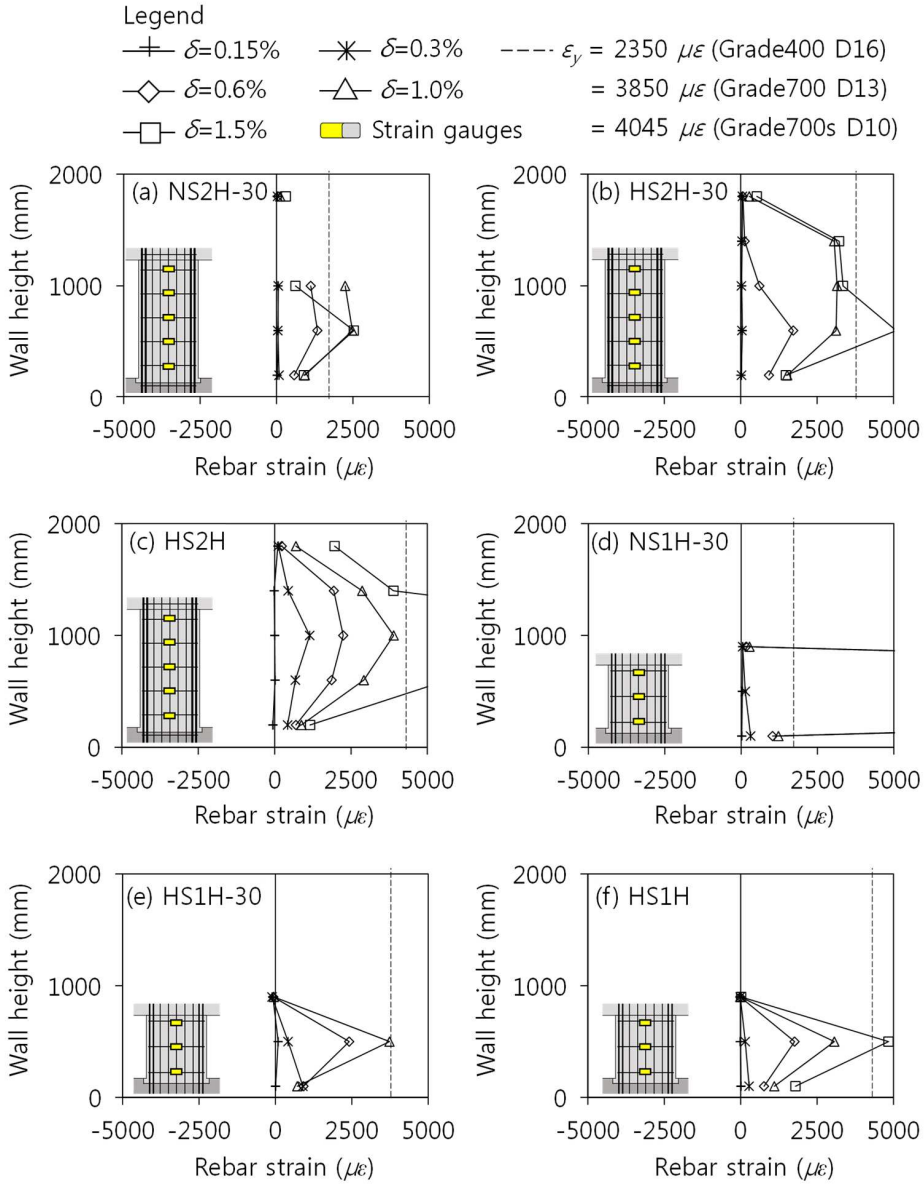

Fig. 3-19 Strain distribution of shear reinforcement in shear failure mode specimens (NS2H-30, HS2H-30, HS2H, NS1H-30, HS1H-30, and HS1H)

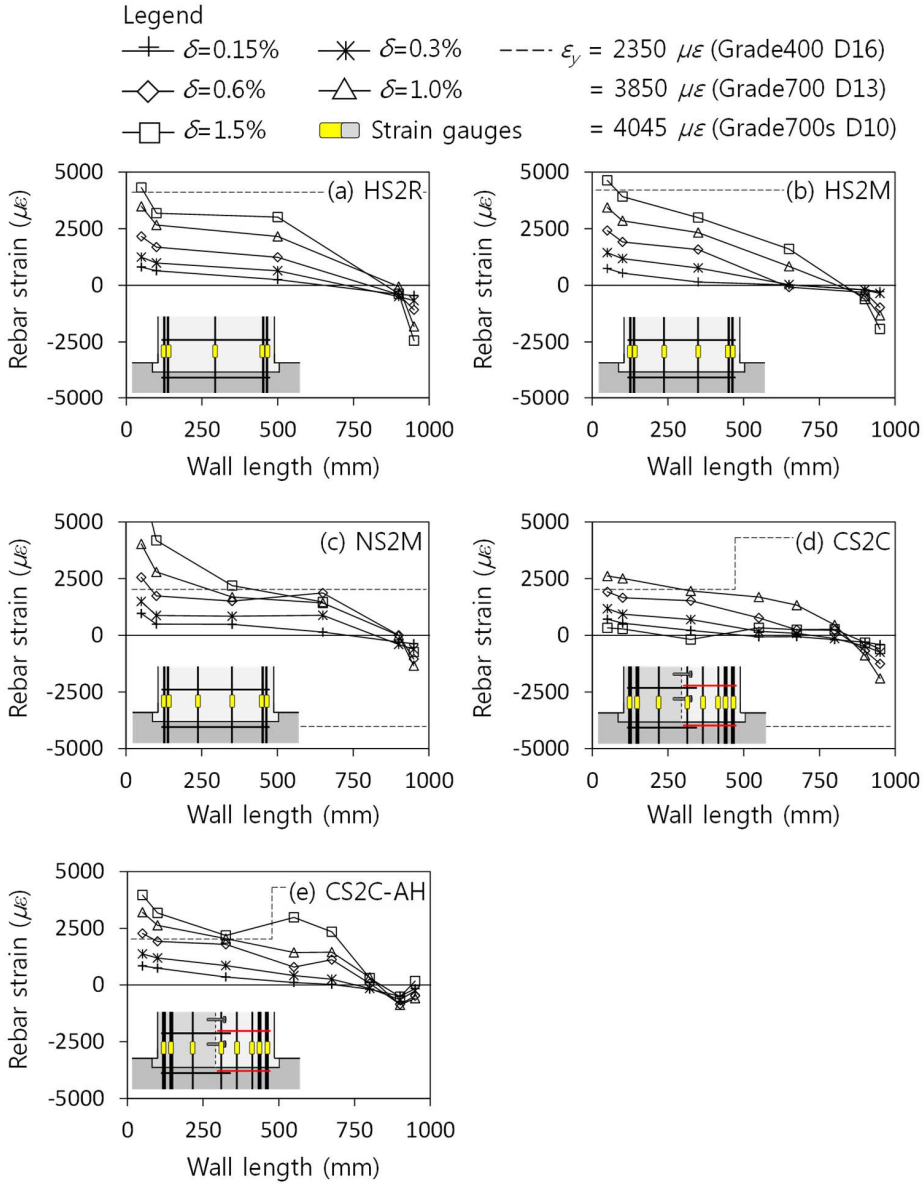

Fig. 3-20 Strain distribution of vertical reinforcement in shear failure mode specimens (HS2R, HS2M, NS2M, CS2C, and CS2C-AH)

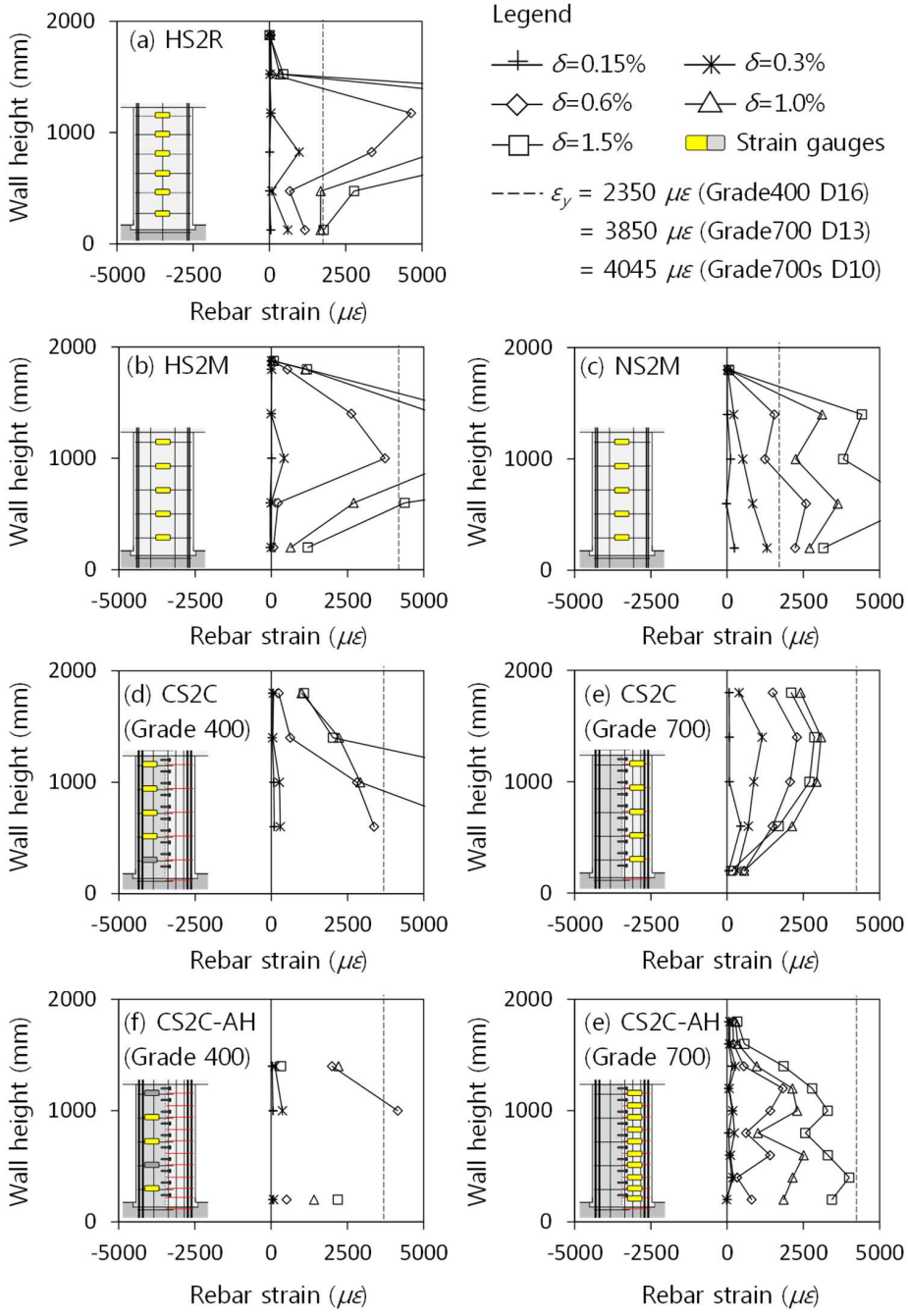

Fig. 3-21 Strain distribution of shear reinforcement in shear failure mode specimens (HS2R, HS2M, NS2M, CS2C, and CS2C-AH)

3.4.4 Contributions of displacement components

Fig. 3-22 to Fig. 3-24 show the contributions of flexural deformation, shear deformation, and wall base slip to total lateral drift. The flexural deformation (circular symbol) was estimated from L4 to L9 (see Fig. 3-6) which measured the vertical deformations in three segments of the wall edge. The average curvature of each wall segment was assumed to be uniform. The shear deformation (triangular symbol) was estimated from the diagonal length changes in the wall panel segments (L10 to L13). The wall base slip (rectangular symbol) was measured at the wall-foundation interface (L15). The overall drift (diamond symbol) was defined as the sum of the contributions of the displacement components. The horizontal dotted line indicates the measured lateral drift of each wall specimen. In all specimens, the overall lateral drift is close to the measured lateral drift, except for those at early loading.

When the lateral drift was small, the major displacement component was flexural deformation regardless of the failure mode and aspect ratio. Particularly in **HF2R**, due to significantly low vertical rebar ratio, the majority of inelastic deformation occurred at the wall base, and the contribution of shear deformation was significantly low. However, as the lateral drift increased, the contribution of shear deformation gradually increased. In particular in the shear failure specimens, the contribution of shear deformation was close to that of flexural deformation. Even in **HF2H-30** with flexural mode, the contribution of shear deformation exceeded that of flexural deformation. This result is attributed to the vertical splitting cracks that occurred at the interface between the web wall and the boundary element after flexural yielding. In all specimen, the contribution of base slip was negligible (0.6 − 3.5 % of the overall lateral drift).

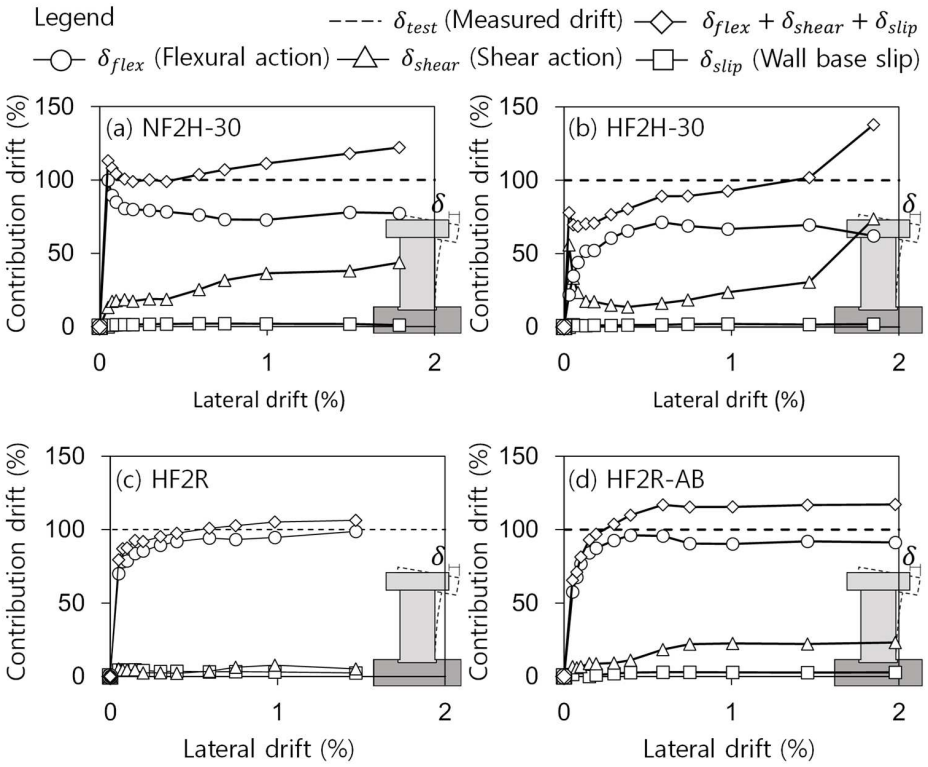

Fig. 3-22 Contributions of deformation components to overall drift

(NF2H-30, HF2H-30, HF2R, and HF2R-AB)

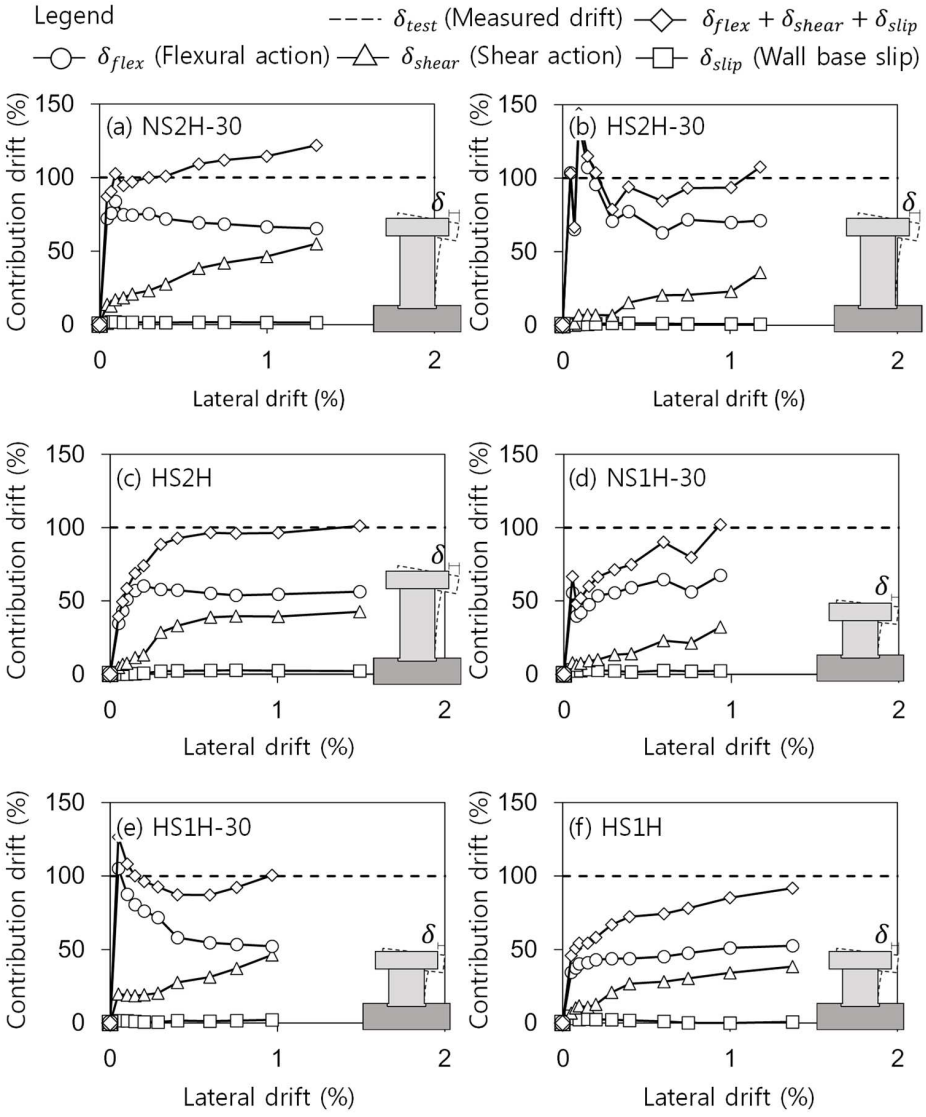

Fig. 3-23 Contributions of deformation components to overall drift

(NS2H-30, HS2H-30, HS2H, NS1H-30, HS1H-30, and HS1H)

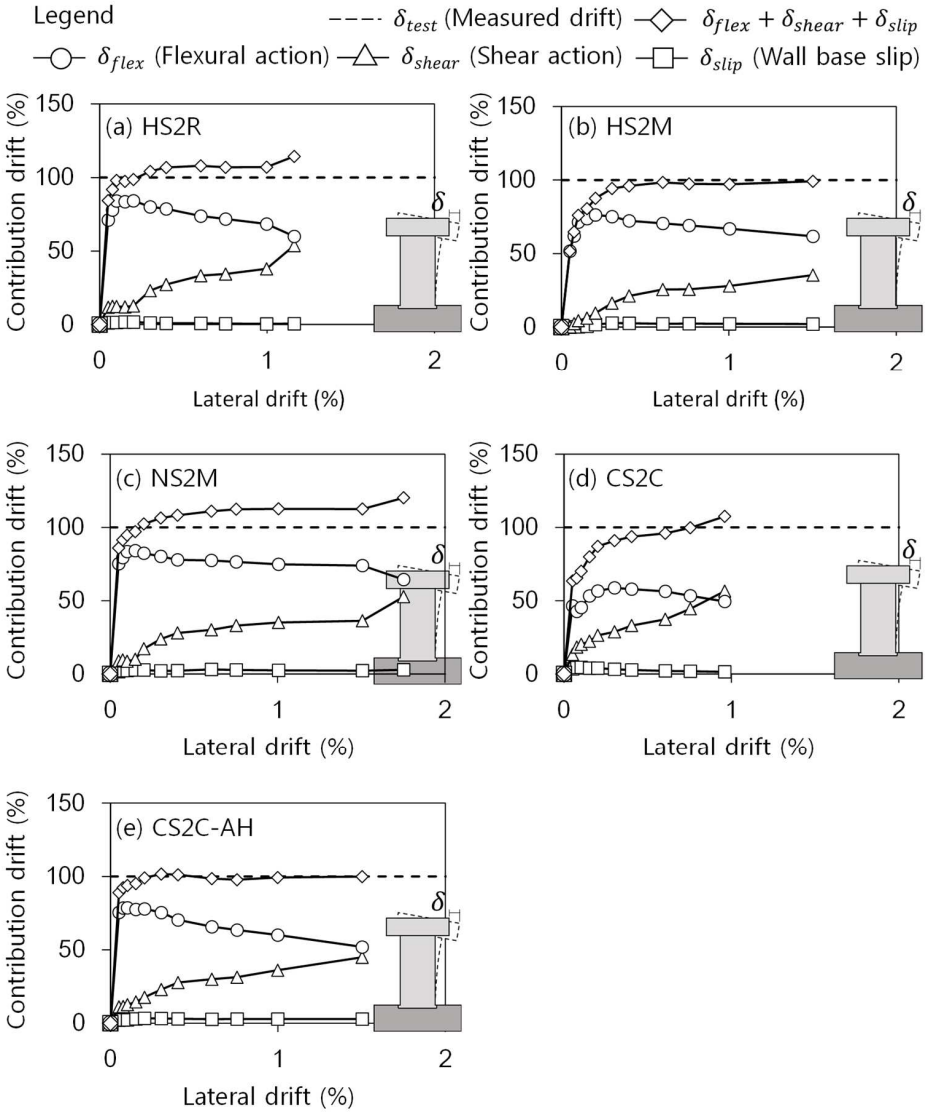

Fig. 3-24 Contributions of deformation components to overall drift

(HS2R, HS2M, NS2M, CS2C, and CS2C-AH)

3.4.5 Average crack width

Fig. 3-25 to Fig. 3-28 show the average crack width of the test specimens. The average crack width was estimated as measured vertical or diagonal deformation divided by the number of cracks crossing the deformation measurement interval.

Fig. 3-25 shows average crack widths of the flexural yielding mode specimens (**NF2H-30**, **HF2H-30**, **HF2R**, and **HF2R-AB**). In **HF2H-30**, the vertical and horizontal reinforcement ratios were less than those of **NF2H-30**, because of the high yield strength of rebar. For the reason, when the lateral drift ratio was 1% or less, the flexural crack width of **HF2H-30** was greater than that of **NF2H-30**. However, after the lateral drift of 1.5% (after the peak strength occurred), the flexural crack width of **HF2H-30** was similar to that of **NF2H-30**. The shear crack width of **HF2H-30** was greater than that of **NF2H-30**. In **HF2R**, due to significantly low vertical rebar ratio, the average width of flexural crack was the greatest**.** The average width of diagonal shear crack was the greatest in **HF2R-AB** due to the web crushing in the plastic hinge zone after flexural yielding.

Fig. 3-26 shows average crack widths of the shear failure mode specimens with aspect ratio = 2.0. At the same lateral drift ratio, the average diagonal shear crack width was the greatest in **HS2R** with the lowest shear reinforcement ratio (ρ_h = 0.14 %). When comparing **NS2H-30** and **HS2H-30**, shear crack width was greater in HS2H-30 with high-strength rebar because of the lower horizontal bar ratio. When comparing **HS2H-30** and **HS2H**, the shear crack width was less in HS2H-30 subjected to axial load. Fig. 3-27 shows the crack width of shear failure mode specimens with aspect ratio = 1.0. The crack width was the least in NS2H-30, because of greater reinforcement ratio.

Fig. 3-28 shows the average crack width of **CS2C**, and **CS2C-AH**. At the same

lateral drift, the average flexural crack width was similar. On the other hand, because the horizontal reinforcement ratio in the expanded wall was increased, the average diagonal shear crack width was greater in **CS2C-AH**.

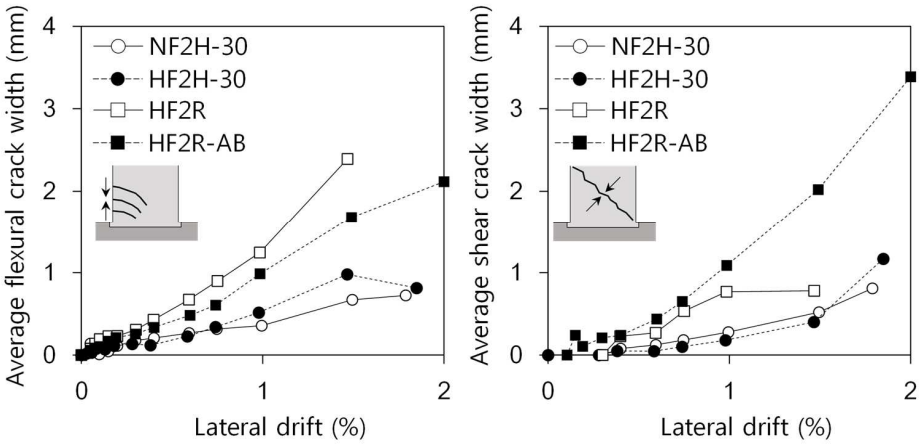

Fig. 3-25 Average crack width of flexural yielding mode specimens

(NF2H-30, HF2H-30, HF2R, and HF2R-AB)

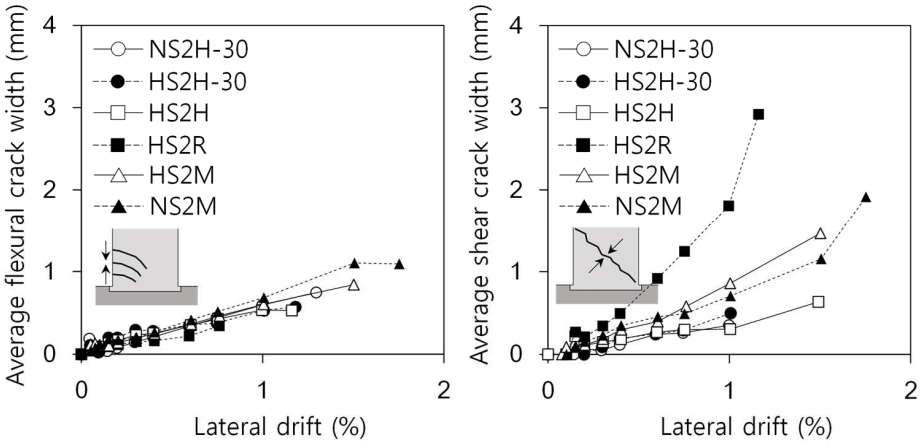

Fig. 3-26 Average crack width of shear failure mode specimens with h_w/l_w = 2.0

(NS2H-30, HS2H-30, HS2H, HS2R, HS2M, and NS2M)

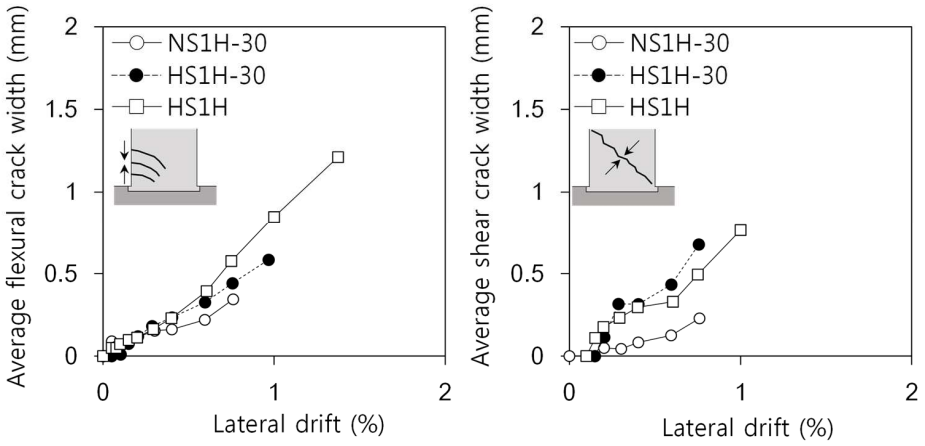

Fig. 3-27 Average crack width of shear failure mode specimens with h_w/l_w = 1.0 (NS1H-30, HS1H-30, and HS1H)

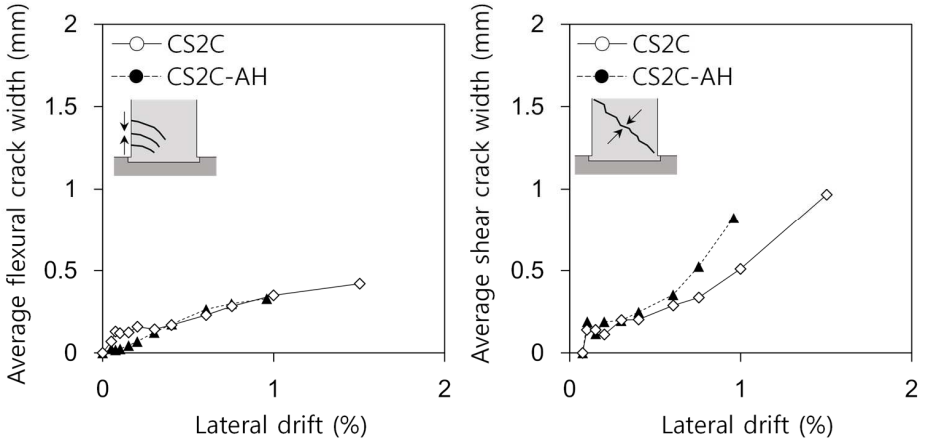

Fig. 3-28 Average crack width of combined bar grade specimens (CS2C, and CS2C-AH)

3.4.6 Energy dissipation and drift ductility ratio

The energy dissipation and drift ductility ratio are the major index to determine the earthquake resistance of RC shear walls. The mechanical properties of 700 MPa reinforcement, such as high yield strain, and decrease in reinforcement ratio, can affect the energy dissipation and drift ductility. Fig. 3-29 compares the load−displacement envelope curves and hysteretic energy dissipation of the flexural yielding mode specimens. From the envelope curve in Fig. 3-29 (a), the lateral ductility ratio μ ($=\delta_u/\delta_y$) was calculated. The yield lateral drift ratio δ_y was determined from an equivalent elasto-plastic curve with secant stiffness at 75 % of the peak strength V_{test}. δ_u indicates the failure drift ratio of the test specimen.

The energy dissipation was defined as the area enclosed by a loading cycle in the load-displacement hysteretic curve (see Fig. 3-29 (b)). The energy dissipation of loading cycle is calculated as follows:

$$E_d = \sum_{i=2}^{N} \frac{(F_i + F_{i-1})}{2} (\Delta_i - \Delta_{i-1}) \quad (3\text{-}1)$$

Where, F_i and $F_{i\text{-}1}$ = i^{th} and i–1 $^{\text{th}}$ force components, Δ_i and $\Delta_{i\text{-}1}$ = i^{th} and i–1 $^{\text{th}}$ displacement components, and N = total number of components included in the loading cycle.

In Eq. (3-1), the equation in the series function indicates the trapezoidal area consisting of the i^{th} and i–1 $^{\text{th}}$ force-displacements. The energy increases in loading phase, due to $(F_i + F_{i\text{-}1})/2 > 0$, and $(\Delta_i - \Delta_{i\text{-}1}) > 0$. On the other hand, in unloading phase, the energy decreases, due to $(F_i + F_{i\text{-}1}) > 0$, $(\Delta_i - \Delta_{i\text{-}1}) < 0$.

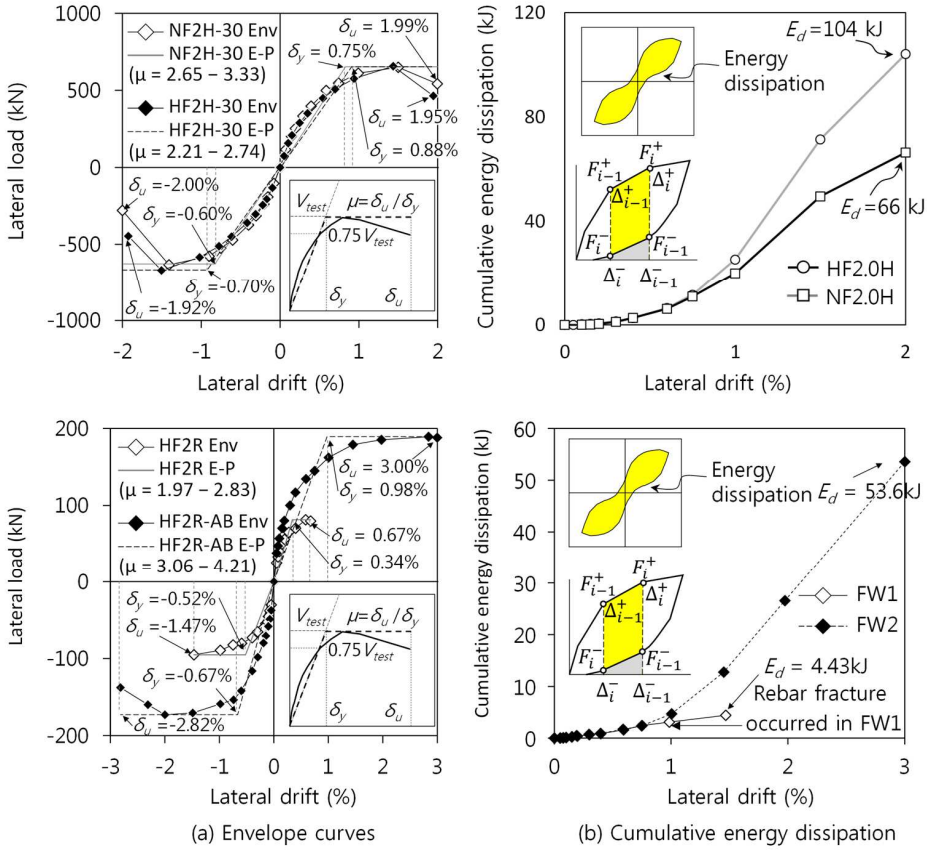

Fig. 3-29 Energy dissipation and drift ductility ratio of flexural yielding specimens

In **HF2H-30** with 700 MPa rebars, because of the lower vertical bar ratio, the initial stiffness the yield drift ratio δ_y was greater than that of **NF2H-30** with 400 MPa rebars (δ_y = +0.75 and -0.60 % in **NF2H-30** vs δ_y = +0.88 and -0.70 % in **HF2H-30**). The ductility ratio μ of **HF2H-30** (μ = 2.21 – 2.74) was also less than that of **NF2H-30** (μ = 2.65 – 3.33). In **HF2R**, the yield lateral drift ratios were δ_y = +0.34 and -0.52 %, the ultimate lateral drift ratios were δ_u = +0.67 and -1.47 %, and the ductility ratios were μ = 1.97 and 2.83. In **HF2R-AB**, δ_y = +0.98 and -0.67 %, δ_u = +3.00 and -2.82 %, and μ = 3.06 and 4.21. In **HF2R**, the drift ductility ratio was limited by unintended premature tensile fracture of vertical rebars.

In Fig. 3-29 (b), the energy dissipation of **HF2H-30** was 0.63 times that of **NF2H-30** (104 kJ in **NF2H-30** vs 66 kJ in **HF2H-30**). The yield strain of 700 MPa bar was much greater than that of 400 MPa bar (ε_y = 0.00385 vs 0.00235). Thus, at the same deformation, the plastic strain of 700 MPa bar was less than that of 400 MPa bar, and the area of 700 MPa bar was less. For this reason, energy dissipated by the flexural rebars was less in the wall with 700 MPa bar. The energy dissipation of **HF2R-AB** was less than that of **HF2H-30** due to smaller total area of vertical rebars. The energy dissipation of **HF2R** was limited by premature tensile fracture.

Table 3-6 shows the summary of effect of bar grade on the wall behavior. Flexural yielding mode specimens, **NF2H-30**, **HF2H**, and **HF2R-AB** are compared. **NF2H-30** used normal grade 400 for vertical reinforcement (f_y = 495 MPa, f_t = 604 MPa, yield ratio f_t/f_y = 1.22). **HF2H-30** used normal grade 700 for vertical reinforcement (f_y = 762 MPa, f_t = 847 MPa, yield ratio f_t/f_y = 1.11). For normal grade rebar, 700 grade bar showed less yield ratio than 400 grade bar. This is because the 700 grade bar has ambiguous yield point, and yield plateau. **HF2R-AB** used seismic grade 700 for vertical reinforcement (f_y = 707 MPa, f_t = 935 MPa, yield ratio f_t/f_y = 1.32). The yield ratio of seismic grade rebar should be greater than 1.25.

As the yield ratio increases, the strength ratio V_{test}/V_f increases, but not significantly. However, the effect of yield ratio on the ductility ratio and energy dissipation is significant. The ductility ratio increases in the order of **HF2H-30**, **NF2H-30**, and **HF2R-AB** (2.21 – 2.74 < 2.65 – 3.33 < 3.06 – 4.21, respectively). Further, the normalized energy dissipation increases as the yield ratio increases. The normalized energy dissipation is defined as a ratio between total cyclic energy dissipation to energy dissipation of equivalent elasto-plastic monotonic curve.

Table 3-6 Summary of effect of bar grade on the test results

Specimen	Vertical reinforcement				Test results		
	Rebar Grade	Yield strength f_y (MPa)	Tensile strength f_t (MPa)	Yield ratio f_t/f_y	Strength ratio V_{test}/V_f	Ductility ratio $\mu = \delta/\delta_y$	Normalized energy E_d/E_0
NF2H-30	400	495	604	1.22	1.05	2.65 – 3.33	1.36
HF2H-30	700	762	847	1.11	1.04	2.21 – 2.74	0.96
HF2R-AB	700s	707	935	1.32	1.09	3.06 – 4.21	1.58

3.5 Shear strength predictions of existing methods

3.5.1 Predictions of existing methods

Table 3-7 shows the test strength V_{test}, and shear strength predictions V_n of KCI 2017 (KCI), ACI 318-19 seismic provision (ACI), Eurocode 8 (EC8), and Gulec & Whittaker (Gulec). To calculate the shear strength of Eurocode 8, the angle of concrete strut θ was assumed as 45 degree. For calculation of all strength predictions, the actual yield strength of the rebar was used in Table 3-3. To verify the applicability of 700 MPa re-bar, the maximum shear strength (i.e. concrete web crushing strength) was not considered.

In the shear design of rectangular wall specified in KCI 2017, effects of aspect ratio and axial load are considered. In conditions of high axial load and aspect ratio = 1.0, the strength prediction is well matched with the tested shear strength. However, without axial load, the strength prediction underestimate the test results (Mean = 1.46, Coefficient of variation (CoV) = 0.19). In the case of ACI 318-19 seismic provision (section 18.10.4), the concrete shear strength of the wall is related to aspect ratio. The strength predictions of ACI 318-19 were better than the other design codes (Mean = 1.22, Coefficient of variation (CoV) = 0.10). On the other hand, Eurocode 8 significantly underestimated the test strength of slender wall ($h_w/l_w \geq 2.0$), not including concrete contribution (Mean = 2.34, Coefficient of variation (CoV) = 0.30). Gulec & Whittaker developed a shear strength equation using statistical optimization on existing wall test data. This equation showed the best predictions regardless of design parameters (Mean = 1.06, Coefficient of variation (CoV) = 0.14).

Table 3-7 Shear strength predictions for test specimens

Specimens	Tested strength V_{test} [kN]	Shear strength predictions				Strength ratio V_{test}/V_{pred}			
		V_{KCI} [kN]	V_{ACI} [kN]	V_{EC8} [kN]	V_{Gulec} [kN]	V_{test}/V_{KCI}	V_{test}/V_{ACI}	V_{test}/V_{EC8}	V_{test}/V_{Gulec}
NS2H-30	829	600	617	373	750	1.38	1.34	2.22	1.11
HS2H-30	749	617	639	304	750	1.21	1.17	2.46	1.00
HS2H	708	468	639	304	750	1.51	1.11	2.33	0.94
NS1H-30	991	840	689	697	737	1.18	1.44	1.42	1.35
HS1H-30	889	857	710	610	737	1.04	1.25	1.46	1.21
HS1H	780	521	710	484	737	1.50	1.10	1.61	1.06
HS2R	347	216	325	101	433	1.61	1.07	3.44	0.80
HS2M	541	323	459	180	554	1.68	1.18	3.01	0.98
NS2M	475	235	352	152	442	2.02	1.35	3.14	1.08
					Mean	1.46	1.22	2.34	1.06
					Std	0.28	0.12	0.71	0.15
					CoV	0.19	0.10	0.30	0.14

3.5.2 Strength and deformation predictions by compression zone failure mechanism model

The compression zone failure mechanism model developed by Park et al. was used to predict the shear strength and deformation capacity of RC walls with or without flexural yielding. Originally, the model was developed for beams. In the present study, the model was applied to walls. The detailed calculations of the compression zone failure mechanism model presents in Chapter 2. Fig. 3-30 and Fig. 3-31 compares the predicted behavior and the test results of the present wall specimens. In the strain-based model, the predicted behavior is defined as the ascending branch of flexural capacity, shear strength at the intersection between the flexural capacity and shear capacity curves, and the descending branch of degraded shear capacity. By using the strain-based model, the deformation capacity, as well as the shear strength, of the test specimens were predicted with reasonable precision.

In the flexural yielding mode specimens (**NF2H-30** and **HF2H-30**), the boundary elements were confined by transverse reinforcement with a spacing of 50 mm. Therefore, in the calculation of moment−curvature relationship, the concrete confinement effect was addressed. As a result, the peak strength V_{test} and lateral drift were accurately predicted in both **NF2H-30** and **HF2H-30** (V_{test}/V_{pred} = 0.98 – 0.99). After the peak strength, the load carrying capacity was decreased by the degradation of shear capacity. However, in the actual test result of **HF2H-30**, the strength degradation was more significant due to vertical cracks between the boundary element and web.

In all shear failure mode specimens (**NS2H-30**, **HS2H-30**, **HS2H**, **NS1H-30**, **HS1H-30**, **HS1H**, **HS2R**, **HS2M**, and **NS2M**) the predicted peak strength and the deformation capacity agree with the tested strengths (V_{test}/V_{pred} = 0.82 – 1.18). The prediction result shows the effects of design parameters. By using 700 MPa bars with

smaller rebar area, the stiffness of the specimen was less than that of walls with 400 MPa bars. Thus, the intersection between flexural demand and shear capacity occurred in a greater deformation. Thus, the strength was less and the deformation was greater than those of walls with 400 MPa bars. For walls subjected to axial force, the compression zone area of concrete increased, which increased the shear strength of the concrete. Thus, the shear strength of the walls increased.

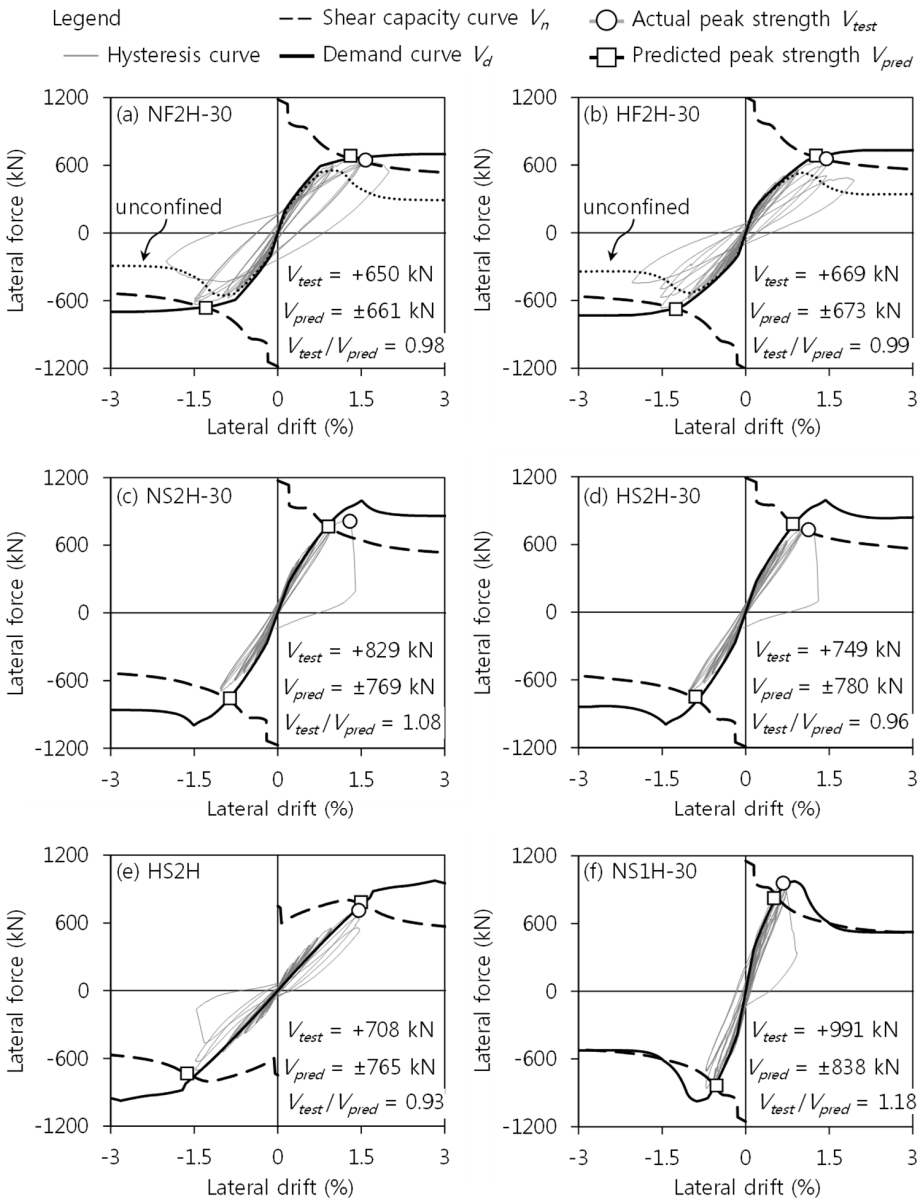

Fig. 3-30 Lateral load-displacement relationship predicted by compression zone failure mechanism model

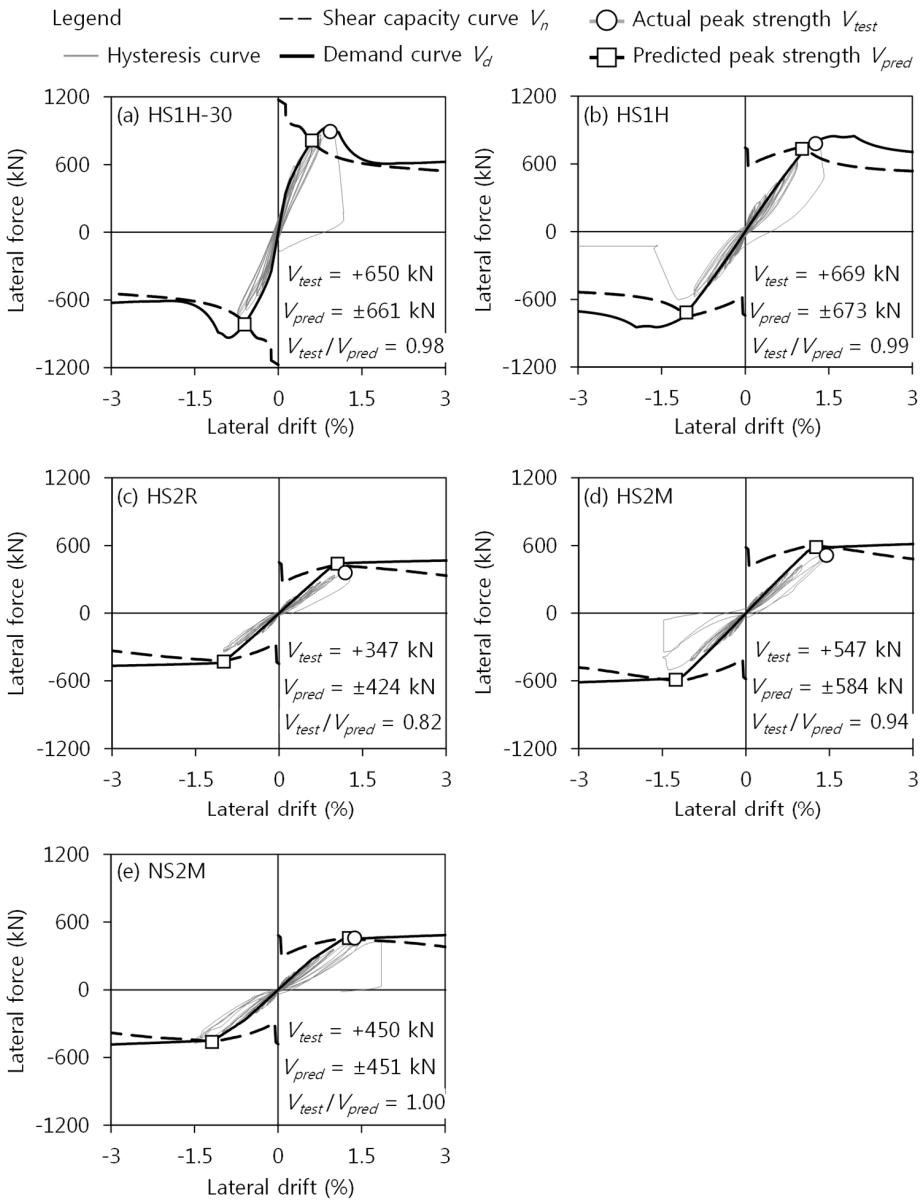

Fig. 3-31 Lateral load-displacement relationship predicted by compression zone failure mechanism model (continued)

3.6 Summary

To investigate the shear strength and deformation capacity of walls with Grade 700 MPa high-strength bars, fifteen wall specimens with aspect ratio 2.0 or 1.0 were tested under cyclic lateral loading. The major results of the present study are summarized as follows:

1) For both flexural specimens with 400 MPa bar or 700 MPa bar, the peak tested strength V_{test} was greater than the nominal flexural strength V_f (V_{test}/V_f = 1.03 ~ 1.20). Comparing **NF2H-30**, and **HF2H-30**, the effect of bar yield strength to flexural strength was not significant. However, ductility of the wall with 700 MPa bar was 17 percent less than that of the wall with 400 MPa bar (2.21 vs 2.65). Further, because of the lower vertical bar ratio of the wall with high-strength bar, energy dissipation was decreased 37 percent (104 kJ vs 66 kJ), and flexural and shear crack widths were increased. In **HF2R**, because of significantly low vertical reinforcement ratio, premature tensile fracture of vertical rebar occurred. As a result, ductility and energy dissipation of **HF2R** were significantly decreased. In **HF2R-AB**, as the lateral drift increased, the web crushing occurred in the plastic hinge zone, because of the significant low shear reinforcement ratio less than the minimum shear reinforcement ratio specified in ACI 318-19. In **HF2R-AB**, the drift ductility ratio was 3.06 – 4.21.

2) Shear failure mode walls with h_w/l_w = 2.0 failed due to diagonal tensile cracking (DT), while the walls with low aspect ratio (h_w/l_w = 1.0) failed in a combined failure mode of diagonal cracking + web crushing. The shear strengths of walls with 700 MPa bar were 10 – 25 percent less than those of walls with 400 MPa bars. In the specimens with 700 MPa shear reinforcement,

yielding occurred in the shear reinforcement and crack width increased because of the higher yield strain and lower reinforcement ratio.

3) In the shear failure mode specimens, the peak tested shear strength V_{test} was greater than the nominal shear strength V_n which was calculated by using actual material strengths. However, the safety margin was decreased in the wall with 700 MPa bar (V_{test}/V_n = 1.07 ~ 1.55 for Grade 700 MPa vs V_{test}/V_n = 1.20 ~ 1.73 for Grade 400 MPa).

4) For test specimens, the shear strength predictions of KCI 2017, ACI 318-19, Eurocode 8, and Gulec & Whittaker were compared with the tested shear strength. The tested shear strength was safely predicted by ACI 318-19 even without the limitation of the rebar yield strength.

Chapter 4. Effects of Design Parameters on Wall Shear Strength and Deformation

4.1 Overview

In Chapter 3, the shear wall tests were conducted to investigate the shear strength of the walls with 700 MPa reinforcement. Further, to improve the shear wall test database, the present shear wall test considers the design parameters, which is not addressed or lack of data, such as high-strength reinforcement (f_y = 770 – 809 MPa), high effective strength of shear reinforcement ($\rho_h f_y$ = 3.30 – 3.23 MPa), significantly low shear reinforcement ratio (ρ_h = 0.14 – 0.25 %), and high axial load ratio ($N_u/A_g f_c'$ = 0.30).

In this Chapter, the effects of design parameters on the shear strength were discussed based on the test results of the present study and existing studies. The major design parameters affecting the shear strength of the walls are the shear reinforcement, the wall aspect ratio, the axial load ratio, the vertical web reinforcement ratio, and the shape of the section.

4.2 Shear reinforcement

According to ACI 318-19, shear strength of shear reinforcement is based on a modified truss analogy. In the truss analogy, the force in ties (generally, horizontal ties in the walls) is resisted by shear reinforcement. Assuming that the diagonal crack is 45 degrees, the contribution of shear reinforcement to the wall shear strength is defined as $\rho_h f_{yh} A_{cv}$, where, ρ_h = shear reinforcement ratio, f_{yh} = yield strength of shear reinforcement, and A_{cv} = total area resisting the shear force. Thus, the design of shear reinforcement directly affects the wall shear strength.

Fig. 4-1 (a) – (c) compares the load-displacement envelope curves of the shear failure specimens of the present study (**NS2H-30**, **HS2H-30**, **HS2H**, **NS1H-30**, **HS1H-30**, **HS2R**, and **NS2M**). The shear strengths of **HS2H-30**, **HS1H-30**, and **HS2R** with 700 MPa bars were 10 – 23 percent less than those of **NS2H-30**, **NS1H-30**, and **NS2M** with 400 MPa bars, respectively, though the failure modes were similar. In the specimens with 700 MPa bars, because of the increased bar strength, the reinforcement ratio was relatively low. Thus, concrete cracking occurred at low lateral deformations and the crack width increased, which degraded the shear strength. Nevertheless, the specimens with 700 MPa bars, shear reinforcement showed a significant safety margin against the nominal shear strength of ACI 318-19: V_{test}/V_n = 1.19 − 1.55.

Fig. 4-1 (d) compares the load-displacement envelope curves of specimens **NS2M**, **HS2H**, **CS2C**, and **CS2C-AH**. In the specimen **CS2C** with combined bar grade, the horizontal and vertical web reinforcement ratio in the old wall with 400 MPa reinforcement had the same those of **NS2M** (ρ_h = 0.25 %, ρ_v = 0.27 %), and the horizontal and vertical web reinforcement ratio in the expanded wall with 700 MPa reinforcement had the same those of **HS2H** (ρ_h = 0.42 %, ρ_v = 1.24 %). The peak

strength of **CS2C** was V_{test} = 495 kN, which was 10 percent greater than the peak strength of **NS2M** (V_{test} = 450 kN). However, the peak strength of CS2C was 30 percent less than the peak strength of **HS2H** (V_{test} = 706 kN). This result indicates that when the wall segments with different rebar grade are connected horizontally, the sum of shear strength of the wall segments can be overestimated the actual shear capacity. In **CS2C** with combined grade shear reinforcement, the yielding occurs in the normal strength reinforcement, the concrete crack width significantly increases in the old wall, and the shear strength of the entire wall is limited. On the other hand, although only the shear reinforcement ratio of the expanded wall increased, the peak strength of **CS2C-AH** was 28 percent greater than that of **CS2C**. As shown in Fig. 3-12 (b), in **CS2C-AH**, due to greater shear reinforcement ratio, the crack width decreased and the number of crack width increased in the expanded wall. Therefore, the peak strength and deformation capacity increased.

Among the existing shear wall test, the shear failure mode specimens with effective shear reinforcement stress of $\rho_h f_{yh}$ = 1.94 – 4.52 MPa were compared. Table 4-1 summarizes the test parameters and test results of the specimens. As the range of $\rho_h f_{yh}$, the specimens were classified by four groups: group 1) $\rho_h f_{yh}$ = 1.08 – 1.26 MPa; group 2) $\rho_h f_{yh}$ = 1.94 – 2.43 MPa; group 3) $\rho_h f_{yh}$ = 3.11 – 3.38 MPa; and group 4) $\rho_h f_{yh}$ = 4.34 – 4.52 MPa. The range of design parameters are as follows: the aspect ratio H/l_w = 0.48 – 2.7, the concrete compressive strength f_c' = 34.7 – 52.9 MPa, the shear reinforcement ratio ρ_h = 0.14 – 0.92 %, the yield strength of shear reinforcement f_{yh} = 454 – 809 MPa, and the axial load ratio $N_u/A_g f_c'$ = 0 – 0.30 (most of the specimens were tested with low axial load $N_u/A_g f_c'$ = 0 – 0.7).

To investigate the effect of shear reinforcement on the shear strength, the contribution of shear reinforcement was calculated form the test strength V_{test}. According to ACI 318-19, the shear strength of the walls is defined as the sum of

contributions of concrete and shear reinforcement to the shear strength ($V_n = V_c + V_s$). The contribution of concrete shear strength is defined as follows:

$$V_c = \alpha_c \sqrt{f_c'} A_{cv} \quad (4\text{-}1)$$

Where, A_{cv} is gross area resisting shear ($= l_w h_w$), and α_c = 1/6 for aspect ratio greater than 2.0 ($H/l_w > 2.0$), and 1/4 for aspect ratio less than 1.5 ($H/l_w < 1.5$).

The effective shear stress of reinforcement $v_{s,test}$ was calculated as follows:

$$v_{s,test} = (V_{test} - V_c)/A_{cv} \quad (4\text{-}2)$$

Fig. 4-2 shows the effects of yield strength of shear reinforcement and shear reinforcement ratio. In Fig. 4-2, the vertical axis indicates the stress ratio of effective shear stress of reinforcement between test and design ($v_{s,test}/\rho_h f_{yh}$). As the yield strength of the shear reinforcement increases, the stress ratio $v_{s,test}/\rho_h f_{yh}$ decreases. When the effective stress of shear reinforcement $\rho_h f_{yh}$ is the same, the greater the yield strength of shear reinforcement is, the less shear reinforcement ratio is. The less shear reinforcement ratio increases the crack width. Further, because of the greater yield strain of high-strength reinforcement, the crack width more increases at the peak strength. According to Vecchio and Collins (1986), the concrete compressive strength of diagonal strut can be decreased by the tensile strain of orthogonal direction, which is called compression softening effect. The contribution of concrete to shear strength is decreased by the increase of crack width. Therefore, as the yield strength of shear reinforcement increases, the shear strength of wall decreases.

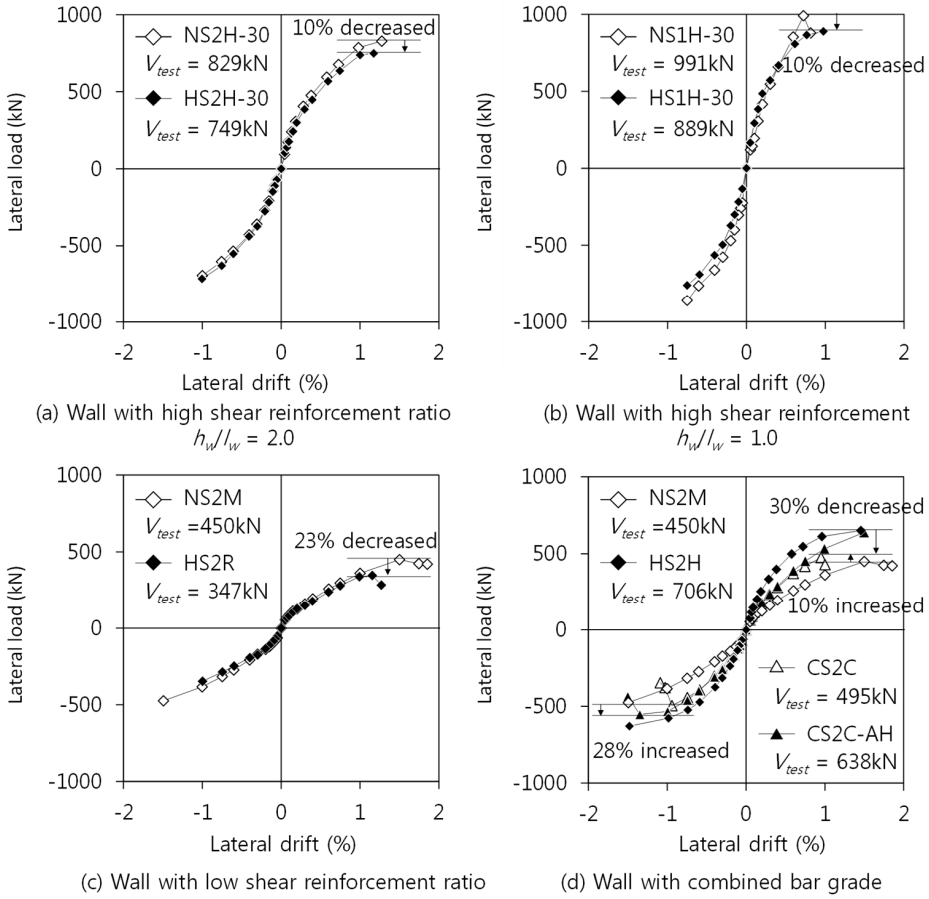

Fig. 4-1 Envelope curves of shear failure mode specimens

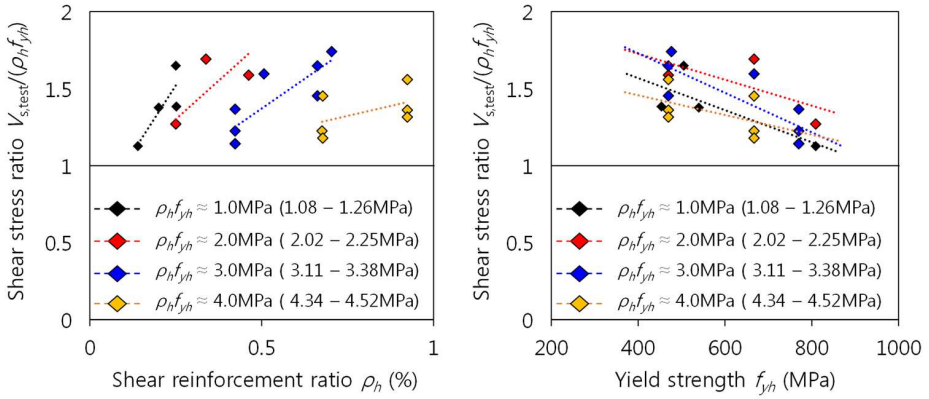

Fig. 4-2 Effect of shear reinforcement on the shear strength

Table 4-1 Summaries of the existing test specimens in Fig. 4-2

Group	Researcher	Specimen ID	Aspect ratio H/l_w	Concrete strength f_c' [MPa]	Axial load ratio $N_u/(A_g f_c')$	Vertical web rebar		Horizontal web rebar			Test results		
						rebar ratio ρ_v [%]	Yield strength f_{yv} [MPa]	rebar ratio ρ_h [%]	Yield strength f_{yh} [MPa]	Effective strength $\rho_h f_{yh}$ [MPa]	Peak shear stress v_{test} [MPa]	Shear stress of rebar $v_{s,test}$ [MPa]	Stress ratio $v_{s,test}/\rho_h f_{yh}$
Group 1) $\rho_h f_{yh} \approx$ 1MPa	Baek (2018)	SW6	2.70	37.1	0.14	0.18	540	0.20	540	1.08	2.51	1.49	1.38
		SW5	2.70	37.1	0.14	0.18	454	0.25	454	1.14	2.60	1.58	1.38
	Present study	HS2R	2.25	38.7	0.00	0.12	809	0.14	809	1.13	2.31	1.28	1.13
		NS2M	2.25	42.3	0.00	0.24	505	0.25	505	1.26	3.17	2.08	1.65
Group 2) $\rho_h f_{yh} \approx$ 2MPa		HS2M	2.25	38.7	0.00	0.24	809	0.25	809	2.02	3.61	2.57	1.27
	Baek (2017a)	NS2L	2.17	36.5	0.07	0.66	470	0.46	470	2.17	4.45	3.45	1.59
		HS2L	2.17	36.5	0.07	0.42	667	0.34	667	2.25	4.82	3.81	1.69
Group 3) $\rho_h f_{yh} \approx$ 3MPa	Present study	NS1H-30	1.25	35.0	0.30	2.21	470	0.66	470	3.11	6.61	5.13	1.65
		NS2H-30	2.25	36.3	0.30	2.21	470	0.66	470	3.11	5.53	4.52	1.45
		HS1H-30	1.25	35.0	0.30	1.41	770	0.42	770	3.25	5.93	4.45	1.37
		HS1H	1.25	35.0	0.00	1.41	770	0.42	770	3.25	5.20	3.72	1.14
		HS2H-30	2.25	36.3	0.30	1.41	770	0.42	770	3.25	4.99	3.99	1.23
		HS2H	2.25	36.3	0.00	1.41	770	0.42	770	3.25	4.72	3.72	1.14
	Park (2015)	NS1T	1.17	46.5	0.07	0.66	653	0.70	477	3.36	7.55	5.85	1.74
		HS1T	1.17	46.5	0.07	0.66	653	0.51	667	3.38	7.10	5.39	1.60
Group 4) $\rho_h f_{yh} \approx$ 4MPa	Baek (2017b)	NS05M	0.67	44.6	0.06	0.92	470	0.92	470	4.34	8.44	6.77	1.56
		NS1M	1.17	52.9	0.07	1.10	470	0.92	470	4.34	7.73	5.91	1.36
		NS2M	2.17	36.5	0.07	1.10	470	0.92	470	4.34	6.72	5.71	1.32
		HS2M	2.17	36.5	0.07	0.56	667	0.68	667	4.51	6.53	5.53	1.23
		HS05M	0.67	37.4	0.06	0.58	667	0.68	667	4.52	8.09	6.56	1.45
		HS1M	1.17	52.9	0.07	0.70	667	0.68	667	4.52	7.15	5.33	1.18

4.3 Wall aspect ratio and axial load ratio

Fig. 4-3 compares the load-displacement envelope curves of specimens **NS2H-30**, **HS2H-30**, **HS2H**, **NS1H-30**, **HS1H-30**, and **HS2H**. In the specimens **NS1H-30**, and **HS1H-30** with 1.0 aspect ratio, the shear strength and initial stiffness were greater than those of specimens **NS2H-30**, and **HS2H-30** with 2.0 aspect ratio. The shear strength of **NS1H-30** was 19 – 24 % greater than that of **NS2H-30**, and the shear strength of **HS1H-30** was 6 – 19 % greater than that of **HS2H-30**. In the specimens with low aspect ratio, the shear strength can be increased by the direct diagonal strut mechanism. On the other hand, in the specimens without axial load ratio, the shear strength was not affected by the wall aspect ratio.

Fig. 4-3 (b) compares the specimens with and without axial loading. The effect of axial loading varied according to the aspect ratio. In **HS2.0H** with aspect ratio of 2.0, shear strength increase was only 1 – 7 % despite the axial force ratio of 0.3, while in **HS1.0H** with aspect ratio of 1.0, the shear strength increase was 14 – 26 %.

To investigate the effects of axial load and wall aspect ratio, the contribution of concrete was calculated form the existing test results, V_{test}. The shear strength is the sum of contributions of concrete and shear reinforcement ($V_n = V_c + V_s$). According to ACI 318-19, the contribution of rebar to the shear strength is defined as follows:

$$V_s = \rho_h f_{yh} A_{cv} \tag{4-3}$$

Where, A_{cv} is gross area resisting shear (= $l_w h_w$), ρ_h = shear reinforcement ratio, and f_{yh} = yield strength of shear reinforcement.

The effective shear stress of concrete $v_{c,test}$ was calculated as follows:

$$v_{c,test} = (V_{test} - V_s)/A_{cv} \quad (4\text{-}4)$$

Fig. 4-4 shows the effects of yield strength of shear reinforcement and shear reinforcement ratio. In Fig. 4-4, the vertical axis indicates the concrete contribution ratio ($\alpha_c = v_{c,test}/\sqrt{f_c'}$). The contribution of concrete decreases as the aspect ratio increases, while it increases as the axial load ratio increases. The effect of aspect ratio increases in the specimens with greater axial load ratio. The effect of axial load ratio increases in the specimens with lower aspect ratio.

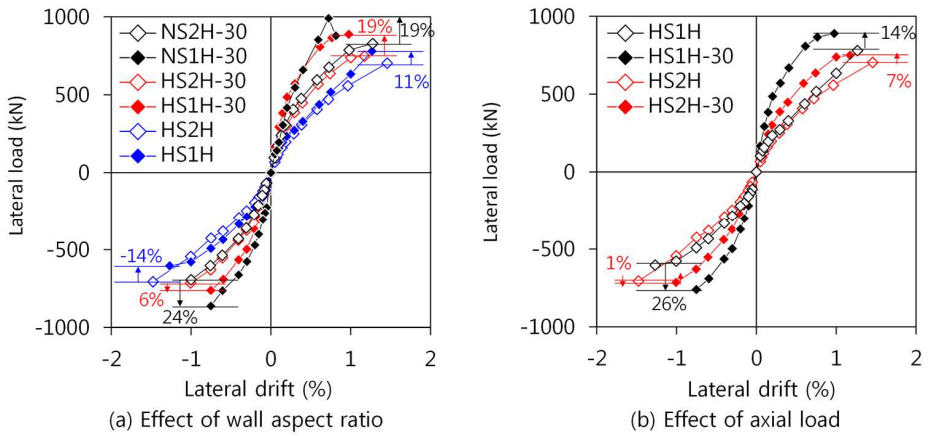

Fig. 4-3 Envelope curves of shear failure mode specimens

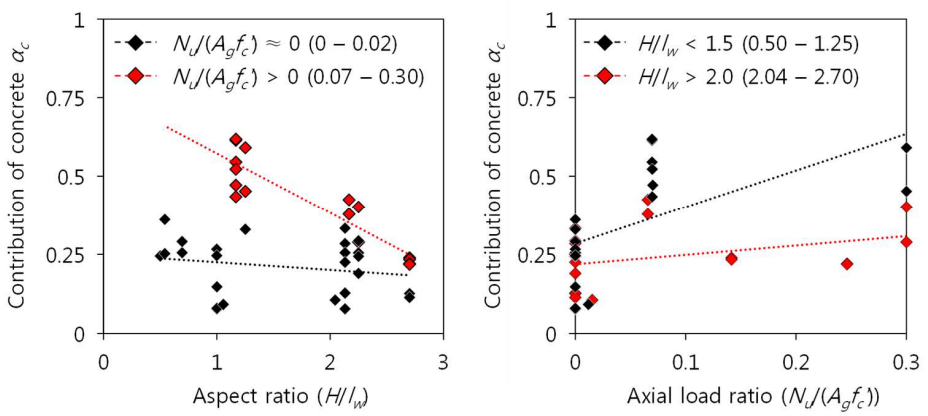

Fig. 4-4 Effects of the aspect ratio and the axial load ratio.

Table 4-2 Summaries of the existing test specimens in Fig. 4-4

Researcher	Specimen ID	Aspect ratio H/l_w	Concrete strength f_c' [MPa]	Axial load ratio $N_u/(A_g f_c')$	Vertical web rebar		Horizontal web rebar			Test results		
					rebar ratio ρ_v [%]	Yield strength f_{yv} [MPa]	rebar ratio ρ_h [%]	Yield strength f_{yh} [MPa]	Effective strength $\rho_h f_{yh}$ [MPa]	Peak shear stress v_{test} [MPa]	Shear stress of concrete $v_{c,test}$ [MPa]	Concrete contribution α_c
Cheng (2016)	H115	1.00	44.0	0.00	0.41	806	0.41	806	3.30	4.28	0.98	0.15
	H60	1.00	44.0	0.00	0.82	475	0.82	475	3.89	4.40	0.51	0.08
Hidalgo (2002)	Hidalgo13	0.50	18.9	0.00	0.26	385	0.26	385	1.00	2.06	1.06	0.24
	Hidalgo7	0.69	18.9	0.00	0.13	490	0.25	490	1.23	2.33	1.11	0.25
	Hidalgo8	0.69	16.3	0.00	0.26	490	0.25	490	1.23	2.40	1.17	0.29
	Hidalgo2	1.00	20.4	0.00	0.25	418	0.25	418	1.05	2.25	1.20	0.27
	Hidalgo4	1.00	20.3	0.00	0.25	418	0.38	418	1.59	2.70	1.11	0.25
Luna (2015)	SW10	0.54	31.7	0.00	1.50	462	0.33	462	1.53	3.56	2.03	0.36
	SW9	0.54	29.7	0.00	1.50	462	0.67	462	3.10	4.47	1.37	0.25
Pilakoutas (1995)	SW4	2.13	36.9	0.00	0.50	550	0.39	550	2.15	2.92	0.78	0.13
	SW5	2.13	31.8	0.00	0.59	550	0.31	400	1.24	3.12	1.88	0.33
	SW6	2.13	38.6	0.00	0.50	550	0.31	400	1.24	3.01	1.77	0.28
	SW7	2.13	32.0	0.00	0.59	550	0.39	550	2.15	3.59	1.44	0.26
	SW8	2.13	45.8	0.00	0.50	550	0.28	400	1.12	2.64	1.52	0.23
	SW9	2.13	38.9	0.00	0.50	550	0.56	400	2.24	2.73	0.49	0.08
Present study	HS1H	1.25	35.0	0.00	1.41	770	0.42	770	3.25	5.20	1.95	0.33
	HS2R	2.25	38.7	0.00	0.12	809	0.14	809	1.13	2.31	1.18	0.19
	HS2M	2.25	38.7	0.00	0.24	809	0.25	809	2.02	3.61	1.58	0.25
	NS2M	2.25	42.3	0.00	0.24	505	0.25	505	1.26	3.17	1.90	0.29
	HS2H	2.25	36.3	0.00	1.41	770	0.42	770	3.25	4.72	1.47	0.24

Table 4-2 Summaries of the existing test specimens in Fig. 4-4 (continued)

Researcher	Specimen ID	Aspect ratio H/l_w	Concrete strength f_c' [MPa]	Axial load ratio $N_u/(A_g f_c')$	Vertical web rebar		Horizontal web rebar			Test results		
					rebar ratio ρ_v [%]	Yield strength f_{yv} [MPa]	rebar ratio ρ_h [%]	Yield strength f_{yh} [MPa]	Effective strength $\rho_h f_{yh}$ [MPa]	Peak shear stress v_{test} [MPa]	Shear stress of concrete $v_{c,test}$ [MPa]	Concrete contribution α_c
Carrillo (2013)	MCL100D	1.06	21.0	0.01	0.27	435	0.27	435	1.17	1.59	0.42	0.09
	MEN100C	2.04	16.2	0.02	0.28	447	0.28	447	1.25	1.68	0.43	0.11
Park (2015)	HS1T	1.17	46.5	0.07	0.66	653	0.51	667	3.38	7.10	3.72	0.55
	NS1T	1.17	46.5	0.07	0.66	653	0.70	477	3.36	7.55	4.19	0.61
	HS1O-B	1.17	46.5	0.07	0.36	653	0.25	667	1.69	5.91	4.22	0.62
	HS1T-H	1.17	70.3	0.07	0.66	653	0.51	667	3.38	7.03	3.64	0.43
	HS1O-H	1.17	70.3	0.07	0.36	653	0.25	667	1.69	6.07	4.38	0.52
	HS1O	1.17	46.1	0.07	0.36	653	0.25	667	1.69	4.89	3.20	0.47
Present study	NS1H-30	1.25	35.0	0.30	2.21	470	0.66	470	3.11	6.61	3.50	0.59
	HS1H-30	1.25	35.0	0.30	1.41	770	0.42	770	3.25	5.93	2.67	0.45
	NS2H-30	2.25	36.3	0.30	2.21	470	0.66	470	3.11	5.53	2.42	0.40
	HS2H-30	2.25	36.3	0.30	1.41	770	0.42	770	3.25	4.99	1.74	0.29
Baek (2017b)	NS2L	2.17	36.5	0.07	0.66	470	0.46	470	2.17	4.45	2.28	0.38
	HS2L	2.17	36.5	0.07	0.42	667	0.34	667	2.25	4.82	2.57	0.42
Baek (20178)	SW1	2.70	19.5	0.00	0.18	454	0.25	454	1.14	1.70	0.56	0.13
	SW2	2.70	19.5	0.25	0.18	454	0.25	454	1.14	2.12	0.97	0.22
	SW3	2.70	19.5	0.00	0.18	540	0.20	540	1.08	1.59	0.50	0.11
	SW4	2.70	19.5	0.25	0.18	540	0.20	540	1.08	2.05	0.97	0.22
	SW5	2.70	37.1	0.14	0.18	454	0.25	454	1.14	2.60	1.45	0.24
	SW6	2.70	37.1	0.14	0.18	540	0.20	540	1.08	2.51	1.42	0.23

Chapter 4. Effects of Design Parameters on Wall Shear Strength and Deformation

A parametric study was performed to investigate the relationships of axial load and wall aspect ratio by using the compression zone failure mechanism model. The detailed procedure of sectional analysis is shown in Chapter 2, and the verification of the model is shown in Chapter 3. For parametric study, the specimen **HS2H** was used as a reference. The controlled design parameters, such as dimensions of section, material strengths, and reinforcement ratios were the same those of **HS2H**.

Fig. 4-5 (a) and (b) shows the effect of axial load. In the figures, horizontal axis indicates a strain coefficient α, which is the ratio of extreme compression fiber strain ε to concrete crushing strain ε_{co} ($\alpha = \varepsilon/\varepsilon_{co}$, $\varepsilon_{co} = 0.002$). In the wall with $h_w/l_w = 1.0$, the initial stiffness of the flexural demand curve is greater than that of wall with $h_w/l_w = 2.0$. Thus, the intersection point is located at a lower strain value. For this reason, the shear strength of the wall with $h_w/l_w = 1.0$ was greater than that of the wall with $h_w/l_w = 2.0$. Also, the shear strength increase due to axial force is greater in the wall with $h_w/l_w = 1.0$. Fig. 4-5 (c) shows the effect of axial force on the effective compression zone depth of the wall with $h_w/l_w = 1.0$. The effective compression zone is defined as a sectional area in compression where concrete crushing does not occur. As the axial force increases, the effective compression zone depth increases, which increases the shear capacity. However, as the strain increases, the effective compressive zone is reduced due to concrete crushing, which results in degradation of the shear capacity. Eventually, V_n is converged to V_s, regardless of the axial load ratio.

The current ACI 318-19 evaluates the concrete shear strength by considering the effect of the wall aspect ratio. However, as discussed, the effect of the aspect ratio depends on the axial load ratio. When the axial load ratio is low, the effect of aspect ratio on the shear strength decreases, whereas the axial load ratio is high, the effect of aspect ratio increases. This is because the concrete shear strength is significantly

affected by the compression zone depth, and the axial load ratio significantly affects the compression zone depth. Therefore, it can be more reasonable to evaluate the concrete shear strength by using the compression zone depth rather than the wall aspect ratio.

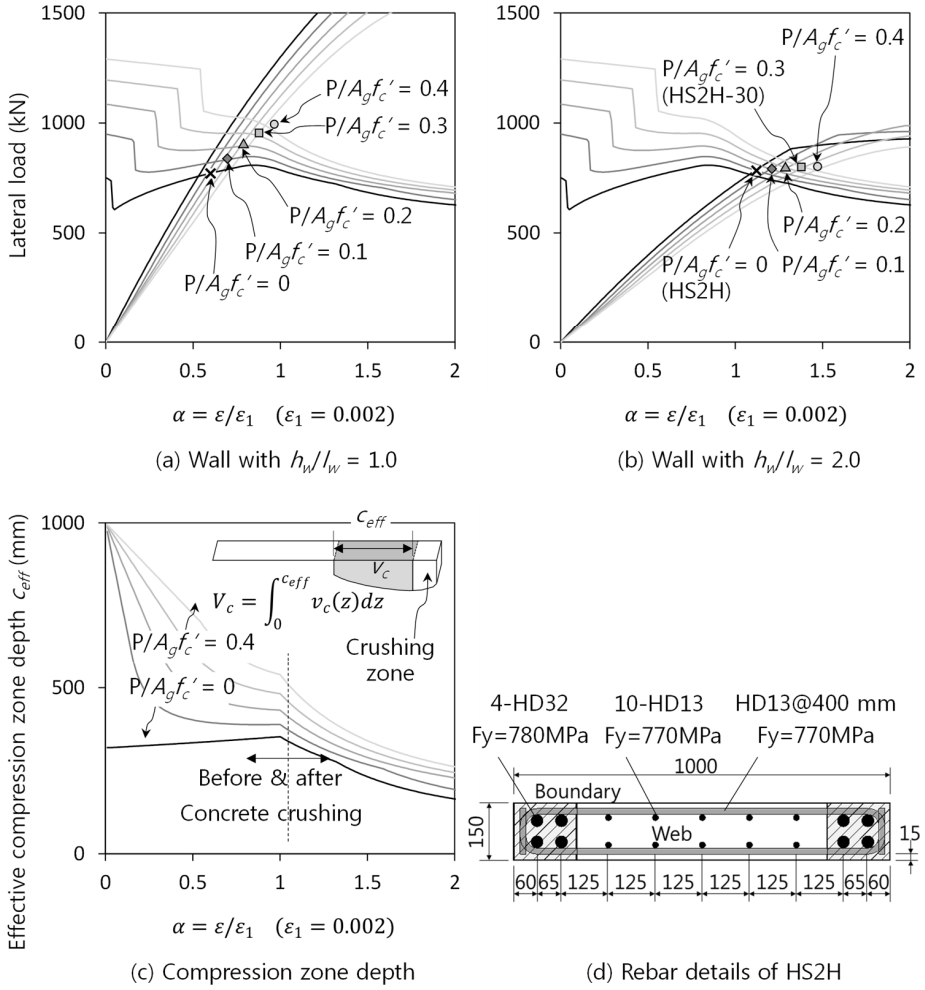

Fig. 4-5 Parametric study on the effect of the aspect ratio and axial load ratio

4.4 Vertical web reinforcement ratio

Vertical web reinforcement ratio is one of the major parameter affecting the compression zone depth. However, in the test of the present study, the vertical reinforcement ratio was controlled. Therefore, the effect of vertical reinforcement ratio is investigated according to the existing test results.

In the study of Cardenas et al. (1973), the effect of vertical web reinforcement was investigated considering three cases of vertical reinforcement distribution: 1) 1/2 +1/2 in two boundary elements without web reinforcement; 2) 1/3+1/3 in two boundary elements and 1/3 in web; and 3) uniformly distributed reinforcement in the cross-section. Fig. 4-6 shows the details of the specimens. The overall vertical reinforcement ratio was 2.3 % in the cases 2) and 3), while the ratio was increased to 3.0 % in the case 3). The nominal moment strengths of three cases were similar. The test results showed that the shear strength of case 3) was 11 % and 14 % greater than those of cases 1), and case 2), respectively.

This result was confirmed by the study of Lopes (2001). In his test, a wall specimen with vertical web reinforcement was directly compared to a counterpart wall without vertical web reinforcement. Fig. 4-7 shows the test specimens and test results. The vertical web reinforcement ratio was 0.40 % (Fig. 4-7 (a)). Despite the similar shear reinforcement ratio (ρ_h = 0.45 – 0.51 %), the peak strength of the wall with vertical web reinforcement was 20 % greater than that of the wall without vertical web reinforcement.

On the other hand, in the study of Hidalgo et al. (2002), when the vertical web reinforcement ratio was significantly low (0.25%), there was a small influence of the vertical reinforcement on the energy dissipation of the specimens (see Fig. 4-8).

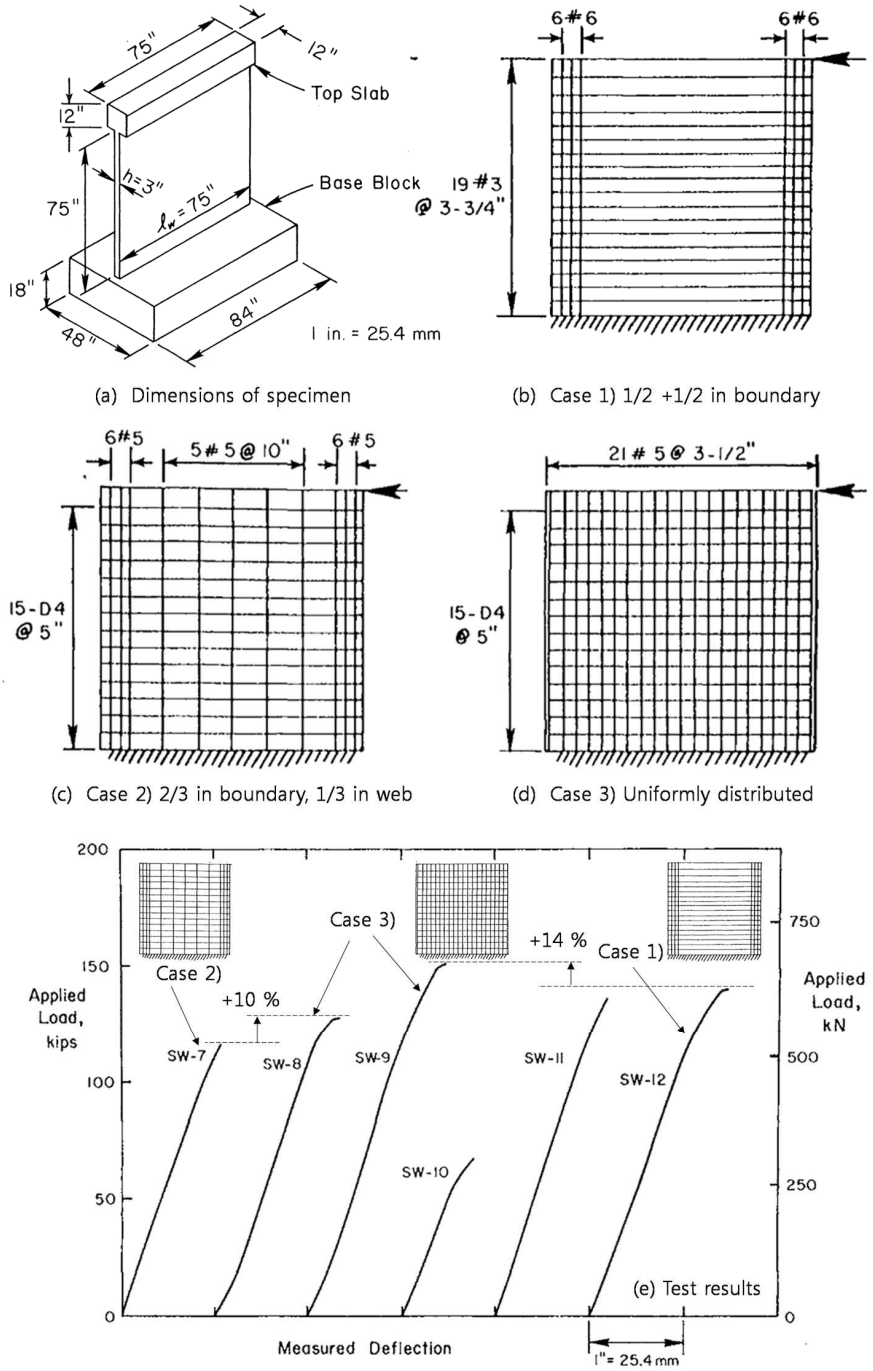

Fig. 4-6 Test specimens and test results of Cardenas et al. (1973)

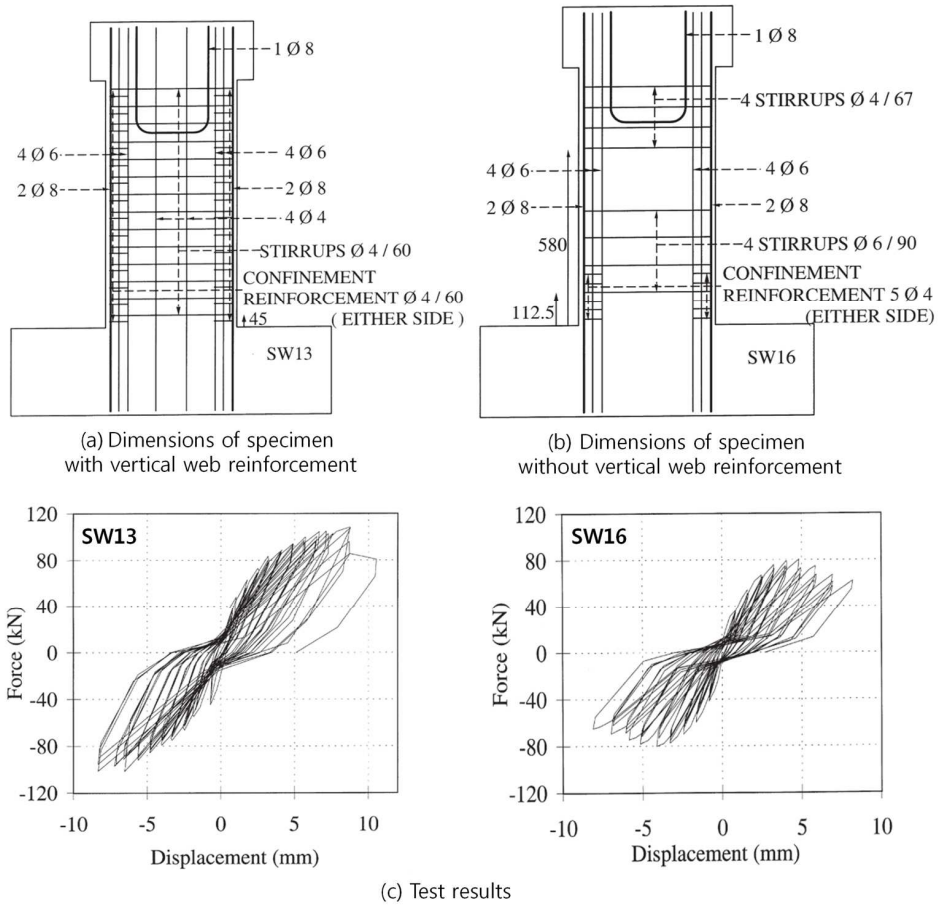

Fig. 4-7 Test specimens and test results of Lopes (2001)

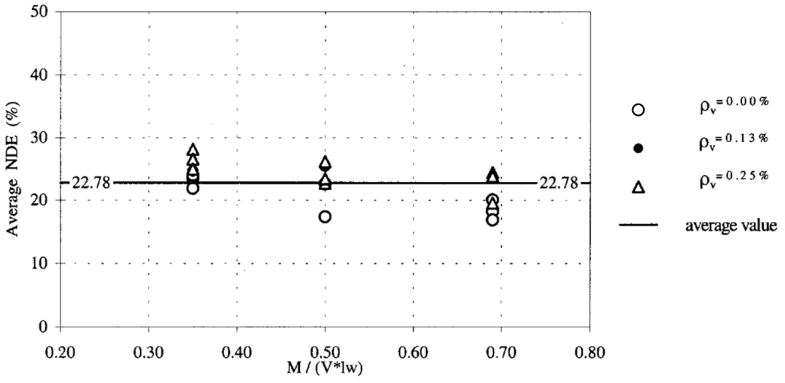

Fig. 4-8 Effect of vertical web reinforcement (Hidalgo et al., 2002)

Fig. 4-9 shows the effect of vertical reinforcement on the shear strength. Test results in Table 4-2 were used. In Fig. 4-9, the vertical axis indicates the concrete contribution ratio ($\alpha_c = v_{c,test}/\sqrt{f_c'}$), and the horizontal axis indicates the average vertical reinforcement ratio ($\rho_{avg} = A_s/A_{cv}$, where, A_s = the total area of vertical reinforcement in the section, A_{cv} = the gross area resisting shear). The contribution of concrete increases as the average vertical reinforcement ratio increases. This result shows that the compression zone depth significantly affects the concrete shear strength.

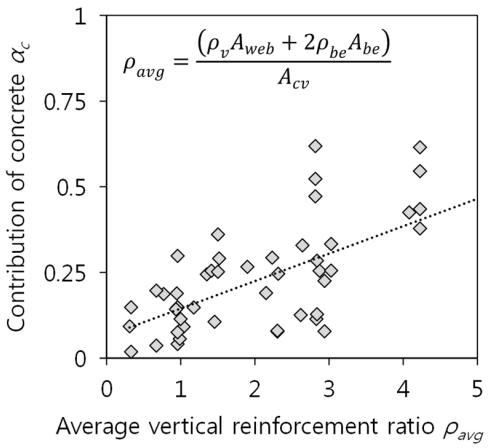

Fig. 4-9 Effect of the vertical reinforcement ratio

4.5 Shape of wall section

The effect of boundary elements and flanges were studied by several researchers. Barda et al. (1977) reported that the shear strength of flanged walls were significantly greater than the nominal shear strength of rectangular wall. Fig. 4-10 shows the effect of test parameters. Compared to shear strength of rectangular wall (calculated by ACI 318), the test strengths of the flanged walls were significantly greater. They proposed a shear strength equation for squat walls with boundary elements, based on the existing test results. The proposed equation was accepted in ASCE/SEI 43-05.

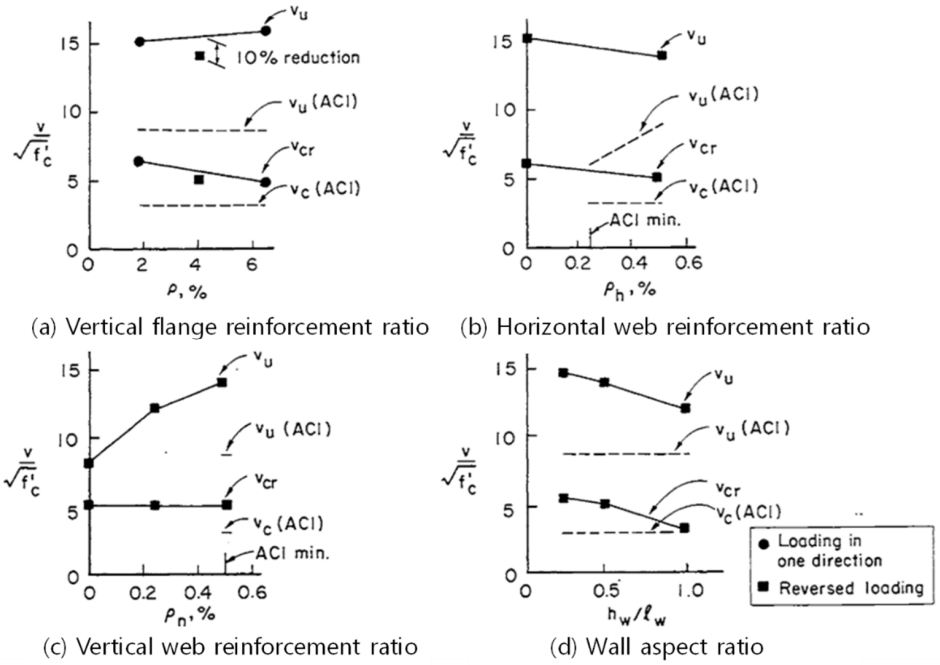

Fig. 4-10 Effect of test parameters on the shear strength of flanged walls (Barda et al., 1977)

Chen et al. (2019) investigated the effect of various wall section shapes, including T-shaped wall, barbell shaped wall, and H-shaped wall. The test results showed that the peak shear strength was greater in the following order: barbell shaped wall < T-shaped wall < H-shaped wall. Further, the specimens with symmetric cross sections (i.e., H-shaped and barbell-shaped ones) showed greater ultimate deformation and ductility than that of specimens with asymmetry cross sections (see Fig. 4-11).

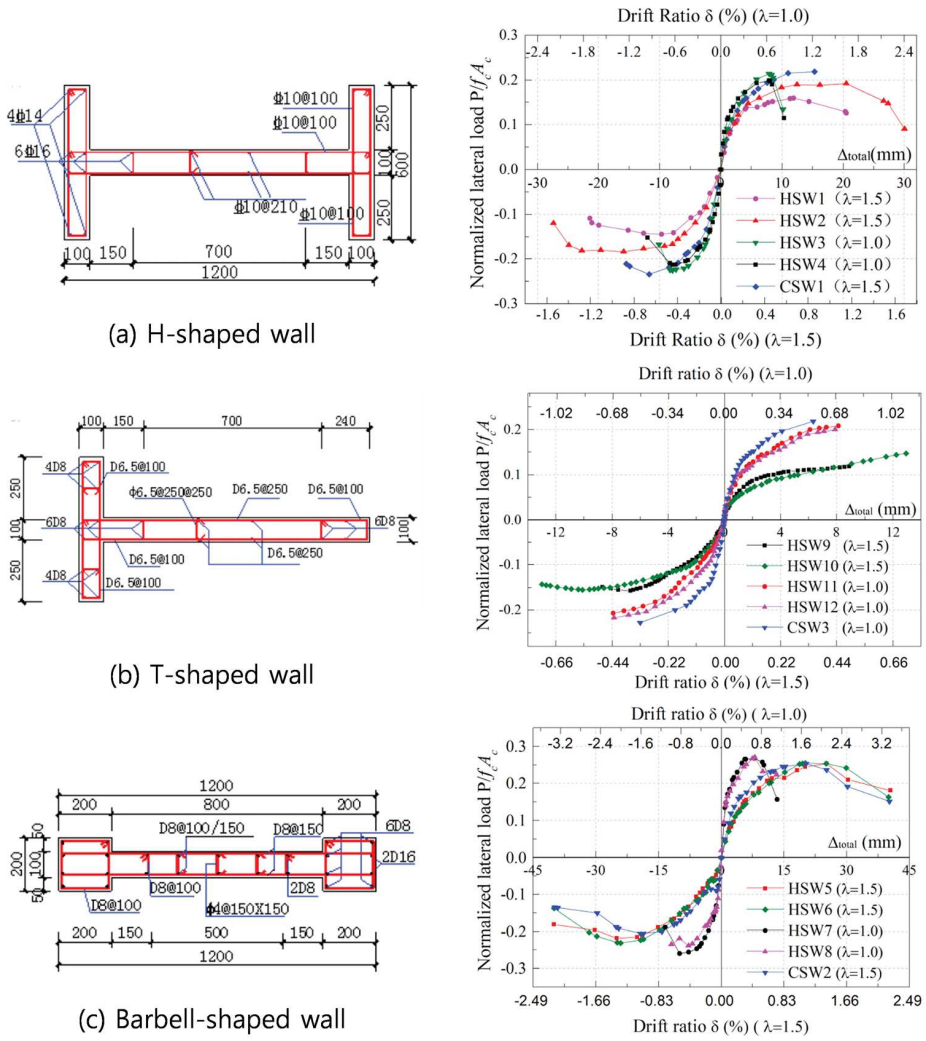

Fig. 4-11 Test specimens and test results of Chen et al. (2019).

Kim and Park (2021) directly compared flanged wall and rectangular wall with the same area of vertical boundary reinforcement. The peak strength was not significantly increased by the wall flange. This result indicates that under the same area of flexural reinforcement, the shear strength of rectangular wall is not significantly different from that of flanged wall (see Fig. 4-12). Further, as the thickness of flange increased, the peak strength increased. On the other hand, the ductility of the flanged wall specimens (μ = 1.9 – 2.5) was greater than that of rectangular wall (μ = 1.5).

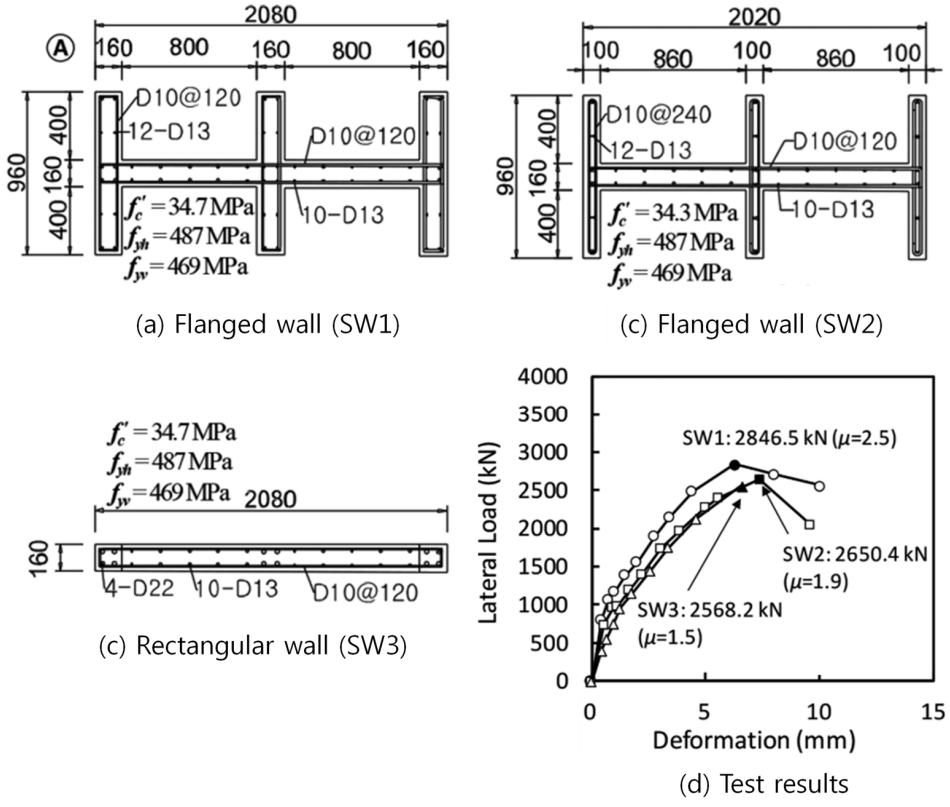

Fig. 4-12 Test specimens and test results of Kim and Park.

Fig. 4-13 shows the effect of vertical reinforcement on the shear strength. In Fig. 4-13, the vertical axis indicates the concrete contribution ratio ($\alpha_c = v_{c,test}/\sqrt{f_c'}$), and the horizontal axis indicates the ratio of the compression zone depth to the wall length (c/l_w). Compared to the rectangle walls, the contribution of concrete is greater in the barbell-shape or flanged walls. When the compression zone depth is the same, the concrete area in compression is significantly increased by the barbell-shaped boundary element or flange. Thus, the contribution of boundary element should be considered in the strength prediction model.

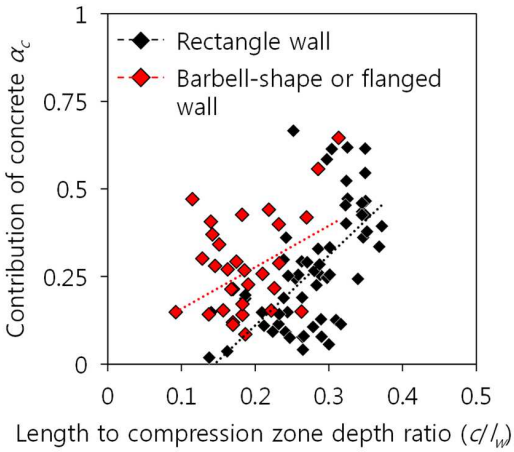

Fig. 4-13 Effect of the vertical reinforcement ratio

4.6 Summary

In the present Chapter, to develop the shear strength model, the effects of design parameters on the wall shear strength were discussed based on the wall test results. The major design parameters affecting the shear strength of the walls are the shear reinforcement, the wall aspect ratio, the axial load ratio, the vertical web reinforcement ratio, and the shape of the section. The major findings are summarized as follows:

1) The shear strength of shear reinforcement is defined by the effective strength of shear reinforcement $\rho_h f_{yh}$. For the same $\rho_h f_{yh}$, as the yield strength of shear reinforcement increases, the shear reinforcement ratio decreases. The shear resistance of concrete is affected by the crack width, and the crack width increases as the shear reinforcement decreases. The safety margin for shear strength decreases in the walls with high-strength shear reinforcement.

2) The shear capacity was significantly affected by the compression zone depth. Thus, the high axial force increased the shear capacity of the wall. The effects of wall aspect ratio and axial load ratio were interdependent. In the present test results, the effect of axial load was less in the wall with aspect ratio of 2.0 than in the wall with aspect ratio of 1.0.

3) The vertical web reinforcement ratio affects the compression zone depth. The walls with uniformly distributed vertical web reinforcement showed greater shear strength than the wall with concentrated vertical reinforcement in the boundary element. However, in the case of significantly low vertical web reinforcement ratio, the effect of vertical web reinforcement was not significant.

4) The shape of the wall section affects the shear strength and deformation capacity of the wall. The shear strength of the wall was increased by the flange. Further, the deformation capacity increased in the wall with the symmetric section. However, in the case of the same amount of vertical reinforcement ratio, the shear strength of flanged wall is not significantly different from that of rectangular wall.

Chapter 5. Simplified Wall Shear Strength Model

5.1 Overview

As explained in Chapter 4, the shear strength of RC walls is affected by various parameters, such as the shear reinforcement, aspect ratio, axial load ratio, vertical reinforcement, and boundary elements. Thus, to accurately predict shear strength of walls, the effect of such major design parameter need to be addressed. In this chapter, a simplified shear strength model was developed addressing the effects of major design parameters: flexural reinforcement, axial force ratio, and boundary element. Two major failure modes were addressed: 1) diagonal tension cracking, and 2) web crushing (Fig. 5-1). The existing mechanism models were adopted to explain the shear strength characteristics, and considering the practical range of the design parameters, the simplified versions of the shear strength models were developed. To verify the proposed shear strength model, the proposed model was applied to existing test specimens. The predictions were compared with the tested strengths.

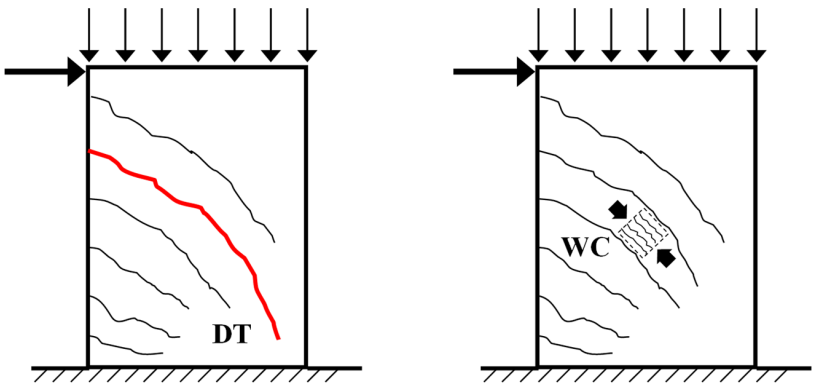

(a) Diagonal tension cracking (b) Web crushing

Fig. 5-1 Major shear failure mechanisms of shear wall

5.2 Background

The shear strength is one of the major design parameters for the design of RC shear walls. Fig. 5-2 shows the typical lateral load-lateral displacement relationships of the RC shear walls. When the shear reinforcement is not insufficient to carry the lateral load corresponding to flexural yielding strength of wall ($V_n < V_f$), the shear strength of wall is drastically decreased by shear failure as the lateral drift ratio increased, which is brittle failure mode. In this case, how to accurately predict the shear strength of wall is important. On the other hand, even if the shear strength is designed to be greater than the flexural strength ($V_n > V_f$), according to existing test results, as the deformation increased, the shear strength of the wall was significantly degraded, and the deformation capacity was limited. In this case, the lateral load-displacement model to simulate the post yield behavior of wall is required.

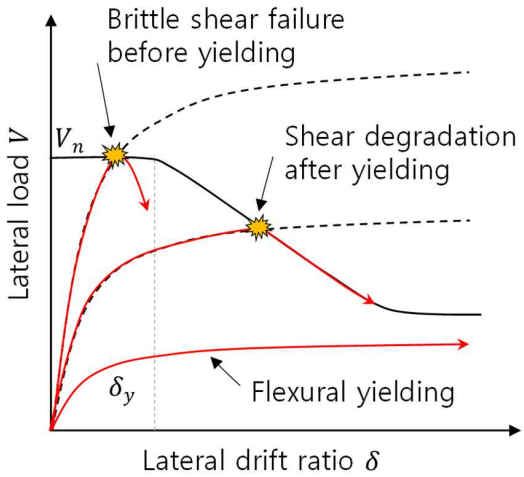

Fig. 5-2 Load-displacement relationships of shear dominant wall

In the recent version of ACI 318, the shear strength provisions for one-way shear was revised: For the shear strength of beams and columns, the effects of longitudinal reinforcement ratio and axial load are considered (ACI 318-19 section 22.5). On the

other hand, the shear strength equation for walls (ACI 318-19 section 11.5.4) was revised to be the same as the seismic provisions (ACI 318-19 section 18.10.4). However, unlike the one-way shear strength equation, the effects of longitudinal reinforcement ratio and axial load were not considered. Furthermore, the properties of walls are different from those of beams and columns: vertical reinforcement is distributed in web, and frequently, columns or flanges are used for boundary elements. Thus, to accurately predict shear strength, such properties of walls need to be addressed. Further, in the high-rise buildings subjected to earthquake, it is known that the shear force is amplified by the nonlinear dynamic mode effects. Such shear amplification was addressed in ACI 318-19 seismic provisions (section 18.10.3). To deal with the increased shear demand, accurate prediction of wall shear strength is required.

The current ACI 318-19 safely predicted the shear strength of wall specimens with conventional range of design parameters. However, for walls with high axial load ratio or high-strength shear reinforcement, the shear strengths were underestimated. In the predictions of Eurocode 8 using the strut-tie mechanism, shear strengths of walls were significantly underestimated, neglecting shear strength of concrete. Gulec and Whittaker (2011) developed a shear strength equation based on statistical optimization on the existing wall test data. This equation showed reasonable strength predictions for existing test specimens, but it is too complex.

5.3 Shear strength of walls controlled by diagonal tension failure

5.3.1 Diagonal tension cracking mechanism model

In the RC slender walls, when horizontal reinforcement is not sufficient, a diagonal tension failure may develop after flexural cracking. The overall shear resistance of concrete is provided by both compression zone and tension zone along the diagonal cracking. However, the intact concrete in the compression zone contributes greater than the damaged (or cracked) concrete in the tension zone.

Choi et al. (2007) developed a compression zone failure mechanism model to predict the shear strength of RC members. Park and Choi (2017) reported that the compression zone depth can be used to describe the major trend of the shear strength; As the flexural reinforcement ratio and axial compression increases, the compression zone depth increases. This trend is the same as that of shear strength; As the concrete strength increases, the compression zone depth does not significantly increase due to the force-equilibrium in the cross section, which is also similar to the trend of shear strength. For this reason, the compression zone depth has been considered as the major design parameter in several recent studies.

Fig. 5-3 (a) shows the concept of the compression zone failure mechanism model. In the compression zone which is subjected to combined (flexural) compression and shear, the shear stress capacity v_c of the concrete is defined as a function of compressive stress σ_c, by using Rankine's failure criteria. The overall shear capacity V_c of a member is defined as the integration of the shear stress capacities of concrete in the compression zone. Thus the concrete shear strength V_c is determined by the flexural compressive stress and compression zone depth.

Since the flexural compressive stress and compression depth are functions of flexural deformation, the shear capacity of a cross-section varies with the flexural deformation or strains (Fig. 5-3 (c)). Before flexural cracking (Stage AB), since the overall cross section can resist shear, the shear capacity is the maximum. However, when the flexural cracking occurs (point B), the shear capacity drastically decreased, due to the cracked region cannot provide the shear resistance. As the flexural deformation increases, the flexural compressive stress and compression zone depth increase. Thus, the shear capacity of concrete increases (Stage BY). However, after flexural yielding, since the compression zone decreases due to the yielding of tensile reinforcement, the shear capacity of concrete gradually degrades (Stage YC). With large deformation, the effective compression zone decreases due to concrete crushing in the compression zone. And the shear capacity of concrete drastically degrades (Stage CE).

The shear strength of a member is determined as the intersection point between the shear capacity curve and shear demand curve (developed by flexural moment) (Fig. 5-3 (b)). For this, nonlinear sectional analysis is carried out. The detailed process is explained in Section 2.3.1.

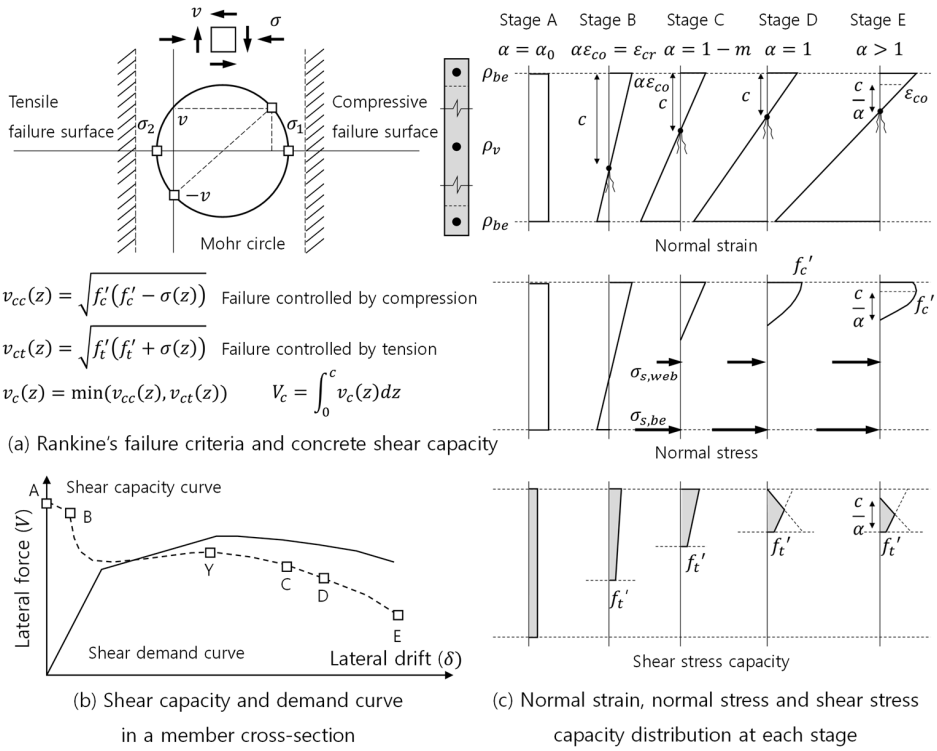

$$v_{cc}(z) = \sqrt{f_c'(f_c' - \sigma(z))}$$ Failure controlled by compression

$$v_{ct}(z) = \sqrt{f_t'(f_t' + \sigma(z))}$$ Failure controlled by tension

$$v_c(z) = \min(v_{cc}(z), v_{ct}(z)) \qquad V_c = \int_0^c v_c(z)dz$$

(a) Rankine's failure criteria and concrete shear capacity

(b) Shear capacity and demand curve in a member cross-section

(c) Normal strain, normal stress and shear stress capacity distribution at each stage

Fig. 5-3 Concept of existing compression zone failure mechanism model

5.3.2 Simplified diagonal tension strength

In the original compression zone failure mechanism model, iterative calculation is needed to define the shear strength. It also requires nonlinear sectional analysis model. For the practical design model, more simple approach is required, such as a closed-form equation.

Shear failure occurs when the flexural strength is greater than the shear strength. Therefore, in RC members showing brittle shear failure, the peak shear strength occurs before or immediately after flexural yielding (Stage BY in Fig. 5-3 (b)): the effect of flexural yielding on shear strength is not significant. On the other hand, to estimate deformation capacity after flexural yielding, shear capacity degradation needs to be evaluated considering inelastic stress-strain relationships of concrete and rebars, which is addressed in the Chapter 6.

For simplified shear strength model, the following assumptions are used:

1) Shear stress of concrete is controlled by tension failure (cracking) rather than compression failure (crushing).

2) Concrete in the compression zone and flexural reinforcement (vertical rebars) show linear stress-strain relationships.

Using the tension failure mechanism (assumption 1)), the shear strength of concrete V_c is defined by Eq. (2-43a) as follows:

$$V_c = \int_0^c \sqrt{f_t\left(f_t + \sigma_c(z)\right)}\, h_w(z) dz \tag{5-1}$$

Where, c is the compression zone depth, f_t is concrete tensile strength ($f_t = 0.2\sqrt{f_c'}$, Mehta and Monteiro, 2014), $\sigma_c(z)$ is concrete normal stress at the distance z, and h_w is the thickness of web.

In Eq. (5-1), the shear capacity of concrete is varied by the concrete normal stress $\sigma_c(z)$. However, considering the linear stress-strain relationship of concrete (assumption 2), the average shear capacity of compression zone depth can be used.

$$\sqrt{f_t\left(f_t + \sigma_c(z)\right)} \approx f_t\sqrt{1 + \sigma_{cm}/f_t} \tag{5-2}$$

Where, σ_{cm} is average concrete compressive stress in the compression zone.

Therefore, the shear strength of concrete can be easily calculated using average shear capacity of compression zone.

For rectangular shape wall,

$$V_c = \int_0^c f_t\sqrt{1 + \sigma_{cm}/f_t}\, h_w dz = f_t\sqrt{1 + \sigma_{cm}/f_t} c h_w \tag{5-3a}$$

For barbell shape or flanged wall,

$$\begin{aligned} V_c &= \int_0^c f_t\sqrt{1 + \sigma_{cm}/f_t}\, h_w(z) dz \\ &= f_t\sqrt{1 + \sigma_{cm}/f_t} c h_w + f_t\sqrt{1 + \sigma_{cm}/f_t}(h_{be} - h_w) t_{be} \end{aligned} \tag{5-3b}$$

where, c is the compression zone depth, f_t is concrete tensile strength, σ_{cm} is average concrete compressive stress, h_w is the thickness of web, h_{be} is the width of boundary element or flange, t_{be} is the thickness of boundary element or flange.

Definitions of geometric dimensions are shown in Fig. 5-4 (a). For barbell shape section, the width of boundary element h_{be} is assumed to be less than 2 times thickness of boundary element ($h_{be} \leq 2t_{be}$). For flanged section, the width of flange h_{be} is assumed to be greater than 2 times thickness of flange ($2t_{be} \leq h_{be}$). In the flange, the vertical strain-stress is not uniformly distributed (Zhang et al. (2021)). Thus, the effective width of flange is limited to 1/2 times the wall height (ACI 318-19).

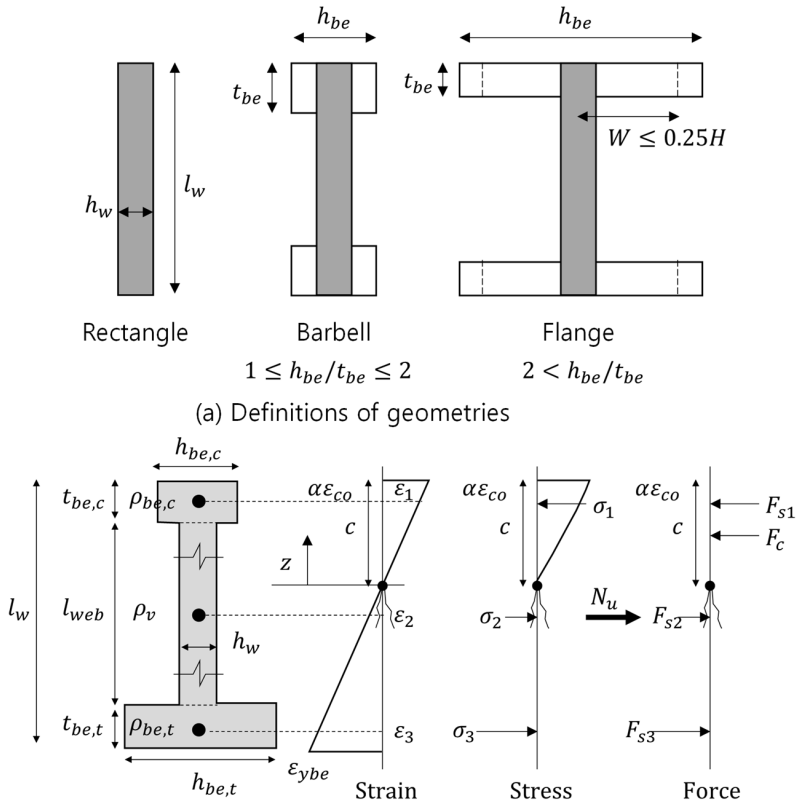

Fig. 5-4 Wall section model

Equations (5-3a) and (5-3b) indicate simplified shear strengths which are defined using the compression zone depth c, and average compressive stress σ_{cm}. Using $f_t = 0.2\sqrt{f_c'}$ (Mehta and Monteiro, 2014), Eqs (5-3a) and (5-3b) can be expressed by similar form specified in ACI 318-19 seismic provisions as follows:

For rectangular shape wall,

$$V_c = \alpha_1\sqrt{f_c}\,l_w h_w \tag{5-4a}$$

For barbell shape or flanged wall,

$$V_c = \alpha_1\sqrt{f_c}\,l_w h_w + \alpha_2\sqrt{f_c}(h_{be} - h_w)t_{be} \tag{5-4b}$$

Where, coefficients α_1 and α_2 are defined as follows:

$$\alpha_1 = 0.2 \cot\theta \, (c/l_w) \tag{5-5a}$$

$$\alpha_2 = 0.2 \cot\theta \, R_{sle} \tag{5-5b}$$

$$\cot\phi = \sqrt{1 + \sigma_{cm}/f_t} \tag{5-5c}$$

where, θ is average crack angle in the compression zone subjected to combined flexural compression and shear, and R_{sle} is reduction factor for equivalent stress block of flange concrete (= 0.25(H/W) ≤ 1, where, H = the wall height, and W = half of the flange width (ACI 318-19)). The coefficient α_1 and α_2 are defined as a function of c/l_w, and cotθ. In the present study, for simplified shear strength model, parameters c/l_w, and cotθ are simplified.

Fig. 5-4 (b) shows a wall section model. A wall cross-section is divided into three elements: boundary element in tension, web wall, and boundary element in compression. The vertical rebars are assumed to be concentrated at the center of each element. The concrete strain at the extreme compression fiber is defined as a ratio to the concrete crushing strain ($\alpha = \varepsilon_c/\varepsilon_{co} \leq 1.0$). Using assumption 2), the concrete normal stress σ_c(z) and average concrete compressive stress σ_{cm} are defined as follows:

$$\sigma_c(z) = \varepsilon_c(z) E_c = 2 f_c' \left(\frac{\alpha z}{c}\right) \tag{5-6a}$$

$$\sigma_{cm} = \frac{1}{c} \int_0^c \sigma_c(z) dz = \alpha f_c' \tag{5-6b}$$

Where, ε_c(z) is the concrete normal strain at the distance z, E_c is the concrete elastic modulus. From the concrete model of Hognestad (1951), the elastic modulus is defined as $E_c = 2f_c'/\varepsilon_{co}$.

The stresses of vertical rebars in the three elements are defined as follows:

$$\sigma_1 = \alpha\varepsilon_{co}E_s\left(\frac{c - t_{be}/2}{c}\right) \quad (5\text{-}7a)$$

$$\sigma_2 = \alpha\varepsilon_{co}E_s\left(\frac{c - l_w/2}{c}\right) \quad (5\text{-}7b)$$

$$\sigma_3 = \alpha\varepsilon_{co}E_s\left(\frac{c - l_w + t_{be}/2}{c}\right) \quad (5\text{-}7c)$$

Where, E_s is the elastic modulus of reinforcement (= 200,000 MPa)

The internal forces of rebars are calculated as follows:

$$F_i = \sigma_i A_i \quad (5\text{-}8)$$

Where, σ_i is the normal stress of the *i*th rebar, and A_i is the sectional area of the *i*th rebars.

From Fig. 5-4 (b), the force equilibrium is defined as follows:

$$\Sigma F_i = \sigma_{cm}A_c + \sigma_1 A_{sbe,c} + \sigma_2 A_{sw} + \sigma_3 A_{sbe,t} - N_u \quad (5\text{-}9)$$

where, σ_{cm} is the average compressive stress in the compression zone (= $\alpha f_c'$), A_c is area of the compression zone, $A_{sbe,c}$, and $A_{sbe,t}$ are areas of vertical reinforcement in the boundary element in compression, and tension, respectively, A_{sw} is area of vertical reinforcement in the web, and N_u is the axial compression force.

Inserting Equations (5-6) and (5-7) to Equation (5-9), and arranging for the compression zone depth to wall length ratio (c/l_w), the equation for compression zone depth is derived as follows:

$$\left(\frac{c}{l_w}\right)^2 + 2\left[\rho_{avg} n\kappa + pn\kappa\psi + \kappa_b\right]\left(\frac{c}{l_w}\right) - \rho_{avg} n(\kappa + \chi) - 2pn\kappa\psi - \kappa_b\kappa_j = 0 \quad (5\text{-}10)$$

where, ρ_{avg} is the average vertical rebar ratio, n is the modulus ratio (= E_s/E_c), ψ is the material strength ratio(=f_c'/f_y), κ is the shape coefficient (= $A_g/(l_w h_w)$), κ_b is the shape coefficient of boundary element in compression (= $(t_{be,c}h_{be,c} - t_{be,c}h_w)/(l_w h_w)$), κ_j is the shape coefficient of joint in compression (= $(t_{be,c}h_w)/(l_w h_w)$), p is the axial load ratio (= $N_u/(A_g f_c')$), and χ is assymetricity of boundary reinforcement (= $0.9(A_{sbe,t} - A_{sbe,c})/(l_w h_w)$). Solving the 2nd order equation for c/l_w, the compression depth to length ratio is defined as follows:

$$\left(\frac{c}{l_w}\right) = -\left(\rho_{avg} n\kappa + pn\kappa\psi + \kappa_b\right) + \cdots \sqrt{\left(\rho_{avg} n\kappa + pn\kappa\psi + \kappa_b\right)^2 + \rho_{avg} n(\kappa + \chi) + 2pn\kappa\psi + \kappa_b\kappa_j} \quad (5\text{-}11)$$

Using the Laurent series, Equation (5-9) can be simplified. The Laurent series is as follows:

$$\sqrt{A^2 + B} = A + \frac{B}{2A} - \frac{B^2}{8A^3} + \cdots \approx A + \frac{B}{2A} \qquad \text{where } A \gg B \qquad (5\text{-}12)$$

Where, the error of the approximation is minimized when A is significantly greater than B. To satisfy this condition, the terms in the square root in Eq. (5-9) is transformed as follows:

$$\sqrt{\underbrace{\left(\rho_{avg} n\kappa + pn\kappa\psi + \kappa_b + \frac{1}{4}\right)^2}_{\text{A}} + \underbrace{\rho_{avg} n\left(\frac{\kappa}{2} + \chi\right) + \frac{3}{2}pn\kappa\psi + \kappa_b\left(\kappa_j - \frac{1}{2}\right) - \frac{1}{16}}_{\text{B}}} \quad (5\text{-}13)$$

Where, B in Eq. (5-13) is very small in the range of design parameters.

Substituting Eq. (5-13) to Eq. (5-11), the compression depth can be simplified as follows:

$$\left(\frac{c}{l_w}\right) = \left(-A + \frac{1}{4}\right) + A + \frac{B}{2A} = \frac{1}{2}\left(\frac{\rho_{avg} n(\kappa + \chi) + 2pn\kappa\psi + \kappa_b\kappa_j + \frac{1}{16}}{\rho_{avg} n\kappa + pn\kappa\psi + \kappa_b + \frac{1}{4}}\right) \quad (5\text{-}14)$$

The parameters in Eq. (5-14) can be further simplified by considering general design values. Assuming that the ranges of concrete strength and rebar yield strength are f_c' = 20 – 100 MPa, and f_y = 400 – 800 MPa, the ranges of n and ψ are n = 6 – 10, and ψ = 0.033 – 0.1. In the present study, simplified values of n = 8 and ψ = 0.05 are used. For rectangular section, κ = 1.0, and κ_b = 0. Therefore, Equation (5-12) is simplified as follows:

$$\left(\frac{c}{l_w}\right) = \frac{1}{2}\left(\frac{8(1 + \chi)\rho_{avg} + 0.8p + \frac{1}{16}}{8\rho_{avg} + 0.4p + \frac{1}{4}}\right) \quad (5\text{-}15)$$

In Equation (5-15), the compression zone depth is a function of average vertical rebar ratio and axial load ratio. Through regression analysis, Equation (5-15) is further simplified as an optimized linear equation which independently addresses the effect of ρ_{avg} and p as follow:

$$\left(\frac{c}{l_w}\right) = (0.9 - 0.45\chi)\left(\left(\rho_{avg}\right)^{1/3} + p\right) + 0.25\chi \leq 0.5 \quad (5\text{-}16)$$

Considering that compression zone depth is usually less than half of wall length, the maximum value of c/l_w is limited to 0.5. In Fig. 5-5, the simplified compression depth Equations (5-14),(5-15), and (5-16) are compared to the detailed compression depth Equation (5-11) for random test parameters: f_c' = 20 – 100 MPa, f_y = 400 – 800 MPa, ρ_{avg} = 0.25 – 6.0 %, p = 0 – 0.3, χ = -0.2, 0, +0.2. Rectangular walls are only

considered (κ = 1.0).

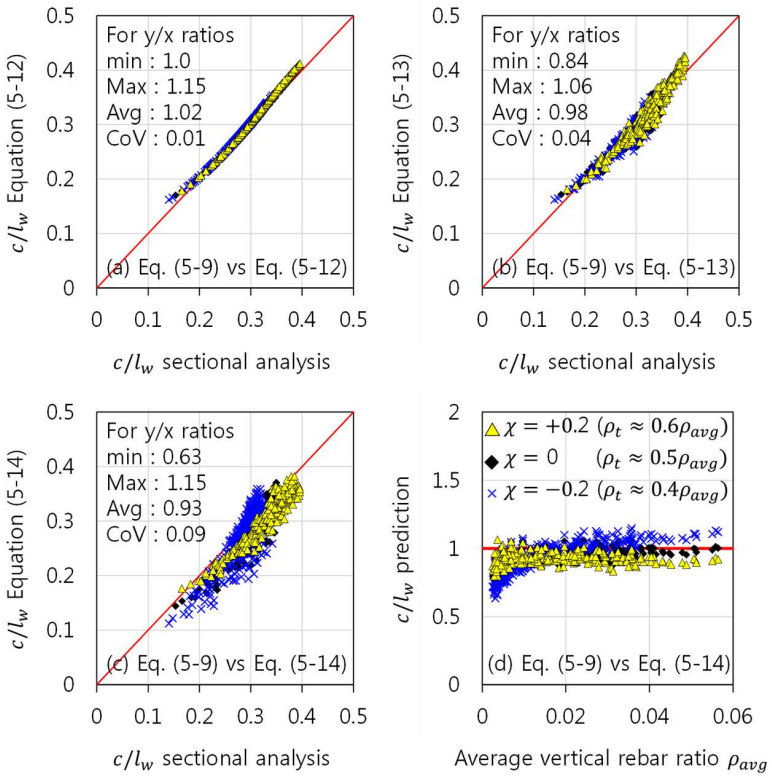

Fig. 5-5 Verification of simplified equations for compression zone depth

Next, parameter cotθ is also simplified. Inserting Eq. (5-6b) into Eq. (5-5c), cotθ can be defined as follows:

$$\cot\theta = \sqrt{1 + \frac{\alpha f_c'}{f_t}} \tag{5-17}$$

Before flexural yielding, shear capacity is degraded as the compression zone depth decreases due to flexural cracking (i.e. when there is no flexural cracking, intact concrete in whole cross-section can provide shear resistance). Thus, for safe estimation of shear capacity, cotθ is defined based on the yield strain of flexural

reinforcement. In Eq. (5-17), α is defined using the yield strain of vertical rebar at the extreme tension fiber ($\alpha = \varepsilon_y/(l_w/c - 1)$). Considering practical ranges of design parameters, f_c' = 20 – 100 MPa and f_y = 400 – 800 MPa, the values of θ ranges 10 – 20°. Thus, the average value θ = 15° is used for crack angle in the compression zone.

Using cotθ = 3.73, the contribution of concrete to shear strength V_c is redefined as follows:

$$V_c = \alpha_c \sqrt{f_c} A_{cv} \tag{5-18}$$

Where, A_{cv} is gross area resisting shear (= $l_w h_w$), and α_c is defined as follows:

For rectangular shape wall

$$\alpha_c = (0.7 - 0.35\chi)\left({\rho_{avg}}^{1/3} + p\right) + 0.20\chi \leq 0.37 \tag{5-19a}$$

For barbell shape or flanged walls

$$\alpha_c = (0.7 - 0.35\chi)\left({\rho_{avg}}^{1/3} + p\right) + 0.20\chi + 0.75 c_s R_{sle} \leq 0.5 \tag{5-19b}$$

Where, c_s is the shape coefficient (= $(h_{be} - h_w)t_{be}/(l_w h_w)$) which is defined as a ratio of net flange area to the web area (see Fig. 5-6 (a)), and R_{sle} is reduction factor for equivalent stress block of flange concrete (= 0.25(H/W) ≤ 1, where, H = the wall height, and W = half of the flange width (ACI 318-19)).

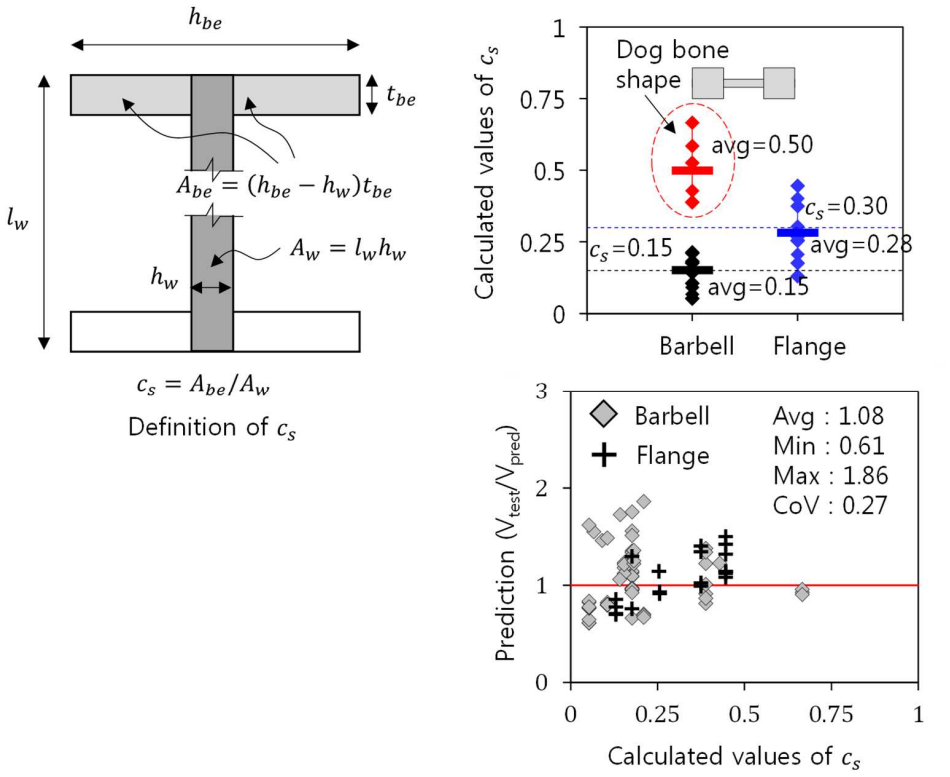

Fig. 5-6 Definition and calculated value of c_s

Based on the existing test results for barbell shaped walls and flanged walls, the recommended values of c_s are c_s = 0.15 for barbell shape walls, and c_s = 0.3 for flanged wall. Fig. 5-6 compares the original definitions and simplified values of c_s for existing test specimens.

Equations (5-18) and (5-19) of the proposed model are similar to one-way concrete shear strength for RC members specified in ACI 318-19 section 22.5:

$$V_c = \left(0.66\rho_w^{1/3}\lambda_s\sqrt{f_c'} + \frac{N_u}{6A_g}\right)b_w d \quad \text{(5-20a)}$$

$$V_c = \left(0.66\rho_w^{1/3}\lambda_s\sqrt{f_c'} + 0.17pf_c'\right)b_w d \quad \text{(5-20b)}$$

where, ρ_w is the longitudinal reinforcement ratio, λ_s is the coefficient for light weight concrete, N_u is axial force, A_g is the gross area of the member, b_w is the breadth of the member, and d is the effective depth. In Eq. (5-20), the effect of axial force is defined as $N_u/(6A_g) = 0.17pf_c'$. Thus, for high strength concrete, the effect of axial force ratio is greater in ACI 318-19.

The contribution of shear reinforcement V_s is defined following ACI 318-19:

$$V_s = \rho_h f_{yh} A_{cv} \tag{5-21}$$

Where, ρ_h is the horizontal reinforcement ratio, and f_{yh} is the yield strength of shear reinforcement. The overall shear strength of a wall controlled by diagonal tension failure is defined as the sum of contributions of concrete and shear reinforcement: $V_n = V_c + V_s$.

5.4 Shear strength of walls controlled by web crushing failure

In RC members, shear force is transferred through the web. Unlike the beam and column, the RC wall usually has thin and wide web, and vertical and horizontal reinforcement is uniformly distributed in the web. Thus, the web can be shear critical region. In particular, when the web in the plastic hinge region is damaged by flexural yielding, the effective concrete strength of web is decreased, and the shear capacity of the web is degraded. In this case, the shear strength is limited by concrete crushing of web, although the web is shear reinforced sufficiently, which is called web crushing failure.

Current design codes address the web crushing failure strength by limiting the maximum shear strength (For example, in ACI 318-19, $V_{nmax} = 2/3\sqrt{f_c'}A_{cv}$). However, according to Baek et al. (2021), the web crushing strength is too conservative for the wall with high-strength concrete. The present study developed the simplified web-crushing strength model based on the truss mechanism model (Eom and Park (2010)).

Fig. 5-7 shows the concept of the model. In this model, the crack angle in the web is assumed to be uniform in the plastic hinge region. The shear force in the plastic hinge zone is resisted by the diagonal concrete strut. Therefore, the diagonal web crushing strength V_{wc} of the web is determined by the effective compressive strength of the web concrete as follows:

$$V_{wc} = f_{ce} l_{web} h_w \cos\theta \sin\theta \tag{5-22}$$

Where, f_{ce} is the effective compressive strength of the web concrete, h_w is the thickness of the web, l_{web} is the length of the web, and θ is the average crack angle in the web.

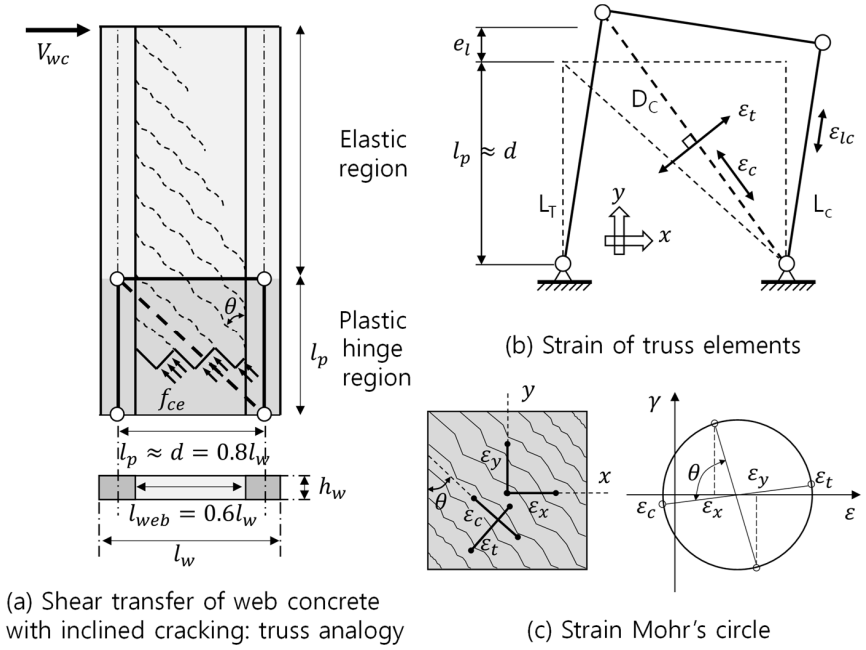

Fig. 5-7 Concept of truss mechanism model for web crushing

Based on this model, the simplified web-crushing strength model is developed. First of all, the effective stress of concrete strut f_{ce} is calculated. When a RC wall is subjected to cyclic lateral loading, elongation of the wall increases as the plastic deformation increases in the plastic hinge region. As the elongation increases, the diagonal tensile strain of the web concrete increases, which degrades the strength of compression strut (compression softening effect). According to Vecchio and Collins (1986), the effective compressive strength of concrete strut f_{ce} is defined as follows:

$$f_{ce} = \left(\frac{f_c'}{0.8 + 0.34(\varepsilon_t/\varepsilon_{co})}\right) \leq f_c' \tag{5-23}$$

Where, ε_t is the principal tensile strain, and ε_{co} is the concrete crushing strain.

In Eq.(5-23), the effective stress of diagonal strut is a function of the principal tensile strain. The principal tensile strain is varied in the web, however, for simple calculation, average principal strain and average effective stress are used. Based on the Mohr's circle, average principal tensile strain ε_t is calculated as follows:

$$\varepsilon_t = \varepsilon_x + \varepsilon_y - \varepsilon_c \tag{5-24}$$

where, ε_x is horizontal strain of web concrete, ε_y is vertical strain of web concrete, respectively, and ε_c is the principal compressive strain of web concrete.

For the web panel, average strain was estimated assuming the ultimate state. At the web crushing failure, the principal compressive strain of concrete reaches the concrete crushing strain $\varepsilon_c = -\varepsilon_{co} = -0.002$. The horizontal strain is represented by strain of horizontal reinforcement. At the ultimate state, since the web-cracking is maximized, it is assumed that the horizontal reinforcement is yielded. Thus, ε_x is greater than the yield strain of horizontal reinforcement ε_{yh}. However, for conservative evaluation, $\varepsilon_x = \varepsilon_{yh}$ is used. The vertical strain is estimated from the elongation of web e_l. From the definition, the vertical strain of web is elongation divided by the original height of the plastic hinge region ($\varepsilon_y = e_l/l_p$).

Therefore, Eq. (5-24) is rewritten as follows:

$$\varepsilon_t \approx \varepsilon_{yh} + \frac{e_l}{l_p} + 0.002 \tag{5-25}$$

Eom et al. (2013) assumed $\varepsilon_{yh} = 0.002$, because the permissible yield strength of wall shear reinforcement was limited to 420 MPa in the past. However, the permissible yield strength of wall shear reinforcement has been increased to 690 MPa in seismic provisions of ACI 318-19, and 600 MPa in most of structural design

codes, including Eurocode 8, Model code, and KCI2017. Therefore, in the present study, $\varepsilon_{yh} = f_{yh}/E_s$ (E_s = elastic modulus of reinforcement (= 200,000 MPa)) is used.

Inserting Eq. (5-25) into Eq. (5-23)), f_{ce} is defined as follows.

$$f_{ce} = \left(\frac{f_c'}{0.8 + 0.34\left(f_{yh}/400\right) + 170\left(e_l/l_p\right)}\right) \leq f_c' \tag{5-26}$$

As shown in Fig. 5-7, a plastic hinge region is defined with the effective depth of wall: $l_p \approx d = 0.8l_w$ (Lee and Watanabe, 2003). For the geometric assumption, the effective length of the web is assumed as $l_{web} = 0.6l_w$. The crack angle is assumed to be 45 degrees. Therefore, the shear capacity of the web V_{wc} is simplified as follows:

$$V_{wc} = \frac{1}{2} f_{ce} 0.6 l_w h_w \approx 0.3 f_{ce} l_w h_w \tag{5-27}$$

Inserting Eq. (5-26) to (5-27), the shear capacity V_{wc} is defined as follows:

$$V_{wc} = \frac{f_c' l_w h_w}{3.8 + 1.13\left(f_{yh}/400\right) + 567\left(e_l/l_p\right)} \tag{5-28}$$

In this section, the maximum shear strength (= web crushing strength) is evaluated, assuming a deformation state before flexural yielding. In this state, a plastic hinge (plastic strain of vertical rebars) is not developed. Thus, in Eq. (5-28), the effect of elongation (e_l/l_p) is negligible.

Therefore, the web crushing strength V_{wcm} can be simplified as follows:

$$V_{wcm} = \beta_c f_c' A_{cv} \tag{5-29}$$

where,

$$\beta_c = \frac{1}{3.8 + 1.13\left(f_{yh}/400\right)} \approx \begin{cases} 1/5 & \left(\text{for } f_{yh} \le 400 \text{ MPa}\right) \\ 1/6 & \left(\text{for } f_{yh} \ge 800 \text{ MPa}\right) \end{cases} \tag{5-30}$$

Where, A_{cv} is the gross area resisting shear (= $l_w h_w$). The value of coefficient β_c was simplified as β_c = 1/5 for $f_{yh} \le$ 400 MPa, β_c = 1/6 for $f_{yh} \ge$ 800 MPa, and linear interpolation between 1/5 to 1/6 can be used for 400 MPa < f_{yh} < 800 MPa.

The proposed web crushing shear strength is similar to that of Eurocode 8:

$$V_{Rd,max} = \alpha_{cw} v_1 f_c' h_w z/(\tan\theta + \cot\theta) \tag{5-31}$$

where, h_w is thickness of the wall, z is inner lever arm corresponding to the bending moment, θ is crack angle between the concrete compression strut and the member longitudinal axis, α_{cw} is a coefficient addressing the state of the stress in the compression chord, and v_1 is a strength reduction factor for concrete cracked in shear. The calculations of α_{cw} and v_1 presents in Chapter 2. In the conditions of no axial load and concrete compressive strength < 60 MPa, α_{cw} = 1.0, and v_1 = 0.6 are used. Further, according to Eurocode 8, the crack angle θ = 45 degrees and the inner lever arm z = 0.8d (≈ 0.8×0.8l_w = 0.64l_w) can be used. Substituting the values of the parameters, Eq. (5-31) becomes as follows:

$$V_{Rd,max} = 0.19 f_c' h_w l_w \tag{5-32}$$

This value is similar to the proposed Equations (5-29) and (5-30).

5.5 Verification of proposed shear strength model

From the previous sections, the proposed shear strength equation can be summarized as follows:

$$V_n = V_c + V_s = \left(\alpha_c\sqrt{f_c'} + \rho_h f_{yh}\right) A_{cv} \le V_{wcm} = \beta_c f_c' A_{cv} \qquad (5\text{-}33)$$

Where, α_c is contribution of concrete to shear strength defined in Eq. (5-19), β_c is effective stress coefficient of web concrete defined in Eq. (5-30), f_c' = concrete compressive strength (MPa), ρ_h = shear reinforcement ratio, f_{yh} = yield strength of shear reinforcement, and A_{cv} = shear resisting area (= $t_w l_w$).

To verify the proposed shear strength model (Eq. (5-33)), the proposed method and existing design methods were applied to existing wall specimens. Total number of the existing specimens was 252: present study, Adajar et al. (1995), Baek et al. (2017a, 2017b, 2018), Barda et al. (1977), Burgueno et al. (2014), Carrillo & Alcocer (2013), Cheng et al. (2016), Favashany et al. (2008), Hidalgo et al. (2002), Hirosawa (1975), Hsiao et al. (2008), Kabeyasawa & Hiraishi. (1988), Kabeyasawa et al. (1996), Kim et al. (2021), Kim & Park (2021), Kimura & Sugano (1996), Looi et al. (2017), Lopes (2001), Luna et al (2015), Maier et al. (1985), Massone et al. (2009), Mo et al. (1996), Oesterle et al. (1976), Park et al. (2015), Pilakoutas (1995), Sato et al. (1989), Seki et al. (1995), Shaingchin, et al. (2006), Sittipunt & Wood (2000), Sugano (1973), Tanabe (1973), Tuboi (2010), Tatsuya (1996), and Wallace et al. (2008). For existing specimens, rectangular shape walls, barbell shape walls, and flanged walls showing shear failure were included, excluding T-shape walls and walls with opening.

Table 5-1 shows the range of test parameters: the wall aspect ratios h_w/l_w = 0.33 – 2.70, concrete strengths f_c' = 5.2 – 137.5 MPa, vertical rebar ratios in the boundary

element ρ_{be} = 0.33 – 27.3 %, vertical rebar ratios in the web ρ_w = 0 – 3.68 %, horizontal rebar ratios in the web ρ_h = 0.11 – 3.68 %, yield strengths of vertical reinforcement f_{yv} = 296 – 1079 MPa, yield strengths of horizontal reinforcement f_{yh} = 289 – 1079 MPa, and axial load ratios $N_u/(A_g f_c')$ = 0 – 0.30. For barbell shaped walls, the dimensions of boundary element was in the following range: barbell thickness to wall length ratio t_{be}/l_w = 0.12 – 0.25, barbell width to wall thickness ratio h_{be}/h_w = 1.50 – 3.34. For flanged walls, flange thickness to wall length ratio t_{be}/l_w = 0.02 – 0.13, and flange width to wall thickness ratio h_{be}/h_w = 2.43 – 20.0.

Fig. 5-8 shows the tested strength-to-prediction ratios V_{test}/V_{pred} by ACI 318-19 seismic provision (section 18.10.4), ACI 318-19 one-way shear provision (section 22.5), Eurocode 8 (EC8), Sanchez and Alcocer (2010), Gulec and Whittaker (2011), and the proposed model (Eq. (5-33)). To calculate the shear strength by one-way shear provisions of ACI 318-19, only equation 22.5.6 (a) (Eq. (5-20)) was considered. In EC8 (for seismic design), 45 degree angle is recommended for angle of concrete strut θ. For the strength predictions, actual material strengths of concrete and rebars were used neglecting strength reduction factors and material factors. The existing prediction methods are presented in Chapter 2.

In the case of ACI 318-19 seismic provision (section 18.10.4), the test strengths of walls were safely predicted. However, the test strengths were significantly underestimated for the walls with flange (see Fig. 5-8 (a)). In Fig. 5-8 (b), one-way shear strength of ACI 318-19 (section 22.5) was applied to walls, though it was developed for beams and columns. The one-way shear strength equation showed better predictions for flanged walls by considering the effect of flexural reinforcement. However, the test strength of squat walls were underestimated. Eurocode 8 significantly underestimated the test results, not including the shear strength contribution of concrete (see Fig. 5-8 (c)). Sanchez and Alcocer developed

a shear strength equation considering the effect of various test parameters, including aspect ratio, vertical rebar ratio, horizontal rebar ratio, and axial load. However, the prediction results were not significantly improved when compared to ACI 318-19 (see Fig. 5-8 (d)). Gulec and Whittaker (2011) developed a shear strength equation using statistical optimization on existing wall tests. This equation showed better predictions (see Fig. 5-8 (e)).

The proposed simplified model (Eq. (5-33)) showed good predictions. Compared to other methods, the proposed model (Eq. (5-33)) showed good prediction for both rectangle and flanged walls. Further, as shown in Fig. 5-9, the proposed method was consistent in the strength predictions, regardless of test parameters. The minimum and maximum strength ratios were 0.61, and 1.99, respectively, and the average strength ratio was 1.08, with Coefficient of variation of 0.24.

Table 5-1 Summary of test parameters of existing wall specimens

Test parameters	Range
Shape of the wall section	Rectangle, Barbell, Flange
Aspect ratio, $M/(Vl_w)$	0.33 – 2.70
Concrete strength, f_c' [MPa]	5.2 – 137.5
Vertical rebar ratio in the boundary element, ρ_{be} [%]	0.33 – 27.3
Vertical rebar ratio in the web wall, ρ_w [%]	0 – 3.68
Horizontal rebar ratio in the web wall, ρ_h [%]	0 – 3.68
Vertical rebar strength, f_{yv} [MPa]	262 – 1079
Horizontal rebar strength, f_{yh} [MPa]	262 – 1079
Axial force ratio, $N_u/(A_g f_c')$	0 – 0.30

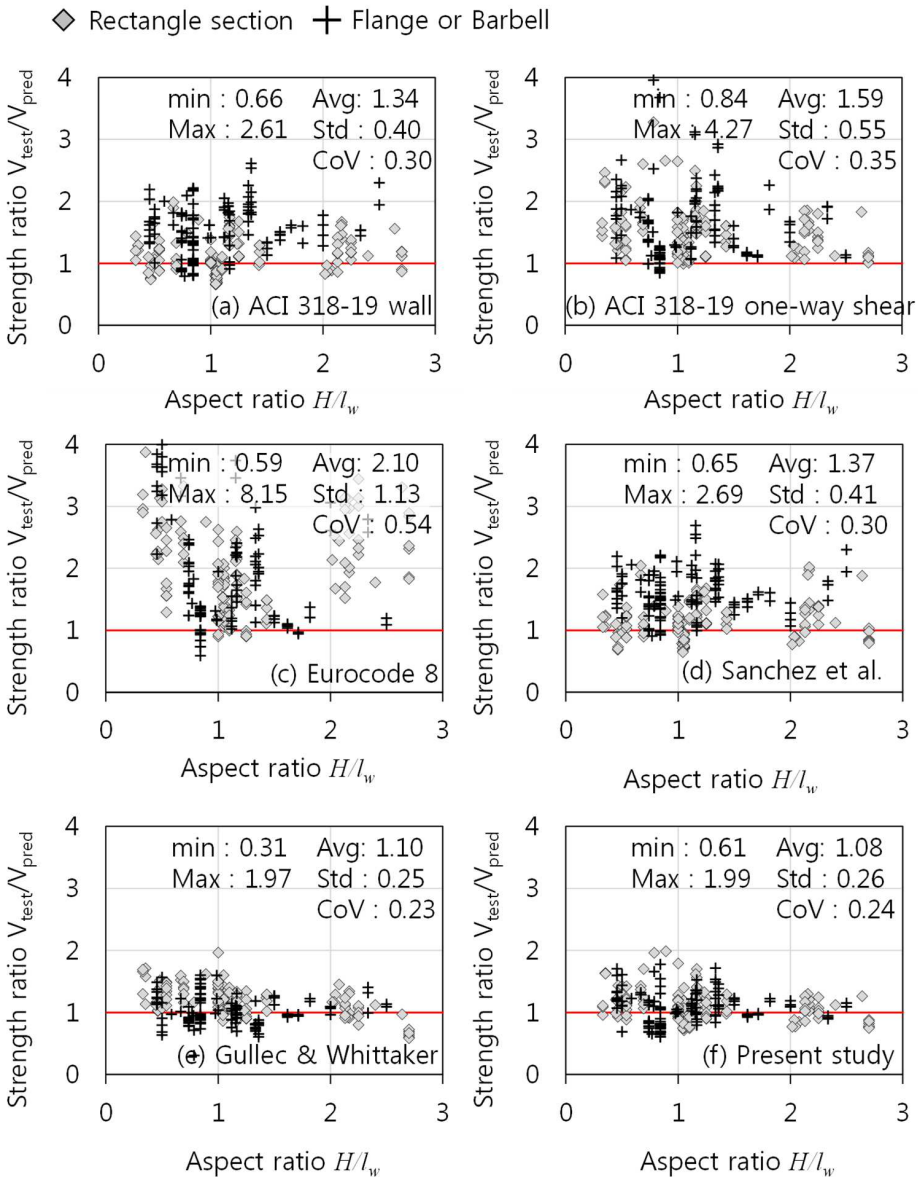

Fig. 5-8 Comparisons of strength predictions

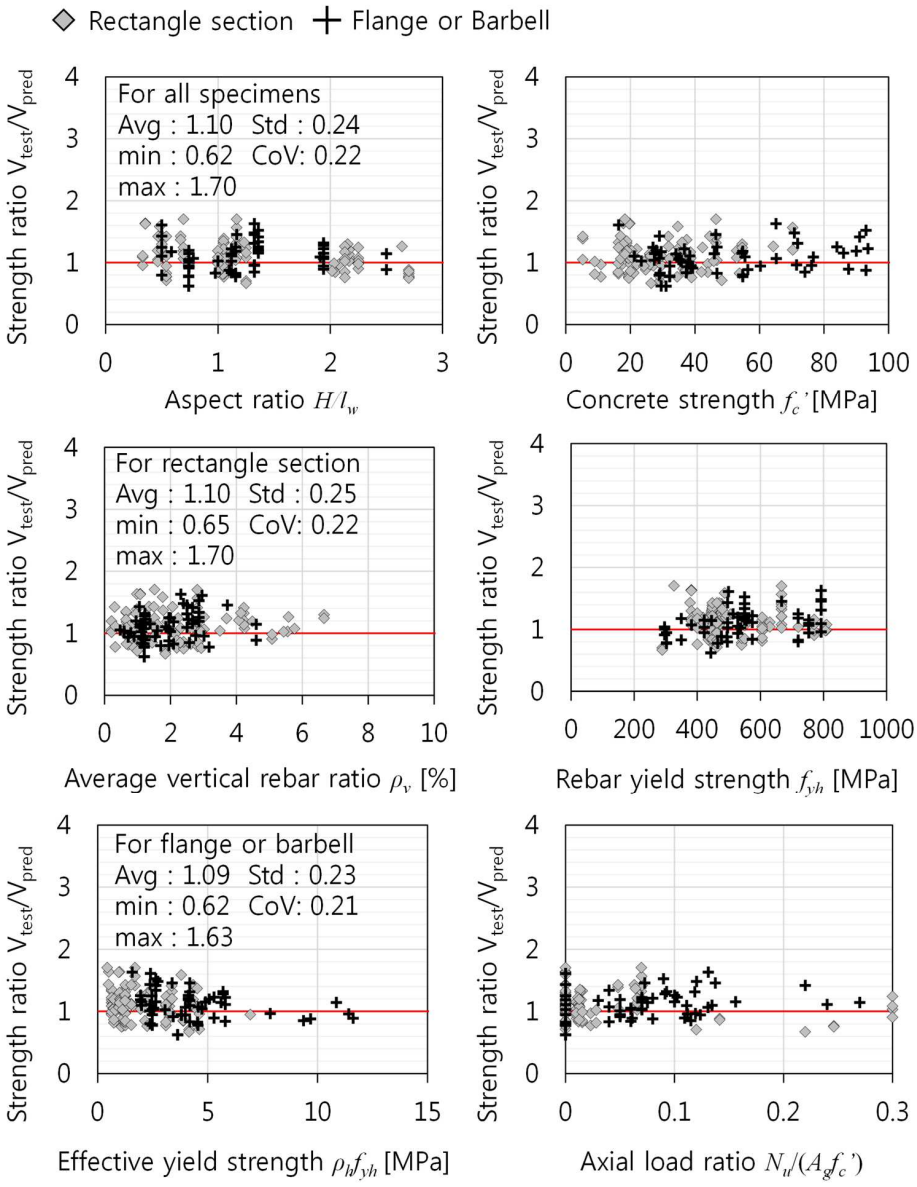

Fig. 5-9 Effect of test parameters on the proposed shear strength prediction

The proposed simplified model (Eq. (5-33)) is compared with the current design code. In KDS 14 20 22 section 4.9.2, which is a shear strength design code, the shear strength of wall is provided. The concrete shear strength V_c is calculated as follows:

$$V_c = \min(V_{c1}, V_{c2}) \geq \frac{1}{6}\sqrt{f_c'}\, t_w d \tag{5-34}$$

Where,

$$V_{c1} = 0.28\sqrt{f_c'} t_w d + \frac{N_u d}{4 l_w} \tag{5-35a}$$

$$V_{c2} = \left[0.05\sqrt{f_c'} + \frac{l_w \left(0.1\sqrt{f_c'} + 0.2\frac{N_u}{4 l_w t_w} \right)}{\frac{M_u}{V_u} - \frac{l_w}{2}} \right] t_w d \tag{5-35b}$$

Where, f_c' is concrete compressive strength, N_u is applied axial force, V_u is required shear force, M_u is required flexural moment, M_u/V_u is shear span, t_w is wall thickness, l_w is wall length, and d is effective wall length (= $0.8l_w$).

V_{c1} in Eq. (5-35a) is a shear strength which occurs the tensile failure of concrete in the web-shear cracking. Thus, it is affected by the axial force applied in the web. V_{c2} in (5-35b) is defined as a flexural-shear cracking strength, and it is affected by axial force and shear span (M/V). The concrete shear strength is determined as the lesser of V_{c1} and V_{c2}. However, it needs not to be less than the well-known equation for shear strength of concrete, $V_c = 1/6\sqrt{f_c'} t_w d$.

In KDS 14 20 80 section 4.7.4, which is a seismic design code, the shear strength of special seismic wall is provided. The shear strength V_n is calculated as follows:

$$V_n = \left(\alpha_c \sqrt{f_c'} + \rho_h f_y \right) A_{cv} \tag{5-36}$$

Where, A_{cv} is net shear area in the cross section, f_c' is concrete compressive strength, f_y is yield strength of horizontal reinforcement, ρ_h is horizontal reinforcement ratio, with α_c is 1/6 for aspect ratio greater than 2.0 ($h_w/l_w > 2.0$), and 1/4 for aspect ratio less than 1.5 ($h_w/l_w < 1.5$).

Fig. 5-10 compares the coefficient for concrete shear strength α_c defined by Eqs. (5-35) and (5-36). The coefficient for concrete shear strength is defined as $\alpha_c = v_c/\sqrt{f_c'}$. Without axial load, the shear strength equations (5-35) and (5-36) are similar. Therefore, in recent revision of ACI 318-19, the wall shear strength equation is unified into one equation (seismic version).

Compared to the current design codes, the proposed model evaluates the shear strength of concrete based on the compression zone failure mechanism. The major parameters affecting the compression depth are the vertical reinforcement ratio (ρ_{avg}) and axial force ratio ($p = N_u/(A_g f_c')$). For symmetric rectangular wall with aspect ratio of 2.0 ($H/l_w = 2$), the proposed model (Eq. (5-33)) is compared with KDS 14 20 22 shear strength model.

Without axial load, the concrete shear stress by the proposed model (Eq. (5-33)) is $v_c = 0.7(\rho_{avg})^{1/3}\sqrt{f_c'}$. The vertical reinforcement ratio ρ_{avg} = 1.35 % showed equivalent concrete shear stress of KDS 14 20 22 ($v_c = 1/6\sqrt{f_c'}$). In general case, the vertical reinforcement ratio of RC walls in the residential buildings is ρ_{avg} = 0.5 – 2.0 %. In this design range, the shear stress of concrete is evaluated as $v_c = 0.12\sqrt{f_c'} – 0.19\sqrt{f_c'}$, which is 0.72 – 1.14 times the current design code.

With high axial load ($p = N_u/(A_g f_c') = 0.2$), the concrete shear stress evaluated by the proposed model (Eq. (5-33)) is $v_c = 0.7[(\rho_{avg})^{1/3}+0.2]\sqrt{f_c'}$, and the concrete shear stress of the current design code (KDS 14 20 22) is $v_c = 0.30\sqrt{f_c'}$. The vertical reinforcement ratio ρ_{avg} = 1.11 % showed equivalent concrete shear stress of KDS

14 20 22. In the practical design range of vertical reinforcement ratio (ρ_{avg} = 0.5 – 2.0 %), the concrete shear stress evaluated by the proposed model is $v_c = 0.26\sqrt{f_c'} – 0.33\sqrt{f_c'}$, which is 0.87 – 1.10 times the current design code.

This indicates that the proposed model does not deviate significantly from the current design code. Rather, the proposed model can consider the various effect of parameters on the compression zone, such as vertical reinforcement ratio, axial load, and shape of compression zone. As shown in Fig. 5-9, the proposed model well predicts the tested shear strength regardless of the design parameters.

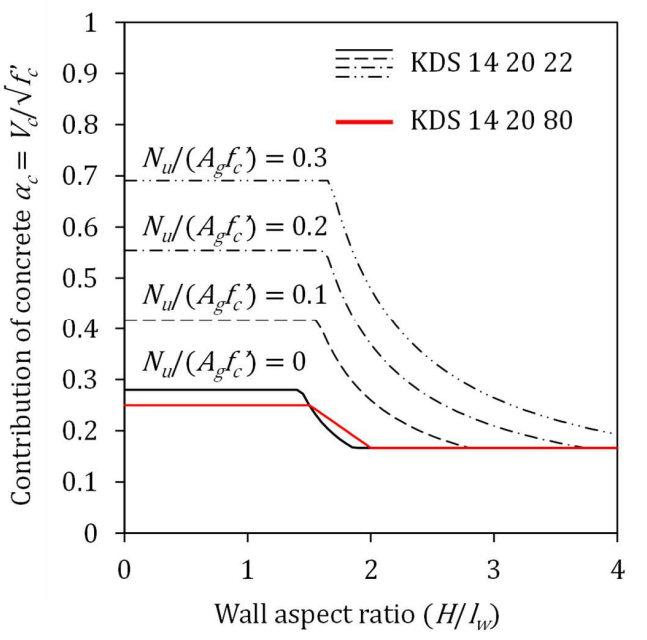

Fig. 5-10 Comparisons of shear strength model of KDS 14 20 22 and KDS 14 20 80

5.6 Summary

In the present Chapter, a simplified design method was developed to predict the shear strength of RC walls. Based on two shear failure mechanisms of diagonal tension cracking and web crushing, simplified shear strength equations were derived, considering the effects of major design parameters: vertical reinforcement ratio, axial load ratio, and the shape of cross-section.

1) For diagonal tension failure criteria, the concept of an existing compression zone failure mechanism model was implemented: The shear strength of concrete was defined as a function of compression zone depth and diagonal tension strength of concrete. For the practical range of design parameters, the compression zone depth and crack angle were simplified. For convenience in design, the proposed model was further simplified to be similar to one-way shear strength equation of ACI 318-19. The web crushing strength of concrete was derived based on an existing truss mechanism model, considering compression softening of diagonal concrete strut. The overall shear strength of wall was defined as the sum of the diagonal tension shear strength of concrete and contribution of shear reinforcement. The maximum of the shear strength is limited by the web crushing strength.

2) The proposed shear strength model was applied to existing test specimens with f_c' = 20 – 100 MPa, f_y = 400 – 800 MPa, ρ_v = 0.25 – 6.0 %, p = 0 – 0.3. The predictions of the proposed design equation agreed with the tested strengths regardless of variations of design parameters.

3) After flexural yielding, the shear strength is degraded due to inelastic deformation. The shear strength degradation is studied in next Chapter to predict deformation capacity of walls after flexural yielding.

Chapter 6. Simplified Wall Shear Strength Degradation Model

6.1 Overview

In this Chapter, for more accurate and simple prediction of shear strength-deformation relationships of the walls, the shear strength degradation model were proposed based on the shear failure mechanisms of the walls. The major shear failure mechanisms were classified to diagonal tension failure and web crushing failure. The proposed models were verified by comparing with the load-displacement response of the existing test results.

6.2 Background

Recently, because of economic reason, performance based seismic design (PBD) is usually used in the design of reinforced concrete structures. The response of the building is simulated by using the nonlinear static or dynamic analysis. Thus, to increase the reliability of the analysis results, the numerical model should accurately simulate the nonlinear behavior of the reinforced concrete members.

Fig. 6-1 shows again the lateral load-lateral displacement relationships of shear walls. When the shear strength is less than the flexural yielding strength of wall ($V_n < V_f$), the brittle shear failure occurs, and the lateral load resistance is drastically decreased. On the other hand, after flexural yielding, even the flexural strength less than the shear strength ($V_n > V_f$), the deformation capacity is limited by the shear strength degradation. In this case, the strength degradation model is required.

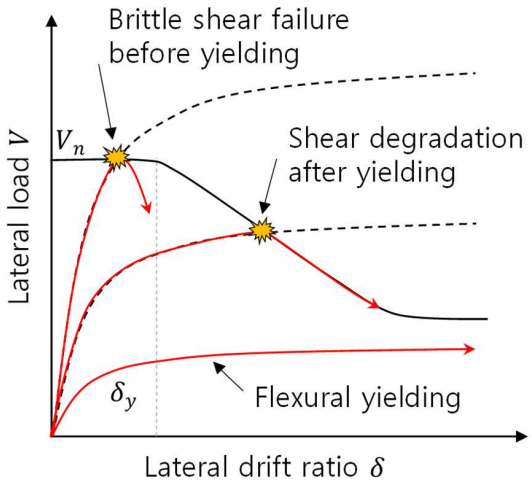

Fig. 6-1 Load-displacement relationships of shear dominant wall

Current design codes and the existing studies have investigated the shear strength-shear deformation relationships of the walls. Table 6-1 and Table 6-2 summarize the modeling parameters of the existing models. Duffey et al (1994) suggested the lateral drift ratio at the peak strength δ_m and the ultimate drift ratio limit δ_u by using the statistical analysis of existing test results. The statistical probability distribution of lateral drift ratio was fitted to lognormal distribution, and the average values of δ_m, and δ_u were suggested as 0.8 % and 1.81 %, respectively. The multi-linear envelope curve is usually used for simplification of load-displacement relationship of the shear wall. Several studies (Hidalgo, Carrillo, Sanchez) suggested the modeling parameters (maximum shear strength, and lateral drift ratios at the initiation of cracking δ_{cr}, peak strength δ_m, and failure δ_u) for multi-linear load-displacement envelope curve based on the structural test results. In their works, the shear strength of wall was defined as a sum of contributions of concrete and shear reinforcement to shear strength ($V_n = V_c+V_s$), where V_c was affected by wall aspect ratio $M/(Vl_w)$. Further, the lateral drift ratios δ_{cr}, δ_m, and δ_u were also defined as a function of aspect ratio. By using a database of existing wall tests, Carlos et al (2016) suggested empirical equations for the lateral drift ratios δ_{cr}, δ_m, and δ_u. They considered effects of various design parameters such as the aspect ratio, the axial load ratio, the concrete strength, the rebar yield strength, the vertical and horizontal reinforcement ratios, and the shape of section. The model well predicted the lateral drift of the wall test specimens, however, the equations were so complicated and inconsistent that it needs improvement.

In ASCE 41-17, FEMA 273, and FEMA 356, which are design guide line for PBD, a trilinear lateral force-lateral deformation relationship was adopted for shear-controlled RC walls based on the work of Wallace (2007). In this model, the shear strength of wall is defined according to ACI 318 code, and the modeling parameters δ_m, and δ_u are 1.0, and 2.0 %, respectively. If the effect of axial load increase, the

modeling parameters δ_m, and δ_u are decreased to 0.75 %, and 1.0 %, respectively. Further, if the axial load ratio is greater than 0.15, the wall member must be treated as a force-controlled component.

Epakachi et al (2016), suggested improvements for ASCE 41 model based on the test results from 240 tests of rectangular, barbell, and flanged shear-critical walls. In this study, for rectangular shape walls, the peak shear strength referred to shear strength provisions of ACI 318-19, whereas for barbell or flanged walls, the peak shear strength was calculated according to Barda et al (1977). Further, the optimized values of lateral drift ratios were suggested considering the effect of aspect ratio, axial load ratio, and shape of wall section.

The existing studies were based on the statistical optimization of the existing wall test data, which indicates that the reliability of the model strongly depends on the quality and quantity of the data. Therefore, it is better that the model is developed on the basis of actual failure mechanism of the wall. Further, most of the existing methods focused on the overall deformation capacity of the wall. However, in the fiber model of the walls, the in-plane shear behavior of the wall is generally defined by the shear stress-strain relationship. Therefore, it is required to define the envelope model by separating the contribution of flexural behavior and shear behavior.

Table 6-1 Summaries of existing load-drift envelope models for rectanglular wall

Researcher	δ_{cr} (%)			δ_{max} (%)	δ_u (%)
ASCE 41-17 (2017)	$\frac{(A_s - A_s')f_y + P}{t_w l_w f_c'} < 0.05$		0.4	1.0	2.0
	$\frac{(A_s - A_s')f_y + P}{t_w l_w f_c'} > 0.05$			0.75	1.0
Duffey (1994)	-			0.8	1.81
Hidalgo (1996)	$0.19\frac{M}{Vl_w}$			$0.185 + 0.45\frac{M}{Vl_w}$	$1.6\frac{M}{Vl_w}$
Carrillo (2012)	$V_{cr}\left(\frac{h_w^2}{1.5EI} + \frac{1}{0.5GA}\right) \times 100$			$\frac{V_{max}}{t_w\sqrt{f_c'}}\frac{1}{5.2}e^{1.3\frac{M}{Vl_w}}$	$\frac{V_{max}}{t_w\sqrt{f_c'}}\frac{1}{3.65}e^{1.35\frac{M}{Vl_w}}$
Sanchez (2013)	$\delta_{cr-f} = 0.01 + 0.005\frac{h_w}{l_w}$ $\delta_{cr} = 0.025 + 0.13\frac{M}{Vl_w}$			$\frac{V_{max}h_w^2}{3EI} + \frac{V_{max}}{A_w\sqrt{f_c'}}\frac{l_w}{h_w}\frac{1}{3}e^{1.33\frac{M}{Vl_w}}$	$\left(\delta_{max} + \frac{900}{\rho_h f_{yh} h_w}\right)\left(0.6\frac{M}{Vl_w} + 0.5\right) \geq 1.2\delta_{max}$
Carlos (2016)	$0.06 + 12.4\rho_{be} + 9.3\rho_h + 0.0024\frac{l_w}{t_w}$			$0.94 - 0.0006f_{yh} + 0.0063f_c' - 0.044\frac{s_h}{t_w}$	$1.30 + 30.2\rho_v - 0.46\frac{s_h}{t_w} + 0.42\frac{s_v}{t_w} + 0.1\frac{P}{A_g}$
Epackachi (2016)	$\frac{M}{Vl_w} < 1$	$0 < \frac{P}{A_g f_c'} < 0.2$	0.4	1.0	2.1
	$1 \leq \frac{M}{Vl_w} \leq 2$	$0 < \frac{P}{A_g f_c'} < 0.2$		1.0	2.5

Table 6-2 Summaries of existing load-drift envelope models for barbell or flanged walls

Researcher	δ_{cr} (%)			δ_{max} (%)	δ_u (%)
Carlos (2016)	$0.08 + 12\rho_{be} + 0.041\frac{h_w}{l_w} - 0.031\frac{s_v}{t_w}$			$0.67 + 0.24\frac{M}{Vl_w} - 0.0077\frac{l_w}{h_w} \ldots$ $+0.006f_c' - 0.0005f_{yb}$	$\left(\begin{array}{c} 2.39 - 0.001f_{yh} - 0.146\rho_{be} \ldots \\ -31.3\rho_h - 0.38\frac{s_h}{t_w} + 0.32\frac{s_v}{t_w} + 10\frac{P}{A_g} \end{array}\right)\delta_{max}$
Epackachi (2016)	$\frac{M}{Vl_w} < 1$	$0 < \frac{P}{A_g f_c'} < 0.05$	0.4	0.7	1.8
		$0.05 < \frac{P}{A_g f_c'} < 0.2$		0.7	1.4
	$\frac{M}{Vl_w} < 1$	$0 < \frac{P}{A_g f_c'} < 0.05$		0.9	2.6
		$0.05 < \frac{P}{A_g f_c'} < 0.2$		0.9	1.6

6.3 Shear strength degradation controlled by tension failure

6.3.1 Compression zone failure mechanism model

Choi et al (2007) developed a compression zone failure mechanism model to simply predict the shear strength of the RC members. Detailed concept of the compression zone failure mechanism model was already explained in the previous Chapter. Fig. 6-2 shows the shear capacity curve. According to the compression zone failure mechanism model, the shear strength is degraded by the disappearance of concrete shear resistance after the flexural yielding of the wall. Therefore, in this Chapter, the present study focused on the shear strength degradation relationships in stage C to E.

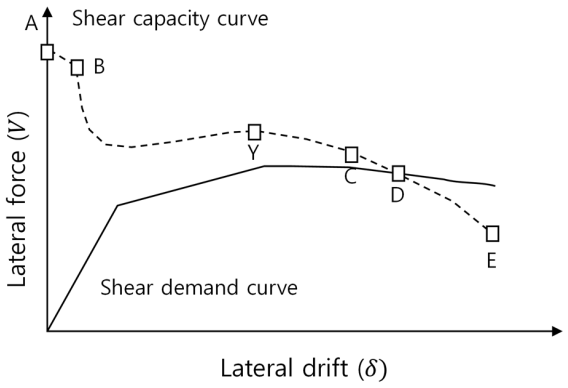

Fig. 6-2 Shear capacity curve

Fig. 6-3 shows the geometric model of the wall for calculation. The shear capacity of the wall concrete was defined as the sum of the shear capacity of the web concrete and flange concrete. The normal strain was assumed to be linearly distributed in the section. The concrete strain of extreme compression fiber was defined using a ratio

to the concrete crushing strain ($\alpha = \varepsilon_c/\varepsilon_{co}$). The normal stress-strain relationship of concrete was assumed as a parabolic relationship as follows:

$$\sigma_c(z) = f_c' \left[2\left(\frac{\varepsilon_c(z)}{\varepsilon_{co}}\right) - \left(\frac{\varepsilon_c(z)}{\varepsilon_{co}}\right)^2 \right] = f_c' \left[2\left(\frac{\alpha z}{c}\right) - \left(\frac{\alpha z}{c}\right)^2 \right] \qquad (6\text{-}1)$$

Where, $\sigma_c(z)$ is the normal stress of concrete at the distance z, $\varepsilon_c(z)$ is the concrete normal strain at the distance z, f_c' is the concrete compressive strength.

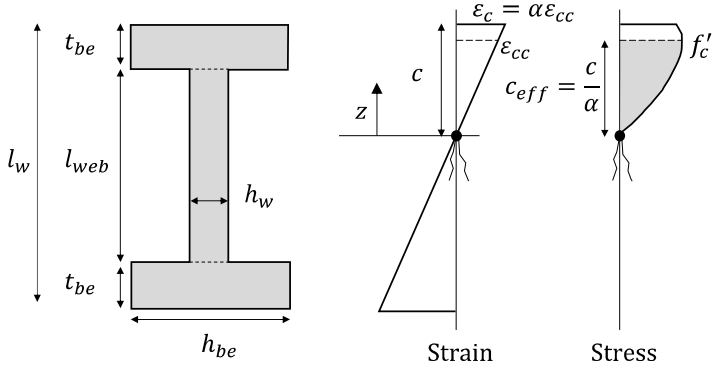

(a) Wall geometries (b) Strain-stress of concrete

Fig. 6-3 Wall section model

From the Rankine's failure criteria, the shear resistance of concrete was calculated as follows:

For shear resistance controlled by tension failure

$$v_{ct} = \sqrt{f_t\left(f_t + \sigma_c(z)\right)} \qquad (6\text{-}2a)$$

For shear resistance controlled by compression failure

$$v_{cc} = \sqrt{f_c'\left(f_c' - \sigma_c(z)\right)} \qquad (6\text{-}2b)$$

In stage CE, the shear resistance is controlled by either tension or compression failure. The critical distance, where the shear resistance controlled by tension or compression is the same ($v_{ct} = v_{cc}$), is calculated as $(1 - m)c/\alpha$, where, m is a strength ratio parameter ($= \sqrt{(f_t/f_c')}$). Therefore, the shear capacity of web concrete is calculated as the sum of the shear capacity controlled by tension and compression:

For stage CD, $1 - m \leq \alpha < 1$

$$V_{CD} = \int_0^c v_c h_w \, dz = \int_0^{(1-m)c/\alpha} v_{ct} h_w \, dz + \int_{(1-m)c/\alpha}^c v_{cc} h_w \, dz \qquad (6\text{-}3a)$$

For stage DE, $1 \leq \alpha$

$$V_{DE} = \int_0^c v_c h_w \, dz = \int_0^{(1-m)c/\alpha} v_{ct} h_w \, dz + \int_{(1-m)c/\alpha}^{c/\alpha} v_{cc} h_w \, dz \qquad (6\text{-}3b)$$

Where, h_w is the thickness of the web concrete. In stage DE, the area where the compressive strain of concrete exceeded the concrete crushing strain ($z > c/\alpha$) is excluded.

From the Eqs. (6-3a) and (6-3a), Park et al (2012) derived the shear strength degradation relationships in stage CE for the web concrete were derived as follows:

$$V_{c,w} = k_e f_c' h_w \frac{c}{\alpha} \qquad (6\text{-}4)$$

where,

For stage CD, $1 - m \leq \alpha < 1$

$$k_e = k_{CD} = m(m^2 + 1)\left(\frac{\pi}{4} - \tan^{-1} m\right) + \frac{m^2 - (\alpha - 1)^2}{2} \qquad (6\text{-}5a)$$

For stage DE, $1 \leq \alpha$

$$k_e = k_{DE} = m(m^2 + 1)\left(\frac{\pi}{4} - \tan^{-1} m\right) + \frac{m^2}{2} \qquad (6\text{-}5b)$$

In Eq. (6-5a), $(\alpha - 1)^2$ can be neglected because the value of $(\alpha - 1)^2$ is significantly less than m^2. Therefore, k_{CD} is equal to k_{DE}, and Park et al (2012) simplified the value of k_{DE} as $k_{DE} = 0.69m$. Further, by the definition of $\alpha = \varepsilon_c/\varepsilon_{co}$, the term c/α in Eq. (6-4) is redefined as ε_{co}/ϕ, where ϕ is the flexural curvature at the wall base (= ε_c/c). For ordinary strength concrete, the concrete crushing strain of ε_{co} = 0.002 can be used. Finally, Eq. (6-4) can be expressed as follows:

$$V_{c,w} = 1.38 \times 10^{-3} m f_c' h_w \frac{1}{\phi} \tag{6-6}$$

On the other hand, the compression zone failure mechanism model assumes that only the concrete in the compression zone depth can resist the shear. When the compressive strain exceeds the concrete crushing strain ($\varepsilon_{cc} = K\varepsilon_{co}$, where, K = confinement coefficient from Kent-Park model (1971)), shear strength degradation occurs due to reduction of effective compression zone depth (see Fig. 6-3 (b)). Therefore, the shear strength degradation can be simplified defined as follows:

$$V_{c,w} = V_{c0}\left(\frac{c_{eff}}{c}\right) = V_{c0}\left(\frac{K\varepsilon_{co}}{\varepsilon_c}\right) = \frac{V_{c0}K\varepsilon_{co}}{c}\left(\frac{c}{\varepsilon_c}\right) = \frac{V_{c0}K\varepsilon_{co}}{c}\left(\frac{1}{\phi}\right. \tag{6-7}$$

Where, V_{c0} is shear strength of concrete before yielding (= $\alpha_c\sqrt{f_c'}$), K is confinement coefficient, ε_{co} is crushing strain of unconfined concrete, ε_c is compressive strain of extreme fiber, c is compression zone depth, and ϕ is the flexural curvature at the wall base (= ε_c/c).

Eq. (6-7) is a simplified version of Eq. (6-6). Both equations are compared in the section 6.2.3.

For flange walls, the contribution of flange needs to be added. In the stage CE, shear resistance of the flange concrete is assumed to be controlled by compression failure. Therefore, the shear capacity of flange concrete is calculated as follows:

For stage CD, $1 - m \leq \alpha < 1$

$$\begin{aligned} V_{CD,f} &= \int_{c-t_{be}}^{c} \sqrt{f_c' \left(f_c' - \sigma(z)\right)} (h_{be} - h_w) dz \\ &= f_c'(h_{be} - h_w) \int_{c-t_{be}}^{c} 1 - \frac{\alpha z}{c} dz \end{aligned} \tag{6-8a}$$

For stage DE, $1 \leq \alpha$

$$\begin{aligned} V_{DE,f} &= \int_{c-t_{be}}^{c/\alpha} \sqrt{f_c' \left(f_c' - \sigma(z)\right)} (h_{be} - h_w) dz \\ &= f_c'(h_{be} - h_w) \int_{c-t_{be}}^{c/\alpha} 1 - \frac{\alpha z}{c} dz \end{aligned} \tag{6-8b}$$

Where, h_{be} is the effective depth of the flange wall, and t_{be} is the thickness of the flange wall.

Eqs. (6-8a) and (6-8b) were calculated as follows:

For stage CD, $1 - m \leq \alpha < 1$

$$V_{CD,f} = \left(1 - \alpha + \frac{\alpha}{c}\frac{t_{be}}{2}\right) f_c'(h_{be} - h_w) t_{be} \tag{6-9a}$$

For stage DE, $1 \leq \alpha$

$$V_{DE,f} = \left(\frac{c}{\alpha t_{be}}\frac{(1-\alpha)^2}{2} + 1 - \alpha + \frac{\alpha}{c}\frac{t_{be}}{2}\right) f_c'(h_{be} - h_w) t_{be} \tag{6-8b}$$

In the range of $1 \leq \alpha$, V_{CD} was always less than V_{DE}. Thus, for safe evaluation, the shear capacity of the flange concrete is evaluated by Eq. (6-9) in stage CE. From the definition of $\alpha = \varepsilon_c/\varepsilon_{co}$, the term c/α is redefined as ε_{co}/ϕ. Therefore, the shear capacity of flange wall $V_{c,f}$ is defined as follows:

$$V_{c,f} = \left(1 - \left(c - \frac{t_{be}}{2}\right)\frac{\phi}{\varepsilon_{co}}\right) f_c'(h_{be} - h_w)t_{be} \tag{6-10}$$

Where, the compression zone depth c can be calculated from the sectional analysis of the flanged walls. Fig. 6-4 shows the calculated compression zone depth of the flanged wall test specimens. For simple evaluation, the compression zone depth is assumed to be quarter of the wall length ($c = 1/4l_w$). Thus, the term $c - t_{be}/2$ in Eq. (6-10) becomes to $1/4l_w - t_{be}/2$, which is equal to the quarter of the web length ($1/4l_{web}$). The length of web wall is assumed as $l_{web} \approx d = 0.6l_w$, where d is the effective depth of the wall (see Fig. 6-5 (b)). The concrete crushing strain of ε_{co} = 0.002 is used. Thus, the Eq. (6-10) is expressed as follows:

$$V_{c,f} = (1 - 75l_w\phi)f_c'(h_{be} - h_w)t_{be} \geq 0 \tag{6-11}$$

The concrete shear capacity of wall is defined as follows.

For rectangular walls

$$V_c = V_{c,w} = 1.38 \times 10^{-3} m f_c' h_w \frac{1}{\phi} \tag{6-12a}$$

For flanged walls

$$\begin{aligned} V_c &= V_{c,w} + V_{c,f} \\ &= 1.38 \times 10^{-3} m f_c' h_w \frac{1}{\phi} + (1 - 75l_w\phi)f_c'(h_{be} - h_w)t_{be} \end{aligned} \tag{6-12b}$$

In Eq.(6-12), the shear capacity of concrete is defined as function of curvature in the plastic hinge zone. Thus, the shear capacity of the wall is degraded as the plastic hinge rotation increases.

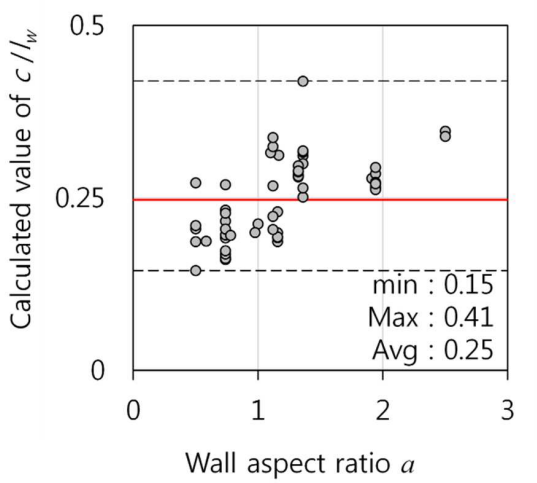

Fig. 6-4 Compression zone depth of the flanged wall test specimens

6.3.2 Deformation model

In Eq.(6-12), the concrete shear capacity of wall was derived as a function of curvature. Therefore, in order to derive the shear strength – lateral deformation relationship, the curvature ϕ should be transformed to lateral deformation Δ.

Fig. 6-5 shows a deformation model for a cantilever wall (Eom et al., 2013). The overall lateral deformation is defined as the sum of contributions of flexure and shear.

$$\Delta = \Delta_f + \Delta_s \tag{6-13}$$

The flexural deformation Δ_f is calculated for the distribution of curvature. At the wall base, the overall curvature ϕ consists of plastic curvature ϕ_p and yielding curvature ϕ_y (see Fig. 6-5 (a)). The distribution of ϕ_p in the plastic hinge region is assumed to be uniform, while the elastic curvature is assumed to be linearly distributed along the height of the wall. After yielding, the flexural deformation is defined as follows:

$$\Delta_f = \Delta_{pf} + \Delta_{yf} \tag{6-14}$$

Where, Δ_{pf} is the flexural deformation developed by plastic curvature, and Δ_{yf} is the flexural deformation developed by yielding curvature. The plastic flexural deformation Δ_{pf} is calculated from distribution of plastic curvature as follows:

$$\Delta_{pf} = \phi l_p \left(H - \frac{l_p}{2}\right) \approx 0.8 l_w \phi (H - 0.4 l_w) \tag{6-15}$$

Where, ϕ_p is the plastic curvature, l_p is the plastic hinge length (assumed as $l_p \approx d = 0.8 l_w \leq H$, Lee and Watanabe, 2003), l_w is the wall length, and H is the wall height.

The yielding flexural deformation Δ_{yf} is calculated as follows:

$$\Delta_{yf} = \frac{H^2}{3}\phi_y \approx \frac{2}{3}\varepsilon_y \frac{H^2}{l_w} \tag{6-16}$$

Where, ϕ_y is the yielding curvature (assumed as ϕ_y = 2/3 ε_y/l_w, Eom et al (2013)), and ε_y is the yield strain of the tensile vertical reinforcement.

Therefore, from Eqs. (6-15) and (6-16), the overall curvature is expressed as follows:

$$\phi = \phi_p + \phi_y = \frac{\Delta_{pf}}{0.8l_w(H - 0.4l_w)} + \frac{2\varepsilon_y}{l_w} \tag{6-17}$$

After diagonal tension cracking and flexural yielding, the shear deformation Δ_{ps} of the wall is significantly increased in the plastic hinge region, whereas the shear deformation Δ_{es} in the elastic region is relatively small. Therefore, the shear drift ratio Δ_s is defined as follows:

$$\Delta_s = \Delta_{ps} + \Delta_{es} \approx \Delta_{ps} \tag{6-18}$$

The shear deformation in the plastic hinge region is defined as a function of plastic hinge deformation:

$$\Delta_{ps} = c_v \Delta_p \tag{6-19}$$

Where, c_v is the contribution ratio of the shear deformation to plastic hinge deformation. The plastic hinge deformation Δ_p is defined as the sum of flexural deformation and shear deformation as follows:

$$\Delta_p = \Delta_{pf} + \Delta_{ps} \tag{6-20}$$

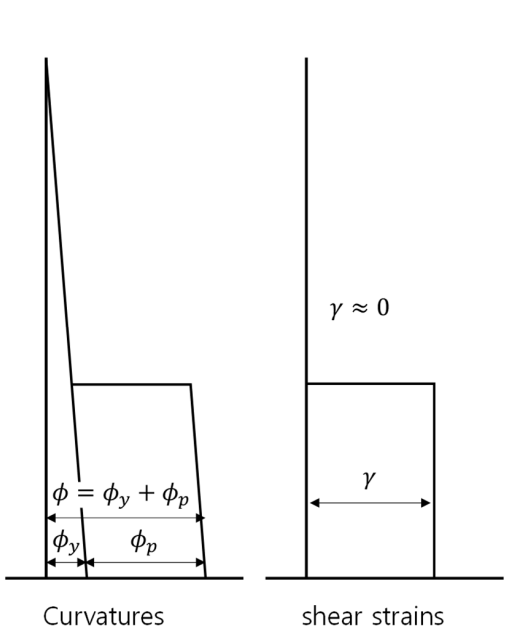

(a) Curvature and shear strain distribution

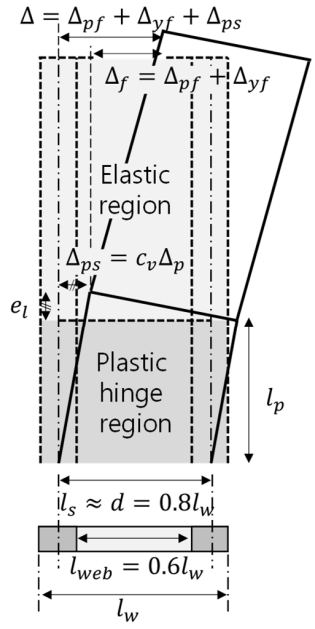

(b) Simplified deformation model

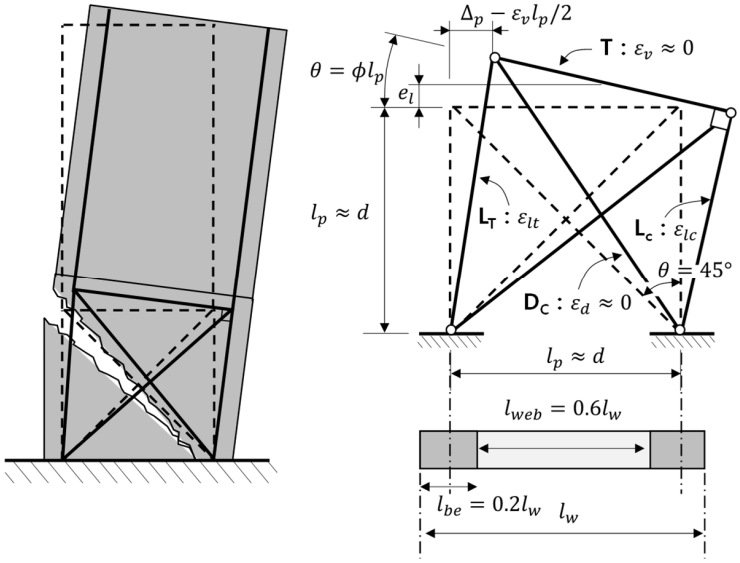

(c) Deformation mechanism of plastic hinge region

Fig. 6-5 Deformation model

The shear deformation of the plastic hinge zone is mainly related to elongation of the wall (Eom et al. (2013)). Fig. 6-5 (c) shows the deformation mechanism in the plastic hinge region. In the shear failure after flexural yielding mode, it is assumed that a major shear crack occurs in the plastic hinge region. In this case, the wall segment above the shear crack can be assumed to rotate rigidly. Therefore, displacement compatibility in the plastic hinge region is derived as follows:

$$-\left(\Delta_p - \varepsilon_v l_p/2\right)\sin\theta + \varepsilon_{lt} l_p \cos\theta = -\varepsilon_d l_p/\cos\theta \tag{6-21}$$

Where, Δ_p is lateral deformation of plastic hinge region, ε_v is tensile strain of horizontal tie **T**, ε_{lt} is tensile strain of vertical tie $\mathbf{L_T}$, ε_c is compressive strain of diagonal strut $\mathbf{D_C}$, θ is crack angle (generally, = 45°), and l_p is plastic hinge length.

From the assumption of rigid rotation, ε_v and ε_c is assumed to be small (ε_v and ε_c = 0). Thus, from Eq. (6-21) the plastic hinge deformation is calculated as follows:

$$\Delta_p = \varepsilon_{lt} l_p \cot\theta = \varepsilon_{lt} l_p \tag{6-22}$$

The curvature and elongation of plastic hinge region is calculated from the vertical strains of vertical truss member $\mathbf{L_T}$ and $\mathbf{L_C}$ as follows:

$$\phi = \frac{\varepsilon_{lt} - \varepsilon_{lc}}{l_p} \tag{6-23a}$$

$$e_l = \frac{\varepsilon_{lt} + \varepsilon_{lc}}{2} l_p \tag{6-23b}$$

From Eqs. (6-23a) and (6-23b), ε_{lt} is calculated as follows:

$$\varepsilon_{lt} = \frac{\phi l_p}{2} + \frac{e_l}{l_p} \tag{6-24}$$

Substituting Eq. (6-24) into Eq. (6-22), the relationship between plastic hinge deformation and elongation is derived as follows:

$$\Delta_p = \frac{\phi}{2} l_p^2 + e_l \tag{6-25}$$

Since $1/2\phi l_p^2 = \Delta_{pf}$, and $\Delta_p = \Delta_{pf} + \Delta_{ps}$, it is resulted that the elongation of the plastic hinge zone is equal to the shear deformation of the plastic hinge zone ($e_l = \Delta_{ps}$).

After yielding of the wall, the elongation of the plastic hinge region is increased by the effect of cyclic loading (Eom and Park (2013)). As the inelastic deformation increases, a significant tensile plastic strain develops in the vertical reinforcement. Even under reversed loading, the tensile stress of vertical reinforcement having been applied by tensile stress is maintained because of the residual tensile strain. Therefore, as cyclic loading progresses, the elongation increases further. From the truss model, Eom and Park (2013) developed an equation for elongation of the wall developed by cyclic loading:

$$e_l = \frac{\Delta_p \frac{l_s}{H}\left(1 + \eta_b \frac{\sigma_{lc}}{2f_y}\right) - \left(1 - \frac{l_p}{2H}\right)\varepsilon_y l_p}{1 - \left(1 + \eta_b \frac{\sigma_{lc}}{f_y}\right)\left(1 - \frac{l_p}{H}\right)} \tag{6-26}$$

where,

$$\sigma_{lc} = -f_y\left(\frac{A_{sbe}}{A'_{sbe}}\right)\left(1 - \frac{l_p}{H}\right) + \left[-\frac{P}{A'_{sbe}} - f_{yw}\left(\frac{A_{sw}}{A'_{sbe}}\right)\right]\left(1 - \frac{l_p}{2H}\right) \tag{6-27}$$

where, Δ_p is the plastic hinge deformation, l_s is center-to-center distance between both boundary elements (assumed as $l_s \approx d = 0.8l_w$), l_p is plastic hinge length (assumed as $l_p \approx d = 0.8l_w$), H is the wall height, ε_{ybe} is yield strain of the vertical

reinforcement in the boundary element, f_y and f_{yw} are yield strengths of the vertical reinforcement in the boundary element and web, respectively, η_b is coefficient addressing the Bauschinger effect (assumed as $\eta_b = 0.6$, Eom and Park, 2010), σ_{lc} is compressive stress of vertical reinforcement in the boundary element ($-f_y < \sigma_{lc} < 0$), A_{sbe} and A'_{sbe} are total cross-sectional areas of the vertical reinforcement in the boundary element in tension and compression, respectively, A_{sw} is total cross-sectional area of the vertical reinforcement in the web, and P is applied compression force.

In this study, following assumptions were used for simple calculation of Eqs. (6-26) and (6-27):

1) Plastic hinge region is square region $l_s \approx l_p \approx d = 0.8l_w$.

2) $\Delta - \Delta_{yf} = \Delta_p$, the plastic hinge deformation.

3) $A_{sbe} = A'_{sbe}$ for symmetric section.

4) $f_{yw} = f_y$ in general design case.

By these assumptions, Eqs. (6-26) and (6-27) become as follows:

$$e_l = \frac{0.8\Delta_p(1 - 0.3s_{be}) - 0.8(a - 0.4)\varepsilon_{ybe}l_w}{0.6as_{be} - 0.48s_{be} + 0.8} \tag{6-28}$$

where,

$$s_{be} = \frac{\sigma_{lc}}{-f_y} = \left(1 - \frac{0.8}{a}\right) + \left[\frac{P}{A_{sbe}f_y} + \left(\frac{A_{sw}}{A_{sbe}}\right)\right]\left(1 - \frac{0.4}{a}\right) \tag{6-29}$$

Where, $a = H/l_w$ is the aspect ratio of the wall (≥ 0.8). $s_{be} = -\sigma_{lc}/f_y$ is the stress level parameter of vertical reinforcement in the boundary element.

From Eq. (6-19), the shear contribution ratio is defined as $c_v = \Delta_s/\Delta_p$. The shear deformation is assumed to be equal to the elongation of the plastic hinge zone ($\Delta_s \approx e_l$, Fig. 6-5 (b)). Therefore, the shear contribution ratio c_v is calculated as follows:

$$c_v = \frac{\Delta_{ps}}{\Delta_p} \approx \frac{e_l}{\Delta_p} = \frac{0.8(1 - 0.3s_{be}) - 0.8(a - 0.4)\varepsilon_{ybe} l_w/\Delta_p}{0.6as_{be} - 0.48s_{be} + 0.8} \quad (6\text{-}30)$$

Because the shear strength degradation occurred after flexural yielding, the inelastic lateral deformation Δ_p is relatively large compared to $0.8(a - 0.4)\varepsilon_{ybe} l_w$. Therefore, in Eq. (6-30), the term $0.8(a - 0.4)\varepsilon_{ybe} l_w/\Delta_p$ is negligible. Further, in Eq. (6-30), the shear contribution ratio is defined as a function of s_{be} and a. In the range of $0.8 < a < 2.5$, and $0.5 < s_{be} < 1.0$, Eq. (6-30) can be simplified as a linear function of s_{be} and a.

$$c_v = \frac{\Delta_{ps}}{\Delta_p} = 1 - 0.19a - 0.25s_{be} \quad (6\text{-}31)$$

For verification, Fig. 6-6 compares the simplified Eq. (6-31) with the original Eq. (6-30), in the following range of design parameters: $a = 0.8 – 2.5$, $s_{be} = 0.5 – 1.0$, $\varepsilon_{ybe} = 0.002 – 0.004$, $l_w = 2000$ mm, and $\Delta_p/H = 2$ %. Eq. (6-31) reasonably simplified Eq. (6-30) as shown in Fig. 6-6. The range of the shear contribution ratio is $c_v = 0.25 – 0.75$.

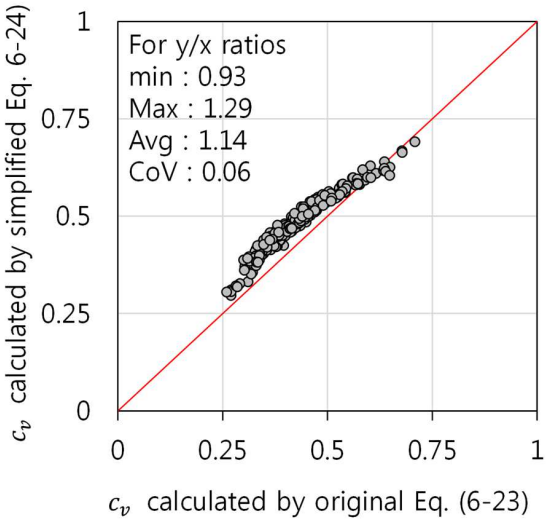

Fig. 6-6 Comparison of the shear contribution ratio

Under axial compression, tensile residual strains disappear in the boundary element in compression. When the compressive stress is σ_{lc} less than $-f_y$ ($s_{be} > 1$), the compressive stress in the boundary element induces yielding of rebars in compression. Therefore, the elongation is not increased by the cyclic loading. In this case, Eom and Park (2013) suggested that the elongation was calculated as follows:

$$e_l = \Delta_p \frac{l_s}{2H} \tag{6-32}$$

Where, Δ_p is the plastic hinge deformation, l_s is center-to-center distance between both boundary elements (assumed as $l_s \approx d = 0.8l_w$), and H is the wall height. By assumptions used in the simplification of Eqs. (6-26) and (6-27), e_l is simplified as follows:

$$e_l = \frac{0.4\Delta_p}{a} \tag{6-33}$$

In this case, the shear contribution ratio is calculated as follows:

$$c_v = \frac{\Delta_{ps}}{\Delta_p} \approx \frac{e_l}{\Delta_p} = \frac{0.4}{a} \leq 0.5 \tag{6-34}$$

Because of the limitation of aspect ratio $a \geq 0.8$, the maximum value of the contribution ratio in Eq. (6-34) is limited to 0.4/0.8 = 0.5. Finally, the shear deformation ratio is summarized as follows:

$$c_v = \frac{\Delta_{ps}}{\Delta_p} = \begin{cases} 1 - 0.19a - 0.25s_{be} & (\text{for } s_{be} \leq 1) \\ \min(0.5, 0.4/a) & (\text{for } s_{be} > 1) \end{cases} \tag{6-35}$$

From Eqs. (6-17), (6-19), and (6-20), the curvature ϕ is transformed to the plastic hinge deformation as follows:

$$\phi = \frac{(1 - c_v)\Delta_p}{0.8 l_w (H - 0.4 l_w)} + \frac{2\varepsilon_y}{l_w} = \frac{c_1 R}{l_w} + \frac{2\varepsilon_y}{l_w} \tag{6-36}$$

where,

$$c_1 = \frac{a(1 - c_v)}{0.8(a - 0.4)} \tag{6-37}$$

Where, R is the plastic hinge rotation (Δ_p/H), and the coefficient c_1 is related to the wall aspect ratio a and the shear contribution ratio c_v.

When, s_{be} was less than 1.0, the value of c_1 ranged 0.70 – 1.05 in the range of parameters: a = 0.8 – 2.5, and c_v = 0.25 – 0.75. When s_{be} is greater than 1.0, the value of c_1 is 1.25 because of $c_v = 0.4/a$. Therefore, the curvature – plastic hinge rotation relationship was summarized as follows:

$$\phi = \left(c_1 R + 2\varepsilon_y\right)/l_w = \begin{cases} \left(c_1 R + 2\varepsilon_y\right)/l_w & (\text{for } s_{be} \leq 1) \\ \left(1.25R + 2\varepsilon_y\right)/l_w & (\text{for } s_{be} > 1) \end{cases} \tag{6-38}$$

6.3.3 Simplified strength degradation model controlled by diagonal tension failure

Substituting Eq. (6-38) into Eq. (6-6), Eq. (6-7) and (6-11), the shear capacity of the concrete is defined as a function of plastic hinge, for both web concrete and flange concrete.

For web concrete

$$V_{c,w} = 1.38 \times 10^{-3} m f_c' l_w h_w \frac{1}{c_1 R + 2\varepsilon_y} \tag{6-39a}$$

$$V_{c,w} = \frac{V_{c0} K \varepsilon_{co}}{c} \left(\frac{1}{c_1 R + 2\varepsilon_y} \right) \tag{6-39b}$$

For flange concrete

$$V_{c,f} = \left(1 - 75\left(c_1 R + 2\varepsilon_y\right)\right) f_c'(h_{be} - h_w) t_{be} \tag{6-39c}$$

Fig. 6-7 shows the shear capacity of the web concrete – plastic hinge rotation ($V_{c,w}$– R) relationship. For calculation, the values of parameters were assumed as follows: c/l_w = 1/4 and 1/3, c_1 = 0.9 and 1.25, f_c' = 20, 50, and 100 MPa, f_y = 400 and 800 MPa, and ε_y = 0.002 and 0.004. In Fig. 6-7, the vertical axis indicates the shear stress which is defined as the shear strength divided by the cross sectional area of web ($V_{c,w}/(l_w h_w)$).

The shear stress of the web concrete is gently decreased as the plastic hinge rotation increases. Further, the shear stress calculated by Eq. (6-39b) is similar to or less than the shear stress calculated by Eq. (6-39a). Therefore, in the simplified shear strength degradation model, the contribution of web concrete to shear capacity $V_{c,w}$ can be calculated by Eq. (6-39b).

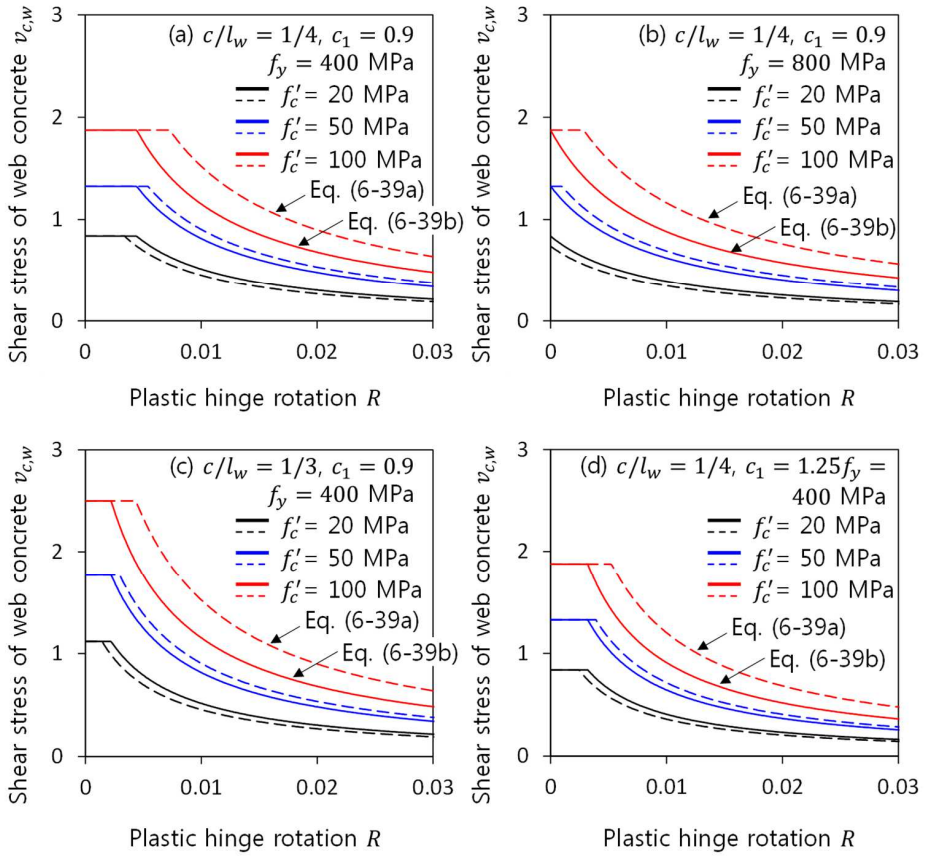

Fig. 6-7 Shear capacity of web concrete

Fig. 6-8 shows the shear capacity of the flange concrete – plastic hinge rotation ($V_{c,f}$ – R) relationship. For calculation, the values of parameters were assumed as follows: c_1 = 0.9 and 1.25, f_c' = 20 – 100 MPa, f_y = 400 – 800 MPa, and ε_y = 0.002 – 0.004. In Fig. 6-8, the vertical axis indicates the shear stress which is defined as the shear strength divided by the cross sectional area of flange ($V_{c,f}/((h_{be} - h_w)t_{be})$).

The shear stress of the flange concrete is significantly decreased and eliminated in the range of plastic hinge rotation 0 < R < 0.01. Therefore, in the simplified shear strength degradation model, the contribution of flange concrete to shear capacity $V_{c,f}$ can be neglected for conservative prediction ($V_{c,f} \approx 0$).

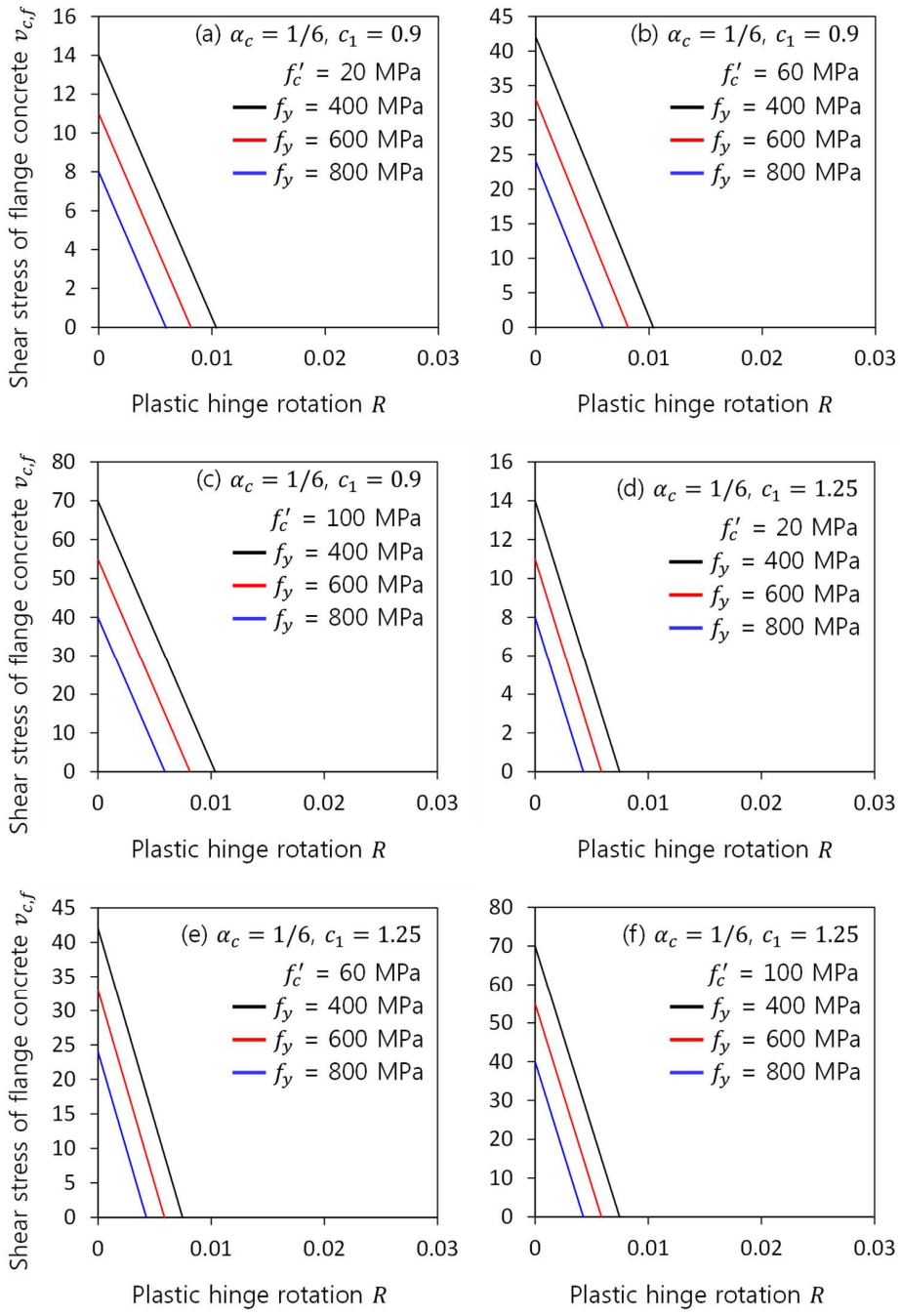

Fig. 6-8 Shear capacity of flange concrete

Therefore, the shear strength degradation of concrete is defined as follows:

$$V_c = \frac{V_{c0} K \varepsilon_{co}}{c} \left(\frac{1}{c_1 R + 2\varepsilon_y} \right) \tag{6-40}$$

Eq. (6-40) is available regardless of cross sectional shape. Eq. (6-40) indicates that the shear capacity of concrete is degraded as the plastic hinge rotation increased.

The shear strength degradation of wall is defined as follows:

$$V_n = \eta V_c + V_s \tag{6-41}$$

where,

$$V_c = V_{c0} = \alpha_c \sqrt{f_c'} A_{cv} \tag{6-42a}$$

$$V_s = \rho_h f_{yh} A_{cv} \tag{6-42b}$$

Where, η is the contribution ratio of the concrete to shear strength ($0 \leq \eta \leq 1$), A_{cv} is gross area resisting the shear ($= l_w h_w$), ρ_h is the shear reinforcement ratio, and f_{yh} is the yield strength of shear reinforcement.

The shear strength degradation is expressed by the contribution ratio of concrete shear strength to the wall shear strength as follows:

$$\eta = \frac{K \varepsilon_{co}}{c/l_w} \frac{1}{\left(c_1 R + 2\varepsilon_y \right)} \leq 1 \tag{6-43}$$

Fig. 6-9 shows the contribution ratio – plastic hinge rotation (η – R) relationship. For calculation, the values of parameters were assumed as follows: c/l_w = 0.25 and 0.50, c_1 = 0.9 and 1.25, f_c' = 20, 50, and 100 MPa, f_y = 400 and 800 MPa, and ε_y = 0.002 and 0.004. The contribution ratio η is significantly decreased in the range of plastic hinge rotation 0 < R < 0.02. Therefore, for safe evaluation, the contribution ratio η is simplified as a linear equation.

The linear equation is defined by a secant line between (R, η) = (0, 1.0) and (R, η) = (R_h, 0.5). From Eq. (6-43), the plastic hinge rotation at η = 0.5 is calculated as $R_h = (2K\varepsilon_{co}/(c/l_w) - 2\varepsilon_y)/c_1$. Thus, the secant slope is calculated as follows:

$$k_{dt} = \frac{1-0.5}{0-R_h} = -\frac{0.25c_1}{\left(\frac{K\varepsilon_{co}}{c/l_w} - \varepsilon_y\right)} \approx -\frac{125c_1}{\left(\frac{K}{c/l_w} - 1.5\right)} \tag{6-44}$$

Here, in the design range of concrete strength f_y = 400, 600 and 800 MPa and ε_y = 0.002, 0.003, and 0.004, the strain ratio $\varepsilon_y/\varepsilon_{co}$ is calculated $\varepsilon_y/\varepsilon_{co}$ = 1 to 2. For simple calculation, $\varepsilon_y/\varepsilon_{co}$ = 1.5 is used.

The simplified linear equation for η is defined as follows:

$$\eta_1 = 1 + k_{dt}(R-0) = 1 - \frac{125c_1}{(Kl_w/c - 1.5)}R \tag{6-45}$$

Where, the range of η_1 should be $0.2 \leq \eta_1 \leq 1$. For diagonal tension failure mechanism, the residual strength of concrete is considered as $0.2V_c$.

In Eq. (6-45), effects of design parameters on deformation capacity are as follows: 1) when the compression depth increases, the slope k_{dt} increases, which causes the decrease of deformation capacity; 2) when the shear contribution increases, the slope k_{dt} increases, and the deformation capacity decreases; and 3) when the confinement effect increases, the slope k_{dt} decreases, and the deformation capacity increases.

Fig. 6-9 also shows the contribution ratio calculated by the simplified Eq. (6-45) (dotted line). Eq. (6-45) is fitted with (6-43) in any plastic hinge rotation.

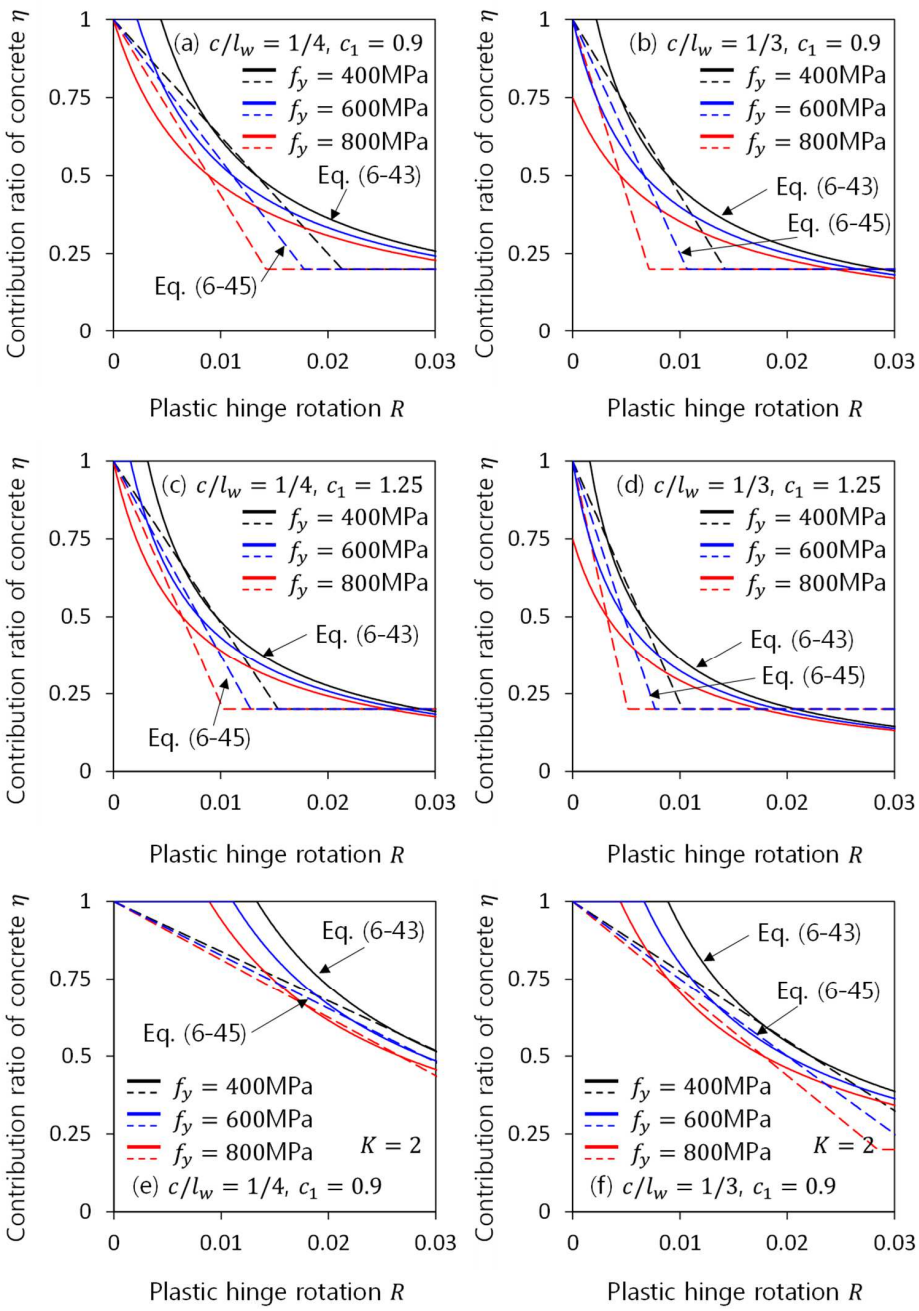

Fig. 6-9 Contribution ratio of concrete to shear strength η

6.4 Shear strength degradation controlled by web crushing failure

6.4.1 Truss mechanism model

Eom and Park (2013) proposed a web crushing strength model by using the truss mechanism model. Fig. 6-10 shows the concept of the model. In Chapter 5, using the truss mechanism model, the web crushing strength of wall is summarized as follows:

$$V_{wc} = \frac{f_c' l_w h_w}{3.8 + 1.13\left(f_{yh}/400\right) + 567\left(e_l/l_p\right)} \tag{6-46}$$

The maximum shear strength (= web crushing strength) of the shear wall is evaluated by assuming the deformation state before yielding. Before yielding of the wall, the plastic hinge is not developed yet, thus, the elongation can be neglected. Therefore, the web crushing strength is defined as follows:

$$V_{wcm} = \beta_c f_c' A_{cv} \tag{6-47}$$

where,

$$\beta_c = \frac{1}{3.8 + 1.13\left(f_{yh}/400\right)} \approx \begin{cases} 1/5 & \left(\text{for } f_{yh} \le 400 \text{ MPa}\right) \\ 1/6 & \left(\text{for } f_{yh} \ge 800 \text{ MPa}\right) \end{cases} \tag{6-48}$$

Where, A_{cv} is the gross area resisting shear (= $l_w h_w$). The coefficient β_c was suggested as β_c = 1/5 for $f_{yh} \le$ 400 MPa, β_c = 1/6 for $f_{yh} \ge$ 800 MPa, and linear interpolation for 400 < f_{yh} < 800 MPa.

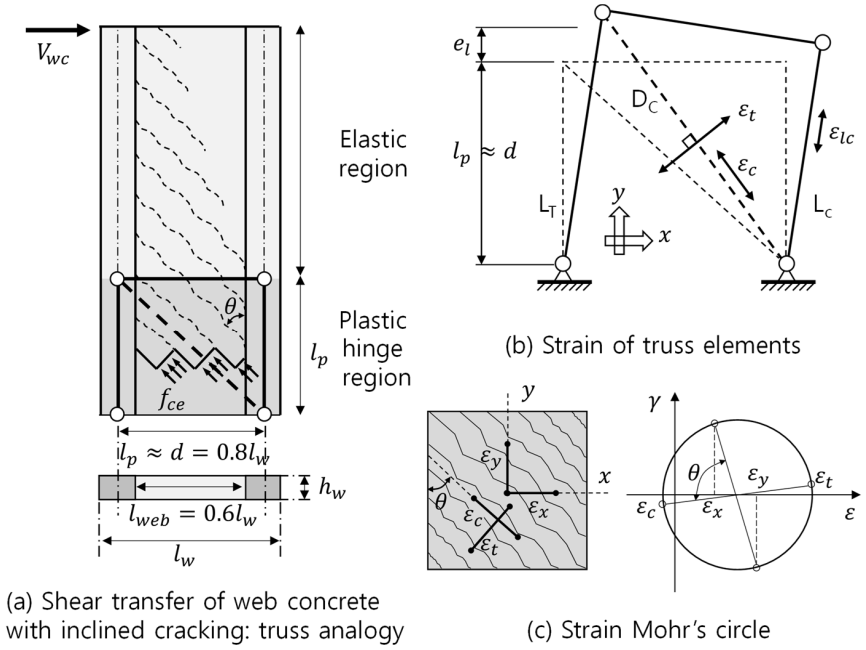

Fig. 6-10 Concept of truss mechanism model for web crushing

6.4.2 Simplified strength degradation model controlled by web crushing failure

After yielding of the wall, as the elongation increases, the effective strength of concrete strut is decreased. According to Eom et al. (2013), the elongation of the wall is related to the shear deformation of the plastic hinge zone. As shown in the deformation model in Fig. 6-5, it is assumed that the elongation of the plastic hinge zone is equal to the shear deformation of the plastic hinge zone ($e_l \approx \Delta_s$), which is defined as $\Delta_s = c_v\Delta$. Further, the plastic hinge length is assumed as $l_p \approx d = 0.8l_w$. Therefore, the term (e_l/l_p) in Eq. (6-46) is simplified as follows:

$$\frac{e_l}{l_p} = \frac{c_v\Delta_p}{0.8l_w}\frac{H}{H} = 1.25c_v aR \tag{6-49}$$

Where, c_v is the shear contribution ratio referring to Eq. (6-35), a is the wall aspect ratio (= H/l_w), and R is the plastic hinge rotation (= Δ_p/H).

Substituting Eqs. (6-49) and (6-48) into (6-46), the shear strength degradation controlled by web crushing failure is defined as follows:

$$V_{wc} = \frac{f_c' A_{cv}}{1/\beta_c + 700c_v aR} = \eta V_{wcm} \tag{6-50}$$

Eq. (6-50) indicates that the web crushing strength is degraded as the plastic hinge rotation increased, and V_{wc} is significantly decreased with large plastic hinge rotation. The shear strength degradation ratio to the maximum web crushing strength is defined as follows:

$$\eta = \frac{V_{wc}}{V_{wcm}} = \frac{1}{1 + 700a\beta_c c_v R} \leq 1 \tag{6-51}$$

Where, a = aspect ratio, β_c is defined by Eq. (6-48), and c_v is defined by Eq. (6-35).

Fig. 6-11 shows the contribution ratio – plastic hinge rotation (η – R) relationship calculated by Eq. (6-51). For calculation, values of parameters were assumed as follows: a = 0.5 – 2.5, β_c = 0.16 – 0.20, c_v = 0.25 – 0.75. As shown in Fig. 6-11, he effect of difference in β_c on the contribution ratio η is negligible. Further, the contribution ratio η is significantly decreased by plastic hinge rotation ($0 < R < 0.03$). Therefore, for safe evaluation, the contribution ratio η is simplified to a linear equation of R.

The linear equation is a secant line between η = 1.0 and η = 0.5. From Eq. (43), the plastic hinge rotation at η = 1.0 is calculated as R = 0, and the plastic hinge deformation at η = 0.5 is $R = 1/(700a\beta_c c_v)$. Thus, the secant slope is calculated as follows:

$$k_{wc} = \frac{1 - 0.5}{0 - 1/(700a\beta_c c_v)} = -350a\beta_c c_v \approx -70ac_v \qquad (6\text{-}52)$$

Here, as shown in Fig. 6-11, since the effect of difference in β_c on η is small, β_c = 1/5 is used to predict conservatively. Therefore, the slope is simplified as $k_{wc} = -70ac_v$.

$$\eta_2 = 1 + k_{wc}(R - 0) = 1 - 70ac_v R \qquad (6\text{-}53)$$

For web crushing failure mechanism, the residual strength is considered as $0.2V_{max}$. The minimum value of the contribution ratio η_2 is determined 0.2 ($0.2 \leq \eta_2 \leq 1.0$). Fig. 6-11 also shows the contribution ratio calculated by simplified model (Eq. (6-53)). In the range of parameters, a = 0.5 – 2.5, β_c = 0.16 – 0.20, c_v = 0.25 – 0.75, the simplified Eq. (6-53) is safely predict the decrease of η in the low plastic hinge rotation.

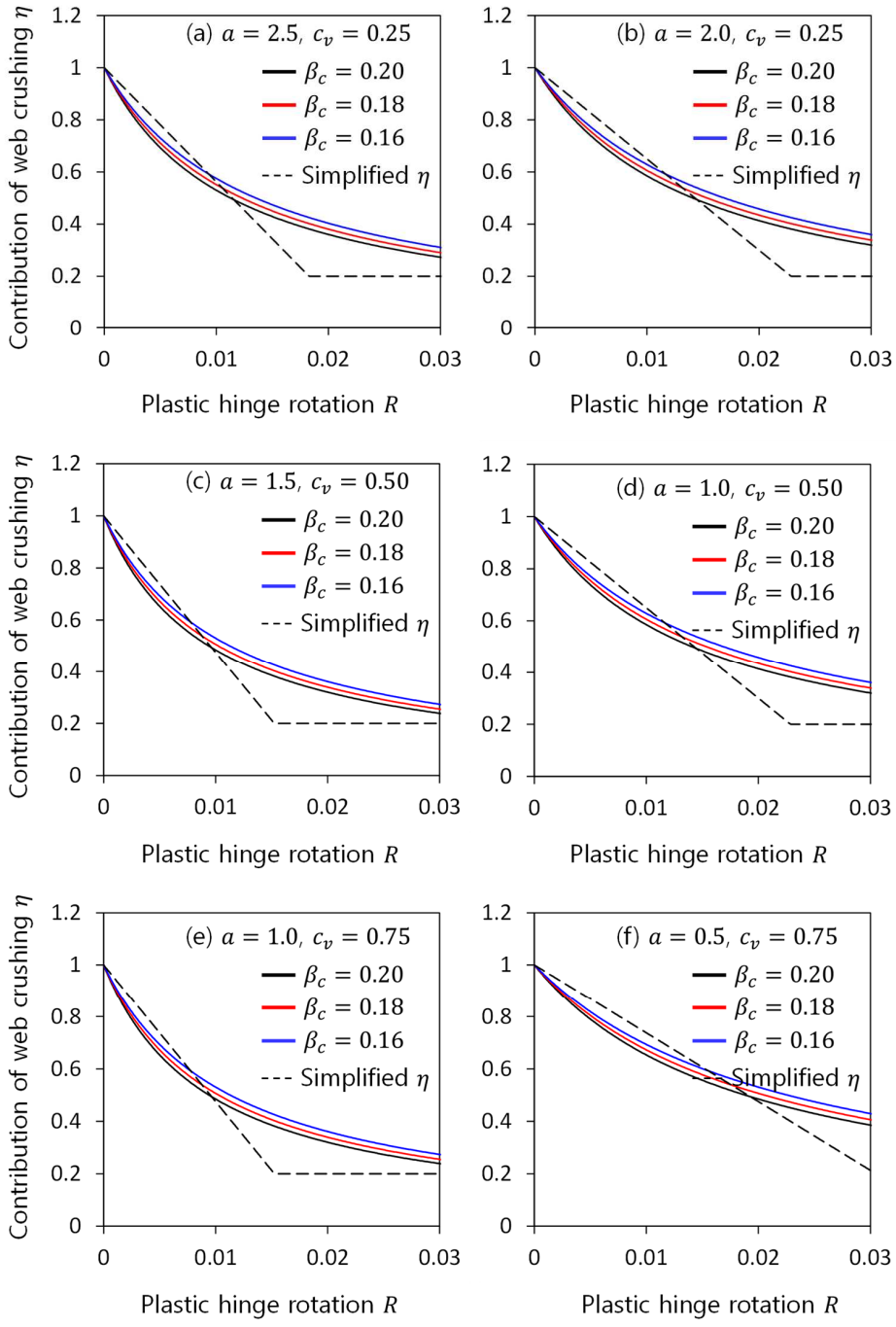

Fig. 6-11 Contribution ratio of web crushing strength η

6.5 Verification of proposed shear strength degradation model

To verify the proposed shear strength degradation model, the load-displacement curves of existing wall specimens (The present study, Adjar et al. (1995), Baek (2017a, 2017b, 2018), Belmouden & Lestuzzi (2006), Burgueno et al. (2014), Cheng et al. (2016), Dazio et al. (1999), Endo (1975), Esaki et al. (1994), Ghorbani et al. (2009), Greifenhagen & Lestuzzi (2006), Hirosawa (1975), Ji (2000), Kabeyasawa & Hiraishi (1998), Kabeyasawa et al. (1996), Kimura and Sugano (1996), Liang et al. (2013), Looi et al. (2017), Luna et al. (2015), Maier et al. (1985), Mo & Chan (1996), Oesterle et al. (1979), Oh et al. (2006), Pilakoutas (1995), Seki et al. (1995), Shaingchin et al. (2006), Sittipunt et al. (2006), Tatsuya (1996), and Zhang (2007)) were predicted by ASCE 41-17 and the proposed model. For existing test results, specimens showing shear failure after flexural yielding were included, excluding the brittle shear failure mode before yielding, and flexural yielding mode without shear failure. For flexural-shear failure mode specimens, the total number of specimens was 144. Table 6-3 and Table 6-4 show the design parameters of the test specimens used for the verification.

From the previous sections, the proposed shear strength degradation models are summarized as follows:

For shear strength degradation defined by diagonal tension cracking

$$V_n = \eta_1 V_c + V_s \tag{6-54a}$$

where,

$$\eta_1 = 1 - \frac{125c_1}{(Kl_w/c - 1.5)}R \tag{6-54b}$$

For shear strength degradation defined by web crushing

$$V_{wc} = \eta_2 V_{wcm} \tag{6-54c}$$

where,

$$\eta_2 = 1 - 70ac_vR \tag{6-54d}$$

In Eq. (6-54), the shear strength of concrete V_c is defined by Eqs. (5-18) and (5-17), and the web crushing strength V_{wcm} is defined by Eqs. (5-29) and (5-30).

In Eqs. (6-54a) to (6-54d), the shear strength degradations are defined as functions of the plastic hinge rotation R. To predict the lateral load-drift ratio of the test specimens, the plastic hinge rotation is transformed to the lateral drift ratio. From Eqs. (6-13), (6-14), (6-18), (6-19), and (6-20), the overall lateral deformation Δ is defined as follows:

$$\Delta = \Delta_f + \Delta_s = \Delta_{pf} + \Delta_{ps} + \Delta_{yf} = \Delta_p + \Delta_{yf} \tag{6-55}$$

where, Δ_f is the overall flexural deformation, Δ_f is the overall shear deformation, Δ_{pf} is the flexural deformation developed in the plastic hinge region, Δ_{ps} is the shear deformation developed in the plastic hinge region, Δ_p is the plastic hinge deformation, and Δ_{yf} is the yield deformation.

Substituting Eq. (6-16) and R = Δ_p/H into Eq.(6-55), the overall lateral drift ratio δ (= Δ/H) is calculated as follows:

$$\delta = R + \frac{2}{3}\varepsilon_y \frac{H}{l_w} = R + \frac{2}{3}a\varepsilon_y \tag{6-56}$$

Where, ε_y is the yield strain of vertical reinforcement, and a is the wall aspect ratio (= H/l_w).

Table 6-3 Summaries of the existing test specimens: Rectangle wall

Shape	Researcher	Specimen ID	Aspect ratio $M/(Vl_w)$	Concrete strength f_c' [MPa]	Axial load ratio $N_u/(A_g f_c')$	Vertical rebar		Horizontal rebar			Test results		
						Rebar ratio ρ_{avg} [%]	Yield strength f_{yv} [MPa]	Rebar ratio ρ_h [%]	Yield strength f_{yh} [MPa]	Effective strength $\rho_h f_{yh}$ [MPa]	Peak shear stress v_{test} [MPa]	Drift at the peak stress δ_m [%]	Drift at the failure δ_u [%]
Rectangle	Present study	HF2R-AB	2.25	38.3	0.00	0.79	737	0.14	809	1.13	1.26	2.84	3.00
		NF2H-30	2.25	37	0.30	3.71	470	0.66	470	3.11	4.33	1.48	1.99
		HF2H-30	2.25	37	0.30	2.64	770	0.42	770	3.25	4.46	1.51	1.89
	Kim et al. (2021)	RF2-0	2.16	47.4	0.00	2.70	466	0.56	445	2.49	2.61	1.50	1.97
	Baek (2017)	NF1M	1.17	50.9	0.06	1.85	653	0.92	470	4.34	4.84	1.21	1.30
		HF1M	1.17	50.9	0.06	1.57	653	0.68	667	4.52	4.37	0.99	1.26
		HF1M_B	1.17	50.9	0.06	1.57	653	0.68	667	4.52	4.74	1.19	2.56
		NF1T_B	1.17	52.9	0.06	1.19	470	0.40	470	1.87	3.68	1.69	2.45
		HF1T_B	1.17	46.5	0.07	0.79	653	0.25	667	1.69	3.59	1.62	3.21
		NF05M	0.67	38.7	0.06	1.06	470	0.92	470	4.34	4.72	1.59	2.00
		HF05M	0.67	38.7	0.06	0.68	667	0.68	667	4.52	4.56	1.03	2.21
		HF05M_B	0.67	37.4	0.06	0.68	667	0.68	667	4.52	4.61	1.64	3.20
		HF2	2.17	36.7	0.07	3.32	617	0.68	667	4.52	4.97	2.08	2.55
		NF2	2.17	38.1	0.07	3.61	617	0.92	470	4.34	4.74	1.60	2.02
		HF2_500	2.17	38.2	0.07	3.41	617	0.79	563	4.46	4.63	1.24	1.89
		HF2_600	2.17	26.1	0.09	3.27	617	0.72	642	4.62	4.65	1.22	2.01

Table 6-3 Summaries of the existing test specimens: Rectangle wall (continued)

Shape	Researcher	Specimen ID	Aspect ratio $M/(Vl_w)$	Concrete strength f_c' [MPa]	Axial load ratio $N_u/(A_g f_c')$	Vertical rebar		Horizontal rebar			Test results		
						Rebar ratio ρ_{avg} [%]	Yield strength f_{yv} [MPa]	Rebar ratio ρ_h [%]	Yield strength f_{yh} [MPa]	Effective strength $\rho_h f_{yh}$ [MPa]	Peak shear stress v_{test} [MPa]	Drift at the peak stress δ_m [%]	Drift at the failure δ_u [%]
Rectangle	Baek (2017)	HF2B	2.17	38.1	0.06	3.32	617	0.68	667	4.51	4.54	1.58	2.00
		HF2B_500	2.17	30.3	0.08	3.41	617	0.79	563	4.46	4.64	2.04	2.04
		HF2B_600	2.17	26.1	0.09	3.27	617	0.72	642	4.62	4.66	2.01	2.22
		FW4	2.70	16.46	0.29	0.48	555	0.20	540	1.08	1.07	1.39	2.84
	Looi et al. (2017)	C30-N-ALR01	1.25	29.1	0.12	1.85	601	1.44	289	4.15	3.95	0.88	1.11
		C30-N-ALR02	1.25	26.4	0.22	1.85	601	1.44	289	4.15	3.83	0.89	1.03
		C30-N-ALR03	1.25	27.6	0.38	1.85	601	1.44	289	4.15	3.90	0.50	0.63
		C30-N-ALR04	1.25	28	0.44	1.85	601	1.44	289	4.15	3.92	0.37	0.47
	Cheng et al. (2016)	H115	1.00	44	0.00	1.17	770	0.41	806	3.30	4.28	1.38	1.87
		H60	1.00	44	0.00	2.30	450	0.82	475	3.89	4.40	1.38	1.64
		H60X	1.00	42	0.00	2.30	450	0.82	475	3.89	4.41	0.90	1.57
		M115	1.00	38	0.00	0.69	770	0.15	786	1.21	2.60	1.44	3.37
		M60	1.00	39	0.00	1.26	450	0.31	453	1.39	2.66	0.69	2.41
	Luna (2015)	SW11	0.54	34.5	0.00	0.89	462	0.67	462	3.10	3.05	0.80	2.35
		SW12	0.54	34.5	0.00	0.77	462	0.33	462	1.53	2.62	1.22	2.00
		SW2	0.54	48.3	0.00	1.00	462	1.00	462	4.62	4.05	1.32	2.20

Table 6-3 Summaries of the existing test specimens: Rectangle wall (continued)

Shape	Researcher	Specimen ID	Aspect ratio $M/(Vl_w)$	Concrete strength f_c' [MPa]	Axial load ratio $N_u/(A_g f_c')$	Vertical rebar		Horizontal rebar			Test results		
						Rebar ratio ρ_{avg} [%]	Yield strength f_{yv} [MPa]	Rebar ratio ρ_h [%]	Yield strength f_{yh} [MPa]	Effective strength $\rho_h f_{yh}$ [MPa]	Peak shear stress v_{test} [MPa]	Drift at the peak stress δ_m [%]	Drift at the failure δ_u [%]
Rectangle	Luna (2015)	SW3	0.54	53.82	0.00	0.67	462	0.67	462	3.10	3.36	2.08	2.95
		SW4	0.54	28.98	0.00	0.33	462	0.33	462	1.53	1.62	1.12	2.30
		SW5	0.33	29.67	0.00	1.00	462	1.00	462	4.62	5.22	1.32	1.40
		SW6	0.33	26.22	0.00	0.67	462	0.67	462	3.10	4.10	0.80	1.40
		SW7	0.33	26.22	0.00	0.33	462	0.33	462	1.53	2.29	0.49	2.95
		SW8	0.54	24.15	0.00	1.50	462	1.50	462	6.93	4.48	0.70	2.30
		SW9	0.54	29.67	0.00	1.50	462	0.67	462	3.10	4.47	0.78	2.30
	Ghorbani et al. (2009)	B2C_end-A	2.08	30	0.00	1.74	413	1.33	413	5.49	1.79	1.17	4.06
	Zhang (2007)	SW1-1	2.00	20.7	0.21	0.97	366	0.36	392	1.42	1.62	0.92	1.06
		SW2-2	1.50	30.8	0.30	0.97	366	0.36	392	1.42	2.98	0.64	0.91
		SW2-3	2.00	30.8	0.30	0.97	366	0.36	392	1.42	1.89	0.55	0.72
		SW4-1	2.00	30.8	0.30	0.70	343	0.36	392	1.42	2.04	0.54	0.81
		SW4-2	2.00	30.8	0.30	0.97	366	0.36	392	1.42	1.85	0.43	0.53
		SW4-3	2.00	30.8	0.30	0.97	366	0.36	392	1.42	1.83	0.60	0.72
		SW5-1	2.00	30.8	0.30	0.93	366	0.36	392	1.42	2.05	0.51	0.90
		SW5-2	2.00	30.8	0.30	0.97	366	0.36	392	1.42	1.81	0.57	0.72

Table 6-3 Summaries of the existing test specimens: Rectangle wall (continued)

Shape	Researcher	Specimen ID	Aspect ratio $M/(Vl_w)$	Concrete strength f_c' [MPa]	Axial load ratio $N_u/(A_g f_c')$	Vertical rebar		Horizontal rebar			Test results		
						Rebar ratio ρ_{avg} [%]	Yield strength f_{yv} [MPa]	Rebar ratio ρ_h [%]	Yield strength f_{yh} [MPa]	Effective strength $\rho_h f_{yh}$ [MPa]	Peak shear stress v_{test} [MPa]	Drift at the peak stress δ_m [%]	Drift at the failure δ_u [%]
Rectangle	Zhang (2007)	SW5-3	2.00	30.8	0.30	1.01	366	0.36	392	1.42	2.33	0.59	0.98
		SW6-1	2.00	30.8	0.30	0.97	366	0.36	392	1.42	2.24	0.67	0.96
		SW6-2	2.00	30.8	0.30	0.97	366	0.36	392	1.42	1.88	0.56	0.72
	Belmouden & Lestuzzi (2006)	WSH6	2.26	51	0.09	0.95	579	0.25	532	1.34	2.00	1.11	2.08
	Greifenhagen & Lestuzzi (2006)	M1	0.69	50.7	0.03	0.40	504	0.32	504	1.63	2.13	0.53	3.70
		M2	0.69	51	0.03	0.40	504	0.14	745	1.07	2.05	1.07	2.25
		M4	0.77	24.4	0.08	0.47	504	0.26	745	1.92	1.87	0.99	1.80
	Oh et al. (2006)	HRI-W2	1.50	27.6	0.10	0.53	449	0.31	342	1.07	1.47	2.52	3.93
		HRI-W5	1.50	27.6	0.10	0.53	449	0.31	342	1.07	1.45	2.53	3.82
	Sittipunt et al. (2006)	W1	1.43	36.6	0.00	0.85	473	0.15	444	0.67	1.31	1.52	2.65
		W2	1.43	35.8	0.00	0.85	473	0.15	444	0.67	1.64	1.50	2.58
		W3	1.43	37.8	0.00	0.85	473	0.15	444	0.67	1.52	1.62	1.75
		W4	1.43	36.3	0.00	0.85	473	0.15	444	0.67	1.65	1.60	1.81
	Oh et al. (2002)	WR-20	1.50	27.6	0.10	0.64	449	0.31	342	1.07	1.47	2.54	3.90
		WR-10	1.50	27.6	0.10	0.64	449	0.31	342	1.07	1.41	2.54	3.83
		WR-0	1.50	27.6	0.10	0.64	449	0.31	342	1.07	1.39	1.33	2.98

Table 6-3 Summaries of the existing test specimens: Rectangle wall (continued)

Shape	Researcher	Specimen ID	Aspect ratio $M/(Vl_w)$	Concrete strength f_c' [MPa]	Axial load ratio $N_u/(A_g f_c')$	Vertical rebar		Horizontal rebar			Test results		
						Rebar ratio ρ_{avg} [%]	Yield strength f_{yv} [MPa]	Rebar ratio ρ_h [%]	Yield strength f_{yh} [MPa]	Effective strength $\rho_h f_{yh}$ [MPa]	Peak shear stress v_{test} [MPa]	Drift at the peak stress δ_m [%]	Drift at the failure δ_u [%]
Rectangle	Lopes (2001)	SW13	1.10	55	0.00	2.92	527	0.93	414	3.85	5.34	1.40	1.75
	Ji (2000)	SW1	3.00	13.5	0.09	2.58	372	0.42	453	1.90	1.52	0.76	0.78
	Dazio et al. (1999)	WSH6	2.26	45.6	0.11	0.87	576	0.25	519	1.30	1.96	1.42	2.10
	Adajar et al. (1995)	RCW1	1.43	46.8	0.01	2.79	598	0.52	490	2.57	3.29	1.03	2.09
		RCW3	1.43	46.6	0.01	2.24	598	0.52	490	2.57	3.87	0.51	1.07
	Pilakoutas & Elnashai (1995)	SW4	2.13	36.9	0.00	2.84	500	0.39	550	2.15	2.92	0.94	1.88
		SW5	2.13	31.8	0.00	3.03	540	0.31	400	1.24	3.12	0.80	0.78
		SW6	2.13	38.6	0.00	2.84	500	0.31	400	1.24	3.01	1.37	1.72
		SW7	2.13	32	0.00	3.03	540	0.39	550	2.15	3.59	1.40	1.72
		SW8	2.13	45.8	0.00	2.94	540	0.28	400	1.12	2.64	1.71	2.04
		SW9	2.13	38.9	0.00	2.94	540	0.56	400	2.24	2.73	1.88	2.04
	Oesterle et al. (1976)	B6	2.40	21.8	0.09	1.23	441	0.20	512	1.04	1.48	1.66	1.70
	Hirosawa (1975)	Hirosawa7-2	1.00	20.8	0.10	1.55	376	0.63	419	2.63	3.11	0.90	0.90
		Hirosawa7-3	1.00	20.8	0.10	1.55	376	1.26	421	5.30	3.07	0.50	1.11
		Hirosawa7-5	1.00	14.7	0.14	1.54	376	2.51	415	10.43	3.02	0.97	1.33

Table 6-4 Summaries of the existing test specimens: Barbell shaped wall and flanged wall

Shape	Researcher	Specimen ID	Aspect ratio $M/(Vl_w)$	Concrete strength f_c' [MPa]	Axial load ratio $N_u/(A_g f_c')$	Vertical rebar		Horizontal rebar			Test results		
						Rebar ratio ρ_{avg} [%]	Yield strength f_{yv} [MPa]	Rebar ratio ρ_h [%]	Yield strength f_{yh} [MPa]	Effective strength $\rho_h f_{yh}$ [MPa]	Peak shear stress v_{test} [MPa]	Drift at the peak stress δ_m [%]	Drift at the failure δ_u [%]
Barbell shaped wall	Burgueno et al. (2014)	M05C	2.50	46	0.08	3.51	491	2.44	445	10.86	4.79	1.49	1.95
		M10C	2.50	56.4	0.06	3.51	457	2.44	476	11.61	4.48	1.66	1.70
		M15C	2.50	102	0.03	3.41	439	1.83	481	8.80	4.87	3.09	3.09
		M20C	2.50	131	0.03	3.51	449	2.44	438	10.69	4.86	3.03	3.03
	Liang et al. (2013)	DHSCW-01	2.10	93	0.11	1.64	463	1.96	494	9.68	5.28	1.48	3.03
		DHSCW-02	2.10	93	0.08	1.64	463	1.96	494	9.68	4.64	0.96	2.91
		DHSCW-03	1.60	93	0.08	1.64	463	1.96	494	9.68	6.54	1.55	2.73
		DHSCW-04	1.60	93	0.08	1.64	463	1.96	494	9.68	6.44	1.11	2.63
		DHSCW-05	1.10	93	0.08	1.64	463	1.96	494	9.68	8.42	1.45	3.54
		DHSCW-06	1.10	93	0.08	1.64	463	1.96	494	9.68	7.66	1.91	3.15
	Oh et al. (2006)	HRI-W7	1.50	27.6	0.10	0.61	342	0.31	342	1.07	1.42	2.40	3.77
	Shaingchin et al. (2006)	WC150	1.50	27.3	0.05	1.39	575	0.81	451	3.64	3.55	1.86	2.40
		WD150	1.50	40.3	0.05	1.39	575	0.81	451	3.64	3.66	0.98	1.70
		WD170	1.50	32.9	0.05	1.33	596	0.71	506	3.60	3.92	1.57	2.01
		WD200	1.50	33.7	0.05	1.26	575	0.60	451	2.73	3.66	2.03	2.39
	Oh et al. (2002)	WB	1.50	27.6	0.08	0.62	342	0.31	342	1.07	1.44	2.43	3.73
	Ji (2000)	SW2	3.00	13.5	0.06	1.85	372	0.42	453	1.90	1.55	1.16	1.88

Table 6-4 Summaries of the existing test specimens: Barbell shaped wall and flanged wall (continued)

Shape	Researcher	Specimen ID	Aspect ratio $M/(Vl_w)$	Concrete strength f_c' [MPa]	Axial load ratio $N_u/(A_g f_c')$	Vertical rebar		Horizontal rebar			Test results		
						Rebar ratio ρ_{avg} [%]	Yield strength f_{yv} [MPa]	Rebar ratio ρ_h [%]	Yield strength f_{yh} [MPa]	Effective strength $\rho_h f_{yh}$ [MPa]	Peak shear stress v_{test} [MPa]	Drift at the peak stress δ_m [%]	Drift at the failure δ_u [%]
Barbell shaped wall	Kabeyasawa & Hiraishi (1998)	NW-1	2.00	87.6	0.11	0.91	776	0.53	1001	5.29	5.77	1.86	3.00
		NW-2	1.33	93.6	0.10	0.91	776	0.53	1001	5.29	7.98	1.54	2.10
		NW-3	2.00	55.5	0.13	0.71	840	0.26	753	1.99	3.90	1.01	1.30
		NW-4	2.00	54.6	0.16	0.87	840	0.26	753	1.99	4.26	0.99	1.40
		NW-5	2.00	60.3	0.12	1.08	840	0.53	753	3.98	4.89	1.50	2.00
		NW-6	2.00	65.2	0.13	1.30	776	0.53	753	3.98	5.74	1.41	1.80
	Kimura & Sugano (1996)	W8N18	1.71	72.8	0.15	1.51	580	1.18	849	10.00	5.54	1.51	1.60
		W8N13	1.71	79	0.10	1.51	580	1.18	849	10.00	4.90	1.99	2.97
		W8N08H	1.71	79.4	0.06	1.51	580	1.18	849	10.00	4.32	1.45	2.98
		W4N18	1.71	43.1	0.26	1.51	580	1.18	849	10.00	4.95	1.00	1.49
		W4N18C	1.71	42.5	0.26	1.51	580	1.18	849	10.00	4.78	0.99	1.52
	Tatsuya (1996)	M35X	1.62	60	0.16	1.09	900	0.71	880	6.22	5.74	1.05	1.45
		M30H	1.62	60	0.13	1.09	900	0.71	800	5.65	5.24	1.09	1.11
		M35H	1.62	60	0.17	1.09	900	0.71	800	5.65	5.76	1.06	1.24
		MW35H	1.62	60	0.15	1.09	900	0.71	800	5.65	5.55	1.09	1.10
		P35H	1.62	60	0.17	1.09	900	0.71	800	5.65	5.59	1.06	1.14

Table 6-4 Summaries of the existing test specimens: Barbell shaped wall and flanged wall (continued)

Shape	Researcher	Specimen ID	Aspect ratio $M/(Vl_w)$	Concrete strength f_c' [MPa]	Axial load ratio $N_u/(A_g f_c')$	Vertical rebar		Horizontal rebar			Test results		
						Rebar ratio ρ_{avg} [%]	Yield strength f_{yv} [MPa]	Rebar ratio ρ_h [%]	Yield strength f_{yh} [MPa]	Effective strength $\rho_h f_{yh}$ [MPa]	Peak shear stress v_{test} [MPa]	Drift at the peak stress δ_m [%]	Drift at the failure δ_u [%]
Barbell shaped wall	Esaki et al. (1994)	H-1.4-N0.25	1.40	21.7	0.14	0.86	359	0.50	291	1.46	2.82	2.01	2.58
		H-1.4-N0.33	1.40	24.2	0.18	0.86	359	0.50	291	1.46	3.37	0.87	1.81
		H-2-N0.33	2.00	18.7	0.18	0.67	359	0.50	291	1.46	1.99	1.60	1.67
	Oesterle et al. (1979)	B2	2.40	53.6	0.00	1.36	410	0.61	532	3.24	2.19	2.52	2.89
		B5	2.40	45.3	0.00	1.36	444	0.61	502	3.06	2.45	2.73	2.86
		B5R	2.40	42.8	0.00	1.37	444	0.61	502	3.06	2.51	3.29	3.37
		B10	2.40	45.6	0.10	0.91	448	0.61	475	2.89	2.39	2.98	3.36
		B11	2.40	53.8	0.00	1.36	436	0.61	434	2.64	2.39	2.86	2.95
		B7	2.40	49.3	0.09	1.36	450	0.61	490	2.98	3.19	2.79	3.28
		B8	2.40	42	0.11	1.36	450	0.61	482	2.93	3.34	2.77	3.64
		B9	2.40	44.1	0.10	1.36	448	0.61	461	2.81	3.21	2.91	3.02
		B9R	2.40	51.8	0.07	1.37	430	0.61	461	2.81	3.21	3.63	5.46
	Endo (1975)	W7101	0.83	26	0.05	0.73	359	1.41	623	8.81	2.48	1.20	2.94
		W7102	0.83	24.6	0.06	0.36	359	0.47	623	2.94	2.13	0.94	1.55
		W7103	0.83	26	0.05	0.36	359	0.47	623	2.94	2.03	0.69	1.20
		W7104	0.83	24.6	0.07	0.47	359	0.75	623	4.70	2.41	0.79	1.11

Table 6-4 Summaries of the existing test specimens: Barbell shaped wall and flanged wall (continued)

Shape	Researcher	Specimen ID	Aspect ratio $M/(Vl_w)$	Concrete strength f_c' [MPa]	Axial load ratio $N_u/(A_g f_c')$	Vertical rebar		Horizontal rebar			Test results		
						Rebar ratio ρ_{avg} [%]	Yield strength f_{yv} [MPa]	Rebar ratio ρ_h [%]	Yield strength f_{yh} [MPa]	Effective strength $\rho_h f_{yh}$ [MPa]	Peak shear stress v_{test} [MPa]	Drift at the peak stress δ_m [%]	Drift at the failure δ_u [%]
Flanged wall	Ji (2000)	SW3	3.00	13.5	0.03	0.75	372	0.42	453	1.90	1.32	1.32	1.86
	Kabeyasawa et al. (1996)	HW-1	1.82	35.5	0.03	0.69	367	0.57	402	2.27	1.29	2.32	2.67
		HW-2	1.82	35.5	0.03	1.33	367	0.57	402	2.27	1.56	0.78	1.70
	Mo & Chan (1996)	HN6-1	0.74	29.5	0.00	0.98	443	0.82	443	3.63	3.29	0.76	1.38
		HN6-2	0.74	29.5	0.00	0.98	443	0.82	443	3.63	2.63	0.24	0.79
		HN6-3	0.74	31	0.00	0.98	443	0.82	443	3.63	2.64	0.56	0.92
	Seki (1995)	RA-15P	0.59	29.5	0.03	1.20	349	1.20	349	4.19	3.76	0.67	0.83
		RB-15P	0.78	28.9	0.04	1.20	381	1.20	381	4.57	3.29	0.52	0.75
		RC-15P	0.98	29.2	0.04	1.20	349	1.20	349	4.19	2.63	0.56	0.83
	Maier et al. (1985)	S1	1.12	36.9	0.07	1.13	574	1.01	574	5.80	3.82	1.70	2.27
		S2	1.12	38.4	0.24	1.13	574	1.01	574	5.80	5.21	0.79	0.94
		S3	1.12	36.7	0.07	2.54	530	1.01	574	5.80	5.49	1.11	1.24
		S5	1.12	37.3	0.06	1.13	574	1.01	574	5.80	3.83	1.60	1.65
		S6	1.12	35.6	0.07	1.13	479	0.57	537	3.06	3.75	1.41	1.86
	Oesterle et al. (1979)	F1	2.40	38.4	0.00	0.65	438	0.70	475	3.31	2.38	2.19	2.35
		F2	2.40	45.6	0.08	0.46	417	0.61	525	3.20	2.55	2.23	3.07

Fig. 6-12 and Fig. 6-13 show the predictions of shear strength degradation of the wall. Among 144 specimens, major 12 specimens are presented. All prediction results are presented in Appendix. In the figures, the gray colored curves indicates the test result, the black dotted line indicates the prediction of ASCE 41-17, the black solid line indicates the flexural strength of the wall, red solid line indicates the proposed model for diagonal tension cracking (Eq.(6-54a), and the blue solid line indicates the proposed model for web crushing (Eq. (6-54c).

The shear strength degradation model of ASCE conservatively predicted the defomation capacity. Since the ASCE model is determined only by the axial load ratio, in the most of the specimens, the drift ratio at the peak strength and the ultimate drift ratio are the same, regardless of the test parameters. Further, in the case of specimens with high-axial load ratio, the ASCE 41-17 model regarded the walls as force controlled members. Thus, the envelope curves of the specimens are presented as linear elastic curves.

On the other hand, the proposed shear degradation model showed better predictions, regardless of the test parameters. However, in order to safely and conveniently applicate the model for the practical design, it is needed to suggest the model as design tables considering the major design parameters.

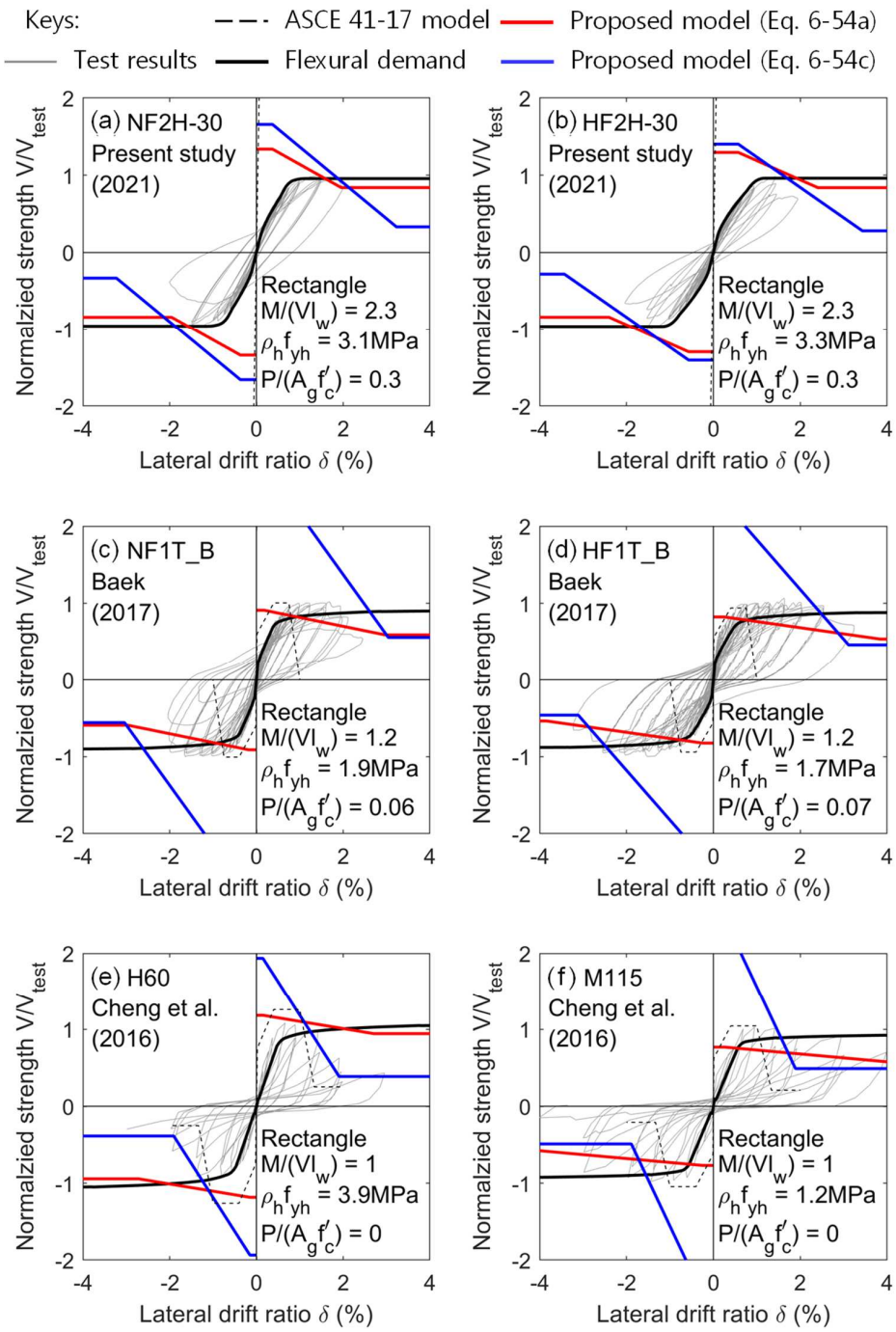

Fig. 6-12 Shear strength degradation predictions of rectangle walls

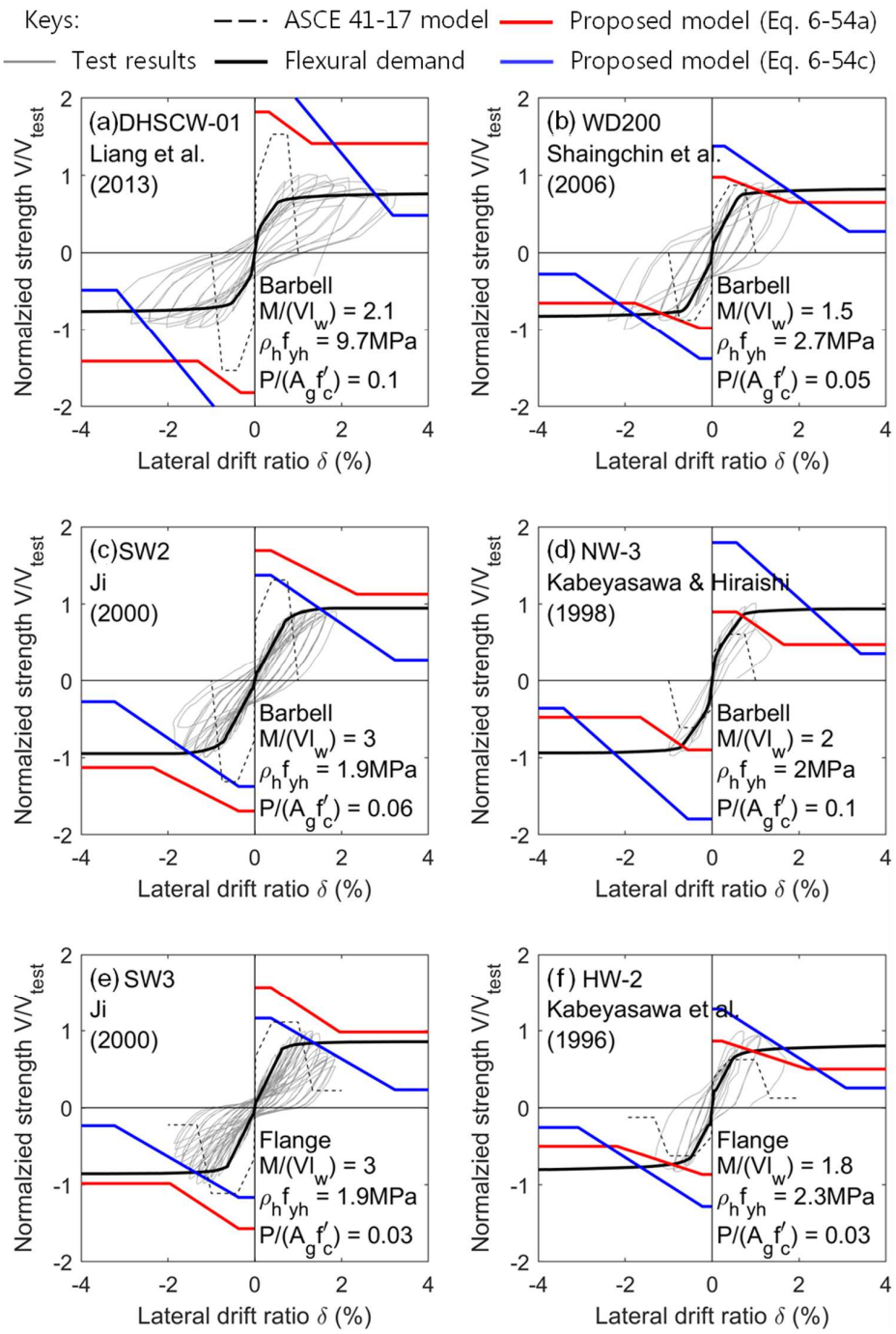

Fig. 6-13 Shear strength degradation predictions of barbell and flanged walls

6.6 Summary

In the present study, the simplified load-deformation model were proposed to predict the shear strength – deformation relationship of the walls. Based on two shear failure mechanisms, diagonal tension failure and web crushing failure, the simplified shear strength – deformation models were developed.

For diagonal tension cracking, the concept of compression zone failure mechanism model was used. The shear resistance of the concrete was provided only in the compression zone. Because the shear strength degradation occurred after yielding, the shear capacity of concrete was derived as a function of plastic hinge rotation. For simple application, the nonlinear curve model was simplified as a linear equation.

For web crushing, the concept of the truss mechanism model was used. The effective strength of the diagonal concrete strut in the web wall decreased as the elongation of the plastic hinge region increased. The elongation was increased by cyclic loading effect after yielding of the wall. Thus, the web crushing strength was degraded as the plastic hinge rotation increased. For simplification, the web crushing strength degradation model was simplified as a linear equation.

For verification, the proposed models were applied with the existing test results. Compared to current ASCE 41-17 method, the proposed model agreed with the test results.

Chapter 7. Application of Proposed Models

7.1 Overview

The proposed shear strength degradation models can be applied to the performance based seismic design/evaluation. The response of the building is simulated by using the nonlinear static or dynamic analysis. Thus, to increase the reliability of the analysis results, the numerical model should accurately simulate the nonlinear behavior of the reinforced concrete members.

In general, there are two modeling methods for RC members used conveniently in practical design, 1) concentrated hinge model, and 2) fiber model. The concentrated hinge model defines the inelastic strength-deformation relationship of the plastic hinge region. In the case of shear wall, shear deformation in the plastic hinge region should be addressed. The wall fiber model consists of two types of components: vertical fibers and shear spring. Axial and flexural behavior of wall is defined by the vertical fibers, while the shear behavior is defined by shear spring.

In the present study, the design tables were developed to define the inelastic plastic hinge model and inelastic shear spring model. The modeling guideline was described for the example wall test specimens.

7.2 Review on Perform 3D wall element

Fig. 7-1 shows the configuration of wall fiber model of Perform 3D. The axial tension, axial compression, and flexural behavior of the wall are defined by vertical springs which represent each fiber of concrete and reinforcing bars. The response of each vertical fiber is defined by nonlinear stress-strain relationships of material. On the other hand, the shear behavior of the wall is defined by a horizontal spring representing the shear strength-shear deformation relationships of the wall panel.

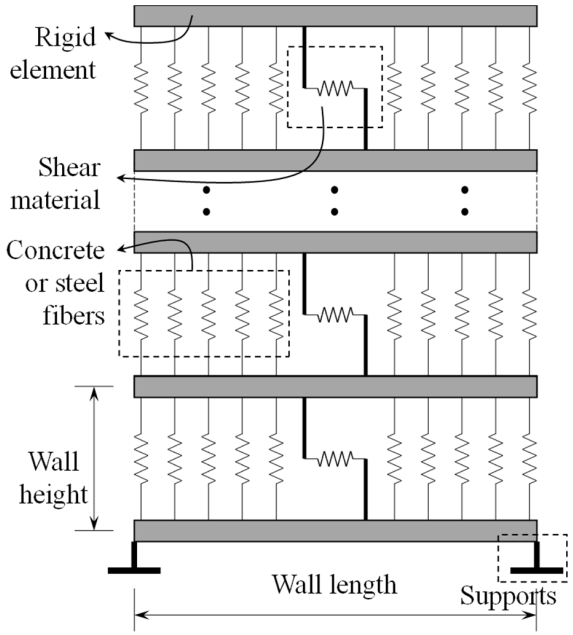

Fig. 7-1 Configuration of wall fiber model

7.3 Envelope curve model for the plastic hinge region

7.3.1 Envelope curve model

In the previous chapters, the simplified shear strength and shear strength degradation model were developed. They are summarized as follows:

Simplified shear strength model

$$V_n = V_c + V_s = \left(\alpha_c\sqrt{f_c'} + \rho_h f_{yh}\right) A_{cv} \le V_{wcm} = \beta_c f_c' A_{cv} \quad (7\text{-}1)$$

Simplified diagonal tension strength degradation model

$$V_n = \eta_1 V_c + V_s \quad (7\text{-}2a)$$

where,

$$\eta_1 = 1 - \frac{125c_1}{(Kl_w/c - 1.5)}R \quad (7\text{-}2b)$$

Simplified web crushing strength degradation model

$$V_{wc} = \eta_2 V_{wcm} \quad (7\text{-}3a)$$

where,

$$\eta_2 = 1 - 70ac_v R \quad (7\text{-}3b)$$

Where, V_c is shear strength of concrete, V_s is shear strength of shear reinforcement, V_{wcm} is web crushing strength, α_c is contribution of concrete to shear strength defined in Eq.(5-19a), β_c is effective stress coefficient of web concrete defined in Eq. (5-30), f_c' = concrete compressive strength (MPa), ρ_h = shear reinforcement ratio, f_{yh} = yield strength of shear reinforcement, A_{cv} = shear resisting area (= $t_w l_w$), R is plastic hinge rotation, c is compression zone depth, l_w is wall length, K is concrete confinement coefficient, a is wall aspect ratio, c_v is shear contribution ratio defined in Eq. (6-35), and c_1 is coefficient related to shear contribution defined in Eq. (6-37).

For convenience in design, design tables were proposed to define the flexural strength-plastic hinge rotation relationship of the wall. Fig. 7-2 shows the envelope curve of the wall affected by shear strength degradation. The post yield shear failure mode wall is defined as a wall in which the flexural strength is less than the shear strength ($V_f < V_n = V_c + V_s$). In this case, the envelope curve model consists of two regions: 1) constant region with the flexural strength V_f, and 2) strength degradation region (see Fig. 7-2). In the ultimate state, it is assumed that the shear resistance of concrete significantly decreases. The residual strength ratio of concrete is assumed as 0.2, which is specified in ASCE 41-17. In the case of diagonal tension cracking mode, the residual strength is defined as $0.2V_c + V_s$, while in the case of web crushing mode, the residual strength is defined as $0.2V_{wcm}$.

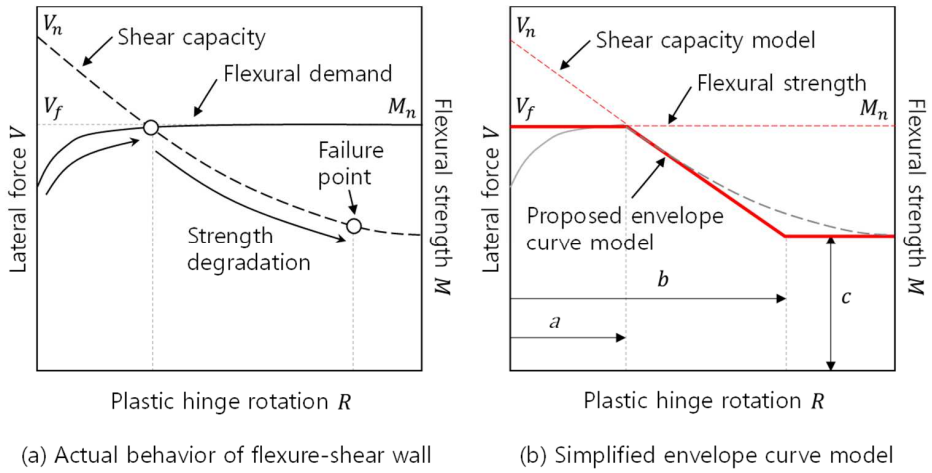

(a) Actual behavior of flexure-shear wall (b) Simplified envelope curve model

Fig. 7-2 Post yielding-shear strength degradation behavior of walls.

In the constant region, the flexural strength V_f is defined as the lateral force corresponding to the nominal flexural strength M_n as follows:

$$V_f = \frac{M_n}{H} = \frac{M_n}{M_u} V_u \tag{7-4}$$

Where, H is the wall shear span length. In the building structure, the shear span length of the wall is calculated as $H = M_u/V_u$, M_u is the demand flexural moment, and V_u is the demand shear force.

In the strength degradation region, the governing shear failure mode is defined. When the residual strength of web crushing mode is greater than that of diagonal tension mode ($0.2V_{wcm}/(0.2V_c + V_s) > 1.0$, or $V_{wcm}/(0.2V_c + V_s) > 5$, case (a) in Fig. 7-3), the strength degradation is defined by diagonal tension failure. Otherwise, the web crushing mode define the shear strength degradation (case (b) in Fig. 7-3).

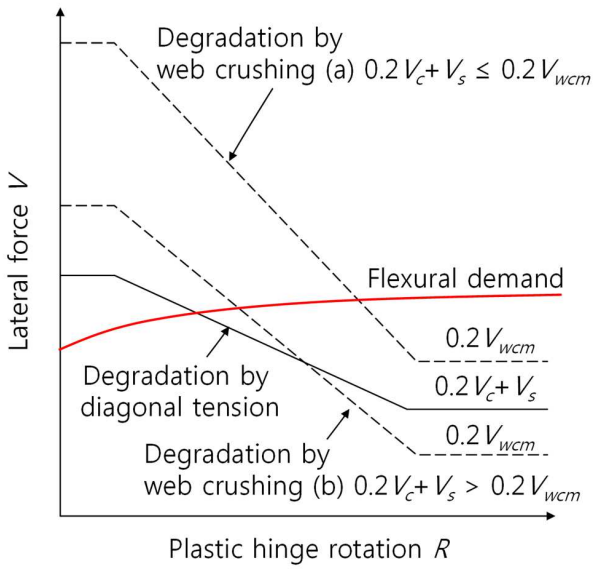

Fig. 7-3 Determination of governing modes.

As shown in Fig. 7-2, the strength degradation function is defined by two reference parameters: 1) "*a*", a plastic hinge rotation where the strength degradation initiates, and 2) "*b*", a plastic hinge rotation where the strength degradation terminates.

The parameter "*a*" is defined as the plastic hinge rotation at the intersection between the flexural demand and the shear capacity ($V_f = V_n$ or $V_f = V_{wcm}$). When the strength degradation is defined by diagonal tension cracking, from Eq. (7-2), the contribution ratio η corresponding to the flexural strength is calculated as follows:

$$\eta_1 = \frac{V_f - V_s}{V_c} \tag{7-5}$$

Substituting Eq. (7-5) into Eq. (7-2), the plastic hinge rotation parameter "*a*" is calculated as follows:

$$a = \left(1 - \frac{V_f - V_s}{V_c}\right)\frac{(Kl_w/c - 1.5)}{125c_1} = 0.008\omega_1 k_c/c_1 \tag{7-6a}$$

where,

$$\omega_1 = 1 - \frac{V_f - V_s}{V_c} \tag{7-6b}$$

$$k_c = (Kl_w/c - 1.5) \tag{7-6c}$$

Where, ω_1 is strength margin ratio ($0 \leq \omega_1 \leq 0.8$), k_c is coefficient related to compression zone depth.

When the strength degradation is defined by web crushing, from Eq. (7-3), the contribution ratio η corresponding to the intersection is calculated as follows:

$$\eta_2 = \frac{V_f}{V_{wcm}} \tag{7-7}$$

Substituting Eq. (7-7) into Eq. (7-3), the plastic hinge rotation of parameter "*A*" is calculated as follows:

$$a = \frac{1 - \frac{V_f}{V_{wcm}}}{70ac_v} = \frac{\omega_2}{70ac_v} = 0.014\omega_2/(ac_v) \quad (7\text{-}8a)$$

where,

$$\omega_2 = 1 - \frac{V_f}{V_{wcm}} \quad (7\text{-}8b)$$

Where, ω_2 is strength margin ratio of web crushing strength ($0 \leq \omega_2 \leq 0.8$), and a is the shear span-to-length ratio ($= M_u/(V_u l_w)$).

The parameter "*b*" is defined as the plastic hinge deformation at the residual strength ($0.2V_c+V_s$ or $0.2V_{wcm}$). When the strength degradation is defined by diagonal tension cracking, from Eq. (7-2), the contribution ratio η corresponding to the residual strength = $0.2V_c + V_s$ is $\eta_1 = 0.2$. Thus, the parameter "*b*" is calculated as follows:

$$b = \frac{0.8k_c}{125c_1} = 0.0064k_c/c_1 \quad (7\text{-}9)$$

Whereas the strength degradation is defined by web crushing, from Eq. (7-3), the contribution ratio η corresponding to the residual strength V_{wcm} is $\eta_2 = 0.2$. Thus, the parameter "*b*" is calculated as follows:

$$b = \frac{0.8}{70ac_v} = 0.011/(ac_v) \quad (7\text{-}10)$$

The residual strength is defined by parameter "*c*". In the case of diagonal tension cracking, the residual strength ratio is $c = (0.2V_c+V_s)/V_f$, while in the case of web crushing, the residual strength ratio is $c = 0.2V_{wcm}/ V_f$.

For performance-based seismic design/evaluation, the acceptance criteria for the performance levels (Immediate Occupancy, IO; Life safety, LS; and Collapse Prevention, CP) are suggested. According to ASCE 41-17 section 7.6.3, the permissible plastic hinge rotations are defined. The plastic hinge rotation of IO level is defined as a deformation at which permanent, visible damage occurred but not greater than 0.67 times the deformation limit for life safety. For LS level, the deformation limit is defined as 0.75 times the ultimate deformation. For CP level, the ultimate deformation in can be use for the limit of the deformation.

Fig. 7-4 shows the acceptance criteria. In the flexural yielding – shear failure wall, at once the shear degradation initiates, the brittle failure can occur due to severe damages on the web. Therefore, the present study defines point "*D*" as the ultimate deformation. To secure the structural safety, the ultimate deformation is limited by the deformation corresponding to the 80 % of nominal strength, $(\theta, V) = (\theta_{0.8V}, 0.8V_f)$. Thus, for the CP level, the deformation limit is $\theta_{CP} = \min(\theta_D, \theta_{0.8V}) = \min(b, \theta_{0.8V})$.

For the life safety level, 0.75 times the CP level is defined as the deformation limit, according to the definitions in the ASCE 41-17. However, when the shear strength degradation occurs, the flexural strength cannot be recovered. To secure the life safety, deformation limit of the LS level should be less than point "*C*". Thus, for the LS level, the deformation limit is $\theta_{LS} = \min(\theta_C, 0.75\theta_{CP}) = \min(a, 0.75\theta_{CP})$.

For the IO level, 0.67 times the LS level is defined as the deformation limit, $\theta_{IO} = 0.67\theta_{LS}$, according to the definitions in the ASCE 41-17. In this deformation limit, the wall is on the flexural yielding state, but the deformation margin is 1.5 times until the strength degradation occurs.

Table 7-1 summarizes the modeling parameters *a*, *b*, and *c*, and the acceptance criteria for IO, LS, and CP level.

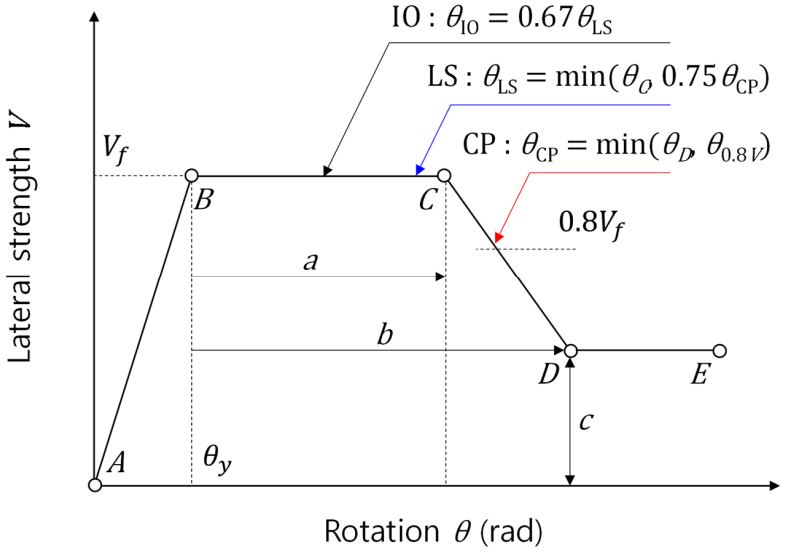

Fig. 7-4 Acceptance criteria

Table 7-1 Modeling parameters for the envelope curve model and acceptance criteria

Governing shear failure mode		Modeling parameters			Acceptable plastic hinge rotation θ		
		Plastic hinge rotation		Residual strength ratio	Performance level		
		a	b	c	IO	LS	CP
Diagonal tension	$V_{wcm}/(0.2V_c+V_s) \geq 5.0$	$0.008\omega_1 k_c/c_1$	$0.0064k_c/c_1$	$(0.2V_c+V_s)/V_f$	$0.67\theta_{IO}$	$\min(a, 0.75\theta_{CP})$	$\min(b, \theta_{0.8V})$
Web crushing	$V_{wcm}/(0.2V_c+V_s) < 5.0$	$0.014\omega_2/(ac_v)$	$0.011/(ac_v)$	$0.2V_{wcm}/V_f$			

Note: $k_c = Kl_w/c - 1.5$, where, K = confinement coefficient, c = compression zone depth, l_w = wall length; Strength margin ratio $\omega_1 = 1 - (V_f - V_s)/V_c$, $0 \leq \omega_1 \leq 0.8$; Strength margin ratio $\omega_2 = 1 - V_f/V_{scm}$, $0 \leq \omega_2 \leq 0.8$.

7.3.2 Design table

Table 7-2 shows the values of plastic hinge rotation *a* and *b* in the range of the design parameters. The major parameters affecting *a* and *b* are the aspect ratio *a*, stress level parameter s_{be}. To linearly interpolate the plastic hinge rotation *a* and *b*, reference values are calculated. For the diagonal tension failure mode wall, the modeling parameter can be amplified by coefficient k_c.

The plastic hinge rotation increases as the aspect ratio decreases. This is because the shear deformation increases in the wall with lower aspect ratio, which increases the plastic hinge rotation.

Table 7-2 Simplified modeling parameters for the envelope curve model

Governing shear failure mode				Modeling parameters		
				Plastic hinge rotation (rad)		Residual strength ratio
				a	*b*	*c*
Diagonal tension failure (k_c = 1)	$V_{wcm}/(0.2V_c+V_s) \geq 5$	$s_{be} \leq 0.5$	$a \leq 1.0$	$0.012\omega_1$	0.0100	$(0.2V_c+V_s)/V_f$
			a = 2.0	$0.010\omega_1$	0.0080	
			a = 3.0	$0.008\omega_1$	0.0065	
			$a \geq 4.0$	$0.006\omega_1$	0.0050	
		s_{be} = 1.0	$a \leq 1.0$	$0.009\omega_1$	0.0070	
			a = 2.0	$0.008\omega_1$	0.0065	
			a = 3.0	$0.007\omega_1$	0.0055	
			$a \geq 4.0$	$0.006\omega_1$	0.0050	
		$s_{be} > 1.0$	For all *a*	$0.006\omega_1$	0.0050	
Web crushing failure	$V_{wcm}/(0.2V_c+V_s) < 5$	$s_{be} \leq 0.5$	$a \leq 1.0$	$0.020\omega_2$	0.0160	$0.2V_{wcm}/V_f$
			$a \geq 2.0$	$0.015\omega_2$	0.0120	
		s_{be} = 1.0	$a \leq 1.0$	$0.025\omega_2$	0.0200	
			$a \geq 2.0$	$0.020\omega_2$	0.0160	
		$s_{be} > 1.0$	For all *a*	$0.035\omega_2$	0.0280	

Note: For diagonal tension failure, modeling parameters can be amplified by k_c, where $k_c = Kl_w/c - 1.5$, where, K = confinement coefficient, c = compression zone depth, l_w = wall length; Strength margin ratio $\omega_1 = 1 - (V_f - V_s)/V_c$, $0 \leq \omega_1 \leq 0.8$; Strength margin ratio $\omega_2 = 1 - V_f/V_{wcm}$, $0 \leq \omega_2 \leq 0.8$. Linear interpolation between values listed in the table shall be permitted.

For the shear material of the wall fiber model, the plastic hinge rotations in Table 7-2 is transformed to the shear strains, by using the shear contribution ratio c_v defined by Eq. (6-35).

From Eq. (6-19), shear strain in the plastic hinge region γ_p is calculated as follows:

$$\gamma_p = \frac{\Delta_{ps}}{l_p} = \frac{c_v \Delta_p}{0.8 l_w} \frac{H}{H} = 1.25 a c_v R \tag{7-11}$$

Where, Δ_{ps} is the shear deformation in the plastic hinge region, c_v is the shear contribution ratio, R is the plastic hinge rotation (= Δ_p/H), H is the wall height, l_p is the plastic hinge length (= $0.8l_w$), and a is the wall aspect ratio (H/l_w).

From Eqs. (7-6a), (7-8a), (7-9), and (7-10), the shear strains corresponding to *a*, and *b* are defined as follows:

For diagonal tension cracking mode

$$\gamma_a = 0.01 \omega_1 k_c a c_v / c_1 \tag{7-12a}$$

$$\gamma_b = 0.008 k_c a c_v / c_1 \tag{7-12b}$$

For web crushing mode

$$\gamma_a = 0.018 \omega_2 \tag{7-12c}$$

$$\gamma_b = 0.014 \tag{7-12d}$$

Table 7-3 shows the values of shear strains in the range of the design parameters.

Table 7-3 Simplified modeling parameters for the shear material

Governing shear failure mode				Modeling parameters		
				Shear strain (mm/mm)		Residual strength ratio
				γ_a	γ_b	c
Diagonal tension failure (k_c = 1)	$V_{wcm}/(0.2V_c+V_s) \geq 5$	$s_{be} \leq 0.5$	$a \leq 2.0$	$0.0120\omega_1$	0.0010	$(0.2V_c+V_s)/V_f$
			a = 3.0	$0.0090\omega_1$	0.0070	
			$a \geq 4.0$	$0.0030\omega_1$	0.0025	
		s_{be} = 1.0	$a \leq 2.0$	$0.0070\omega_1$	0.0055	
			a = 3.0	$0.0045\omega_1$	0.0035	
			$a \geq 4.0$	$0.0030\omega_1$	0.0025	
		$s_{be} > 1.0$	For all a	$0.0030\omega_1$	0.0025	
Web crushing failure	$V_{wcm}/(0.2V_c+V_s) < 5$	For all s_{be}	For all a	$0.018\omega_2$	0.0140	$0.2V_{wcm}/V_f$

Note: For diagonal tension failure, modeling parameters can be amplified by k_c, where $k_c = Kl_w/c - 1.5$, where, K = confinement coefficient, c = compression zone depth, l_w = wall length; Strength margin ratio $\omega_1 = 1 - (V_f - V_s)/V_c$, $0 \leq \omega_1 \leq 0.8$; Strength margin ratio $\omega_2 = 1 - V_f/V_{wcm}$, $0 \leq \omega_2 \leq 0.8$. Linear interpolation between values listed in the table shall be permitted.

7.4 Perform 3D modeling procedure

7.4.1 Overview

The present section describes how to apply the model in numerical analysis program, Perform 3D (Computer & Structures Inc.).

Fig. 7-5 shows the modeling procedure of wall element in the Perform 3D. To construct the numerical analysis model in Perform 3D, following steps are required: 1) the geometric information, such as nodes, elements, coordination, connectivity, and inelastic & elastic regions; 2) the material properties of vertical fibers and shear spring; 3) the loading conditions; and 4) boundary conditions.

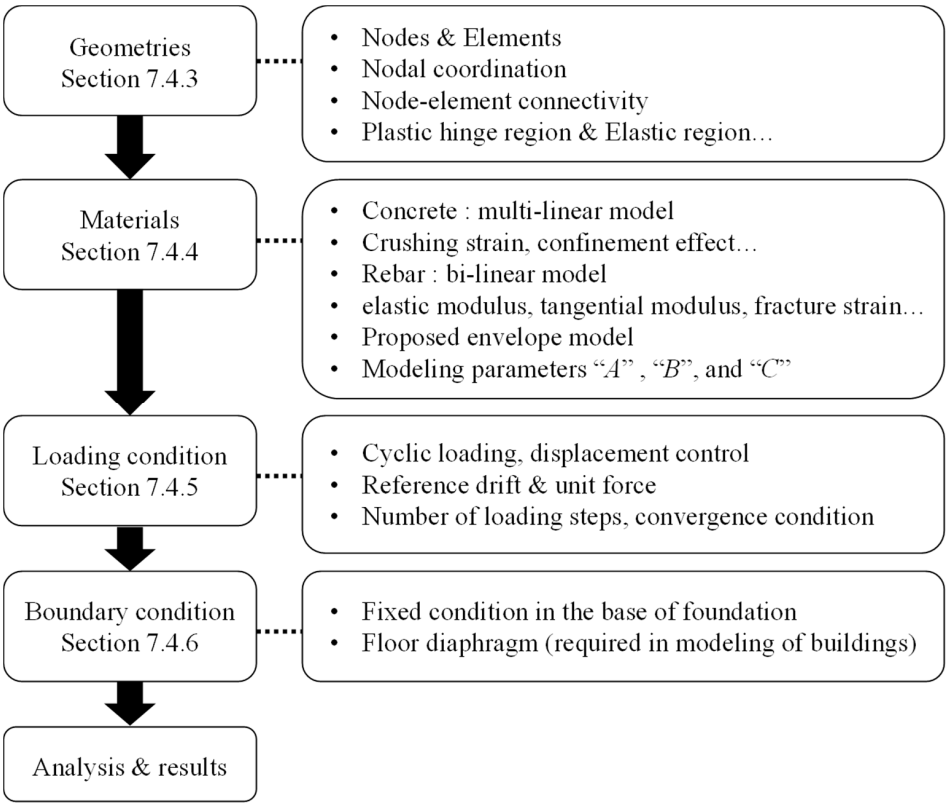

Fig. 7-5 Modeling procedure of wall element

7.4.2 Example walls

Specimens **NF2H-30**, and **HF2H-30** in Chapter 3 were used as example walls. As already reported, these specimens were failed by flexural–shear failure. Table 7-4 summarizes the design parameters of example walls.

In **NF2H-30**, for material properties of vertical fibers, the concrete compressive strength is $f_c' = 37$ MPa, yield strength of vertical web reinforcement is $f_{yv} = 470$ MPa, vertical web reinforcement ratio is $\rho_v = 2.21$ %, yield strength of vertical boundary element reinforcement is $f_{ybe} = 470$ MPa, and vertical boundary element reinforcement ratio is $\rho_b = 5.96$ %. The nominal flexural strength of **NF2H-30** is $V_{test} = 650$ kN, and the shear stress corresponding to the nominal flexural strength is $v_f = 4.33$ MPa. The nominal shear strength of **NF2H-30** calculated by Eq. (5-33) is $V_n = 807$ kN, and the shear stress corresponding to the nominal shear strength is $v_n = 5.38$ MPa. The concrete and rebar shear strengths of **NF2H-30** calculated by Eq. (5-33) are $V_c = 342$ kN, and $V_s = 465$ kN, respectively. The web crushing strength of **NF2H-30** calculated by Eq. (5-33) is $V_{max} = 1078$ kN. The strength margins are $\omega_1 = 1 - (V_f - V_s)/V_c = 0.46$, and $\omega_2 = 1 - V_f/V_{max} = 0.40$. From Table 7-3, the shear strains corresponding to a and *b* are calculated as $\gamma_a = 4.6\times10^{-3}$, and $\gamma_b = 7.9\times10^{-3}$, respectively. The residual strength ratio is $c = (0.2V_c + V_s)/V_f = 0.82$.

In **HF2H-30**, for material properties of vertical fibers, the concrete compressive strength is $f_c' = 37$ MPa, yield strength of vertical web reinforcement is $f_{yv} = 770$ MPa, vertical web reinforcement ratio is $\rho_v = 1.41$ %, yield strength of vertical boundary element reinforcement is $f_{ybe} = 770$ MPa, and vertical boundary element reinforcement ratio is $\rho_b = 2.08$ %. The nominal flexural strength of **HF2H-30** is $V_{test} = 669$ kN, and the shear stress corresponding to the nominal flexural strength is $v_f = 4.46$ MPa. The nominal shear strength of **HF2H-30** calculated by Eq. (5-33) is $V_n = 827$ kN, and the shear stress corresponding to the nominal shear strength is $v_n = 5.52$

MPa. The concrete and rebar shear strengths of **HF2H-30** calculated by Eq. (5-33) are V_c = 342 kN, and V_s = 485 kN, respectively. The web crushing strength of **HF2H-30** calculated by Eq. (5-33) is V_{max} = 939 kN. The strength margins are $\omega_1 = 1 - (V_f - V_s)/V_c$ = 0.46, and $\omega_2 = 1 - V_f/V_{wcm}$ = 0.290. From Table 7-3, the shear strains corresponding to a and *b* are calculated as $\gamma_a = 5.1\times10^{-3}$, and $\gamma_b = 14.3\times10^{-3}$, respectively. The residual strength ratio is $c = 0.2V_{max}/V_f$ = 0.28.

Table 7-4 Design parameters of example walls

Specimens	Vertical fibers					Plastic hinge rotation				Nominal strength		Governing shear failure mode
	f_c' [MPa]	f_{yv} [MPa]	ρ_v [%]	f_{yb} [MPa]	ρ_b [%]	ω_1, ω_2	γ_a [$\times10^{-3}$]	γ_b [$\times10^{-3}$]	c	v_f [MPa]	v_n [MPa]	
NF2H-30	37	470	2.21	470	5.96	0.46	4.6	7.9	0.82	4.33	5.39	DT+WC
HF2H-30	37	770	1.41	770	4.49	0.29	5.1	14.3	0.28	4.46	5.52	WC

Note:
f_c' = concrete compressive strength
f_{yv} = yield strength of vertical web reinforcement
ρ_v = vertical web reinforcement ratio
f_{yb} = yield strength of vertical boundary element reinforcement
ρ_b = vertical boundary element reinforcement ratio
ω_1 = Strength margin ratio of diagonal tension failure, $\omega_1 = 1 - (V_f - V_s)/V_c$, $0 \le \omega_1 \le 0.8$,
ω_2 = Strength margin ratio of web crushing failure, $\omega_2 = 1 - V_f/V_{wcm}$, $0 \le \omega_2 \le 0.8$.
a = Plastic shear strain from yielding to start of shear stress degradation
b = Plastic shear strain from yielding to ultimate state
c = Residual shear stress
v_f = shear stress corresponding to nominal flexural strength (test strength)
v_n = shear stress corresponding to nominal shear strength (Eq. (5-33))
WC = Web crushing mode
DT = Diagonal tension mode

7.4.3 Geometries of model

Fig. 7-6 and Fig. 7-7 show the geometries of Perform 3D model for example walls. Because the wall element in Perform 3D is 2D-plane element, only degrees of freedom related to the in-plane behavior were considered (dir. x, dir. z, and rot. y). The degrees of freedom related to the out-of-plane direction, the out-of-plane rotation, and the torsion were not considered. However, in case of the building structure, all degrees of freedom should be considered.

The wall model was consists of three parts: 1) wall, 2) elastic foundation, and 3) elastic loading beam. The wall model was established by considering the actual geometric dimensions of the wall specimens. The dimensions of wall was 1,000 mm (length) × 2,000 mm (height). According to program manual of Perform 3D, in case of single wall, it is suggested that the wall is divided by several parts to increase the accuracy of analysis. Therefore, the wall was divided by two regions, plastic hinge region and elastic region. The plastic hinge length was $l_p = 0.8l_w = 800$ mm. Generally, in the building structures, the floor slabs divide the walls by several parts. In this case, it is not required to divide the wall by plastic hinge region and elastic region.

The dimensions of elastic foundation was 2,000 mm (length) × 750 mm (height), and the dimensions of elastic loading beam was 1,500 mm (length) × 500 mm (height). The net height between the loading point and the wall base is 2,250 mm. For the foundation and loading beam, elastic concrete model was used.

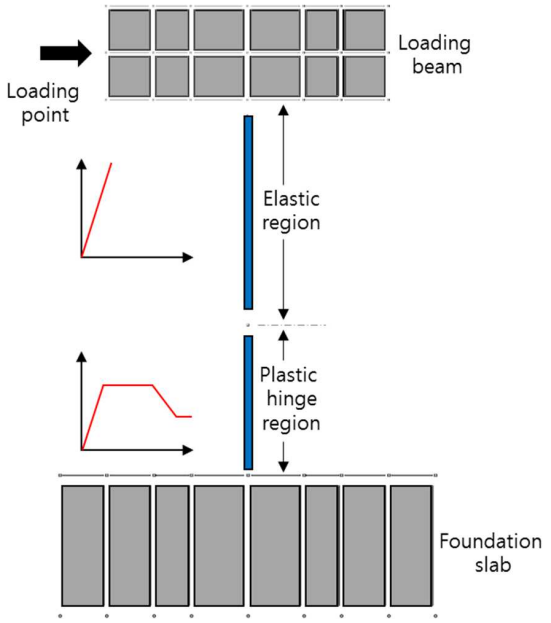

Fig. 7-6 Geometries of Perform 3D model (Concentrated hinge model)

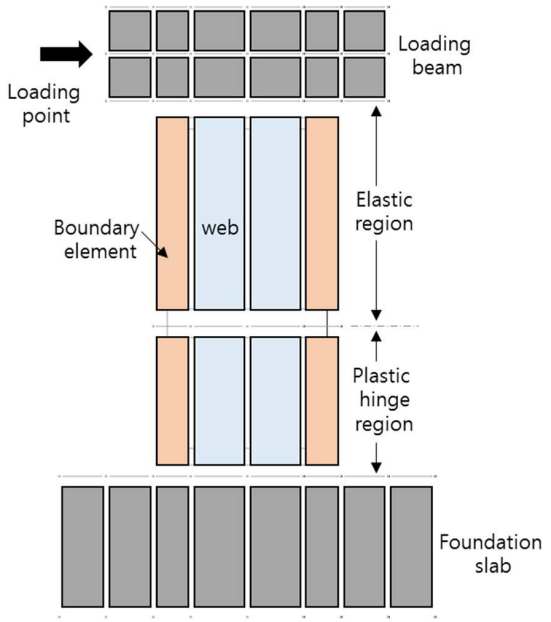

Fig. 7-7 Geometries of Perform 3D model (Fiber model)

7.4.4 Materials

In case of the concentrated hinge model, the flexural strength-plastic rotation relationship should be defined. Unfortunately, the Perform 3D does not provide the concentrated hinge model for the wall. Instead, the present study uses the FEMA beam-column element.

The sectional properties are defined by using "Cross Sects: Column Reinforced Concrete Section" function (see Fig. 7-8). Defining the dimension of section, the sectional stiffness are automatically calculated. For effective shear modulus of wall "G", the user guide of Perform 3D suggests $G = \rho_h E_s$, where, ρ_h = shear reinforcement ratio, and E_s = elastic modulus of reinforcement (= 200,000 MPa).

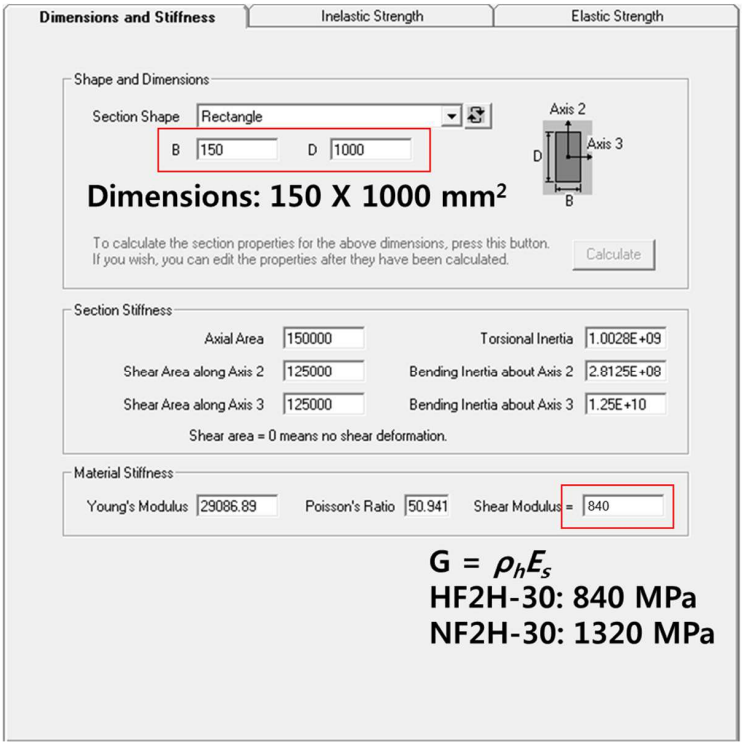

Fig. 7-8 Input values of wall cross section

The envelope curve model for the plastic hinge is defined by using “Inelastic: FEMA Column Concrete Type” function. In the Perform 3D, the envelope curve model is defined by “YULRX” rule. Meaning of each letter is as follows: index “Y” indicates point at the elastic limit, index “U” indicates point at the reaching of peak strength, index “L” indicates point at the start of degradation, index “R” indicates point at the end of degradation, and index “X” indicates point at ultimate state. The “YULRX” rule is combined with both force related index “F” and displacement related index “D”. For example, in the shear material for a wall of Perform 3D “FU” indicates the peak strength. Similarly, “DU” indicates the deformation corresponding to the peak strength.

Table 7-5 shows the input parameters of the proposed model in the Perform 3D concentrated hinge model. Because the proposed model defines the post-yielding behavior, only parameters for “ULRX” were required. For the flexural strength “FU”, the nominal flexural strength M_n is assigned. For the plastic rotation, “DL” and “DR”, which are the plastic rotation corresponding to the initiation and termination of strength degradation, the modeling parameters *A* and *B* are assigned, respectively. For residual stress ratio “FR/FU”, the modeling parameter *C* is assigned.

Table 7-5 also shows the calculated values of input parameters for the example walls. For **NF2H-30**, *G* = 1,320 MPa, FU = 1,461 kNm, DL = 0.0091 rad, DR = 0.0158 rad, and FR/FU = 0.82. For **HF2H-30**, G = 840 MPa, FU = 1,505 kNm, DL = 0.0103, DR = 0.0286, and FR/FU = 0.28.

Fig. 7-9 and Fig. 7-10 show input values of plastic hinge model in the Perform 3D.

Table 7-5 Summary of the input parameters for concentrated hinge model

Parameters of Perform 3D	Parameters of the proposed model	Calculations for example walls	
		NF2H-30	HF2H-30
G	$G=\rho_h E_s$	1,320 MPa	840 MPa
FU	M_n	1,461 kNm	1505 kNm
DL	A	0.0091 rad	0.0103 rad
DR	B	0.0158 rad	0.0286 rad
FR/FU	C	0.82	0.28

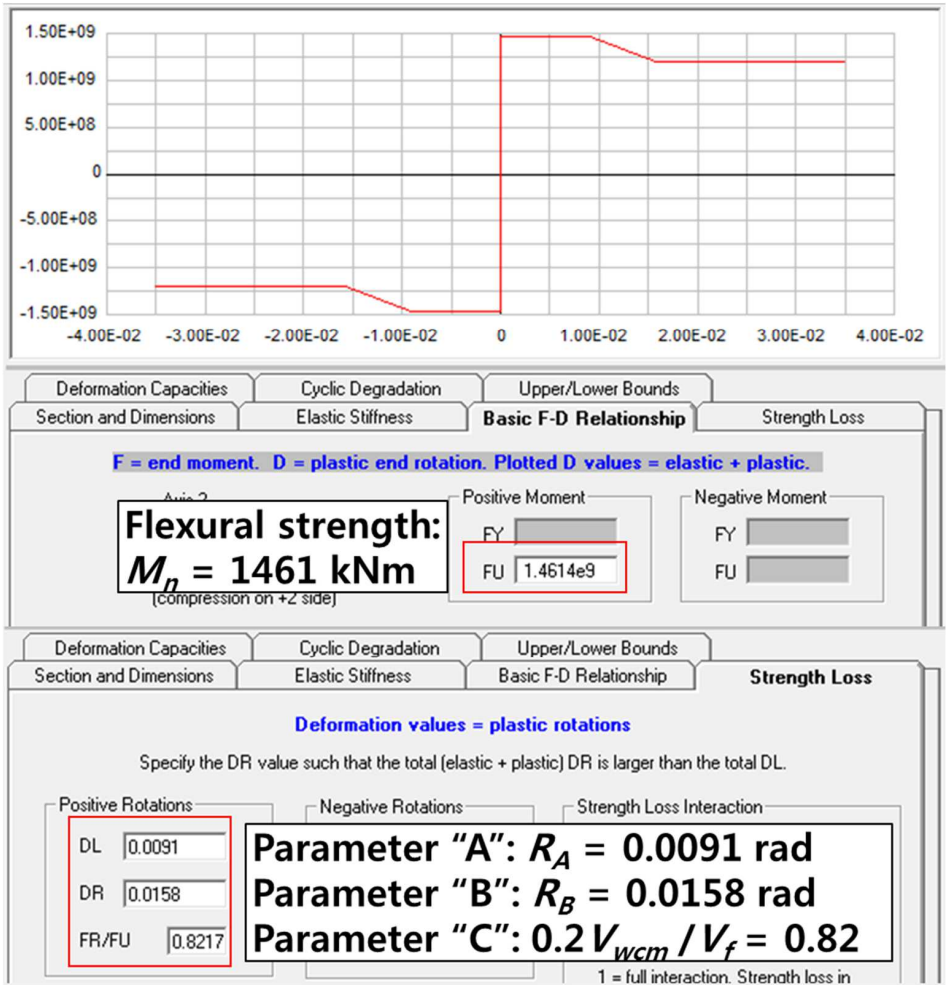

Fig. 7-9 Input values of plastic hinge model for the wall (**NF2H-30**)

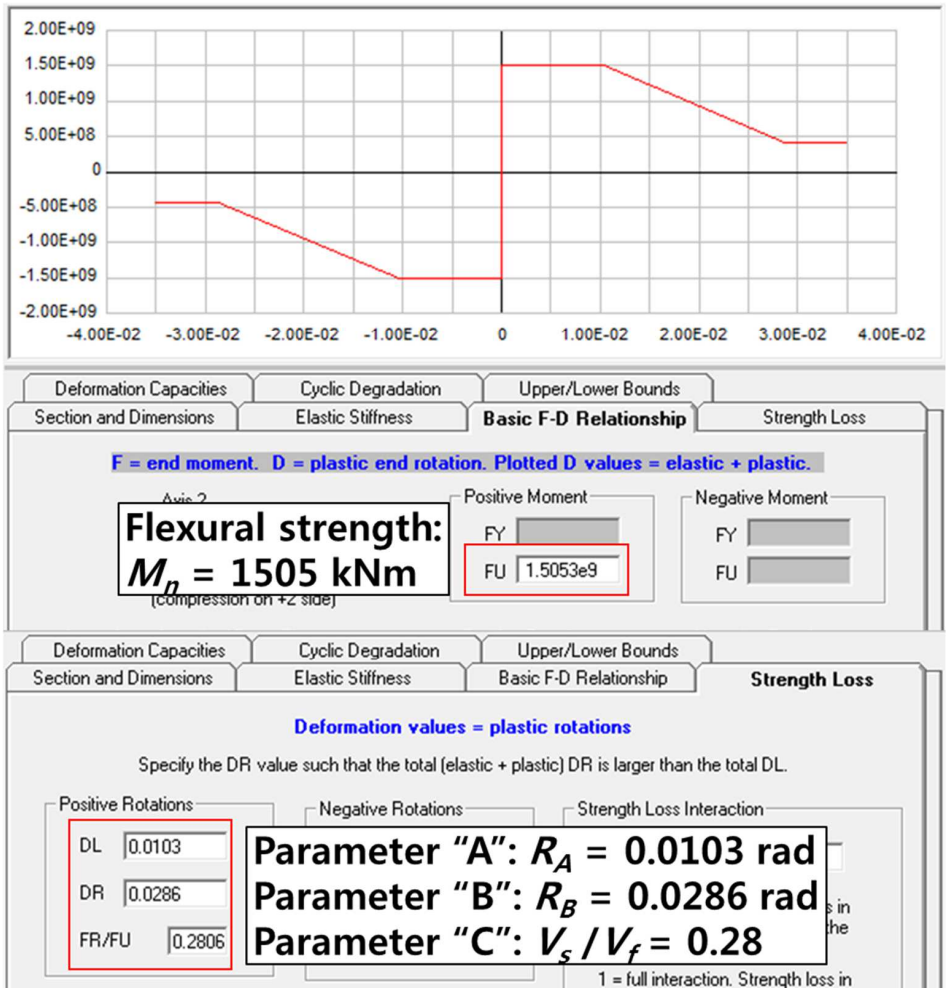

Fig. 7-10 Input values of plastic hinge model for the wall (**HF2H-30**)

The wall fiber model of the Perform 3D is consists of vertical fibers and shear spring (see Fig. 7-1). In Perform 3D, the properties of vertical fibers, such as area and material of the fiber, are defined by using "Cross Sects: Shear Wall Inelastic Section." Function. Fig. 7-11 shows the input values in the Perform 3D. To define the fiber model, the material model and the number of fibers are defined. For concrete, the section is divided into five fibers uniformly. For rebar, the area of fiber is calculated from the rebar ratio. The number of steel fibers is two.

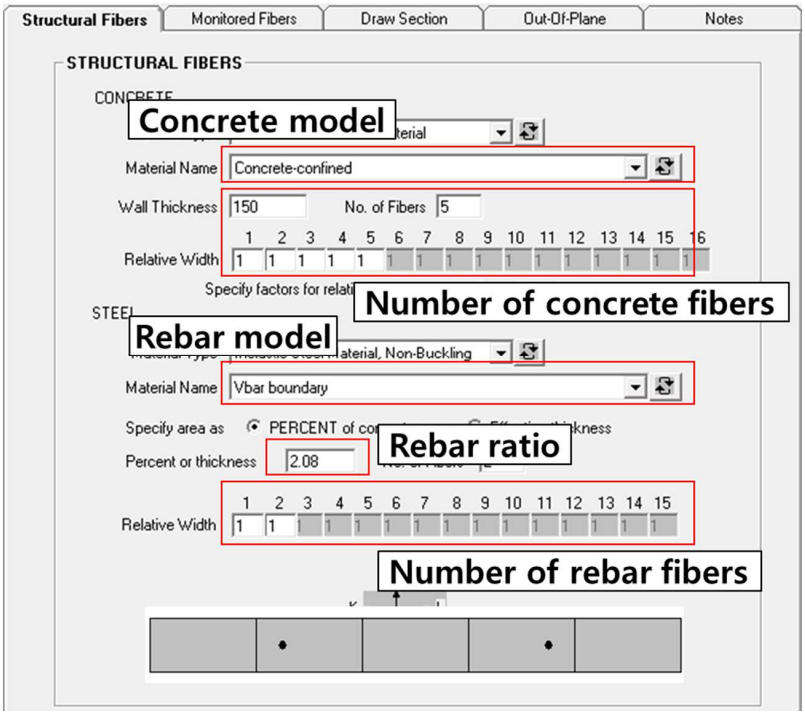

Fig. 7-11 Shear wall inelastic section in the Perform 3D (fiber model)

The material models of concrete and rebar are defined by using "Materials" function. Fig. 7-12 shows the stress-strain relationship of concrete and rebar. For concrete, multi-linear strain-stress curve corresponding to Kent Park concrete model was used. For unconfined concrete, the concrete crushing strain was assumed to be ε_{co} = 0.002, and the concrete ultimate strain was assumed to be ε_{cu} = 0.003. The residual stress of concrete was assumed to be $0.2f_c'$. For confined concrete in the boundary elements, ε_{co} and ε_{cu} were increased considering the confinement effect. The elastic modulus of concrete was assumed as $E_c = 4700\sqrt{f_c'}$, according to ACI 318-19.

For rebar, bilinear elasto-plastic strain curve was used. The buckling of rebar was not considered. Elastic modulus of rebar was assumed to be E_s = 200,000 MPa. Tensile fracture strain of rebar was assumed to be ε_t = 0.025.

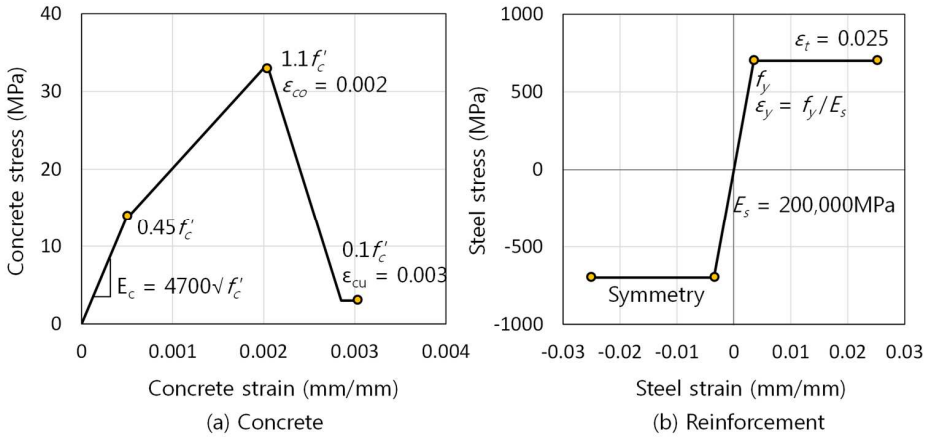

Fig. 7-12 Material models of concrete and rebar

The material model of shear spring is defined by using “Inelastic/elastic shear material for a wall” function. Table 7-6 shows the summary of input parameters in the Perform 3D shear material model. Because the proposed model defines the post-yielding behavior, only parameters for “ULRX” were required. For the peak stress “FU”, the nominal flexural stress v_f is assigned. For shear strains, “DL” and “DR”, which are the shear strains corresponding to the initiation and termination of the strength degradation, $\gamma_a + \gamma_y$ and $\gamma_b + \gamma_y$ (where, γ_y = shear strain corresponding to yielding) are assigned, respectively. For residual stress ratio “FR/FU”, C is assigned.

Table 7-6 also shows the calculated values of input parameters for example walls. For **NF2H-30**, G = 1,320 MPa, FU = 4.33 MPa, DL = 0.0063, DR = 0.0097, and FR/FU = 0.82. For **HF2H-30**, G = 840 MPa, FU = 4.46 MPa, DL = 0.0080, DR = 0.0172, and FR/FU = 0.28.

Fig. 7-13 and Fig. 7-14 show input values of shear material model in Perform 3D.

Table 7-6 Summary of the input parameters for fiber model

Parameters of Perform 3D	Parameters of the proposed model	Calculations for example walls	
		NF2H-30	HF2H-30
G	$G=\rho_h E_s$	1320 MPa	840 MPa
FU	v_f	4.33 MPa	4.46 MPa
DL	$\gamma_a + \gamma_y$	0.0063	0.0080
DR	$\gamma_b + \gamma_y$	0.0097	0.0172
FR/FU	C	0.82	0.28

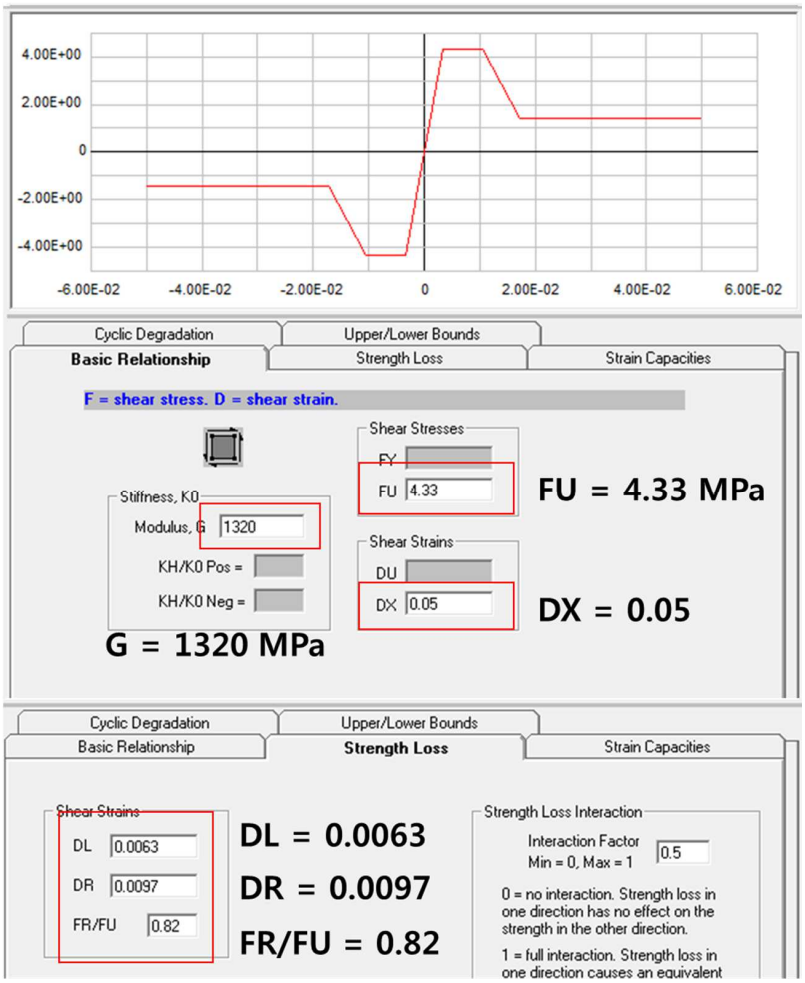

Fig. 7-13 Input values of shear material for a wall (**NF2H-30**)

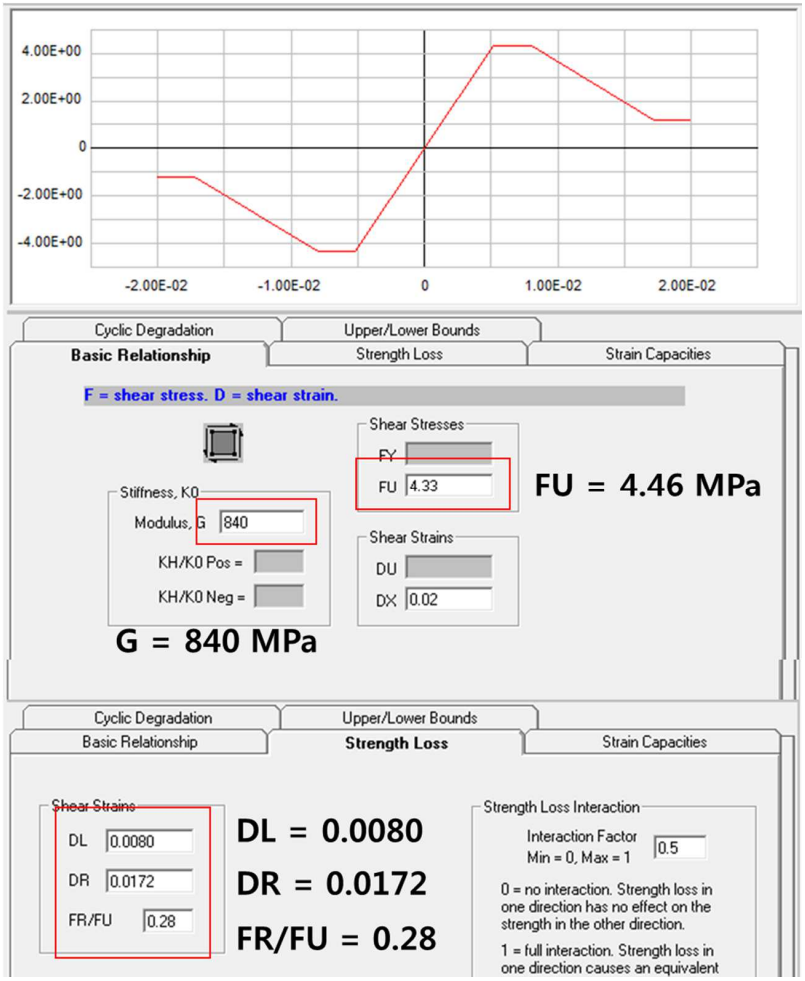

Fig. 7-14 Input values of shear material for a wall (**HF2R-AB**)

7.4.5 Cyclic properties

To simulate the cyclic response of RC walls, hysteretic model should be defined. In Perform 3D, to define the cyclic degradation, energy factor and unloading stiffness can be defined. Pinching effect cannot be considered.

The energy factor is defined as a ratio between energy dissipation in a loading cycle to energy dissipation of equivalent elasto-plastic curve (E_d/E_0). Fig. 7-15 shows the energy factors calculated in the existing test specimens listed in Table 6-3 and Table 6-4. The energy factor decreases as the drift ductility ratio increases. Further, the energy factor decreases as the yield strength of vertical reinforcement increases. From the existing cyclic loading test results, an empirical equation for energy factor is recommended as follows:

$$\frac{E_{d,i}}{E_{0,i}} = \frac{0.6}{\mu - 0.4} \geq 0.2 \quad (f_y < 400 \text{ MPa}) \tag{7-13a}$$

$$\frac{E_{d,i}}{E_{0,i}} = \frac{0.4}{\mu - 0.6} \geq 0.15 \quad (f_y = 400 - 600 \text{ MPa}) \tag{7-13b}$$

$$\frac{E_{d,i}}{E_{0,i}} = \frac{0.2}{\mu - 0.8} \geq 0.1 \quad (f_y > 600 \text{ MPa}) \tag{7-13c}$$

Where, μ = drift ductility ratio (δ/δ_y), f_y = yield strength of vertical reinforcement.

According to Lowes and Altoontash (2003), the cyclic deterioration is reasonably simulated by using a damage index. Using the energy factor, a linear damage index model can be utilized (Han et al. (2019)). In Perform 3D, unloading stiffness factor is defined as a value between -1 to +1. When the unloading stiffness factor is plus 1, the unloading stiffness is maximized with minimum elastic range (Fig. 7-16 (a)). While the unloading stiffness factor is minus 1, the unloading stiffness is minimized with maximum elastic range (Fig. 7-16 (c)). According to Lowes et al. (2018), for modeling of RC member, unloading factor is recommended to use 0.5.

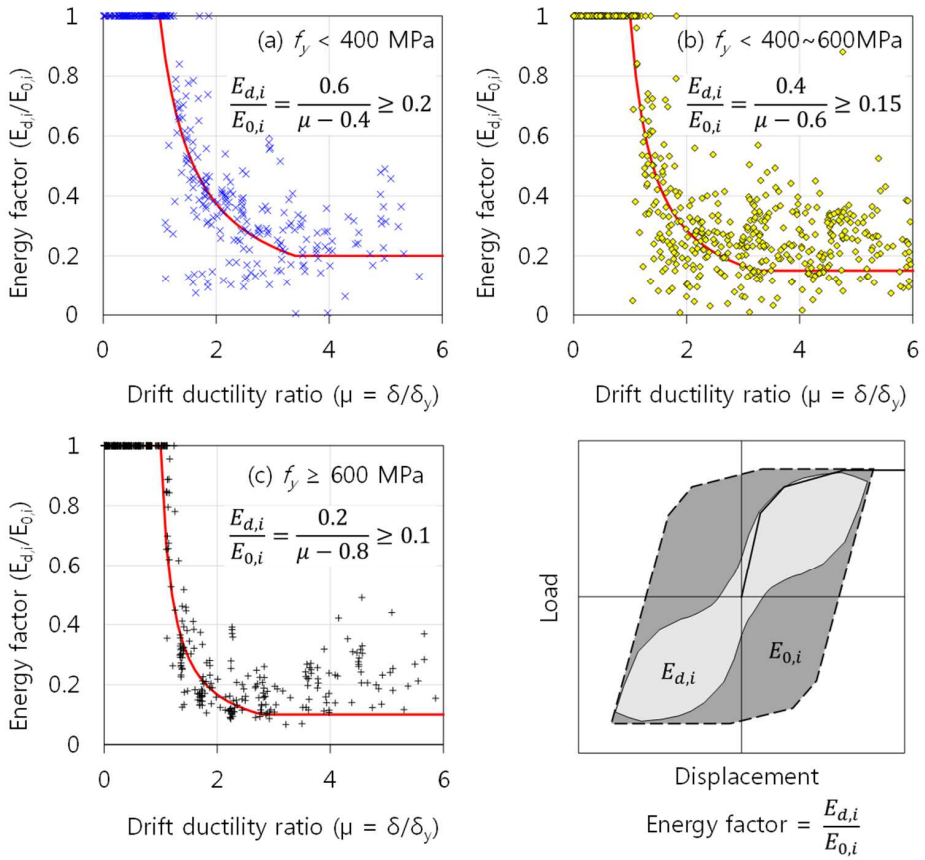

Fig. 7-15 Energy factor calculated in the existing test specimens

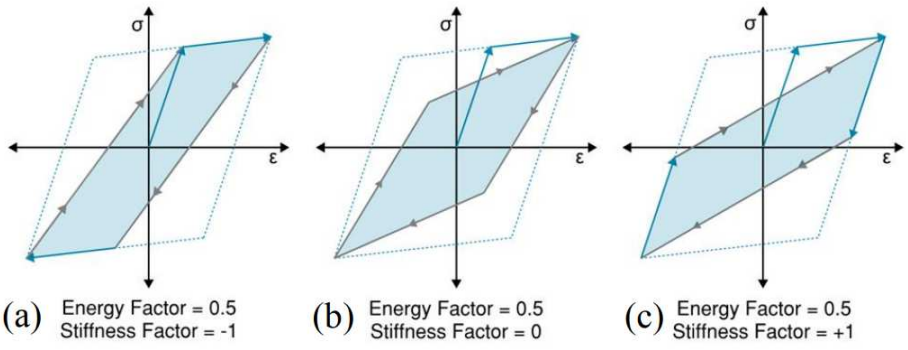

Fig. 7-16 Unloading stiffness factor of Perform 3D.

7.4.6 Loading conditions

To simulate the cyclic response of the example walls, cyclic loading was applied to the model by displacement control. The same loading protocol used in the cyclic loading test (see Fig. 3-7) was used in Perform 3D analysis. In Perform 3D, using "Static push-over" load case, lateral load can be applied by displacement control. For each loading step, target drift was defined by loading protocol for positive and negative loading direction, respectively. A loading step was divided by 10 sub-steps. The maximum number of iterations was limited by 100 times. The convergence condition of error < 1% was used.

Fig. 7-17 shows procedure of loading application. For specimens **NF2H-30** and **HF2H-30** with axial loading, the gravity load case was applied first, and then cyclic lateral loadings are followed. A loading cycle was consists of following steps: 1) positive loading step 2) negative loading step (unloaded to zero displacement), 3) negative loading, and 4) positive loading step (unloaded to zero displacement).

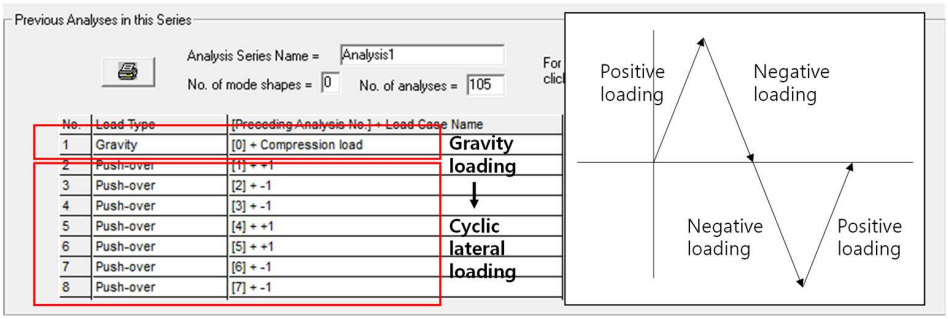

Fig. 7-17 Procedure of loading application

7.4.7 Boundary conditions

Fig. 7-18 shows boundary conditions of the Perform 3D model. For the base of the foundation, fixed support was used. Further, because the wall element in Perform 3D is 2D-plane element, only degrees of freedom related to the in-plane behavior were considered (dir. x, dir. z, and rot. y). The degrees of freedom related to the out-of-plane direction, the out-of-plane rotation, and the torsion were constrained. Because the example wall model was a single wall, floor diaphragm was not considered for the example walls. However, in the modeling of building structures, the walls in the same floor are restrained by the slab. In this case, floor diaphragm is required.

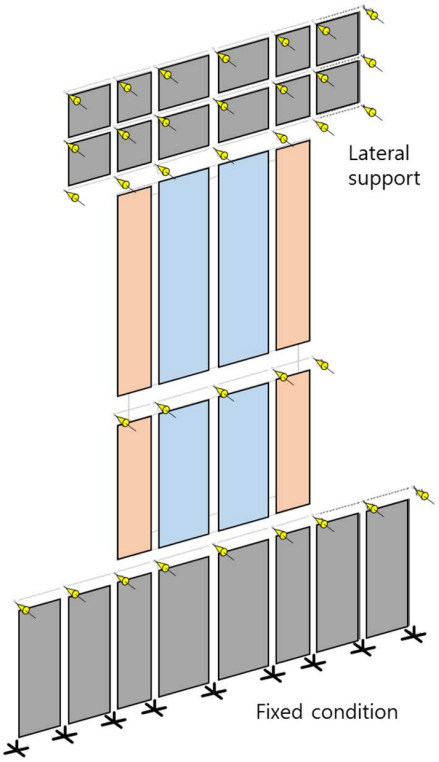

Fig. 7-18 Boundary conditions of the wall model

7.4.8 Analysis results

Fig. 7-19 and Fig. 7-20 show the analysis results. In the figures, gray solid line indicates the load-displacement relationship measured in the test, blue solid line indicates the proposed strength degradation model, red solid line indicates the load-displacement relationship of Perform 3D cyclic loading analysis, Black solid line indicates the load-displacement envelope of Perform 3D push-over analysis with the strength degradation model, and black dotted line indicates the load-displacement of Perform 3D push-over analysis without strength degradation.

Before flexural yielding, the Perform 3D analysis showed accurate prediction of the load-displacement relationships of the wall specimens, regardless of type of the modeling methods. On the other hand, after flexural yielding, as the plastic deformation increased, the shear strength degradation occurred in the wall model with the strength degradation model. Using the concentrated hinge model, the proposed strength degradation model is exactly defined in the Perform 3D, while fiber model shows rapid strength degradation than the proposed model. This phenomenon will be discussed in the next section “7.5 Limitation”. The deformation capacity is limited by the strength degradation.

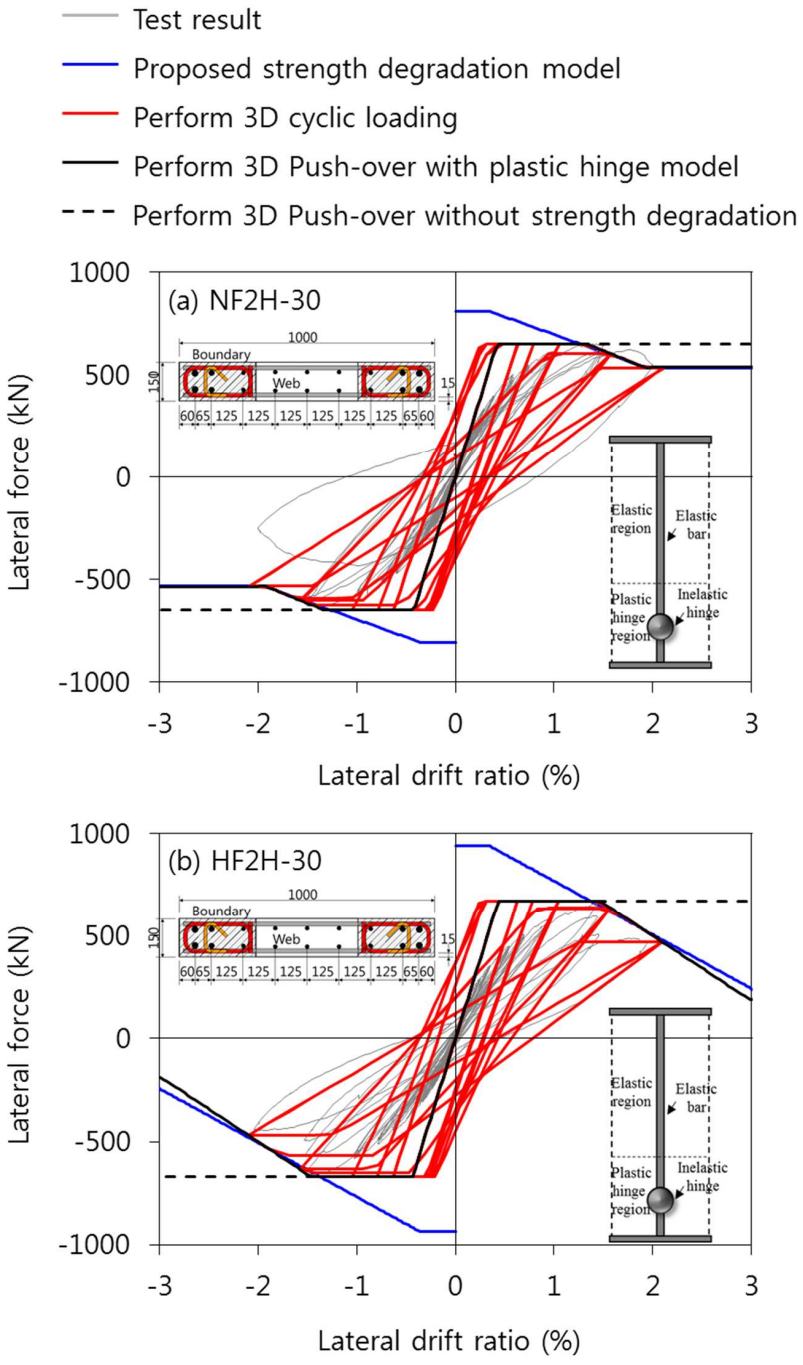

Fig. 7-19 Perform 3D analysis results (Concentrated hinge model)

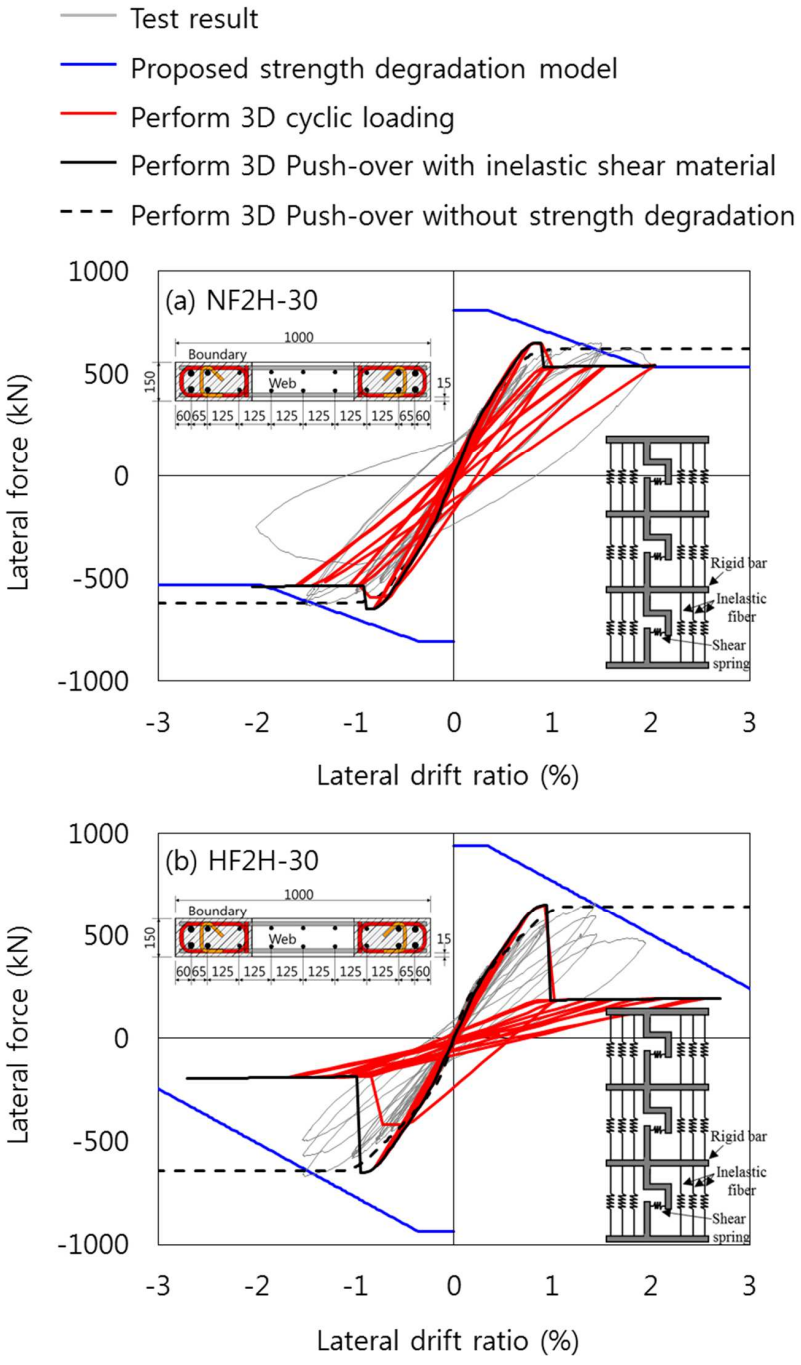

Fig. 7-20 Perform 3D analysis results (Fiber model)

7.5 Limitations

Using the fiber model of the Perform 3D, the shear strength degradation occurs more rapidly than the proposed strength degradation model (see Fig. 7-20). This is because of the characteristics of the fiber model.

Fig. 7-21 shows a working mechanism of wall element in Perform 3D. The flexural strength – rotation relationship of vertical fibers is represented by flexural spring, and the shear stress – shear strain relationship of shear material is represented by shear spring. The flexural spring and the shear spring are connected in series. The lateral forces applied to each spring are the same, and the total lateral deformation is sum of flexural deformation and shear deformation.

In Perform 3D, the flexural spring and shear spring are working independently. If flexural yielding occurs before reaching shear stress (Case 1 in Fig. 7-21 (a)), the stiffness of flexural spring is significantly decreased. Total lateral deformation is governed by flexural deformation, while the shear deformation is limited. In this case, the shear strength degradation model is not working as intended. On the other hand, if shear yielding occurs before flexural yielding (Case 2 in Fig. 7-21 (b)), total lateral deformation is governed by shear deformation. In this case, the shear strength degradation occurs by the defined shear stress-strain model. However, the flexural deformation does not increase or even decreases by the strength degradation, which results in significant underestimation of plastic hinge rotation.

Thus, for future study, an integrated wall model is required to address the flexural-shear interaction (i.e. strength degradation affected by plastic hinge rotation).

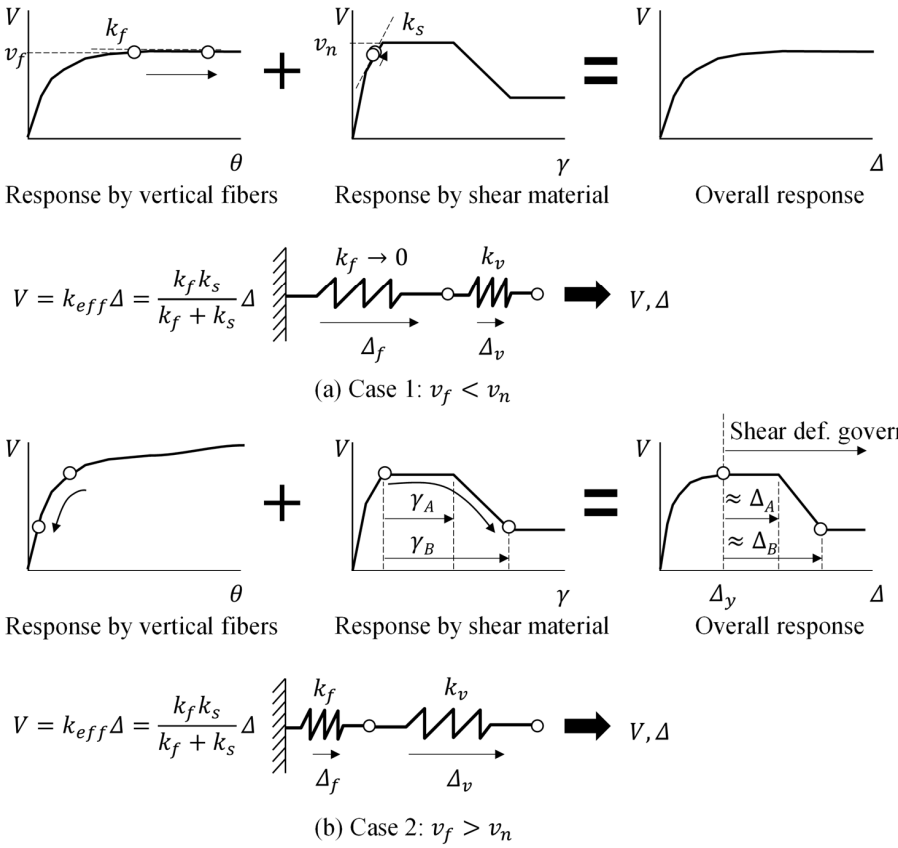

Fig. 7-21 Working mechanism of a wall model in Perform 3D.

7.6 Summary

Based on the proposed model, the envelope curve model was developed for practical design. The strength degradation was defined by three parameters: plastic hinge rotation *A*, and *B*, and residual strength ratio *C*. For modeling parameters, a design table was suggested in the range of design parameters.

The proposed shear strength degradation model was applied in the practical design. The envelope curve model for plastic hinge model was developed. The plastic hinge model was defined by the plastic rotation and flexural strength. Further, for the fiber model, shear spring model was developed. The shear spring model was defined by the shear strain and shear stress. For convenient design, the design tables were developed for both plastic hinge model and shear spring model.

For verification, the proposed model was applied to the example wall test specimens. The specimens **NF2H-30**, and **HF2H-30** were used as example wall models. The lateral cyclic loading was applied to the wall model by displacement control.

The analysis results showed that the shear strength degradation after flexural yielding occurred in the wall model with inelastic strength degradation model. Using the concentrated hinge model, the proposed strength degradation model was exactly defined in the Perform 3D. However, using the fiber model, the lateral displacement limited by shear strength degradation was underestimated.

Chapter 8. Conclusions

In this dissertation, experimental and theoretic studies were conducted, to develop the simplified design model to predict the shear strength and deformation capacity of walls accurately. The experimental studies investigated the effects of various design parameters on the shear strength. Based on the test results, simplified shear strength and strength degradation models were developed. Followings summarize the conclusions of this dissertation.

1. Shear strength of RC walls with 700 MPa reinforcing bars

To investigate the shear strength and deformation capacity of walls with Grade 700 MPa high-strength bars, fifteen wall specimens with aspect ratio 2.0 or 1.0 were tested under cyclic lateral loading. The major findings are summarized as follows:

1) For flexural yielding mode specimens, the peak strength V_{test} was greater than the nominal flexural strength V_f (V_{test}/V_f = 1.03 ~ 1.20). Comparing **NF2H-30**, and **HF2H-30**, the effect of bar yield strength to flexural strength was not significant. However, because of the greater yield strain and lower vertical bar ratio of the wall with high-strength bar, the wall with 700 MPa bar showed 17 percent less drift ductility ratio, 37 percent less energy dissipation, and increase of flexural and shear crack widths. In **HF2R**, due to significantly low vertical reinforcement ratio, premature tensile fracture of vertical rebar occurred. Ductility and energy dissipation of **HF2R** were significantly decreased. **HF2R-AB** showed the combined failure mode (FY+DT+WC), because of the significantly low shear reinforcement ratio. **HF2R-AB** showed ductility of 3.06 – 4.21, due to greater yield ratio of the tensile rebar.

2) Shear failure mode walls with h_w/l_w = 2.0 failed due to diagonal tensile cracking (DT), while the walls with low aspect ratio (h_w/l_w = 1.0) failed in a combined failure mode of diagonal cracking + web crushing. The shear strengths of walls with 700 MPa bar were 10 – 25 percent less than those of walls with 400 MPa bars. In the specimens with 700 MPa shear reinforcement, yielding occurred in the shear reinforcement and crack width increased because of the higher yield strain and lower reinforcement ratio.

3) In the shear failure mode specimens, the peak tested shear strength V_{test} was greater than the nominal shear strength V_n which was calculated by using actual material strengths. However, the safety margin was decreased in the wall with 700 MPa bar (V_{test}/V_n = 1.07 ~ 1.55 for Grade 700 MPa vs V_{test}/V_n = 1.20 ~ 1.73 for Grade 400 MPa).

2. Shear strength & Shear strength degradation model

Based on the test results, the effects of design parameters on the shear strength were investigated. The shear strength and strength degradation models were developed considering the shear failure mechanisms, diagonal cracking and web crushing. The major findings are as follows:

1) The major design parameters affecting the shear strength are vertical reinforcement ratio, axial load ratio, and the shape of cross-section. Such parameters are closely related to the compression zone depth, which indicates that the shear failure mechanism is explained based on the effective compressive stress of concrete and effective area of concrete in compression. Based on the considerations the simplified shear failure mechanism models were developed for diagonal tension cracking and web crushing.

2) For the diagonal tension cracking, it was assumed that only the concrete in

the compression zone resists the shear. Before flexural yielding, the concrete shear strength is defined by the average concrete compressive stress and the compression zone depth. From the simplified sectional analysis model, the compression zone depth, average concrete compressive stress, crack angle were simplified. After flexural yielding, the compression zone gradually decreases as the concrete crushing occurs. Thus, the shear strength of concrete is degraded.

3) Assuming that the diagonal strut of plastic hinge region is critical section for web crushing failure, the web crushing strength was defined based on the effective strength of diagonal strut. By the compression softening effect, the average effective compressive stress of diagonal strut is degraded as the transverse strain increases. The transverse strain was calculated from the strain compatibility with diagonal, horizontal and vertical strains ($\varepsilon_t = -\varepsilon_c + \varepsilon_x + \varepsilon_y$). Therefore, before yielding, since the vertical residual strain is negligible, the web crushing strength was related to the horizontal reinforcement. After yielding, in the plastic hinge region, the elongation occurs by the cyclic loading effects. As the elongation increases, the transverse strain of diagonal strut increases, and effective strength of diagonal strut decreases. Therefore, web crushing strength is degraded.

4) Considering the shear failure mechanisms, simplified shear strength and strength degradation model were developed. The proposed shear strength model was applied to existing test specimens with f_c' = 20 – 137 MPa, f_y = 400 – 1079 MPa, ρ_{avg} = 0.25 – 6.0 %, p = 0 – 0.3. The proposed model agreed with the existing test results regardless of variations of design parameters.

3. Application of the proposed model

For application in the practical design, the proposed model was applied in the Perform 3D. The design tables and modeling guideline were suggested. The major findings are as follows:

1) The strength degradation was defined by three parameters: plastic hinge rotation *A*, and *B*, and residual strength ratio *C*. For modeling parameters, a design table was developed in the range of design parameters.

2) The performance based seismic design, the acceptance criteria was suggested for each performance level, according to ASCE 41-17. Assuming that the brittle failure by shear strength degradation, the deformation limit of collapse prevention level was defined as the modeling parameter *B*. The deformation limit of life safety level was defined as 0.75 times CP. The modeling parameter A was used for immediate occupancy level.

3) The Perform 3D modeling guideline was suggested. Both plastic hinge model and fiber model were used. The modeling guideline includes: dimensions, material models, envelope curve models, cyclic properties, loading conditions, and boundary conditions.

4) For verification, the proposed model was applied to the test specimens. The lateral cyclic loading was applied to the wall model by displacement control. The analysis results showed that the shear strength degradation after flexural yielding occurred in the wall model with the strength degradation model. The lateral displacement was limited by the shear strength degradation.

References

[1] American concrete institute 41-17, A. (2017). Seismic evaluation and retrofit of existing buildings.

[2] Adorno-Bonilla, C. M. (2016). Shear strength and displacement capacity of squat reinforced concrete shear walls. UNIVERSITY OF PUERTO RICO MAYAGÜEZ CAMPUS,

[3] AIK. (2020). Design guideline for performance based design of RC structure. Retrieved from Seoul, Korea:

[4] Baek, J.-W., Park, H.-G., Choi, K.-K., Seo, M.-S., & Chung, L. (2018). Minimum Shear Reinforcement of Slender Walls with Grade 500 MPa (72.5 ksi) Reinforcing Bars. ACI Structural Journal, 115(3).

[5] Baek, J.-W., Park, H.-G., Lee, B.-S., & Shin, H.-M. (2018). Shear-Friction Strength of Low-Rise Walls with 550 MPa (80 ksi) Reinforcing Bars under Cyclic Loading. ACI Structural Journal, 115(1).

[6] Baek, J.-W., Park, H.-G., Lee, J.-H., & Bang, C.-J. (2017). Cyclic Loading Test for Walls of Aspect Ratio 1.0 and 0.5 with Grade 550 MPa Shear Reinforcing Bars. ACI Structural Journal, 114(4). doi:10.14359/51689680

[7] Baek, J.-W., Park, H.-G., Shin, H.-M., & Yim, S.-J. (2017). Cyclic Loading Tests for Reinforced Concrete Walls (Aspect Ratio 2.0) with Grade 550 MPa (80 ksi) Shear Reinforcing Bars. ACI Structural Journal, 114(3). doi:10.14359/51689437

[8] Barda, F., Hanson, J. M., & Corley, W. G. (1977). Shear strength of low-rise walls with boundary elements. Special Publication, 53, 149-202.

[9] Burgueño, R., Liu, X., & Hines, E. M. (2014). Web crushing capacity of high-strength concrete structural walls: experimental study. ACI Structural Journal, 111(2), 235.

[10] Cardenas, A. E., Hanson, J. M., Corley, W. G., & Hognestad, E. (1973). Design provisions for shear walls. ACI Journal, 70(3), 221-230.

[11] Carrillo, J., & Alcocer, S. M. (2012). Backbone model for performance-based seismic design of RC walls for low-rise housing. Earthquake Spectra, 28(3), 943-964.

[12] Carrillo, J., & Alcocer, S. M. (2013). Shear strength of reinforced concrete walls for seismic design of low-rise housing. ACI Structural Journal, 110(3), 415.

[13] Chen, X. L., Fu, J. P., Hao, X., Yang, H., & Zhang, D. Y. (2019). Seismic behavior of reinforced concrete squat walls with high strength reinforcements: An experimental study. Structural Concrete, 20(3), 911-931.

[14] Cheng, M.-Y., Hung, S.-C., Lequesne, R. D., & Lepage, A. (2016). Earthquake-resistant squat walls reinforced with high-strength steel.

[15] Choi, K.-K., & Hong-Gun, P. (2007). Unified shear strength model for reinforced concrete beams-Part II: Verification and simplified method. ACI Structural Journal, 104(2), 153.

[16] Committee, A., & Standardization, I. O. f. (2019). Building code

requirements for structural concrete (ACI 318-19) and commentary.

[17] Committee, N. S. (2005). Seismic Design Criteria for Structures, Systems, and Components in Nuclear Facilities. American Society of Civil Engineers, Reston, VA.

[18] CSI. (2006). Components and Elements for PERFORM 3D and PERFORM-Collapse ver 4. Retrieved from

[19] Dazio, A., Beyer, K., & Bachmann, H. (2009). Quasi-static cyclic tests and plastic hinge analysis of RC structural walls. Engineering Structures, 31(7), 1556-1571.

[20] Deger, Z. T., & Basdogan, C. (2021). Empirical Equations for Shear Strength of Conventional Reinforced Concrete Shear Walls. ACI Structural Journal, 118(2), 61-71.

[21] Duffey, T., Farrar, C., & Goldman, A. (1994). Low-rise shear wall ultimate drift limits. Earthquake Spectra, 10(4), 655-674.

[22] Elwood, K. J., & Eberhard, M. O. (2009). Effective Stiffness of Reinforced Concrete Columns. ACI Structural Journal, 106(4).

[23] Eom, T.-S., & Park, H.-G. (2010). Elongation of reinforced concrete members subjected to cyclic loading. Journal of structural engineering, 136(9), 1044-1054.

[24] Eom, T.-S., & Park, H.-G. (2013). Evaluation of Shear Deformation and Energy Dissipation of Reinforced Concrete Members Subjected to Cyclic Loading. ACI Structural Journal, 110(5).

[25] Eom, T.-S., Park, H.-G., Kim, J.-Y., & Lee, H.-S. (2013). Web Crushing and Deformation Capacity of Low-Rise Walls Subjected to Cyclic Loading. ACI Structural Journal, 110(4).

[26] Epackachi, S., Sharma, N., Whittaker, A., Hamburger, R. O., & Hortacsu, A. (2019). A cyclic backbone curve for shear-critical reinforced concrete walls. Journal of structural engineering, 145(4), 04019006.

[27] Farvashany, F. E., Foster, S. J., & Rangan, B. V. (2008). Strength and deformation of high-strength concrete shearwalls. ACI Structural Journal, 105(1), 21.

[28] fib. (2013). fib Model Code for Concrete Structures 2010: Wiley.

[29] Gulec, C. K., & Whittaker, A. S. (2011). Empirical Equations for Peak Shear Strength of Low Aspect Ratio Reinforced Concrete Walls. ACI Structural Journal, 108(1).

[30] Hawkins, N. M., & Ghosh, S. (2004). Acceptance criteria for special precast concrete structural walls based on validation testing. PCI journal, 49(5), 78-92.

[31] Hidalgo, P., & Jordan, R. (1996). Strenght and Energy Dissipation Characteristics of Reinforced Concrete Walls under Shear Failure. Paper presented at the Proceedings of The Eleventh World Conference on Earthquake Engineering, Acapulco, Mexico.

[32] Hidalgo, P. A., Ledezma, C. A., & Jordan, R. M. (2002). Seismic behavior of squat reinforced concrete shear walls. Earthquake Spectra, 18(2), 287-308.

[33] Hirosawa, M. (1975). Past experimental results on reinforced concrete shear walls and analysis on them. Kenchiku Kenkyu Shiryo, 6, 33-34.

[34] Hognestad, E. (1951). Study of combined bending and axial load in reinforced concrete members. Retrieved from

[35] Huq, M. S. (2018). High-Strength Steel Bars in Earthquake-Resistant T-Shaped Concrete Walls. University of Kansas,

[36] Institute, K. C. (2017). Concrete Design Code and Commentary. Seoul, Korea: Kimoondang Publishing Company.

[37] Kabeyasawa, T., & Hiraishi, H. (1998). Tests and analyses of high-strength reinforced concrete shear walls in Japan. Special Publication, 176, 281-310.

[38] Kent, D. C., & Park, R. (1971). Flexural members with confined concrete. Journal of the Structural Division.

[39] Kim, J.-H., & Park, H.-G. (2020). Shear and Shear-Friction Strengths of Squat Walls with Flanges. ACI Structural Journal, 117(6).

[40] Kim, S.-H., & Park, H.-G. (2021). Shear Strength of Reinforced Concrete Wall with 700 MPa Shear Reinforcement. ACI Structural Journal, 118(2).

[41] Kimura, H., & Sugano, S. (1996). Seismic behavior of high strength concrete slender wall under high axial load. Paper presented at the 11th World Conference on Earthquake Engineering, Paper.

[42] Lee, J.-Y., & Watanabe, F. (2003). Shear deterioration of reinforced concrete beams subjected to reversed cyclic loading. Structural Journal, 100(4), 480-489.

[43] Liang, X., Che, J., Yang, P., & Deng, M. (2013). Seismic Behavior of High-Strength Concrete Structural Walls with Edge Columns. ACI Structural Journal, 110(6).

[44] Looi, D., Su, R., Cheng, B., & Tsang, H. (2017). Effects of axial load on seismic performance of reinforced concrete walls with short shear span. Engineering Structures, 151, 312-326.

[45] Luna, B. N., Rivera, J. P., & Whittaker, A. S. (2015). Seismic behavior of low-aspect-ratio reinforced concrete shear walls. ACI Structural Journal, 112(5), 593.

[46] Maier, J., & Thürlimann, B. (1985). Bruchversuche an stahlbetonscheiben. Bericht/Institut für Baustatik und Konstruktion ETH Zürich, 8003(1).

[47] Mehta, P. K., & Monteiro, P. J. (2014). Concrete: microstructure, properties, and materials: McGraw-Hill Education.

[48] Mo, Y., & Chan, J. (1996). Behavior of reinforced-concrete-framed shear walls. Nuclear Engineering and Design, 166(1), 55-68.

[49] Oesterle, R., Fiorato, A., Johal, L., Carpenter, J., Russell, H., & Corley, W. (1976). Earthquake resistant structural walls-tests of isolated walls. Research and Development Construction Technology Laboratories, Portland Cement Association.

[50] Park, H.-G., Baek, J.-W., Lee, J.-H., & Shin, H.-M. (2015). Cyclic Loading Tests for Shear Strength of Low-Rise Reinforced Concrete Walls with Grade 550 MPa Bars. ACI Structural Journal, 112(3).

[51] Park, H.-G., & Choi, K.-K. (2017). Unified shear design method of concrete beams based on compression zone failure mechanism. Concrete International, 39(9), 59-63.

[52] Park, H.-G., Yu, E.-J., & Choi, K.-K. (2012). Shear-strength degradation model for RC columns subjected to cyclic loading. Engineering Structures, 34, 187-197.

[53] Pilakoutas, K., & Elnashai, A. S. (1995). Cyclic behavior of reinforced concrete cantilever walls, Part I: Experimental results. ACI Structural Journal, 92(3), 271-281.

[54] Sánchez-Alejandre, A. (2013). Comportamiento sísmico de muros de concreto para vivienda. Ph. D. Dissertation,

[55] Sánchez-Alejandre, A., & Alcocer, S. M. (2010). Shear strength of squat reinforced concrete walls subjected to earthquake loading—trends and models. Engineering Structures, 32(8), 2466-2476.

[56] Sato, S., Ogata, Y., Yoshizaki, S., Kanata, K., Yamaguchi, T., Nakayama, T., . . . Kadoriku, J. (1989). Behavior of Shear Wall Using Various Yield Strength of Rebar Part 1: An Experimental Study.

[57] Seki, M., Kobayashi, J., Shibata, A., Kubo, T., Taira, T., & Akino, K. (1995). Restoring force verification test on RC shear wall.

[58] Standard, B. (2004). Eurocode 2: Design of concrete structures—.

Part 1-1: General rules and rules for buildings, 230.

[59] Standard, B. (2005). Eurocode 8: Design of structures for earthquake resistance. Part, 1, 1998-1991.

[60] Vecchio, F. J., & Collins, M. P. (1986). The modified compression-field theory for reinforced concrete elements subjected to shear. ACI J., 83(2), 219-231.

[61] Wallace, J. W. (2007). Modelling issues for tall reinforced concrete core wall buildings. The structural design of tall and special buildings, 16(5), 615-632.

[62] 국토교통부. (2016). KDS 14 20 22 콘크리트 전단 및 비틀림 설계기준.

[63] 김성현, 황현종, & 박홍근. (2018). 세장한 RC 벽체의 비선형 동적 거동에 의한 전단력 증폭효과. 콘크리트학회 논문집, 30(2), 135-146.

[64] 행정안전부. (2018). 2017 포항지진 백서. (11-1741000-000123-01). 재난관리실 지진방재관리과: 행정안전부

Appendix: Verification of Simplified Strength Degrdation Models

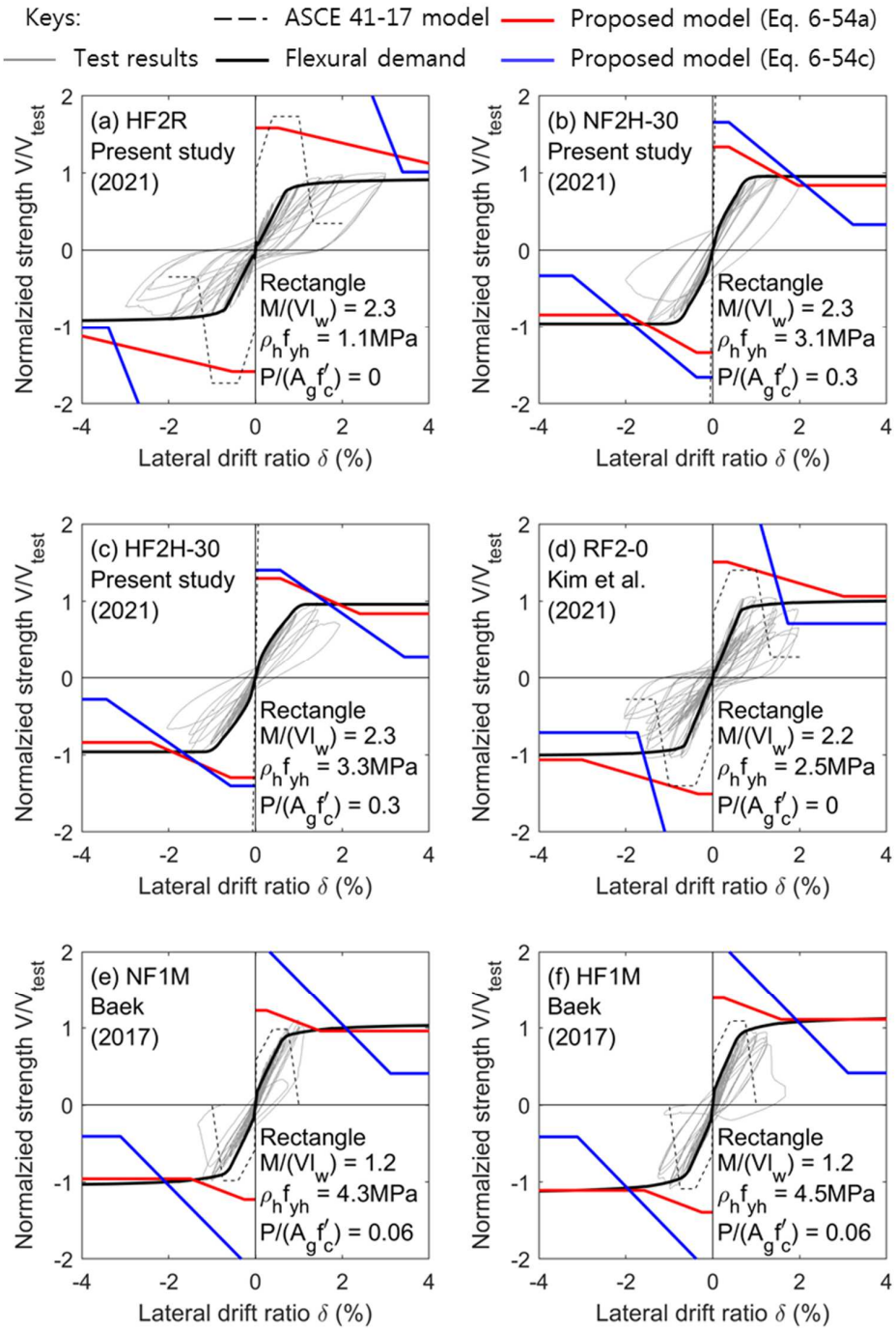

Fig. A-1 Shear strength degradation of rectangle walls

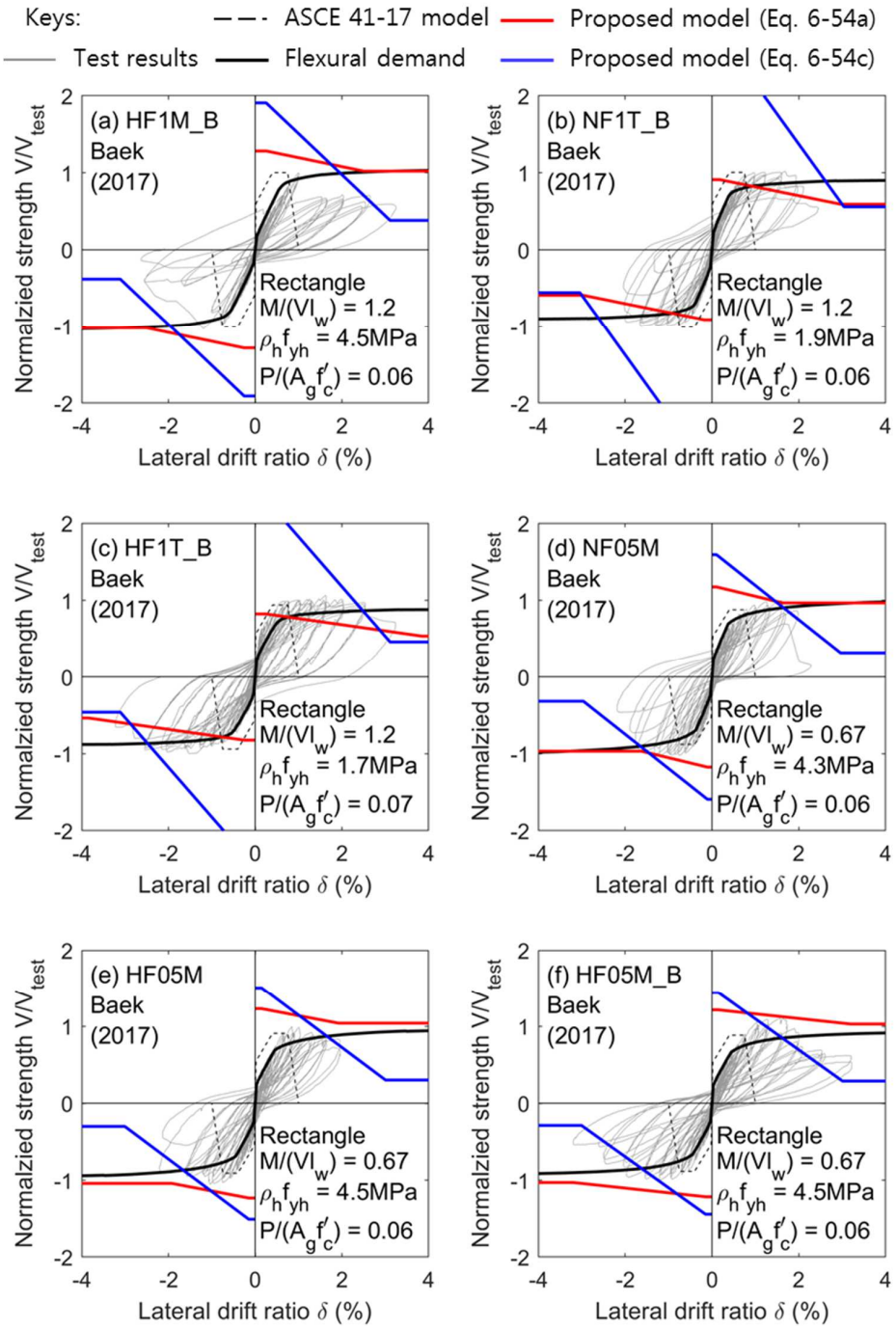

Fig. A-1 Shear strength degradation of rectangle walls (continued)

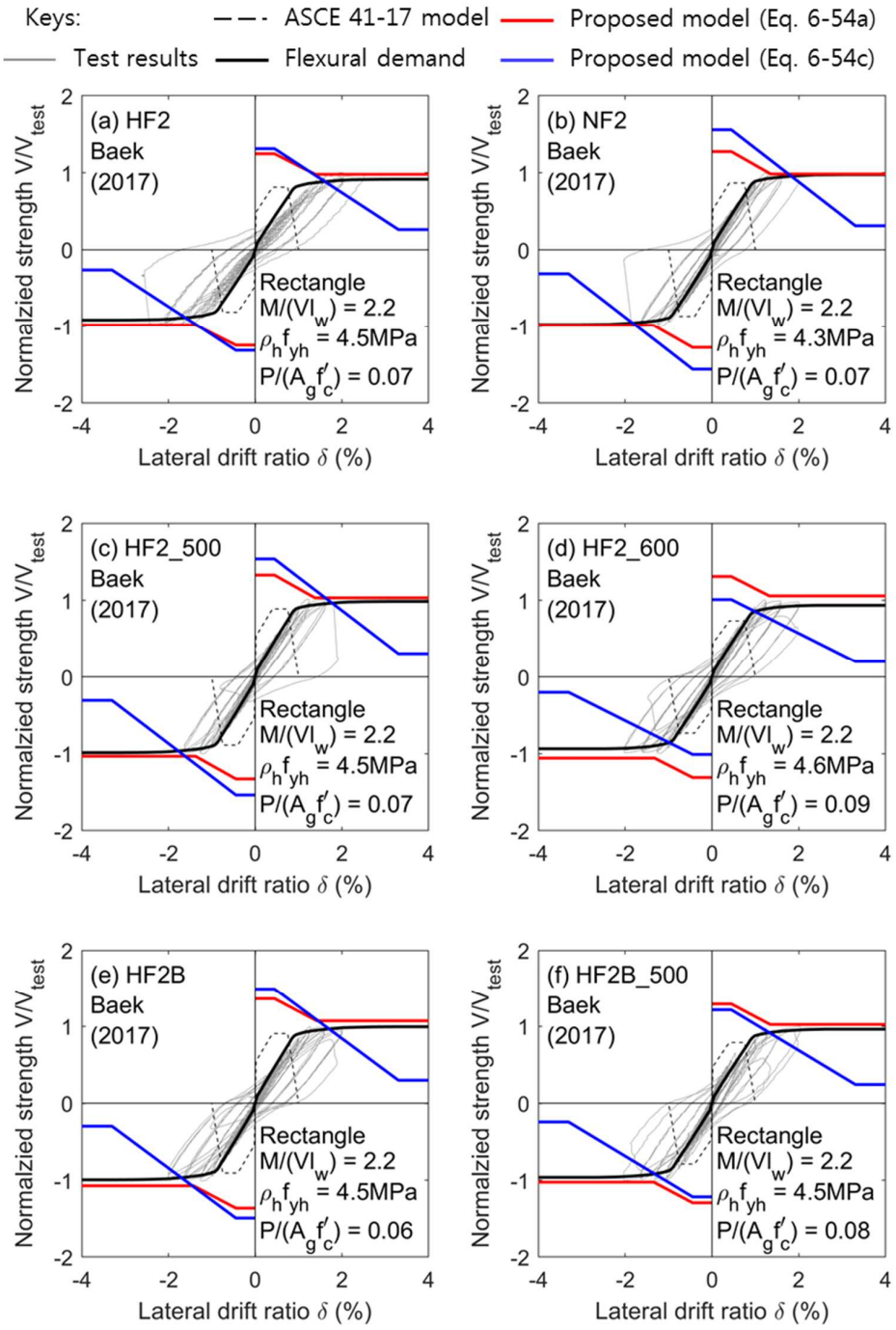

Fig. A-1 Shear strength degradation of rectangle walls (continued)

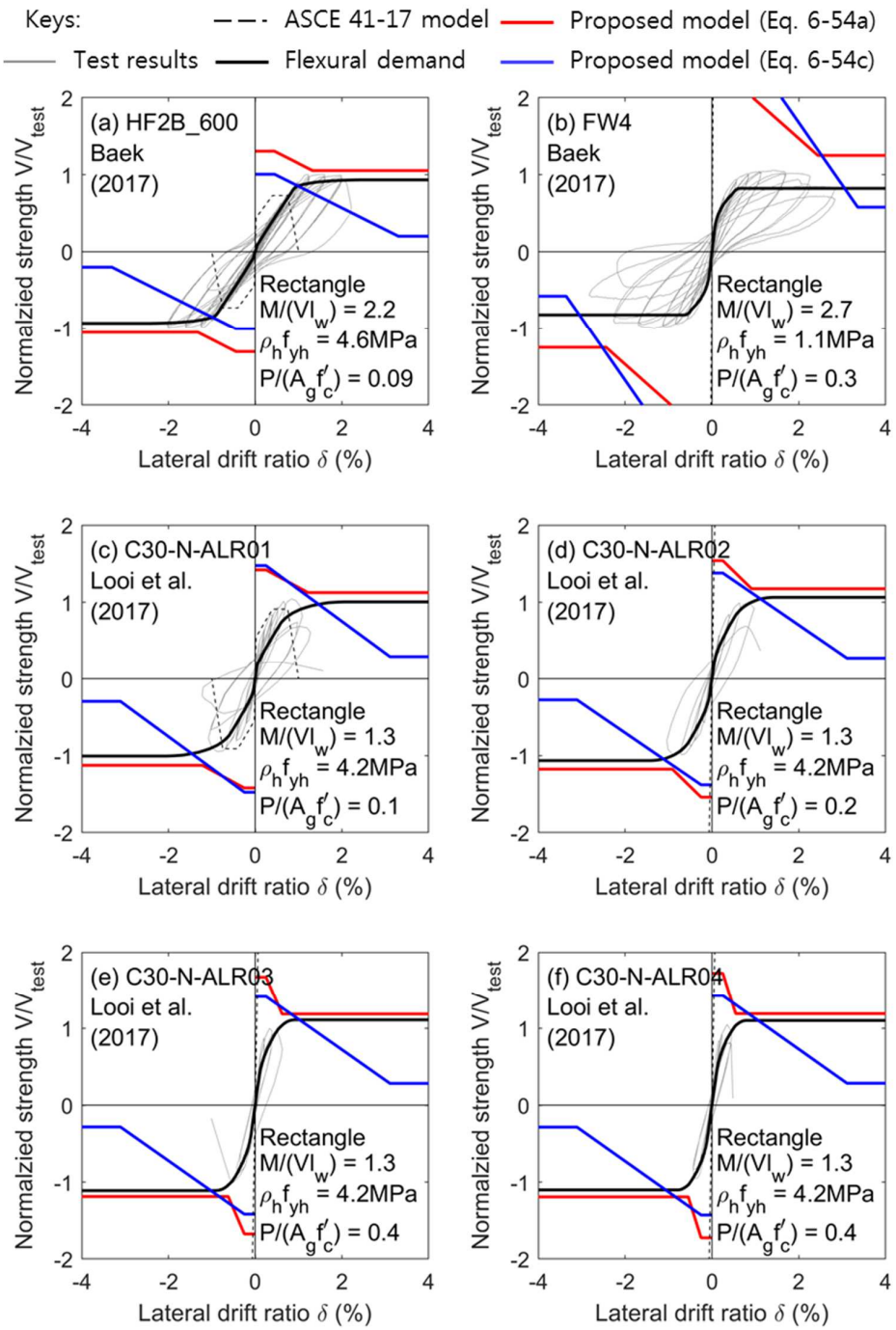

Fig. A-1 Shear strength degradation of rectangle walls (continued)

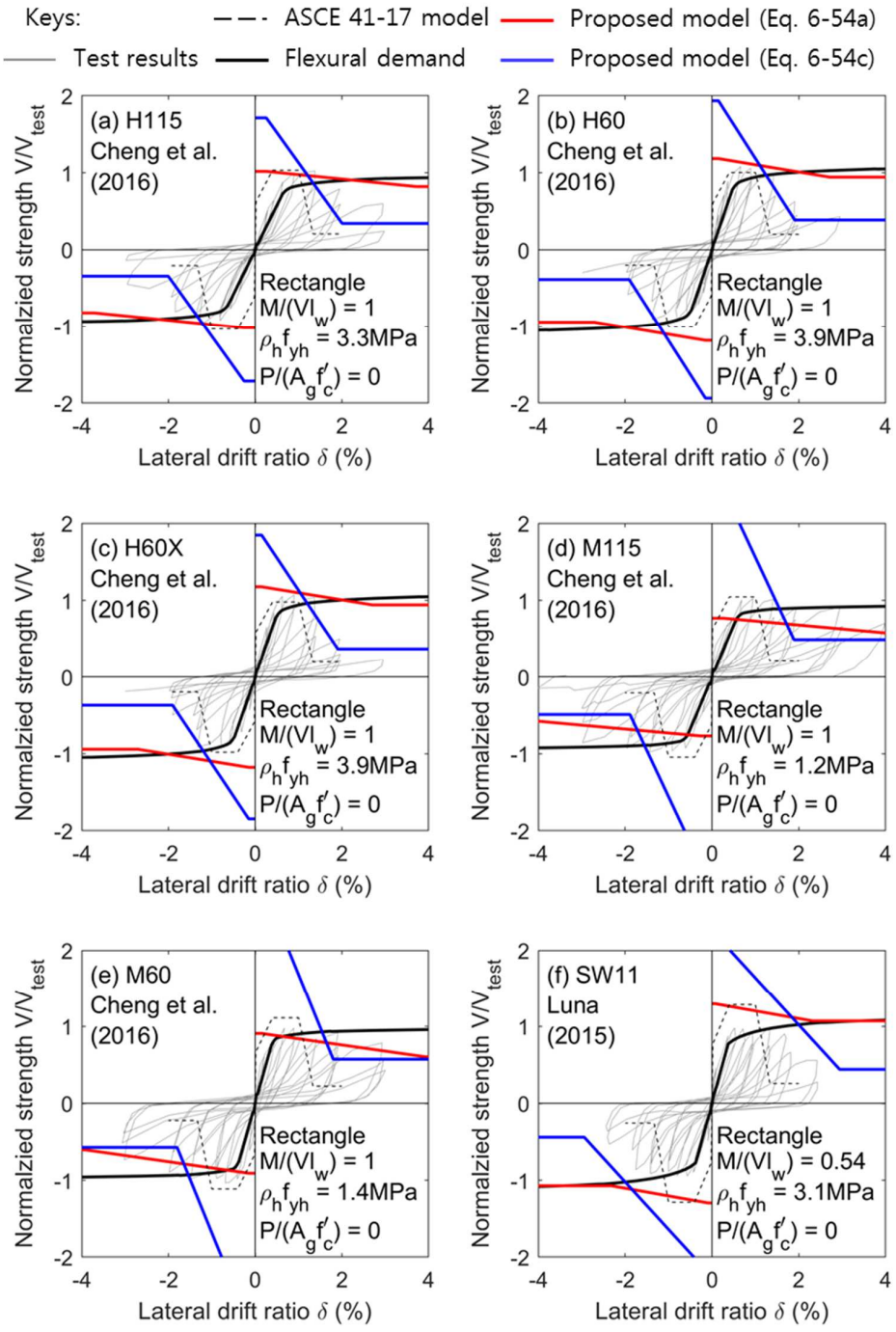

Fig. A-1 Shear strength degradation of rectangle walls (continued)

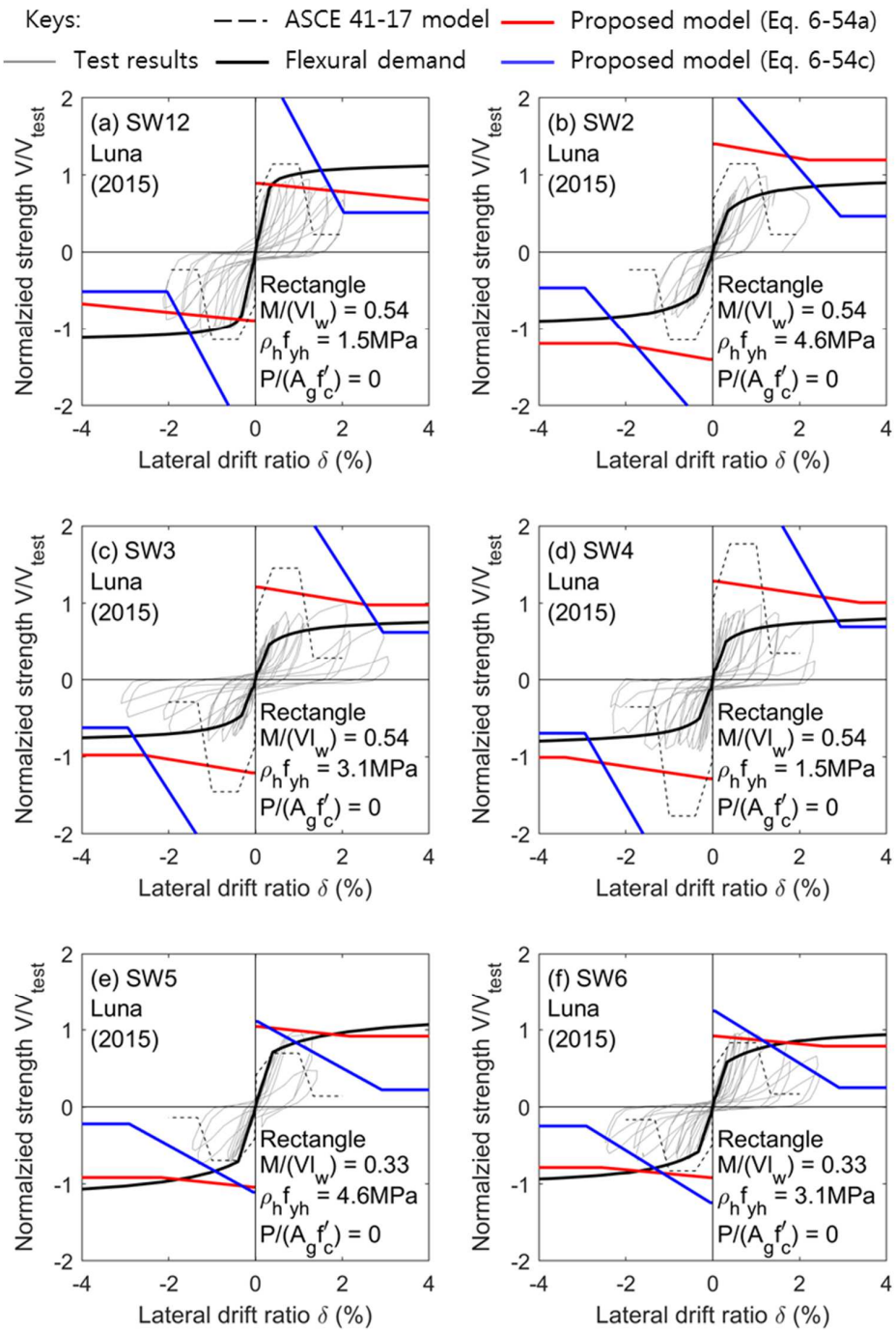

Fig. A-1 Shear strength degradation of rectangle walls (continued)

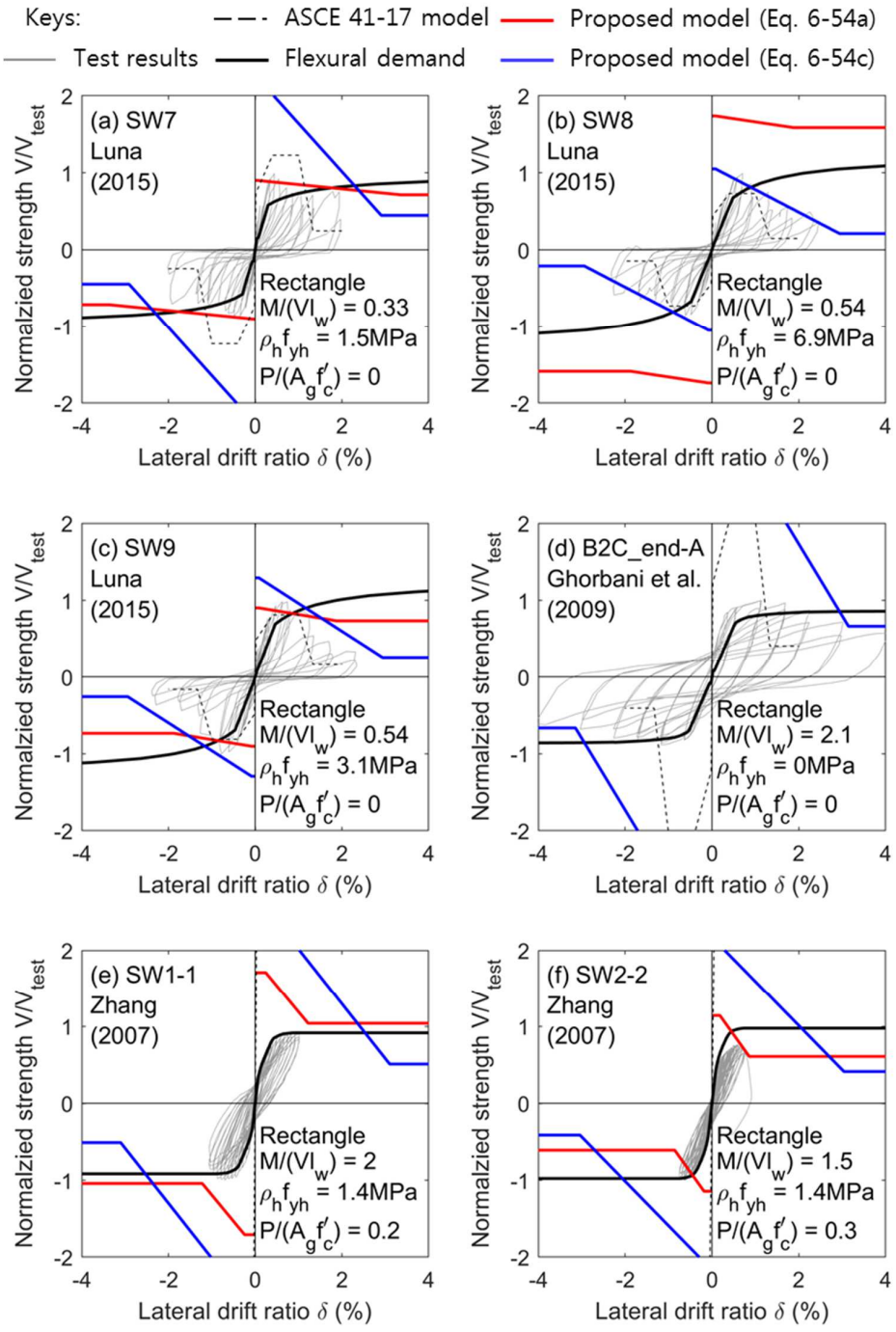

Fig. A-1 Shear strength degradation of rectangle walls (continued)

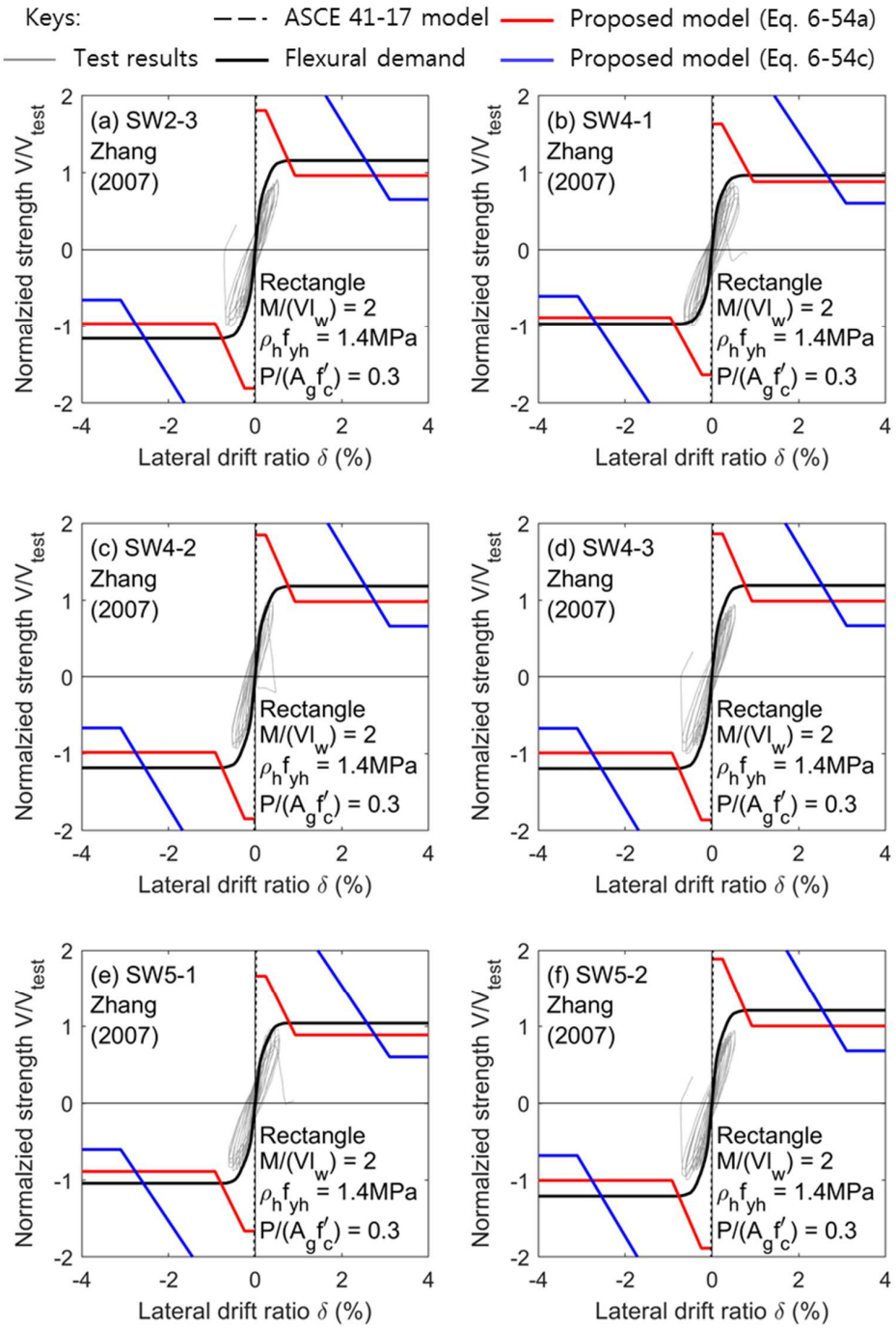

Fig. A-1 Shear strength degradation of rectangle walls (continued)

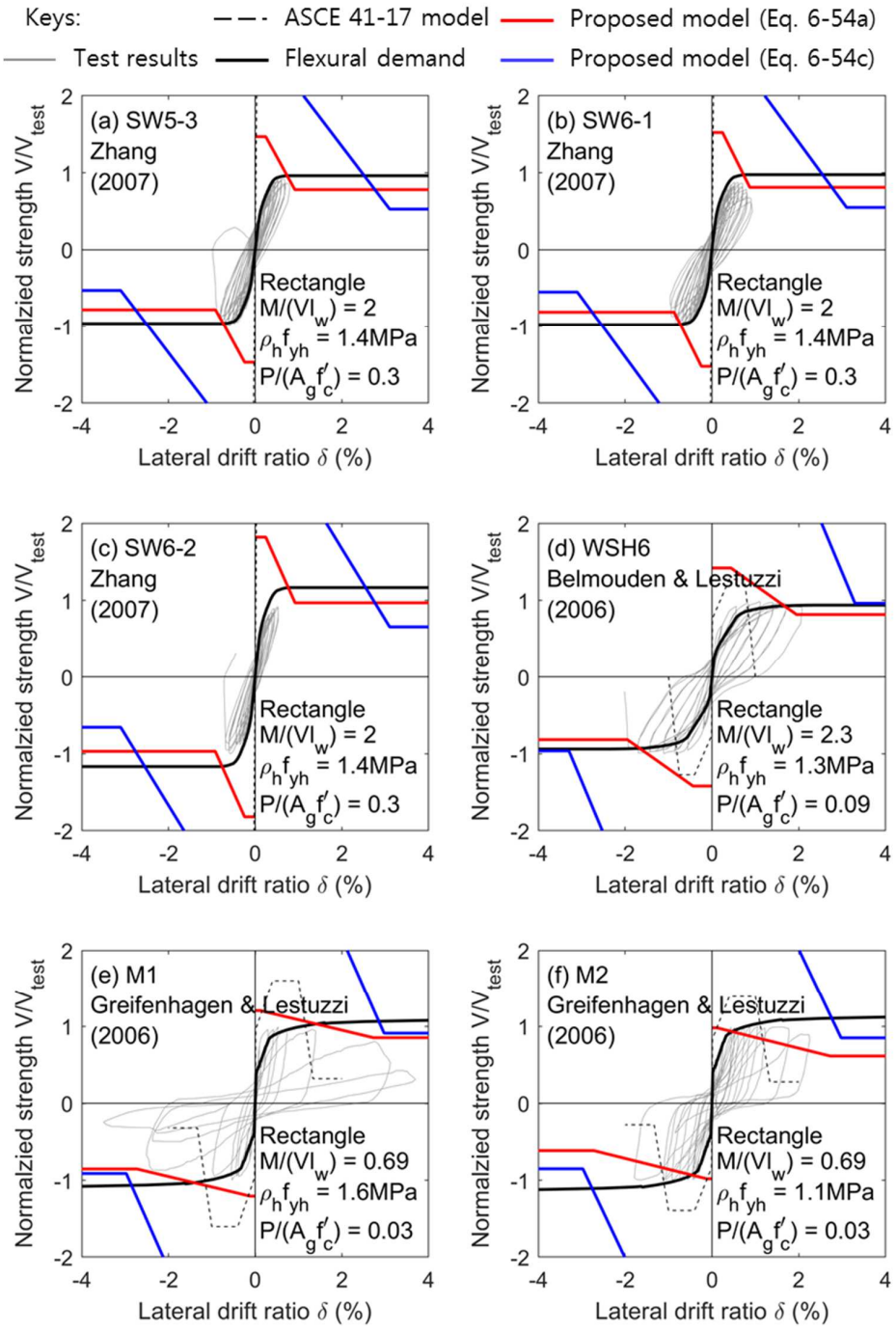

Fig. A-1 Shear strength degradation of rectangle walls (continued)

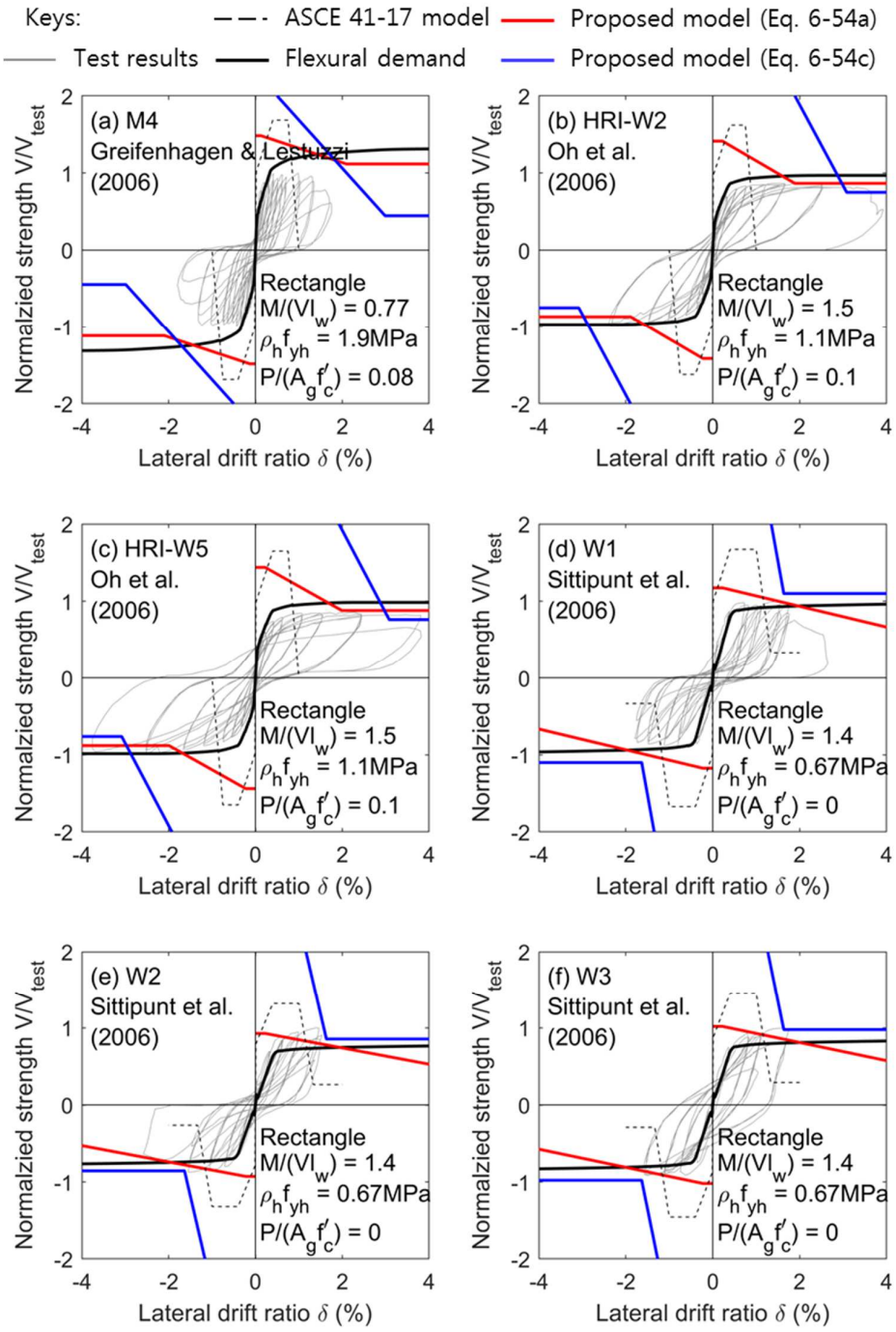

Fig. A-1 Shear strength degradation of rectangle walls (continued)

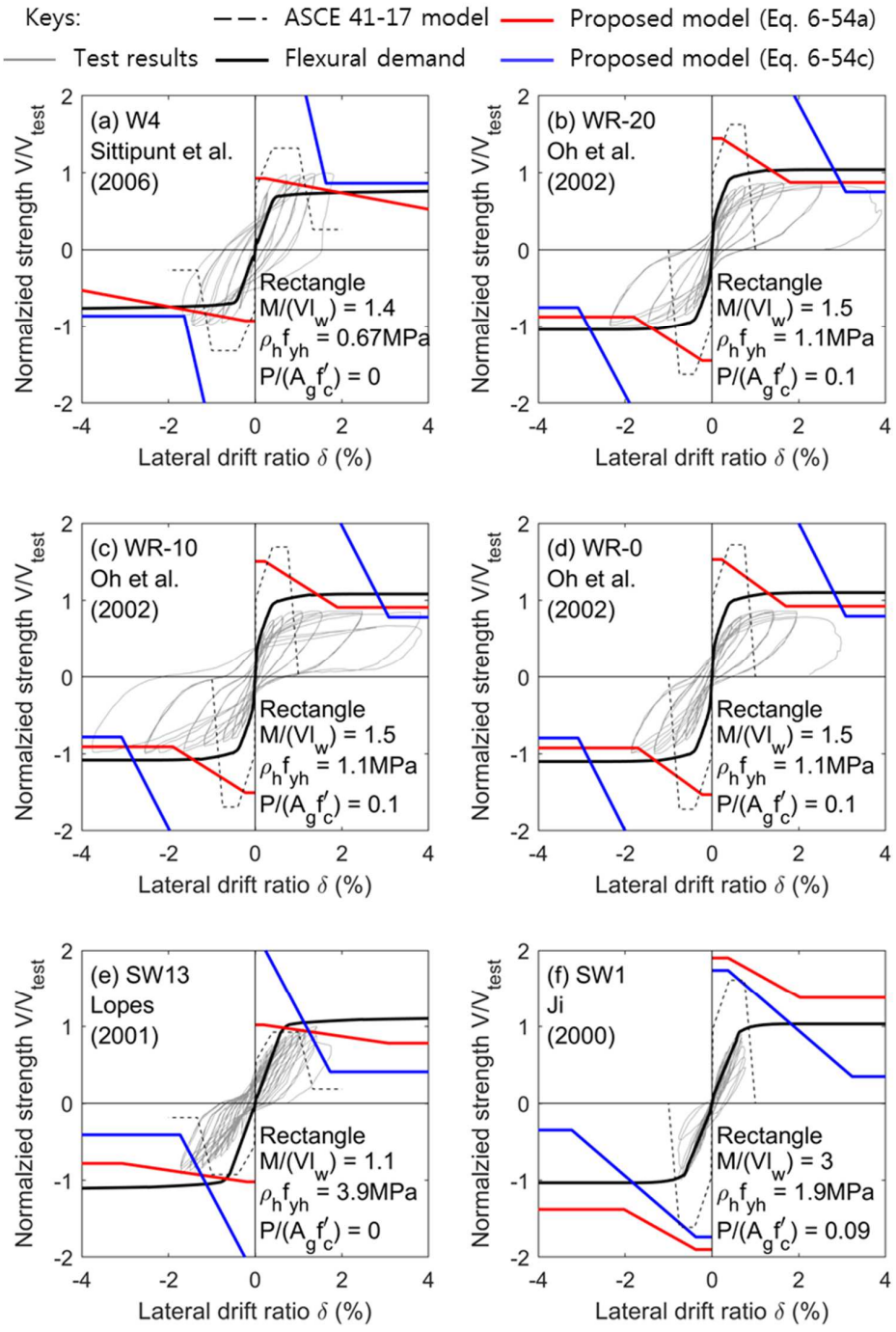

Fig. A-1 Shear strength degradation of rectangle walls (continued)

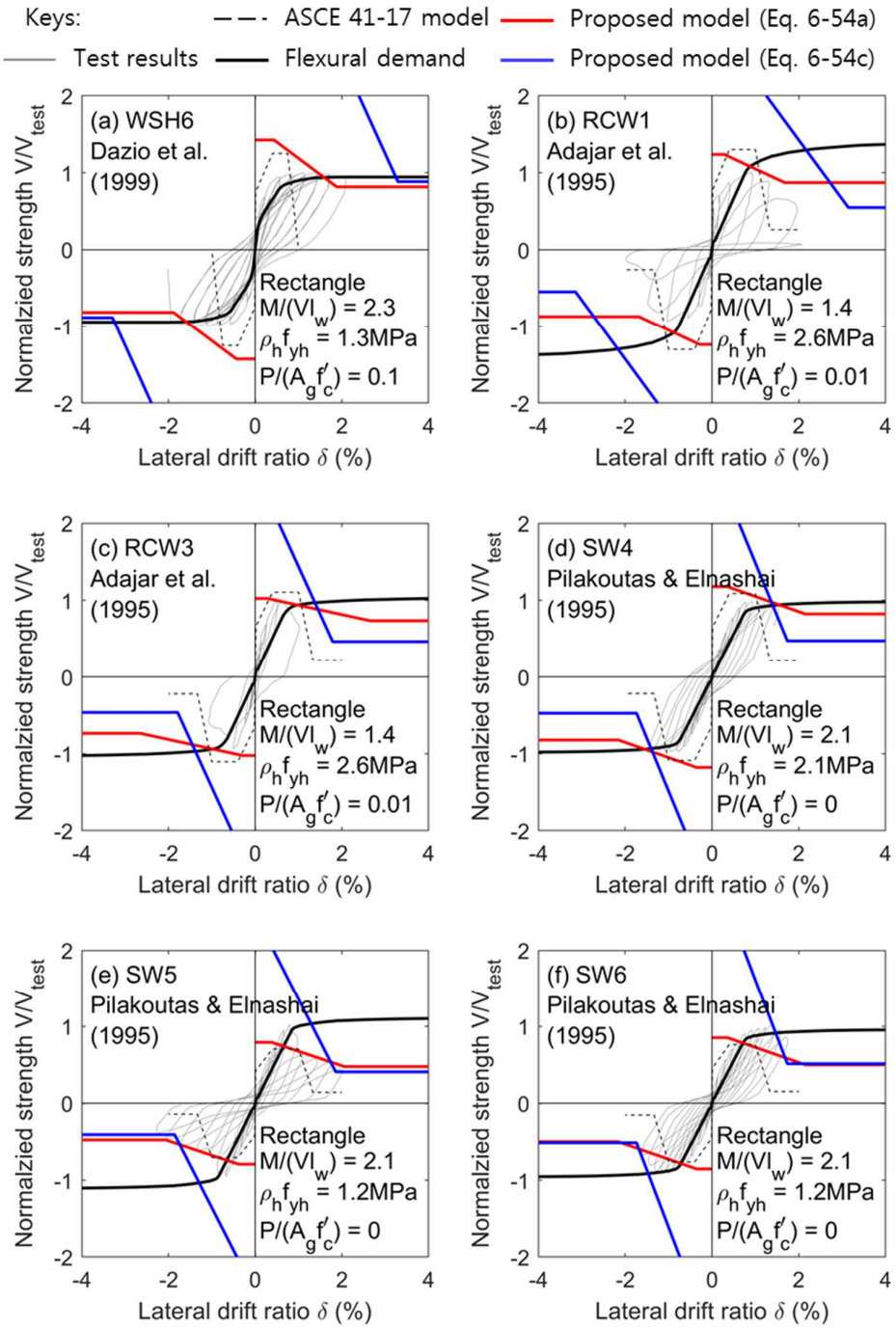

Fig. A-1 Shear strength degradation of rectangle walls (continued)

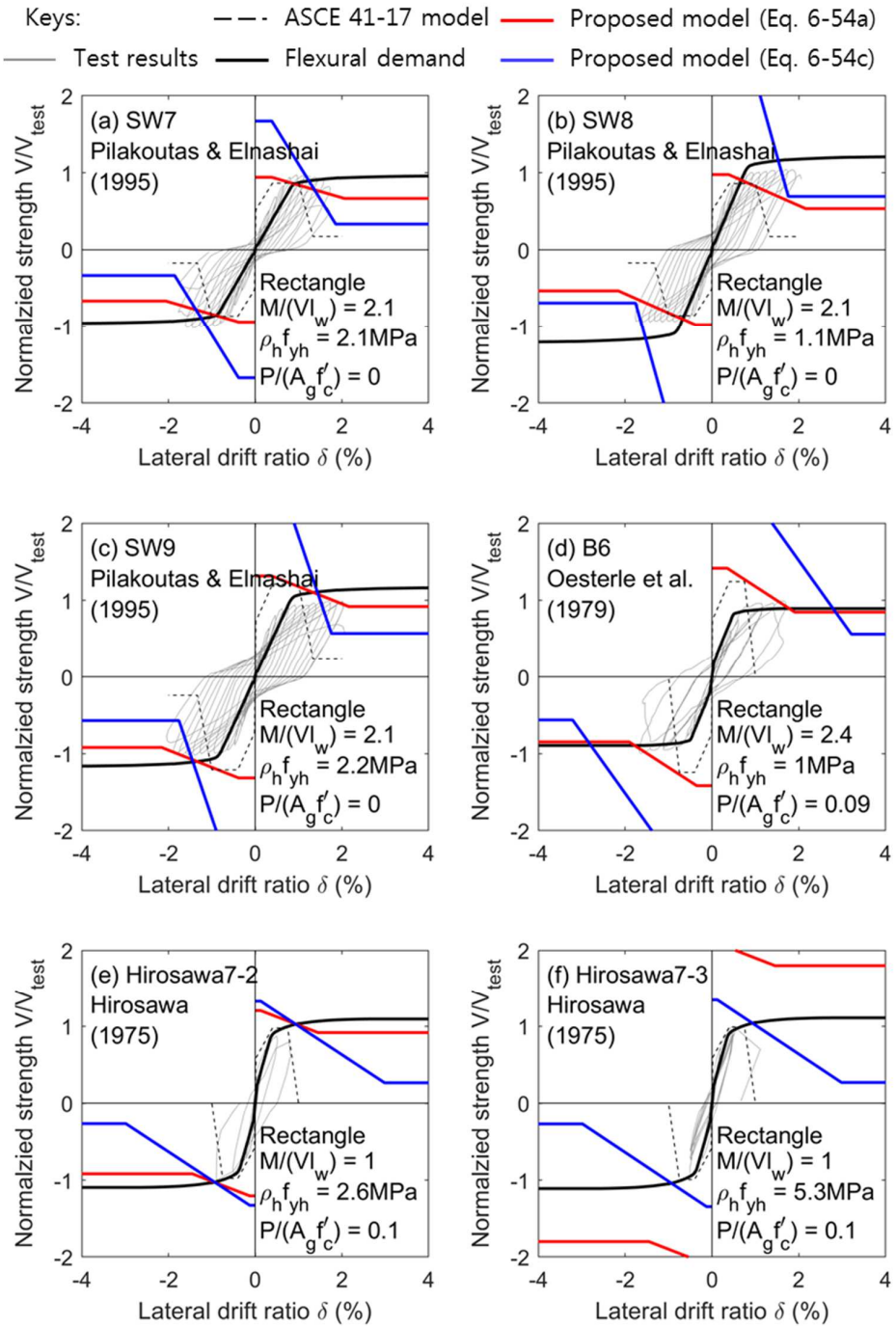

Fig. A-1 Shear strength degradation of rectangle walls (continued)

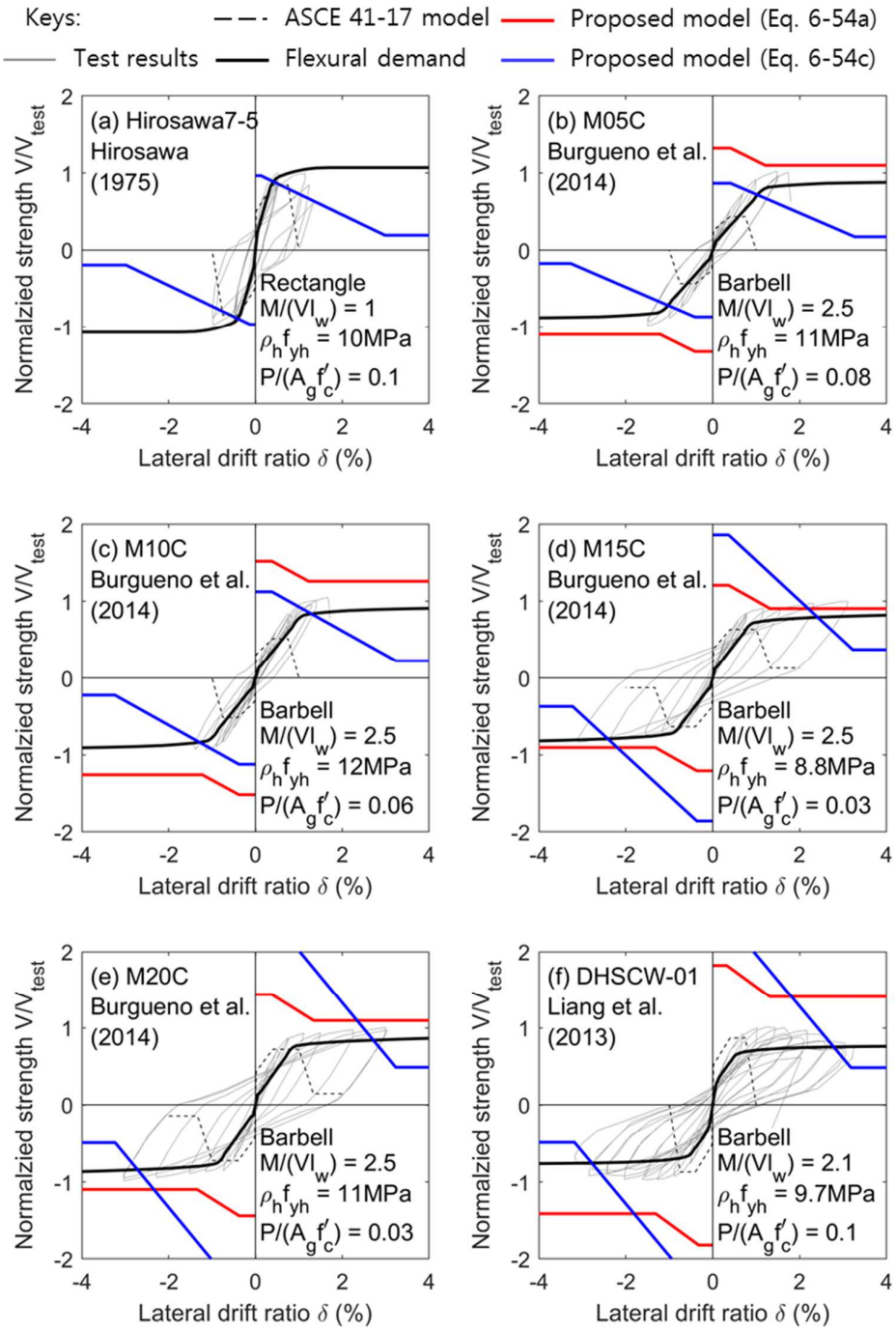

Fig. A-2 Shear strength degradation of barbell and flanged walls

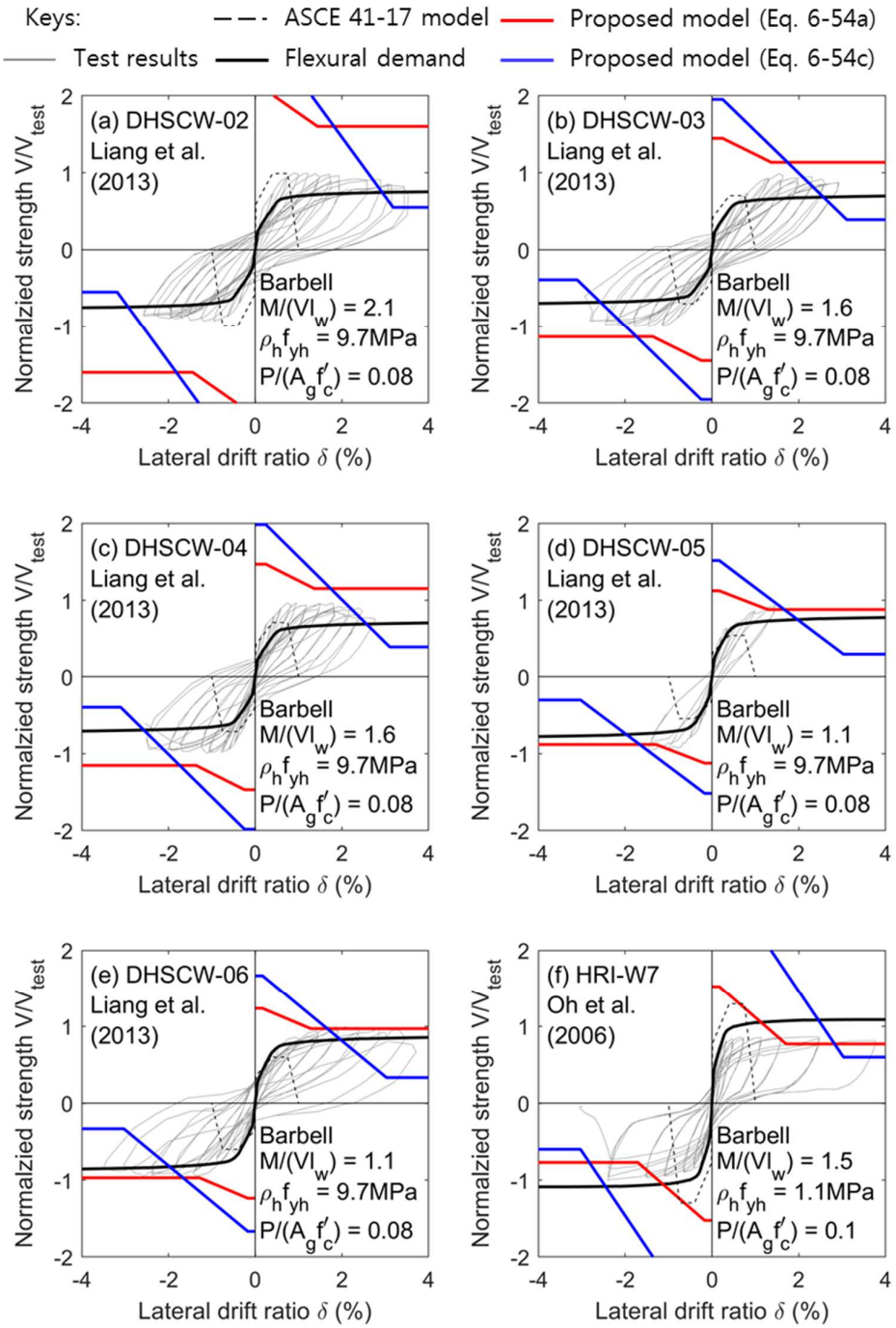

Fig. A-2 Shear strength degradation of barbell and flanged walls (continued)

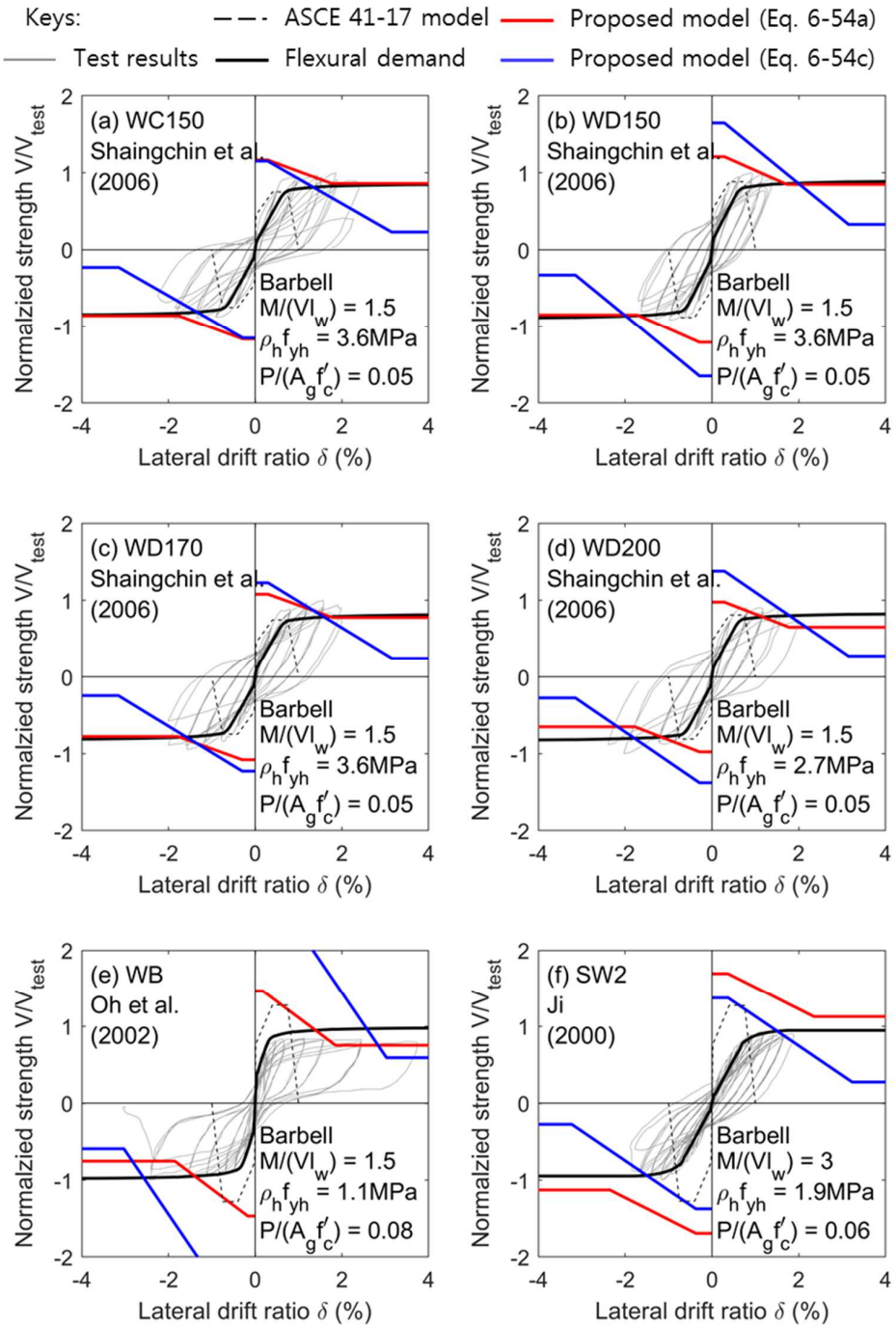

Fig. A-2 Shear strength degradation of barbell and flanged walls (continued)

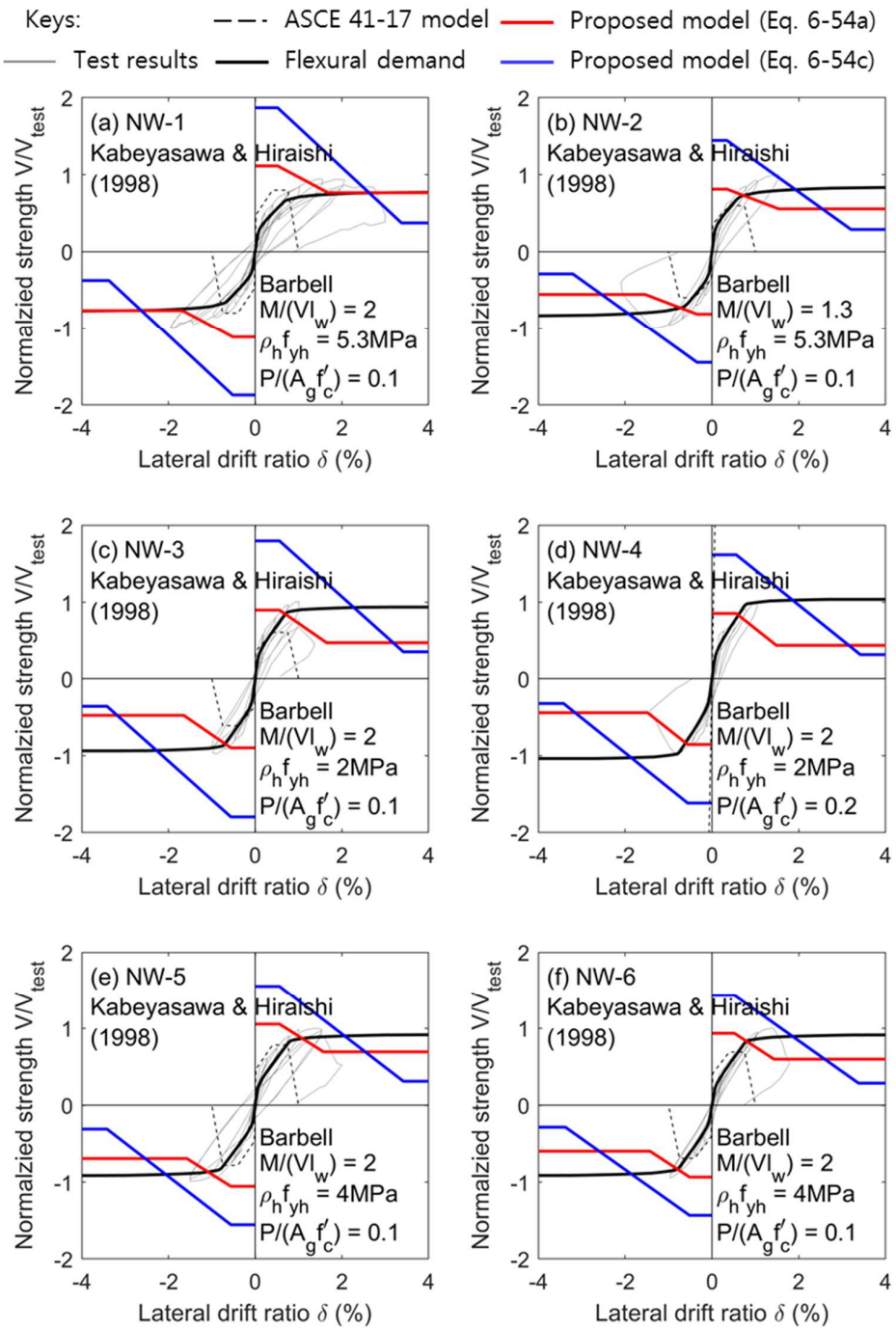

Fig. A-2 Shear strength degradation of barbell and flanged walls (continued)

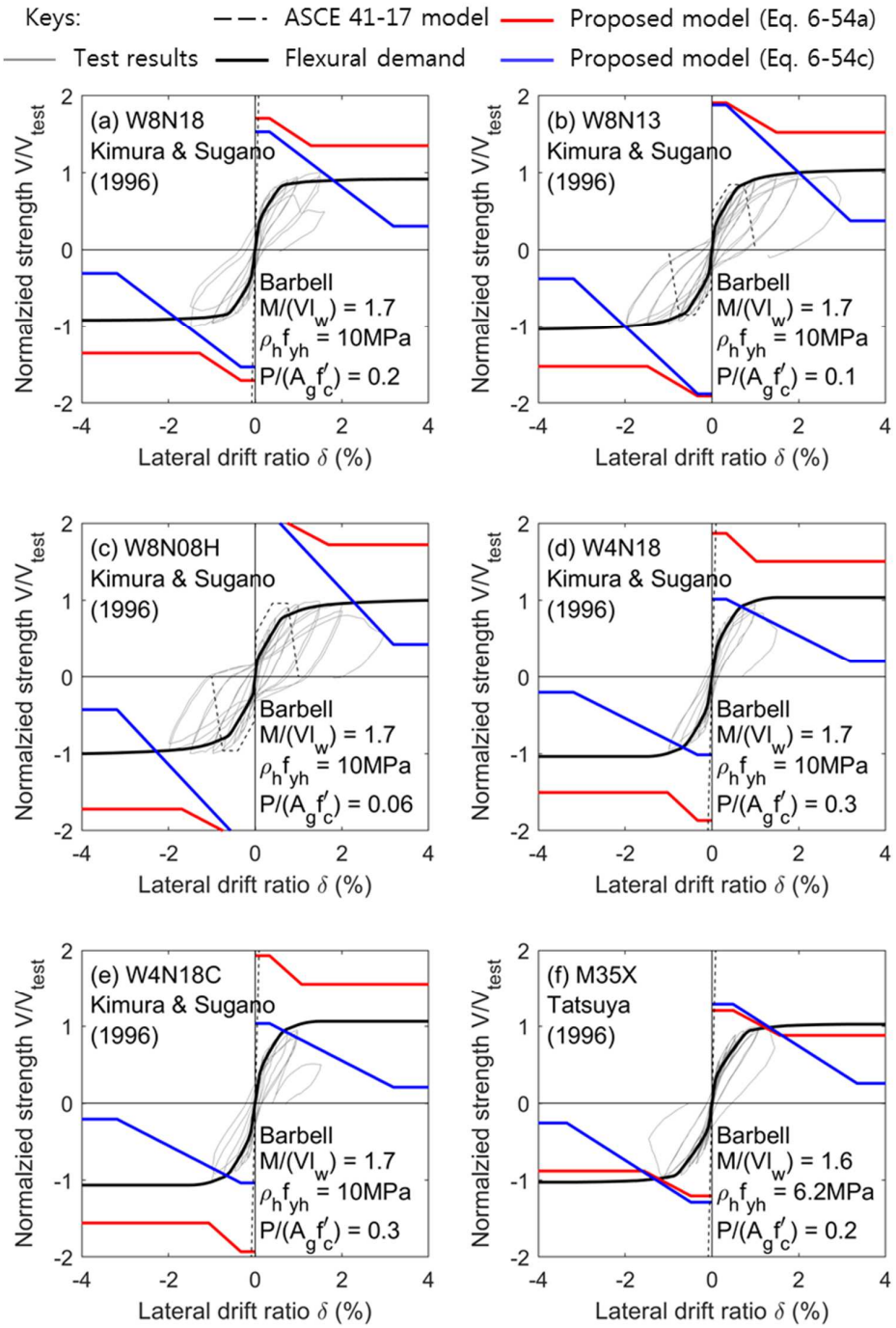

Fig. A-2 Shear strength degradation of barbell and flanged walls (continued)

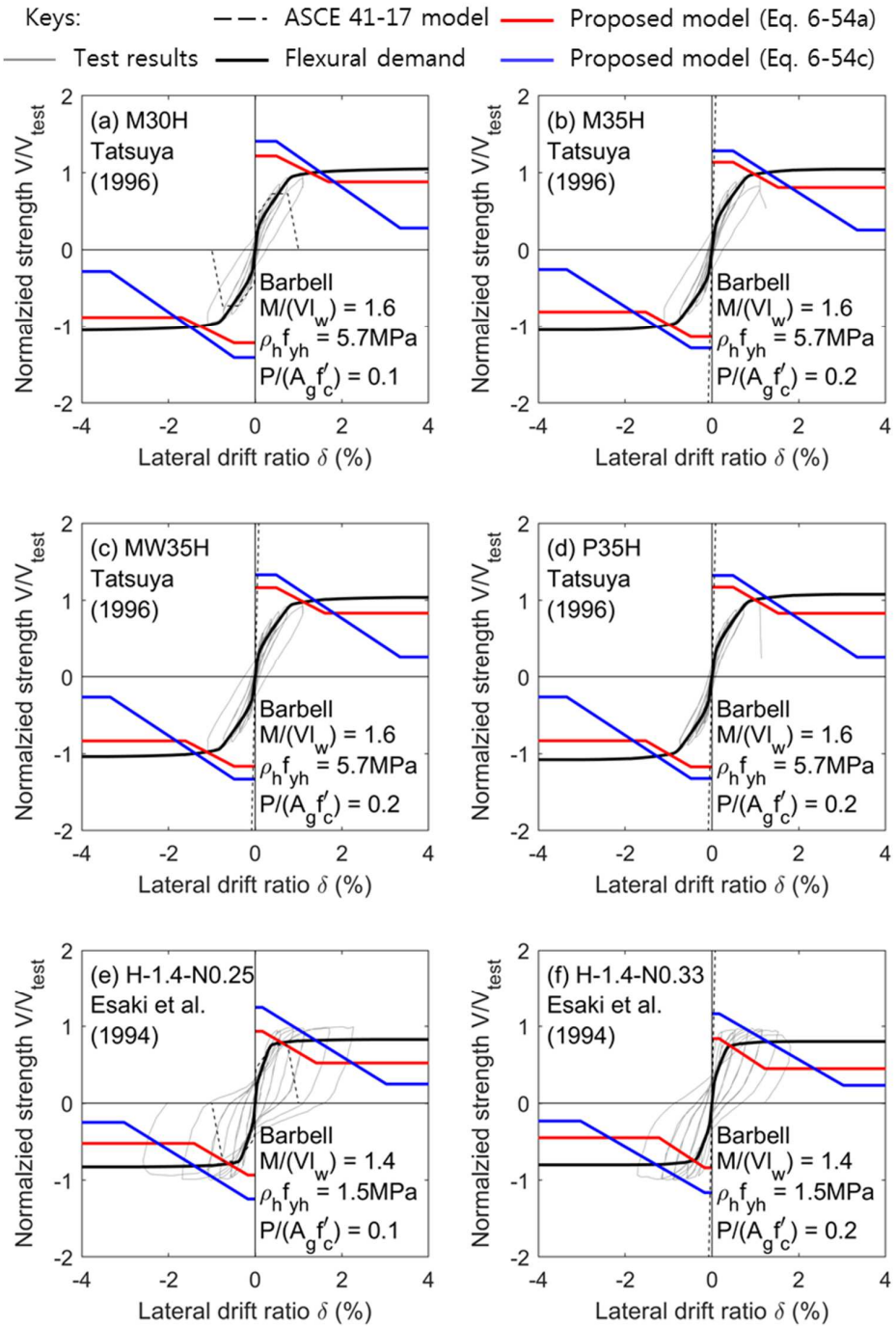

Fig. A-2 Shear strength degradation of barbell and flanged walls (continued)

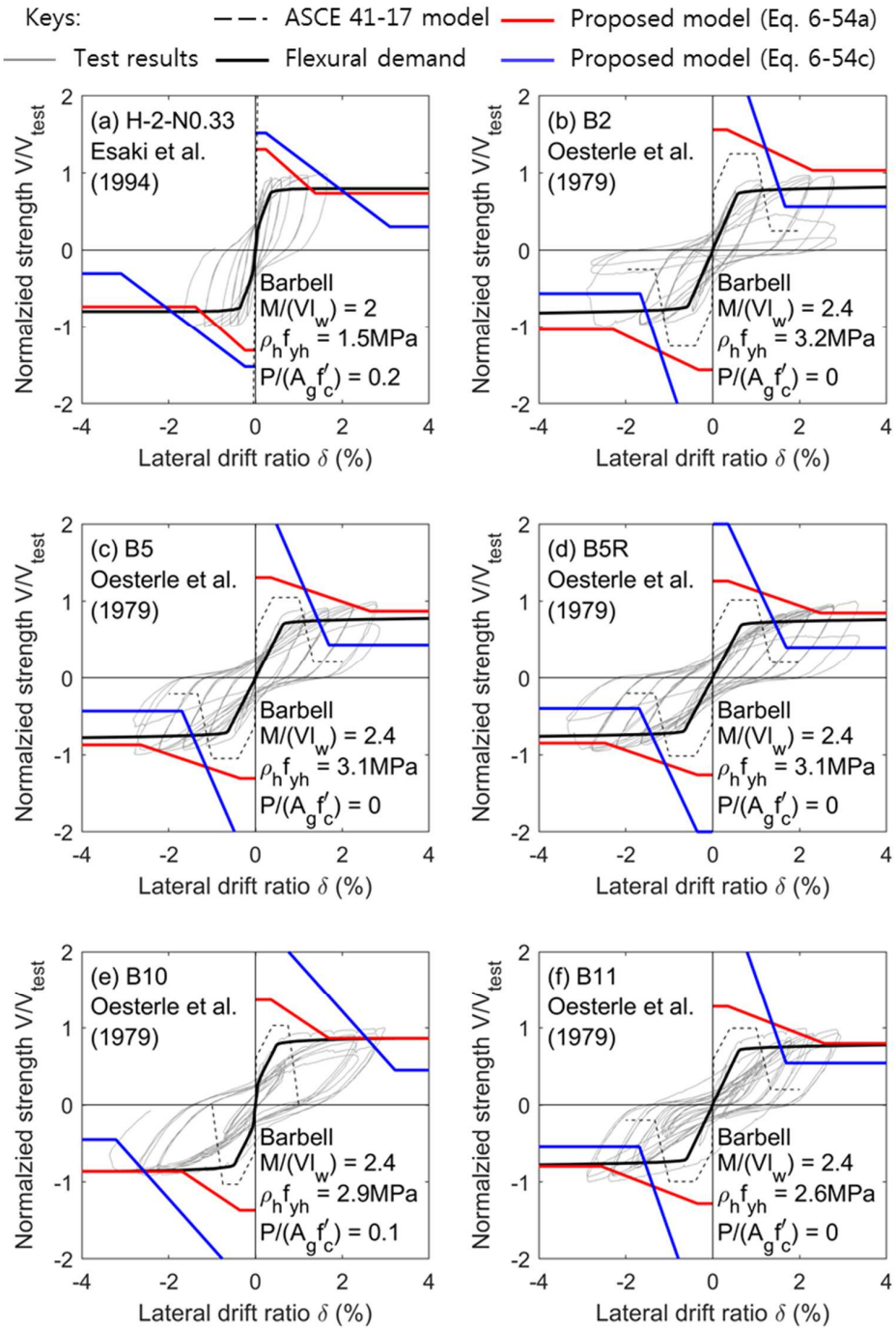

Fig. A-2 Shear strength degradation of barbell and flanged walls (continued)

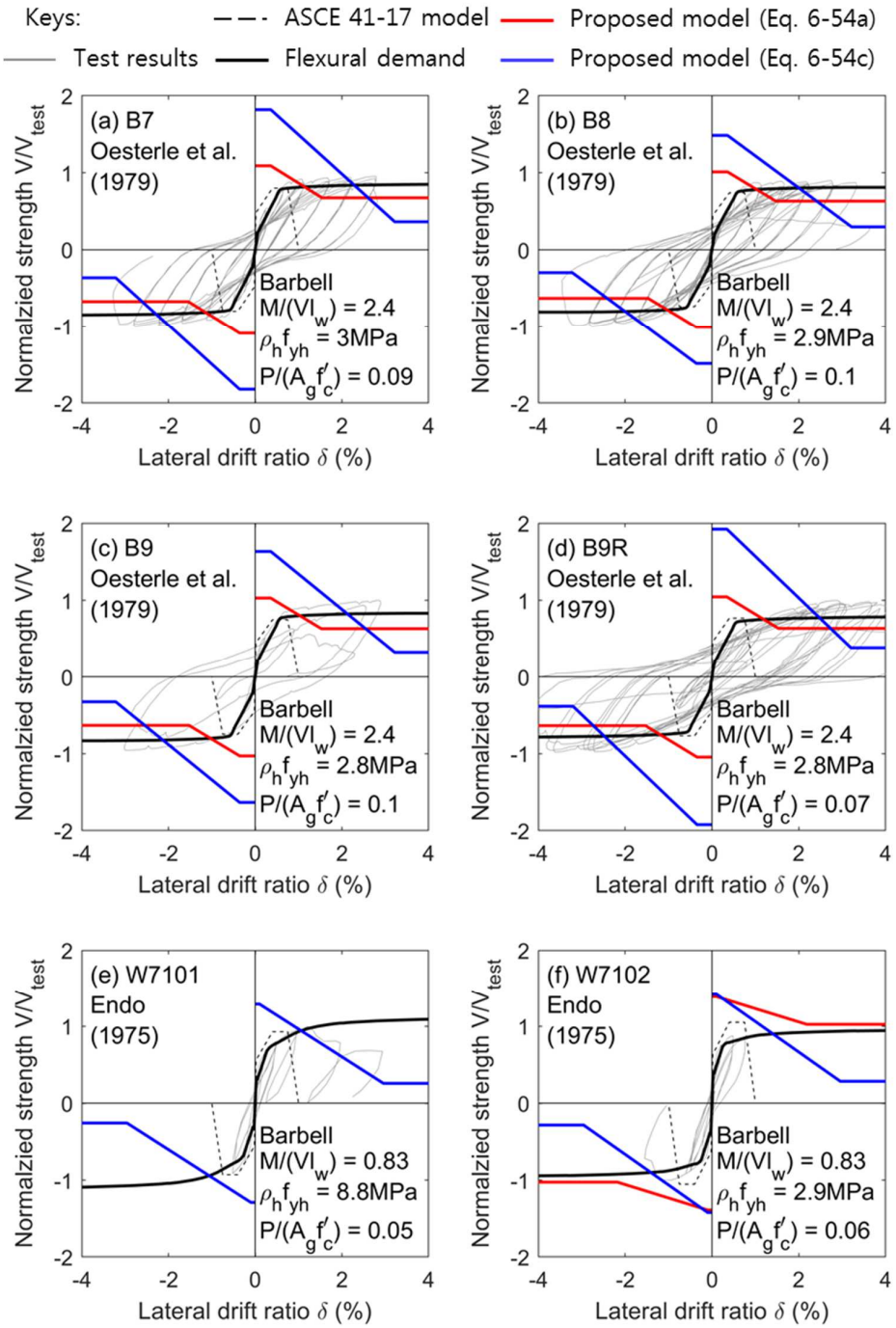

Fig. A-2 Shear strength degradation of barbell and flanged walls (continued)

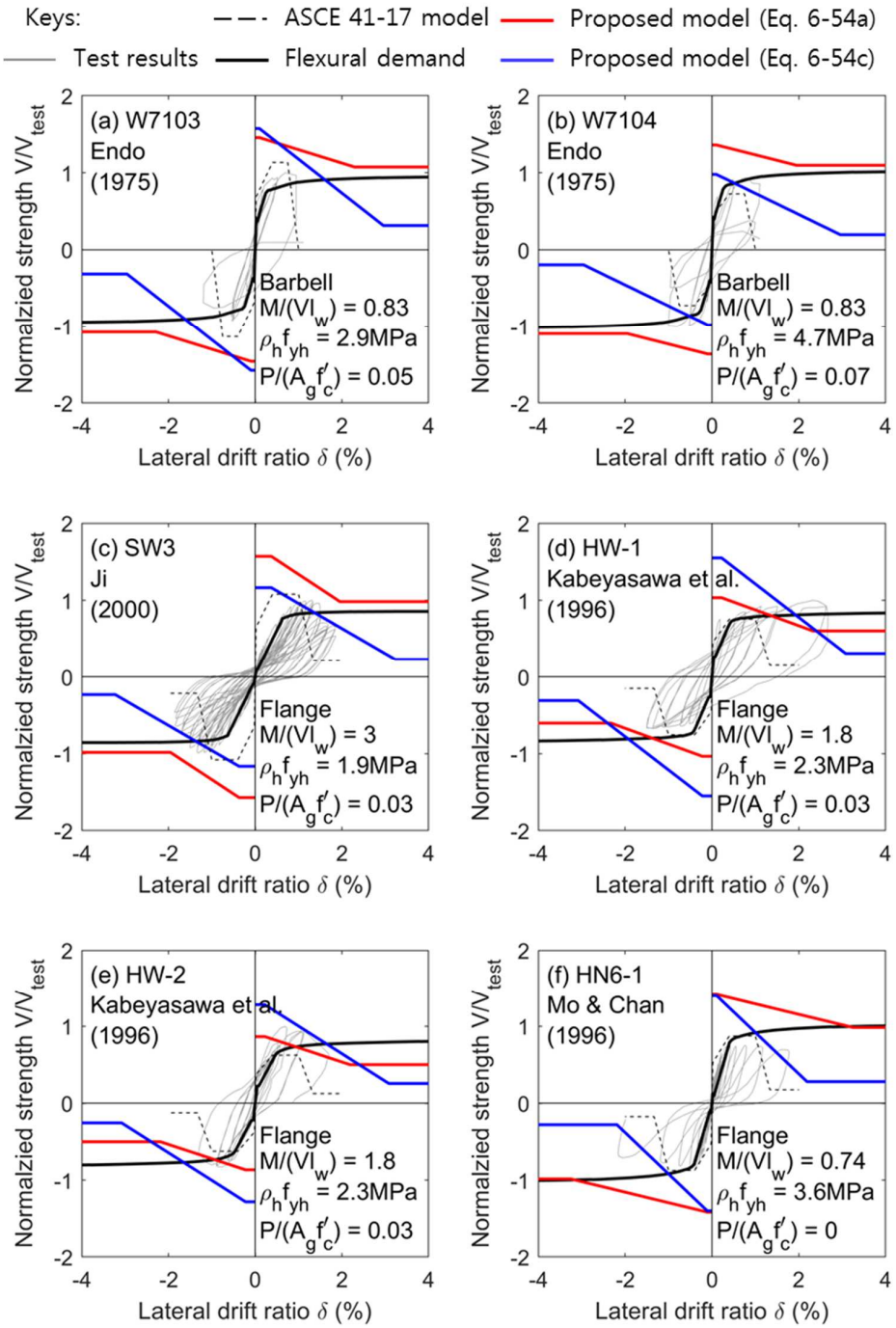

Fig. A-2 Shear strength degradation of barbell and flanged walls (continued)

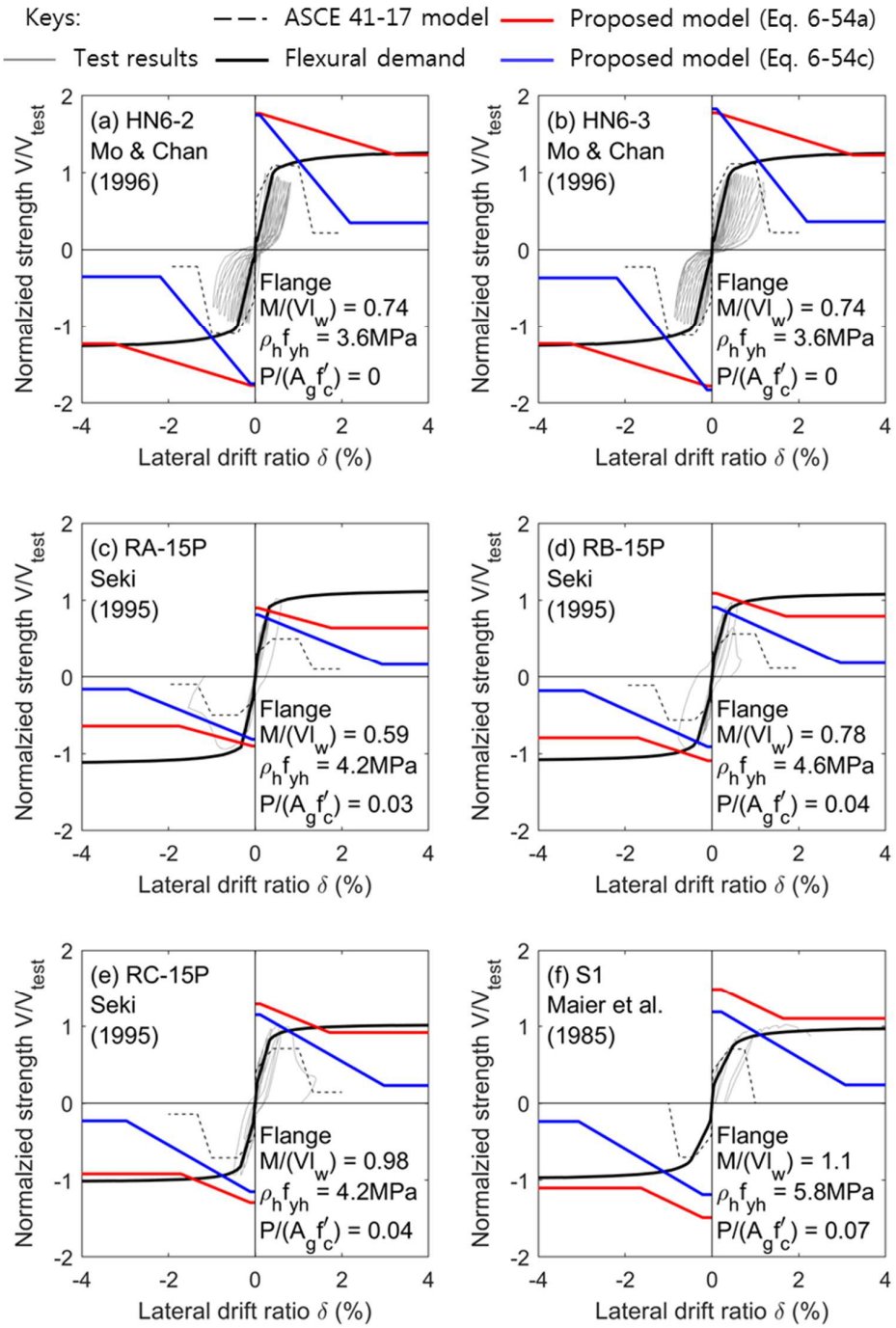

Fig. A-2 Shear strength degradation of barbell and flanged walls (continued)

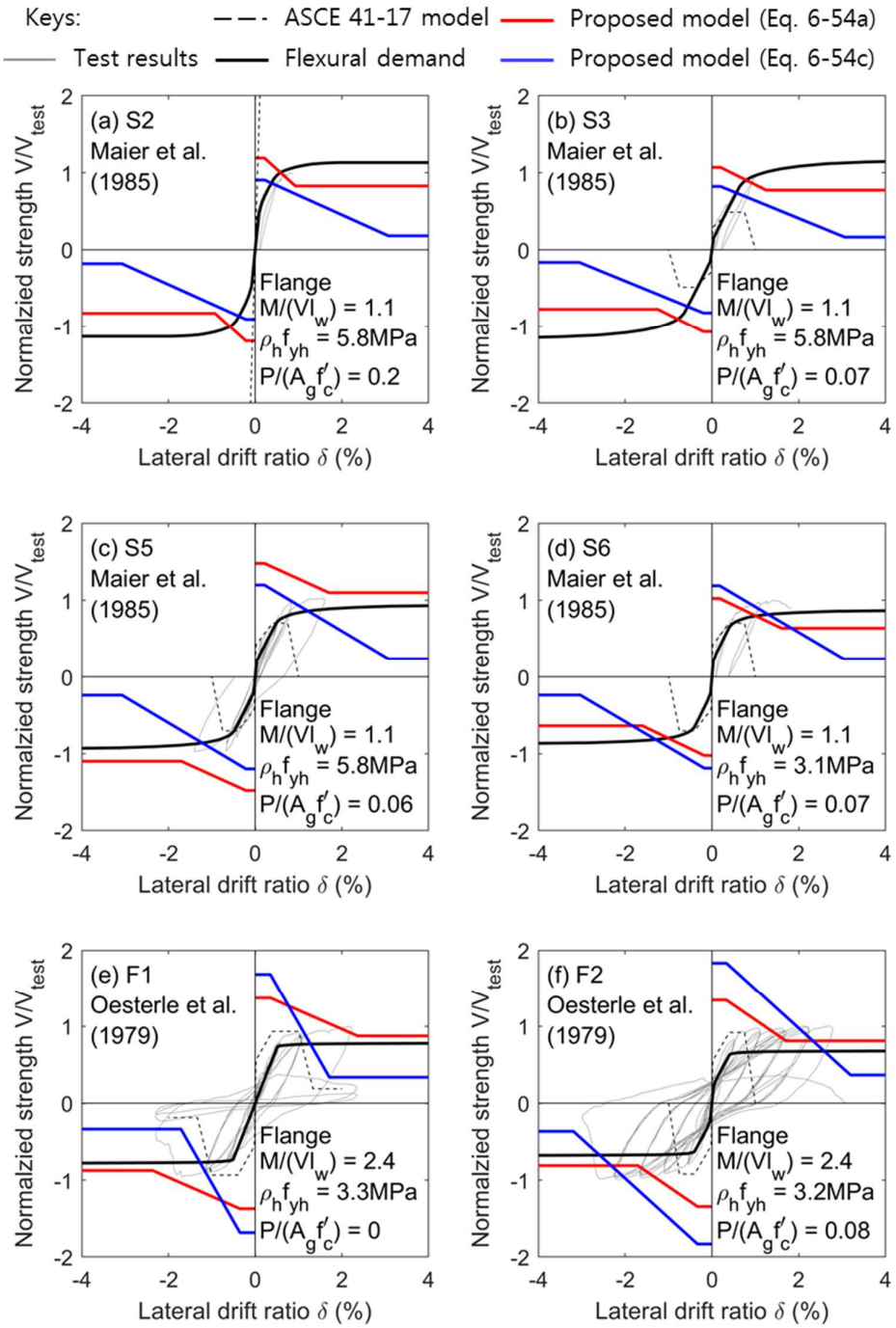

Fig. A-2 Shear strength degradation of barbell and flanged walls (continued)

초 록

RC 벽체의 성능기반 내진설계 및 평가를 위한 전단 강도와 강도저하 예측모델

김 성 현

서울대학교 건축학과 대학원

성능기반 내진설계 및 평가 기법에서는 비선형 해석을 통해 지진에 의한 건축물의 거동을 평가한다. 성능설계 시, 고층 공동주택의 세장한 벽체는 구조적 동적 특성으로 인해 지진하중에 의해 큰 전단력이 벽체에 작용하므로 경제적인 설계를 위해 고강도 철근의 사용이 요구된다. 이를 위하여 본 연구에서는 실험적 연구를 바탕으로 700 MPa 철근을 사용한 벽체의 유효성에 대하여 입증 자료를 제공하였다. 한편, 기존 건물의 벽체는 내진설계가 미비하여 연성능력이 부족하고 전단파괴에 취약하기 때문에, 성능 평가 시 벽체의 전단강도와 변형능력을 정확히 평가하는 것이 중요하다. 따라서, 벽체의 전단거동에 영향을 미치는 주요 요인을 조사하고, 벽체의 전단 거동 메커니즘을 기반으로 전단 강도와 변형능력을 평가하는 설계모델을 개발하였다.

고층 공동주택의 벽체에는 중력하중과 지진하중에 의하여 큰 요구하중이 작용한다. 따라서 높은 축력비가 작용하고 철근비가 높은 벽체에 대하여 700 MPa 철근의 유효성이 검증되어야 한다. 한편

요구강도가 크지 않더라도 현행 설계 기준은 벽체의 사용성 및 안전성을 확보하기 위하여 최소 철근비를 규정하고 있다. 따라서 낮은 철근비가 벽체의 강도와 변형능력에 미치는 영향이 평가되어야 한다. 이를 위하여 700 MPa 철근을 사용한 벽체에 대하여 반복 주기 횡 하중 실험이 수행되었다. 실험 결과, 700 MPa 철근을 사용한 벽체는 파괴모드 및 설계변수와 관계없이 설계 강도 이상의 전단 강도를 나타냈다. 700 MPa 전단철근은 최대강도에서 항복하였다. 그러나 700 MPa 철근은 항복 변형률이 크고 철근비가 감소하기 때문에 일반강도 (400 MPa) 철근을 사용한 벽체와 비교하여 강도 여유치는 감소하였고, 균열폭 증가, 에너지 소산량 감소, 연성능력 감소가 나타났다.

실험 연구 결과를 바탕으로 벽체 전단 강도에 영향을 미치는 설계 변수를 분석하였다. 주요한 설계변수는 전단철근 강도, 복부 수직철근비, 축력비, 단면 형상 등이었다. 이러한 설계변수들은 압축대 깊이와 밀접한 관련이 있으므로 콘크리트의 압축 응력을 기반으로 전단강도와 강도저하를 설명할 수 있다. 이러한 고찰을 바탕으로 본 연구에서는 전단강도와 강도저하 예측모델을 개발하였다. 대표적인 전단파괴 메커니즘인 대각 인장 균열 파괴와 복부 압괴 파괴를 고려하였다.

대각인장 균열 강도는 콘크리트 압축대의 깊이와 압축대에 작용하는 평균 응력으로부터 산정하였다. 비탄성 변형이 증가하면 콘크리트 압괴가 압축대에서 발생한다. 유효 압축대 깊이가 감소함에 따라 대각 인장 균열 강도는 저하된다.

복부 압괴 강도는 대각 압축 스트럿의 유효 응력을 사용하여

정의하였다. 콘크리트의 압축강도 연화 작용에 의하여 유효 콘크리트 응력은 균열폭이 증가함에 따라 감소한다. 따라서 횡 변형이 증가할수록 복부 압괴 강도는 저하된다.

이러한 전단거동 메커니즘을 바탕으로 단순 모델을 개발하였다. 기존 설계 기준과 비교하여 제안 모델은 실험 결과를 비교적 잘 예측하였다.

본 연구의 제안 모델을 실무설계에 적용하기 위하여 설계 테이블과 가이드라인이 제시되었다. Perform 3D 해석 프로그램을 기반으로 제안 모델을 적용하고 실험결과와 비교하였다. Perform 3D를 사용한 해석 결과는 항복 이후 강도 저하를 모사할 수 있었으며, 벽체의 변형능력이 강도저하에 의하여 제한되었다.

주제어: 성능기반 내진설계 및 평가; 700 MPa 철근; 주기하중; 벽체 전단강도; 벽체 변형능력; 대각인장파괴; 복부압괴파괴.

학 번: 2017-35111